Development of sustainable cement composites: understanding the effect of cellulosic additives and waste biomass

by

Sreenath Raghunath

B. TECH, Manipal Institute of Technology, 2017

M.TECH, Manipal Institute of Technology, 2019

MSc, University of Bristol, 2020

A THESIS SUBMITTED IN PARTIAL FULFILLMENT OF

THE REQUIREMENTS FOR THE DEGREE OF

DOCTOR OF PHILOSOPHY

in

THE FACULTY OF GRADUATE AND POSTDOCTORAL STUDIES

(Chemical and Biological Engineering)

THE UNIVERSITY OF BRITISH COLUMBIA

(Vancouver)

November 2025

The following individuals certify that they have read, and recommend to the Faculty of Graduate and Postdoctoral Studies for acceptance, the dissertation entitled:

Development of sustainable cement composites: understanding the effect of cellulosic additives and waste biomass

submitted by Sreenath Raghunath in partial fulfilment of the requirements for

the degree of Doctor of Philosophy

in Chemical and Biological Engineering

Examining Committee:

Dr. E Johan Foster, Associate Professor, Department of Chemical and Biological Engineering, UBC
Supervisor

Dr. Mark Martinez, Professor, Department of Chemical and Biological Engineering, UBC
Supervisory Committee Member

Dr. Feng Jiang, Associate Professor, Department of Wood Science, UBC
Supervisory Committee Member

Dr. Dana Grecov, Professor, Department of Mechanical Engineering, UBC
University Examiner

Dr. Qingshi Tu, Assistant Professor, Department of Wood Science, UBC
University Examiner

Dr. Yoan Simon, Associate Professor, Biodesign Center for Sustainable Macromolecular Materials and Manufacturing, Arizona State University
External Examiner

Abstract

Fiber reinforced cement is widely used in non-structural building applications due to its improved toughness, strength, and durability. However, continued reliance on ordinary Portland cement and synthetic chemical additives raises concerns regarding environmental impact and long-term sustainability. This thesis addresses these challenges through two strategies: first, replacing petrochemical or silica-based additives with nano- to micro-scale cellulosic biomaterials, and second, reducing ordinary Portland cement use by partially substituting it with processed waste biomass and by developing a cement-free hybrid geopolymer binder.

In the first approach, nano- and micro-scale cellulosic additives were investigated in fiber cement reinforced with softwood kraft pulp. Among the nanocellulosic materials, cellulose nanocrystals at optimal concentrations (2–4 wt.%) produced notable improvements in workability, early hydration, and flexural strength compared to systems containing conventional chemical additives. These improvements were attributed to the high surface area and network-forming morphology of cellulose nanocrystals, which enhanced water transport, supported early hydration reactions, and promoted matrix densification. Micro-scale cellulosic additives also provided distinct benefits: alpha cellulose improved post-cracking toughness and workability by reducing yield stress, while microcrystalline cellulose enhanced peak flexural strength. Despite differences in absolute strength, the strength-to-weight ratios of systems modified with alpha cellulose and microcrystalline cellulose were comparable, suggesting that low-cost alpha cellulose can deliver similar performance benefits.

In the second approach, biochar derived from woody biomass was used to partially replace Portland cement. At an optimal dosage of 8 wt.%, biochar improved rheology, time-dependent thixotropy, and mechanical strength while reducing global warming potential by 18 % relative to a pure cementitious system. These effects were linked to its porous morphology and reactive surface, which enhanced water retention and hydration. Furthermore, a cement-free geopolymer binder composed of metakaolin and biochar was developed through mechanochemical processing and reinforced with pulp fibers, achieving flexural strengths of 13–15 MPa with substantially lower embodied carbon, demonstrating a viable route toward sustainable, high-performance fiber cement.

Lay Summary

Fiber cement is a widely used building material known for its strength and durability. However, its production depends on cement and additives derived from fossil fuels or mined materials, which are harmful for the environment. This thesis explores natural, biobased alternatives to make fiber cement more environmentally friendly. Different forms of cellulose, extracted from wood/plant sources and refined into micro- to nano-sized additives, were tested for their potential to improve the mixing, setting, and hardening behaviour of fiber cement. Additionally, biochar, a carbon-rich material produced by heating waste biomass in a low-oxygen environment, was used to partially replace cement and reduce carbon emissions. Finally, a fully cement-free system was also developed using a blend of biochar and metakaolin, a clay-based material, as a hybrid binder. These materials proved to be strong and easy to fabricate with lower environmental impact. Overall, this work supports the development of greener construction materials, using renewable low-impact resources.

Preface

This thesis is structured around four primary studies, each of which has been prepared in the form of a manuscript that has either been published, submitted, or is currently under preparation for submission to peer reviewed journals. The details of each manuscript, along with author-specific contributions are summarised below:

Chapter 3: The author of this thesis was the primary author of this work, involved with conceptualization, developing experimental protocols, conducting and validating experiment, data analysis and drafting the original manuscript. A version of this work was published as "Raghunath S, Hoque M, Foster EJ (2023). On the Roles of Cellulose Nanocrystals in Fiber Cement: Implications for Rheology, Hydration Kinetics, and Mechanical Properties. *ACS Sustainable Chemistry and Engineering* 11(29),10727 10736. https://doi.org/10.1021/acssuschemeng.3c01392 "

Dr. Mahfuzul Hoque contributed to designing experimental protocols and editing. Dr. E. Johan Foster jointly contributed to editing the manuscript, acquired funding, and supervised the work.

Chapter 4: The author of this thesis was the primary author of this work, involved with conceptualization, developing experimental protocols, conducting and validating experiment, data analysis and drafting the original manuscript. A version of this work was published as "Raghunath, S., Hoque, M., Zakani, B., Gondaliya, A. M., & Foster, E. J. (2024). Sustainable micro-cellulosic additives for high-density fiber cement: emphasis on rheo-mechanical properties and cost–performance analysis. *RSC Sustainability*. https://doi.org/10.1039/D4SU00287C ".

Dr. Mahfuzul Hoque contributed to conceptualization and editing the manuscript. Dr. Behzad Zakani contributed to rheological analysis. Akash Madhav Gondaliya contributed to experiments and editing the manuscript. Dr. E. Johan Foster jointly contributed to editing the manuscript, acquired funding, and supervised the work.

Chapter 5: The author of this thesis was the primary author of this work, involved with conceptualization, developing experimental protocols, conducting and validating experiment, data analysis and drafting the original manuscript. A version of this work was published as "Raghunath, S., Hoque, M., Gondaliya, A. M., Jalaee, A., Zakani, B., Santos, F. B. dos, Tu, Q., & Foster, E. J. (2025). Engineering low-carbon fiber cement with biochar: understanding its physicochemical properties and their impact on the composite performance and carbon footprint. *Green Chemistry*. https://doi.org/10.1039/D5GC01405K".

Dr. Mahfuzul Hoque contributed to designing experimental protocols and editing the manuscript. Akash Madhav Gondaliya and Dr. Qingshi Tu contributed to Life Cycle Analysis. Dr. Adel Jalaee and Dr. Fernanda Brito dos Santos contributed to experiments. Dr. Behzad Zakani contributed to rheological analysis and manuscript editing. Dr. E. Johan Foster contributed to conceptualization, manuscript editing, acquired funding, and supervised the work.

Chapter 6: The author of this thesis was the primary author of this work, involved with conceptualization, developing experimental protocols, conducting and validating experiment, data analysis and drafting the original manuscript.

This is an original unpublished work currently being drafted into a manuscript. Dr. Mahfuzul Hoque contributed to conceptualization. Dr. Adel Jalaee and Farah Sadek contributed to experiments. Akash Madhav Gondaliya and Dr. Qingshi Tu contributed to Life Cycle Analysis. Dr. E. Johan Foster acquired funding and supervised the work.

The use of Generative AI in this thesis was limited to employing ChatGPT for checking sentences and paragraphs for grammatical correctness and clarity. All 'AI' generated outputs were subsequently reviewed and verified by me for technical accuracy and factual correctness. The use of these tools aligns with UBC's guidelines on ethical and transparent use of Generative AI in graduate research.

Table of Contents

List of Tables

List of Figures

List of Symbols

$\boldsymbol{\alpha}$	Degree of hydration
$\boldsymbol{G''}$	Elastic modulus
$\boldsymbol{G'}$	Storage modulus
$\dot{\boldsymbol{\gamma}}$	Shear rate
$\boldsymbol{\eta}$	Shear viscosity
$\boldsymbol{m}$	Consistency factor of power law fluid model
$\boldsymbol{n}$	Flow index of power law fluid model
$\boldsymbol{Q^0}, \boldsymbol{Q^1}, \boldsymbol{Q^2}, \boldsymbol{Q^3}, \boldsymbol{Q^4}$	Silicon environments in silicate structures in ^{29}Si MAS NMR
$\boldsymbol{\rho}$	Density
$\boldsymbol{\rho_{BC}}$	Density of biochar
$\boldsymbol{\rho_C}$	Density of cement
$\boldsymbol{t}$	Time
$\boldsymbol{\tau}$	Shear stress
$\boldsymbol{\tau_{Dynamic}}$	Dynamic yield stress
$\boldsymbol{\tau_{Static}}$	Static yield stress
$\boldsymbol{\tau_{y_{CO}}}$	Yield stress (Crossover)
$\boldsymbol{\tau_{y_{HB}}}$	Yield stress (Herschel–Bulkley)

List of Abbreviations

ASTM	American Society for Testing Materials
BC	Biochar
C/P	Cost to Performance
DIA	Dynamic Image Analysis
FR-BEMG	Fiber Reinforced Metakaolin Based Geopolymer
GHG	Greenhouse Gas
GWP	Global Warming Potential
ITC	Isothermal Calorimetry
MOR	Modulus of Rupture
NBSK	Northern Bleached Softwood Kraft
OPC	Ordinary Portland Cement
PCEs	Polycarboxylate
PFI	Paper and Fiber Research Institute
PXRD	Powder X-Ray Diffractometry
rheo-mechanical	Rheological and Mechanical
SCMs	Supplementary Cementitious Materials
SDGs	Sustainable Development Goals
UN	United Nations
w/c	Water to Cement
w/b	Water to Binder

Acknowledgements

I would like to thank my supervisor Dr. E Johan Foster for his endless support, guidance, encouragement and patience throughout my PhD journey. His immense knowledge and expertise were instrumental in helping me navigate through my PhD journey.

I would like to thank my committee members Dr. Mark Martinez and Dr. Feng Jiang for their valuable feedback and guidance throughout my PhD journey.

I would like to thank my lab colleagues both past and present for their endless support throughout my PhD journey - especially Dr. Mahfuzul Hoque, whose guidance and encouragement over the years have been invaluable. I'm also deeply grateful to my lab mates Akash Gondaliya, Adel Jalaee, Victoria French, Ruby Osei-Bonsu, Fernanda Brito dos Santos, Philip McMichael, Dr. Sara Fleetwood, Dr. Behzad Zakani and Akshai Bose for their unwavering support and continued friendship throughout my PhD journey.

I gratefully acknowledge the financial support provided from the NSERC Canfor Industrial Research Chair in Advanced Bioproducts (#553449-19), NSERC Discovery GRANT (RGPIN – 2021- 03172), the Canada foundation for Innovation (Project number 022176) and the Pacific Economic Development Canada (PacifiCan). Their support has been instrumental in facilitating this research.

Dedication

To my loving wife, **Dr. Nigitha Prasad**, whose unwavering support, patience, and love has been my greatest strength throughout this journey.

To my precious daughter **Siara Menon Sreenath**, whose innocent smile brings endless joy and has given new meaning to my life.

To my beloved parents, **Raghunath Cherukkat** and **Sudha Raghunath**, whose endless love, sacrifices and encouragement propelled me to the person I'm today, and to my dear brother **Sriram Raghunath**, for his constant love & support.

To my late maternal grandfather, **Kunikrishna Kurup**, whose wisdom and kindness continues to guide me in spirit.

Lastly, a special mention to my amazing mother**, Sudha Raghunath**, for her unconditional love & sacrifices, for instilling in me with strong moral values and for cultivating my love for science. I owe everything to her!

With deepest love and gratitude, I dedicate my thesis to you all.

Chapter 1: Introduction

1.1 Cement industry: global significance, scale of production and environmental impact

Cement is one of the most important materials in the world, often regarded as the backbone of modern construction and infrastructure. It serves as the binding agent in mortar and concrete, which is the most widely produced man-made material in the world and the second most consumed substance on Earth after water. Cement is essential for constructing durable structures such as buildings, bridges, harbors, runways and roads, which are critical to supporting growing communities and expanding cities. As the global population increases and urbanization accelerates, the demand for cement is expected to grow, making it a key contributor to economic development worldwide [1].

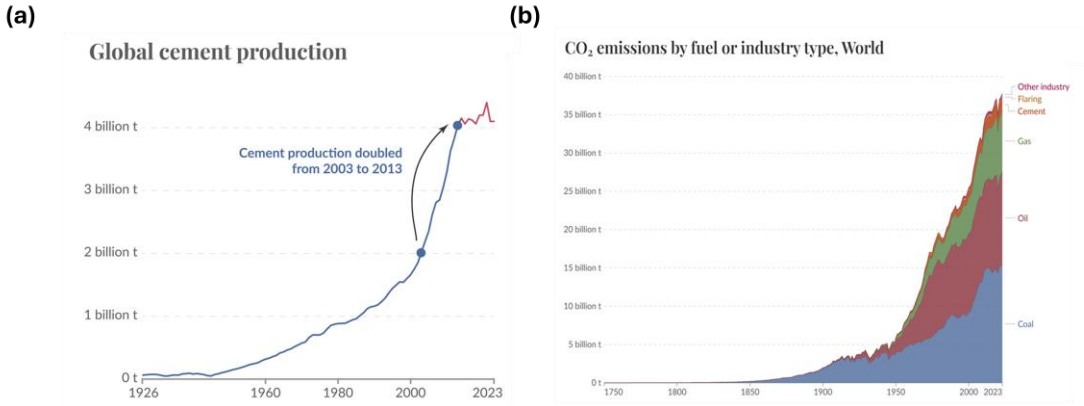

Figure 1.1 a) Global cement production (1926–2023). Source: U.S. Geological Survey, 2024 [2,3]. **(b) Annual CO_2 emissions by fuel type. Source: Global Carbon Budget (2024)** [4].

Cements are primarily characterized into two types: hydraulic and non-hydraulic cements. Hydraulic cements (OPC) are those in which anhydrous cement components react with water to

form strength-imparting hydrates, whereas the setting of non-hydraulic cements depends on carbonation reactions with CO_2 in the dry state (e.g., slaked lime or lime putty). Among these hydraulic cements are predominantly used for mortar / concrete applications. The global scale of hydraulic cement production is vast, reaching a production scale of 4.2 billion metric tons annually (see **Figure 1.1(a))** [5].

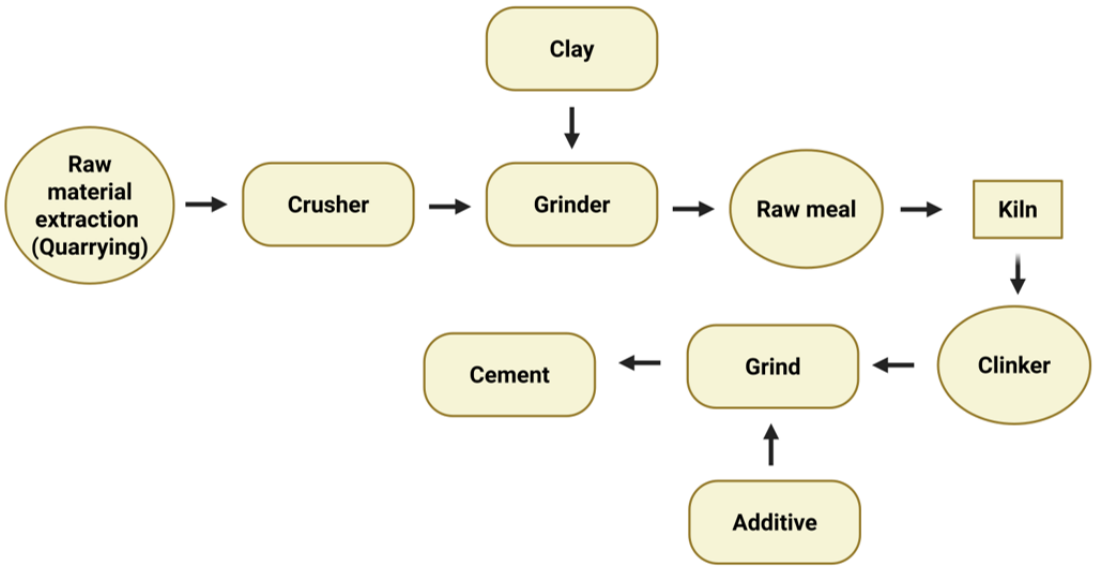

Figure 1.2 Flow sheet of cement manufacturing process.

Cement production involves calcination of limestone in rotary kilns at very high temperatures (1450°C), making its production energy intensive [6]. While cement plays a vital role in meeting the growing demands of the construction industry and contributes significantly to global economic development, its production is also a major source of GHG emissions, accounting for an estimated 7 – 8 % of global CO_2 emissions (see **Figure 1.1(b)**) [7,8]. These emissions primarily arise from the calcination of limestone (50 – 60%) and from the energy (usually burning of fossil fuels) that needs to be provided to facilitate this reaction in the rotating kiln (see **Figure 1.2** for

steps involved in cement production) [8]. In addition to this, cement production requires extensive quarrying / mining to extract limestone and clay, posing severe threat to the environment [9]. Furthermore, the particulate matter ejected into the atmosphere in addition to the GHG emissions possesses severe health hazards as well as air pollution [9].

Thus, given the scale and carbon footprint associated with the cement industry, it's imperative that we look for sustainable options that could offset or reduce the GHG emissions and curb the global warming potential (GWP) associated with building materials [10]. Advancements in low-carbon cement formulations and the use of green/sustainable materials as additives/reinforcement are crucial in paving the way towards sustainable construction practices [10].

1.2 Setting the stage: fiber cement

Fiber cement (FC) is a class of construction material that incorporates fiber into the cement matrix (inherently brittle in nature) to enhance the composite's mechanical properties, durability and to facilitate improved crack resistance. FC has been predominantly employed for non-structural applications – potential use case involves materials for – siding/cladding, roofing sheets and partition walls applications. Over the years a variety of fibers have been explored to reinforce cement. Among them fibers extracted from earth-based materials (fibrous silicate minerals, i.e., asbestos) have dominated the 20^{th} century. Asbestos, due to its low cost, abundant availability coupled with high strength, good workability and durability was long considered to be the core of FC[11]. Asbestos reinforced FC composites were fabricated using a novel technique called "Hatschek process" (named after the inventor Ludwig Hatschek in 1894). This method, inspired by paper manufacturing, deposits a slurry of cement, water and fibers onto rotating sieves, to form

thin laminae that are pressed, cured, and cut to size. [11,12]. This process was easily commercialisable and over the next few decades, dominated the FC industry. However, from the late 20th century, the production and use of asbestos fibers were restricted and eventually banned (in most countries) due to their severe health hazards (known to be carcinogenic in nature and cause severe respiratory illness), posing risk to factory workers with long term exposure [13].

1.2.1 Setting the stage: wood fiber as a green alternative to asbestos / petrochemical derived fibers in FC

The development of wood/cellulose FC composites begins in Australia in the 1940s, when James Hardie & Co. pty Ltd (now referred to as James Hardie industry Ltd) initiated efforts to replace asbestos with cellulose fibers in cement [14]. The primary reason for this drive was facilitated due to the shortage of asbestos fiber in Australia during post World War II [15] and the wide availability of high quality plantation grown softwood and hardwood species and well-established pulp and paper industry in the region [14]. Initial work focused on evaluating the mechanical performance of utilizing fibers such as bagasse, groundwood, wheat straw, brown paper and cement bags as reinforcement in cement matrix [14]. Among these brown paper (produced as a result of kraft process) as reinforcement, imparted the greatest strength to autoclaved FC composite. These initial findings were instrumental in advancing the use of chemical pulp / dissolving pulp for use as reinforcement in FC composites [14]. However, the research interest in utilizing cellulosic fibers declined and later discontinued, when asbestos supply was reinstated. Later, concerns (in terms of health of workers and environment) regarding the handling and extraction of Asbestos fiber for

FC applications led researchers to adopt natural fibers (predominantly cellulose fibers) as reinforcement [14]. Cellulose due to its wide availability, renewable nature and compatibility with cement matrix emerged as a promising replacement [16].

1.3 Wood anatomy and chemical structure

Understanding wood anatomy is critical to FC applications as it governs fiber morphology, porosity and moisture retention which are key factors influencing the rheology, hydration kinetics and mechanical reinforcement of the resulting FC composite.

1.3.1 Hierarchical structure of wood

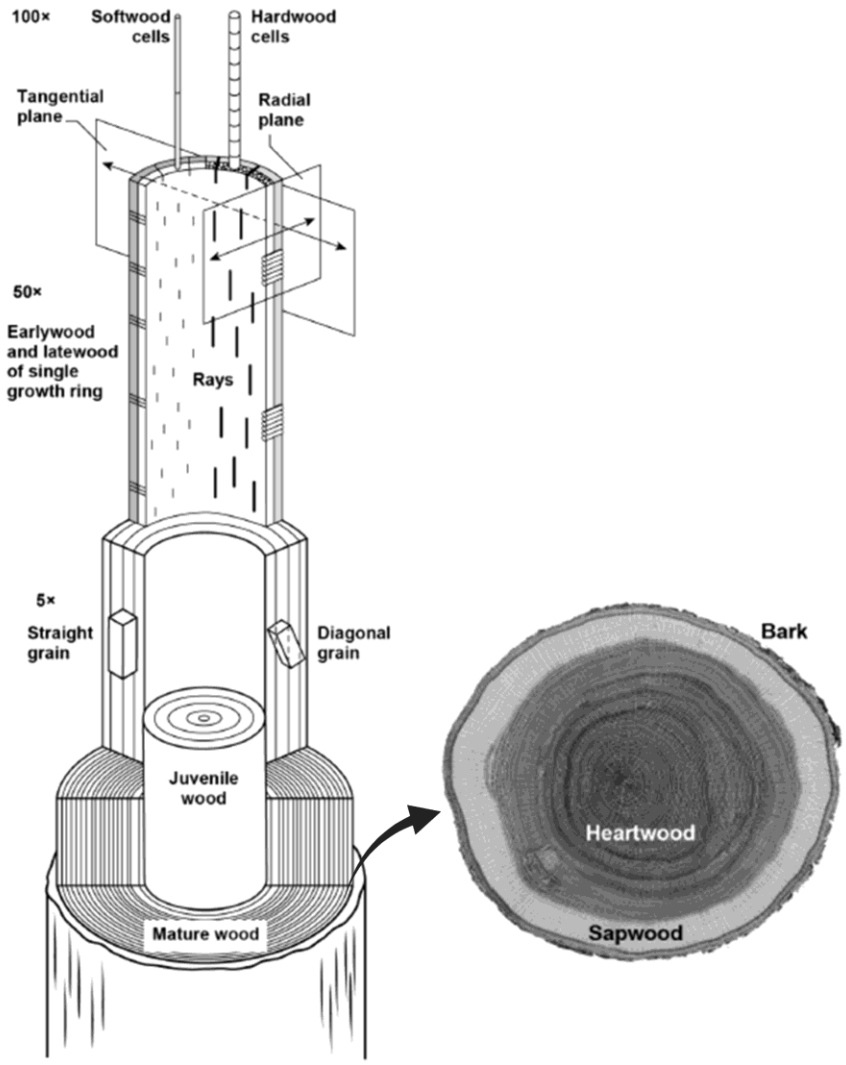

Figure 1.3 Hierarchical structure of wood under different magnification scales. Source: "Wood Handbook-Wood as an Engineering Material," U.S. Forest Service [17].

Wood is a naturally occurring, three-dimensional biopolymer composite that functions as a xylem tissue. It provides mechanical support to trees and woody plants, facilitates the transport of water and nutrients, and serves as a reservoir for various biochemicals [18]. Wood exists as a

hierarchical structure, organized in distinct layers at both the macro and microscale, ranging from cellular and tissue level organization to molecular arrangement of its primary constituent biopolymers (see **Figure 1.3**) [17,18]. At the macroscopic level, the outermost layers make up the bark and cambium, responsible for protection against biological attack/mechanical damage and growth-related functions, respectively [17]. The underlying layers is differentiated into sapwood and heartwood, which support nutrient and water transport and provide mechanical strength, respectively. [17]. The growth rings (which indicate early /late wood growth characteristics) reflect the seasonal variability in cell development and contribute to the mechanical anisotropy of wood. Additionally, wood rays enable radial transport within the structure [18].

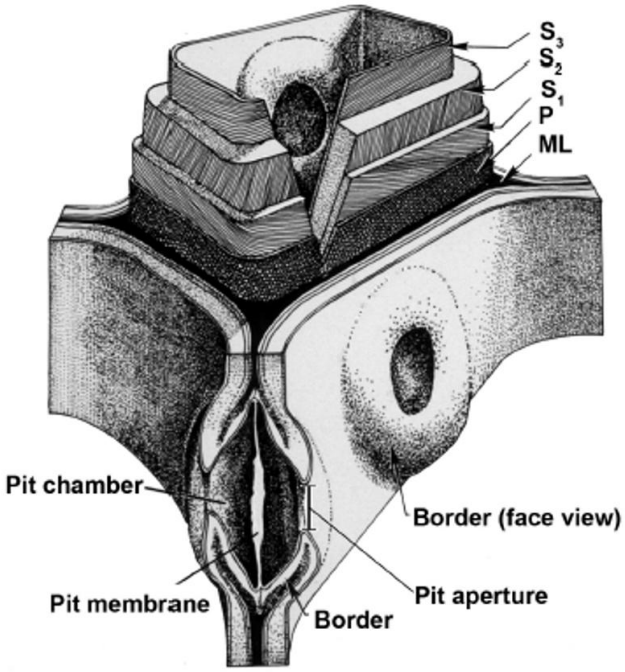

Figure 1.4 Cut-away schematic of a plant cell wall showing the middle lamella (ML), primary cell wall (P) with randomly oriented cellulose microfibrils, and the three layers of the secondary wall (S1, S2, S3) with their

respective microfibril angles. The lower portion illustrates bordered pits in sectional and face views. Source: Wood Handbook-Wood as an Engineering Material, U.S. Forest Service [17].

At the cellular level, wood is composed of elongated, tube-like cells termed as tracheids / vessels, responsible for effective water conduction, while fibers provide mechanical strength. Each cell is enclosed by multilayered cell wall, which dictates the mechanical performance of wood [17,18]. The multilayered cell is composed of three main layers: primary cell wall, secondary cell wall and the middle lamella (**Figure 1.4**) [17]. The secondary cell wall is further differentiated into three layers S1, S2 and S3 respectively (**Figure 1.4**). The S1 and S3 layers contribute to dimensional stability and resist deformation. On the other hand, S2 layer (which contains cellulose microfibrils aligned parallel to the axis of cell wall) imparts high tensile strength and stiffness and provides majority of the fiber's mechanical strength [17,18]. The middle lamella, which is rich in lignin, acts as a glue and binds the adjacent cell walls together, providing rigidity to the wood structure. This region also contains pectin, a gel-like matrix structure that facilitates cell wall adhesion and maintains water retention. At this juncture, it is important to note that hemicellulose (a branched polysaccharide) is interspersed throughout the cell wall (majorly concentrated in primary and secondary cell wall, with little or no presence in the middle lamella) and plays a crucial role in crosslinking cellulose microfibrils and stabilizing the cell wall structure [17,18].

1.3.2 Wood composition and classification

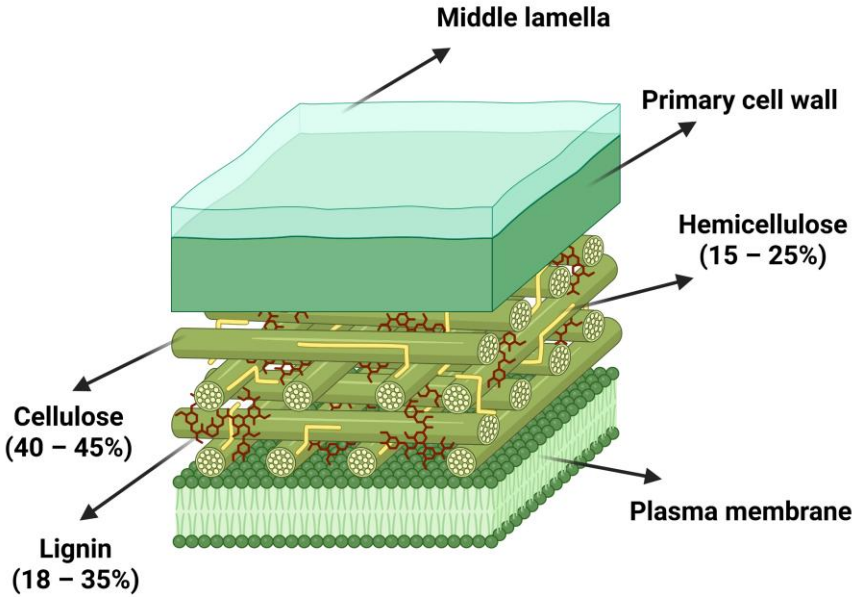

Figure 1.5 Schematic of the plant secondary cell wall showing its lignocellulosic constituents: cellulose microfibrils, hemicellulose and lignin network.

Compositionally, wood is made up of approximately 40 – 45% of cellulose and 15 – 25% of hemicellulose (**Figure 1.5**). Together, cellulose and hemicellulose, collectively termed as holocellulose, constitutes around 65-70% of the wood dry mass. In addition, wood contains 18 – 35% lignin, while the remaining fraction consists of pentosans, extractives, and inorganic components (**Figure 1.5**) [19]. In terms of elemental composition, dry wood is composed of about 50% carbon, 6% hydrogen, 44% oxygen and trace amount of inorganics [19]. This intricate architecture of cellulose, hemicellulose, lignin and other derivates at cellular level, dictates the physical properties of wood fibers, influencing their ability to reinforce materials (**Figure 1.5**). However, the composition of wood varies significantly depending on the type of wood, which is broadly classified into two main categories: softwood and hardwood (see **Figure 1.6**). Hardwood refers to wood derived

from flowering or fruit bearing plants known as angiosperms (e.g., deciduous trees such as maple and birch), whereas softwood comes from gymnosperms (for e.g., trees with needles like leaves such as pine and spruce [17,18]).

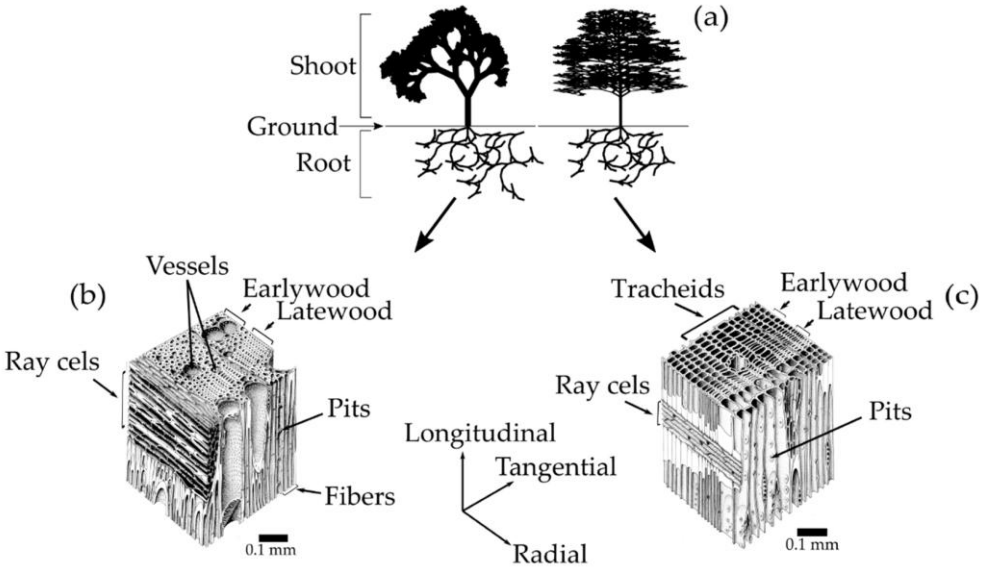

Figure 1.6 Generic representation of hardwood (left) and softwood (right) trees (a), and their corresponding cellular structures: hardwood (b) and softwood (c). The tangential, longitudinal, and radial directions indicate the three principal orientations in wood. Growth increments, or growth rings, consist of groups of cells formed over distinct time intervals. Earlywood cells develop during the initial phase of growth, whereas latewood cells form later in the season and are generally denser than earlywood [20].

At cellular level, softwood contains tracheids, serving dual role by facilitating both water/nutrient transport and mechanical reinforcement and lack vessels (**Figure 1.6(a,c)**), whereas hardwood contains vessels (for nutrient transport) and fibers for mechanical support (**Figure 1.6(a,b))**[17,18]. Due to this reason, softwood tracheids are generally longer and slender than hardwood fibers (which are short) – main reason why softwoods are preferred over hardwoods as reinforcing materials for various applications in composites. In terms of composition, softwoods

generally contain high cellulose (40 – 49%), high lignin (26 –34%) and lower pentosan (7 – 14%) content, compared to hardwood – cellulose (38 – 45%), lignin (23 – 30%) and pentosans (19 – 26%) [19]. Additionally, softwoods are known to contain higher proportions of extractives compared to hardwood species [21].

1.4 Initial advancements in wood pulp reinforced FC

Researchers R.S.P Cottus and Cambel (in association with Commonwealth Scientific and Industrial Research Organization (CSIRO) Australia) were instrumental in this shift, exploring the potential of wood derived cellulose pulp as a reinforcement for cement mortar/concrete applications. In their 1979 study, Cottus *et al*. explored how pulping techniques affects the dispersion and mechanical performance of FC composite [22]. Their analysis revealed that for 12wt.% fiber dosage, Asplund fibers (mechanical pulping) did not require slushing before integration with the pulp slurry, whereas kraft fibers (with closed lumina) required slushing (slushed fibers could be more easily incorporated into the Hatschek process, thereby making commercialization viable) which later opened the domain of utilizing refined fibers (wet refining) for FC applications [22]. In addition to this, their subsequent studies expanded on these findings and explored the effect of coupling agents and the effect of curing conditions (air curing vs autoclave curing) on composite performance [23]. For example, their studies pertaining to curing conditions revealed that different environments (air vs autoclave) can significantly alter the curing kinetics and influence the formation of hydration products, which in turn affect the mechanical properties of the hardened FC composite (it was observed that that autoclaved FC resulted in exhibiting improved flexural strength compared to air-cured FC samples [23]). The exact mechanism behind this improvement was not identified at the time, but later studies indicate that autoclave curing promotes the formation of

tobermorite – a crystalline calcium silicate hydrate (C-S-H) , typically formed at higher temperatures and pressure, and is more stable and provides better mechanical integrity to the hardened FC composites when compared to semi-crystalline or amorphous C-S-H phases formed during ambient air curing conditions [24]. With regards to the use of coupling agents, initial researchers focused specifically on using a range of commercially available titanium alkoxides containing at least two reactive alkoxide groups, which were commonly used for composite development at that time but not typically for FC applications. This was found to improve the interfacial bond between fibers and the cement matrix, contributing to enhanced stress-transfer and improved durability [25]. However, the use of coupling agents for FC applications did not gain prominence due to their increased cost, environmental concerns and meticulous processing conditions, suppressing their commercial viability. Insights from these initial research works not only advanced the fundamental understanding of the wood-pulp reinforced cement system but also led to optimizing FC fabrication process. In addition to this, their work laid a foundation for further innovations in the domain of fiber modification and fiber refining techniques [26]. In particular, wet refining / beating of pulp fibers as a preprocessing step in FC manufacturing gained traction as a method of producing highly fibrillated fiber networks, which in turn help improve the interfacial bond strength between the cement matrix and the pulp fibers, enhancing the mechanical properties of FC [27,28].

1.4.1 Synthetic fibers as a reinforcement material for FC applications

During similar timelines (late 1970s – early 1980s), researchers also explored the potential of using petrochemical derived fibers such as polypropylene (PP), Polyvinyl alcohol (PVA), Polyethylene (PE) and silica based glass fibers as reinforcements for FC composites (inspired from

their predominant use in textile and fiber reinforced composites (FRC) [29,30]). These fibers benefited from low cost (and relatively less expensive than cellulose pulp), improved chemical resistance, low density and ease of processing. However, despite these benefits, these fibers failed to succeed in the market, predominantly due to their inherent hydrophobicity [31], which limited their ability to facilitate efficient interfacial bonding within the cement matrix, crucial for load transfer, mechanical integrity and durability of FC composites. Moreover, the ban on use and production of asbestos further fueled researchers to navigate towards non-toxic, biodegradable and renewable fibers, as a result of which, pulp fibers (kraft and mechanical) became a dominant choice for non-asbestos FC composites, during the transitional phase [14].

1.4.2 Effect of pulp fibers on the mechanical performance and durability of FC

Over the years a variety of studies focused on evaluating the rheo-mechanical characteristics of utilizing chemical/dissolving pulp fiber as a reinforcement in FC composites. Fibers derived using kraft process from softwood (e.g., pine), hardwood (e.g., eucalyptus) and plant sources (e.g., sisal) and their implications on the resulting FC composites performance were investigated. Fiber dosages ranging from as low as 0.039 to high as 33 wt.% (recycled waste kraft pulp) were reported in literatures spanning applications ranging from non-structural (FC) to structural applications (concrete), with average fiber dosages ranging from 1-12 wt.%. The incorporation of kraft fibers consistently reported to have enhanced the flexural strength and fracture toughness of the FC composite, which was attributed to the ability of kraft fibers to bridge cracks thereby facilitating enhanced load transfer and delaying crack propagation.

In addition to these crucial mechanical properties, another important parameter that caught the researchers' attention was the dimensional stability of kraft pulp fibers which dictates the durability and shelf life of these FC composites. Research works from Mohr *et al*. were instrumental in this investigation, especially in understanding the durability of kraft pulp fibers in mimicking wet/dry cycles [25,32]. Their studies revealed that, after subjecting the FC to 25 wet dry cycles, significant reduction in first crack strength, peak strength, post crack toughness was observed, and they also indicated that majority of these loses occurred within the first five cycle itself [25]. They proposed a three-part degradation mechanism to address these losses (a) due to fiber-matrix debonding, (b) reprecipitation of hydration products upon cycling, and (c) due to fiber cell wall mineralization. Another important take away from this study was that unbleached fibers were less prone to degradation compared to bleached fibers upon repeated cycling. The alkaline environment present in the cement matrix could prove detrimental for the cellulosic fibers, gradually weakening their reinforcing ability, which in turn affects the mechanical property of the FC composite [25]. Unbleached fibers, contain quite a bit of lignin and other extractives in them and the alkalinity of the cement matrix, tend to attack the lignin first, followed by hemicellulose and then cellulose. On the other hand, bleached pulp, made up predominantly of cellulose, is more prone to degradation in the alkaline environment of the cement matrix – as the alkalinity attacks cellulose first (Though this effect was not well known at that time, recent research works have confirmed this degradation mechanism [33]).

In addition to wet/dry cycling, another critical environmental factor that affect the durability of the FC composites is its ability to withstand repeated freeze/thaw cycles [34]. This is particularly important in cold countries, wherein frequent freeze-thaw cycles may lead to freezing water

within the pore structure of the cement matrix, leading to the development of internal tensile stresses, which aids in the propagation of existing micro cracks and formation of new cracks [35]. It is believed that the presence of macroscopic pulp fibers in the matrix could bridge these cracking to an extent, however the exact effect of these repeated cycles on the degradation/shelf-life of this cellulosic pulp is still unknown [36].

However, the speculation is that the ice crystal formation, due to entrapped moisture present within/in the vicinity of fibers, could potentially degrade the fibers and restrain its ability to resist crack propagation [36]. Results from repeated cycling tests suggest that the mechanical properties (especially compressive strength) decreased by 50 %, when the FC is subjected to 252 freeze thaw cycles, whereas research conducted for fewer cycles (25), reported no change in mechanical properties [37]. Further research in this domain targeting concrete applications revealed that, incorporation of pulp fibers significantly improved freeze thaw resistance [34].

1.4.3 Effect of cellulose fibers on the rheology of cement paste

While mechanical integrity and environmental durability are critical for long term performance and use of FC composites, other key properties that dictate the early age workability and strength development of FC composites should not be overlooked. Rheology (Greek *rhéō*, 'flow' and *logia*, 'study of') is the investigation of the deformation and flow of matter under shear stress, crucial to the manufacturing process (i.e., Hatschek process) of FC since the ability to place (or transfer) the slurry in a facile manner could aid in reducing the processing cost and improved performance.

Cement pastes exhibit complex, time dependent rheological behaviour that evolves significantly during the early stages of hydration. This behaviour can be categorised s thixotropic or rheopectic depending on the degree of structural evolution in the paste [38]. In freshly prepared pastes, prior to the onset of substantial hydration reactions (i.e., during the dormant period), thixotropy typically dominates. Thixotropy refers to a reversible decrease in viscosity under applied shear, where the internal flocculated structure of the cement paste breaks down, allowing it to flow, and gradually rebuilds when the shear is removed, restoring a more rigid or consolidated state [39]. As hydration progresses and chemical interactions begin to dominate, the paste may transition from thixotropy to rheopectic behaviour, where viscosity increases under sustained shear due to irreversible structural evolution [40].

Another important parameter governing the flow of cement slurry is yield stress, a defining characteristic of non-Newtonian fluids like cement paste [41]. Yield stress represents the minimum stress required to initiate and sustain flow, and in cementitious systems, it is typically described using two distinct forms: static and dynamic yield stress [41]. The static yield stress refers to the stress needed to initiate flow in a resting paste, reflecting the strength of the interparticle network that develop over time due to flocculation and physical interactions. Once shear is applied and the structure breaks down, dynamic yield stress defines the minimum stress that must be applied to maintain that flow [41].

Additionally, the flow characteristics of the cement paste can affect various cement chemistries, e. g., hydration kinetics [42–44], setting time [44], drying shrinkage [45–48], curing [49–51] to name a few, other hardened state (macroscopic) properties such as flexural & compressive

strength [32,52–57] and durability of these materials [32,58]. Thus, understanding of the FC rheology is of paramount importance since addition of pulp fibers can alter the paradigm of its rheological behaviour, *vis a vis*, introduction of shear-thinning (viscosity reduces with shear strain) behaviour and yield stress [59]. The origin of such a change lies at the microscopic level, i.e., alignment/ordering of FC constituents which in turn forms a pattern or strings in a direction which is along/parallel [60,61] to the loading direction or in some cases owing to the formation of particle layers (formation of particle chains) [62]. Now, in terms of application (transferring slurry, pumping cement mortars, and 3D printing), shear thinning property is desirable since the viscosity (low/high) depends on the rate (high/low) of the applied shear.

In terms of rheological characterization, the number of studies focusing on the rheology of FC containing pulpfibers in literature is relatively low compared to broader research, focused on the rheological implications of cement mortars / cement system incorporating synthetic fibers. The influence of bleached pulp on the rheological properties of cement pastes was discussed by Nilson *et al.* [63]. They employed recycled paper and superplasticizers, observed the improvement of plastic viscosity of the cement paste (0.3 Pas for non-plasticized mortars to 1.5 Pas for plasticized mortars) with the increase in superplasticizer dosage (from 0.94 to 13.38 wt.% of cement) & MFC dosage from (1 - 3 Kg / m^3) [63].

Karimi *et al*. explored the flexibility of using milled paper pulp as a possible viscosity modifying admixtures (VMAs) in cementitious materials [64]. They employed two sets of cellulose microfibers depending upon their refining intensity, namely high energy milled paper pulp (HPP) containing fine / ultrafine aggregates with (length < 100μm to width < 50μm) and low energy milled paper pulp (LPP), mostly containing coarse aggregates (length > 200μm) which was

incorporated into the cement matrix in varied proportions (0.04 wt.% to 0.12 wt.%). Their analysis revealed that addition of HPP improved the plastic viscosity and dynamic yield stress of the slurry than the LPP, indicating that refining of fibers does improve the rheology of cementitious materials [64].

1.4.4 Effect of cellulose fibers on the hydration kinetics of FC

When cement clinker phases encounter water, a highly exothermic reaction takes place, consisting of a series of complex reactions leading to the formation of strength imparting hydrate – phenomenon collectively termed as cement hydration [65]. Cement hydration is perceived in 4 stages: first stage, known as the pre-induction period – typically occurs within first few minutes after cement clinker phases encounters water [66]. This stage is marked by the rapid dissolution of cement clinker phases, which result in the sudden release of cations and anions (such as Ca^{2+}, OH^{-}, SO_4^{2-}, Al^{3+}) in the aqueous phase [67]. This triggers an exothermic reaction, which results in the formation of a supersaturated cement pore solution and the subsequent nucleation of initial hydration products. The second stage is called the induction stage (also known as dormant period), which lasts anywhere between 1 – 3 hours. This stage is characterized by a slow reaction rate, allowing time for workability (mixing and pumping) or consolidation in a designated mold or structure. The next stage in cement hydration is called the acceleration phase, where the predominant cement clinker phases (i.e., C_3S) react to form a semicrystalline C-S-H gel along with portlandite (Calcium hydroxide) and calcite (calcium carbonate). At this stage, C_3A reacts with gypsum (which is added into the cement mix) to form ettringite which controls the setting time an prevent early age cracking [67]. This stage is accompanied by a rapid increase in temperature (measured through ITC analysis) and this results in the formation of a solid matrix framework, which drastically reduces

fluidity. After this phase, the hydration slows down and enters a diffusion-controlled regime. During this period, the hydration products encompass unhydrated cement grains, there by limiting their water accessibility. At this period, C_2S hydration dominates, contributing to long term strength development and durability. Additionally, the ettringite formed may convert into monosulphates, if gypsum get depleted [68]. This stage is marked by pore refinement and matrix densification, which is an integral part of strength development.

1.5 Climate change, SDGs, and its impact on FC

Growing human population has led to a rapid rise in infrastructure development, placing increasing demand on construction materials and natural resources. This surge directly contributes to GHG emissions and environmental degradation, leading to climate change [69]. According to UN, Climate change refers to "long-term shifts in the temperatures and weather patterns, primarily caused by human activities, especially the burning of fossil fuels that release GHGs" [69]. As mentioned in the previous sections of literature review, in the context of FC, cement production is a major contributor to global CO_2 emissions. Moreover, to tackle FC formulation challenges, often petrochemical/silica-based additives/ cement admixtures are employed, which are conventionally sourced as byproduct of petrochemical industries or extracted via quarrying, raising environmental concerns.

To tackle this, UN has emphasized the importance of sustainable infrastructure through several SDGs [70], particularly SDG 9 (Industry, innovation and infrastructure), SDG 11 (sustainable cities and communities) and SDG 13 (climate action) – which iterates the need for development / utilizing low-carbon construction materials for a sustainable future [70].

1.5.1 Possible decarbonization pathway in FC: capitalizing the opportunity for developing low-carbon footprint construction materials

To advance sustainability and to curb emissions related to the fabrication and use of FC, two key strategies have emerged and researched about in literature : fiber/additive modification and matrix modification. The first strategy involves transitioning from the use of conventionally employed synthetic fibers and petrochemical/silica based additives to green and sustainable alternatives to facilitate various role that aid the FC processing whilst enhancing its performance. The second strategy, on the other hand primarily focuses on reducing the GWP impact related to cement production, by partially replacing cement with low-carbon SCMs (such as FA, GBFS, MK, SF or more recently processed was biomasses such as BC) or by complete transition into geopolymer system (which is devoid of OPC and uses aluminosilicate binders in conjunction with alkaline activators to initiate geopolymerization process).

Together these two complementary strategies offer a strategic and promising approach to decarbonization pathways for the development of low carbon cementitious composites –boosting material innovation whilst combating climate change and enhancing sustainability.

1.6 Roles of additives in FC

In FC composites, additives play a critical role in addressing challenges related to workability (rheological behaviour), curing kinetics/ strength development (hydration kinetics and mechanical properties) and long-term durability. Additives are employed at the processing / fabrication stage to tweak both wet state and dry / hardened state properties of the resulting FC composite.

In case of FC containing pulp fibers, often it is difficult to incorporate high aspect ratio fibers (improves flexural strength) without jeopardizing the mixed consistency of the cement paste. Now this can be attributed to the hydrophilic nature of cellulosic fibers, that reduces the overall water / cement ratio, effectively reducing the free water that is available in the FC slurry during mixing, eventually leading to poor fiber dispersion. In addition to this, fibers due to their surface charges and Van der Waals forces tend to flocculate in cement pore solution, leading to formation of clumps or agglomerates. Moreover, the process of FC mixing can result in possible entanglement (due to possible hinging/bending/stretching of fibers), which can again hamper the workability of the FC slurry. To negate this, FC industries often employ additives, such as VMAs, which are water soluble admixtures (semi-synthetic, synthetic, or natural elements) that alter the rheological behaviour as well as influence other phenomena such as hydration and setting time, and impact key physicochemical properties including porosity and mechanical performance in the hardened state. [71–73]. As such, a broad range of polymeric VMAs, also known as superplasticizer, has been developed in the past few decades, and in FC industry, it is the PCEs based superplasticizer that has found success in finding the balance between rheology, micromechanics, and cement chemistry. Indeed, PCEs is derived from petrochemicals, thus, to reduce the carbon dioxide foot-print, the current research trend is shifting into biobased superplasticizers, i.e., functionalized lig-nin (PCEs-class). To that end, interest in nanocellulose has also gathered momentum to tune the rheological characteristic of cement paste, cement mortar, and FC slurry.

1.7 Cellulosic biomaterial as an additive for cementitious system (mortar, concrete, FC)

1.7.1 Cellulose: structure and classification

Cellulose is the most abundant renewable material found in the biosphere. Cellulose is widely present in plants, animals and to a lower extent in algae, fungi and amoeba. As mentioned in the previous literature review section, cellulose is a fibrous, water insoluble material that provides structural support to plant cell walls. Cellulose was first discovered and isolated by French chemist Anselme Payen in 1838 [74]. This marked the beginning of understanding cellulose as a structural material in plants and laid the foundation for its use in various industries such as textiles, paper and bioplastics. Irrespective of the source from which cellulose was isolated, cellulose can be characterized by a high molecular weight, amphiphilic homopolymer comprising of repeating units of β-1,4-linked anhydro-D-glucose, in which every unit is rotated 180° relative to its neighboring unit (note that the basic structural repeating units of cellulose is cellobiose rather than glucose) [75,76]. This linear arrangement allows for extensive intra/inter molecular hydrogen bonding, contribute to cellulose's high tensile strength and resistance to enzymatic degradation. Based on the source, processing method and structure, cellulose can be classified into many forms/polymorphs. The most common naturally occurring form of cellulose is referred to as cellulose I. Cellulose I can be further characterized based on its two allomorphs: cellulose Iα (produced by microbes, triclinic lattice arrangement) and cellulose Iβ (present in higher plants, monoclinic lattice structure) characterized by parallel cellulose strands [16]. Furthermore, cellulose I can exist in different polymorphs – Cellulose II, produced upon chemical treatment or regeneration, cellulose transforms into cellulose II, marked by its antiparallel chain configuration and greater thermody-

namic stability [77]. Further chemical modifications can yield cellulose III (amine/ammonia treatment) [78] and cellulose IV (heating cellulose III) [79]. However, these polymorphs are less commonly produced and used due to their lower crystallinity [79].

1.7.2 Processed/purified cellulose

Cellulose can further be classified based on the nature and extent of its processing/structural refinement as well as from its purity. Processed forms of cellulose such as alpha cellulose, microcrystalline cellulose and cellulose nanocrystals – offers high purity, and its physicochemical characteristics allows them to be widely used across various industries ranging from pharmaceuticals to construction industry [80]. These cellulosic biomaterials are highly versatile –facilitating various functions by serving as binders, thickeners, reinforcing materials or as rheology modifier [80].

1.7.2.1 Alpha cellulose (AC)

Alpha cellulose is the richest and purest form of cellulose, which is extracted from plant material like wood pulp or cotton. It is a white powdery substance, which is insoluble and has the highest degree of polymerization (compared to MCC and CNCs). The extraction of AC involves subjecting the lignocellulosic biomass (such as pulp / cotton) to alkaline treatment (using 17.5% sodium hydroxide solution at elevated temperatures [81]. The purpose of this step is to dissolve the soluble fraction of cellulose (i.e., beta and gamma cellulose), leaving behind the insoluble fraction (i.e., AC) [81]. AC is then filtered, washed thoroughly and dried, followed by bleaching step, involving agents such as hydrogen peroxide or chlorine chloride to obtain better purity and

brightness. Typical applications of AC include its use as a bulking agent in pharmaceuticals formulations/food industry [82]. Morphologically, AC is characterized by microfibrillar networks which are tightly packed together, giving it a rigid morphology [82]. The fibers are usually long and thick with high aspect ratio and typically appear coarse and irregular, reflecting its minimal refinement compared to processed cellulose derivatives (such as MCC/CNCs) [82]. Moreover, due to the presence of both crystalline and amorphous region, AC typically has lower crystallinity (crystallinity index (*CI*) in the rage of 65 – 70%) compared to other processed derivatives [82]. In addition to this AC often serves as a starting material to produce highly crystalline micro/nano crystalline biomaterials.

1.7.2.2 Microcrystalline cellulose (MCC)

MCC is purified, partially depolymerized type of cellulose, often derived from AC through mild acid hydrolysis process [83]. This process selectively isolates/removes the amorphous regions of the cellulose structure, retaining the crystalline part – responsible for MCCs higher degree of crystallinity [84]. Typically, MCC are extracted via hydrochloric acid hydrolysis, where the starting cellulosic biomaterial is treated with a controlled concentration of HCL (usually around 2 -2.5 M at temperatures ranging from 60° - 105°C) for 15 – 2 hours, depending upon the desired degree of depolymerization [85–88]. After this, the reaction is quenched, washed, charge neutralized and dried to obtain white powdery substance. Typical applications include use as binders/texturizer/stabilizer in applications ranging from cosmetics, pharmaceuticals, food industry to construction sectors [89]. Morphologically, MCC is characterized by short, rod-like or irregularly shaped granular particles. These particles are generally fragmented from cellulosic precursor (such as AC) through acid hydrolysis, as a result MCC appears to be more compact comprising of granular micro

particles (with rough surface containing minimal functional groups) with typical particle sizes in the range of 50 – 70 μm [82]. Additionally, since most of the amorphous region has been isolates, MCC generally exhibit higher crystallinity (with reported '*CI'*, in that range of 75 – 80 %) [82].

1.7.2.3 Cellulose nanocrystals (CNCs)

CNCs are the highest refined form of cellulose (isolated down to nanoscale crystalline regions with most of the amorphous regions removed – this is marked by its high crystallinity, with typical 'CI' in the range of 80% [90]). CNCs are extracted via acid hydrolysis (typically extracted via sulfuric acid hydrolysis, where starting cellulosic material is treated with concentrated sulfuric acid, typically 55-65wt.% at temperatures ranging from 40° to 60°C for 30 to 90 minutes. These conditions preferentially hydrolyze amorphous cellulose regions, while preserving the crystalline regions. In addition to this, the process of hydrolysis also imparts surface functional groups onto the CNCs surface (sulfate ester groups in this case – since sulfuric acid was employed) introducing negative surface charge – enhancing their colloidal stability in water [91]. Morphologically, CNCs is characterized by rod shaped (or whisker shaped morphology), with high aspect ratios with length ranging from approximately 100-300 nm and diameter ranging from 3 to 10 nm.[90] This rod like morphology contributes to their excellent mechanical strength and stiffness (100 -160 GPa [90,92]), with its nanoscale dimensions impart high surface area. In addition to this, the added advantage of CNCs over the other processed crystalline cellulosic derivatives is their ease of surface chemical modifications. The availability of abundant CNCs can be readily functionalized through various chemical modifications such as (esterification, oxidation, grafting or silanization) - making it a versatile nanoscale substance [90,93]. These properties enable CNCs to be employed

in a wide range of applications involving structural composites, cementitious materials, packaging materials, rheology modifiers, drug delivery etc. [90,93].

1.8 Role of processed/purified cellulosic biomaterials on the performance of cementitious system

Based on the source, extraction techniques and the solvent employed, cellulosic biomaterials can facilitate multifunctional roles, when employed as an additive in cementitious system. This section highlights some of the recent advances, employing cellulosic biomaterials as additive in cement/concrete applications. Note that the number of studies involving the use of MCC and AC is some what limited compared to the extensive research available on CNCs. Therefore, this literature review (*Vide infra*) primarily focuses on the effects of CNCs in various cementitious systems.

1.8.1 Rheology

The positive impact of the macro-sized cellulosic fibers on cement rheology further inspired more research activities involving the nano-sized cellulosic materials, i.e., CNCs. The rheological properties of cellulose nanomaterials (reinforcement) in cementitious materials (cement paste) were first reported by Cao *et al*. focusing on the understanding of how the shear stress of the cement paste varies as a function of CNCs content (0 – 3.5 vol%) [57]. Notably, at fixed w/c of 0.35, at low CNCs content (i.e., <0.3 vol%), the yield stress was reduced and reached a minimum of 15 Pa (at 0.04 vol%) and thereafter increased (reaching a maximum of 600 Pa at 0.15 Vol% of CNCs concentration) as the concentration of CNCs increased[57]. They attributed this reduction in shear stress due to a phenomenon called steric stabilization [94] - a well-known mech-

anism observed in water reducing admixtures (WRAs) such as poly(carboxylate) based superplasticizer [57,94]. On the other hand, the increase in shear stress observed by Cao *et al*. (when the CNCs concentration was increased beyond 0.3 %) is attributed to the CNCs agglomeration effect [27] in fresh cement paste pore solution [57,62,95]. This could be vital because the excess CNCs could act as defects or stress concentrators which could be detrimental to the resulting mechanical properties of the cementitious materials [57,95]. In order to negate this problem Cao *et al.* in their subsequent research, proposed tip ultrasonication [96] as a processing technique that could be employed to disperse CNCs more uniformly in the cement matrix [96]. Their rheological studies indicated that, when CNCs concentration increased above 0.18 vol % in the pore solution, agglomeration starts to develop which increases the yield stress, and employing tip sonication would result in better dispersion and increase in mechanical properties to over 50% [96].

Studies by researchers [57,96,97] employed CNCs from the same source and tested only a fixed w/c ratio of 0.35., To gain a broader perspective regarding the influence and physical properties of CNCs on the w/c ratio, Montes *et al*. utilised three different w/c ratios (0.30, 0.35,0.40). Their results revealed a reduction in yield stress as the CNCs content and w/c ratio increased [98]. This suggest that a higher w/c ratio can accommodate a greater amount of CNCs (acting as VMAs) in the cement matrix, before the excess CNCs start to increase the yield stress (due to agglomeration effect). At lower dosages, CNCs primarily functions as WRAs [98]. When the CNCs concentration is less, the particles remain dispersed and mobile, lacking the critical concentration needed for alignment or network formation. As a result, the shear-thinning behaviour becomes less pronounced at lower CNCs dosages.[98].

1.8.2 Hydration kinetics

When cement encounters water, an exothermic reaction occurs between the cement clinker phases (e.g., calcium silicate/aluminate) and water, which can be monitored via ITC experiments, which measure the heat released as a function of reaction time (expressed in hours). In the recent literature [99,100], it was shown that hydration kinetics is affected by the pulp fibers and/or a variety of nanocellulose (additive). However, one of the major limiting factors in FC is that there is a retardation effect on hydration by the non-crystalline saccharides (additives). Kochova *et al*. reported that the incorporation of lignocellulosic fibers in cementitious system can significantly retard (up to 48 hours) OPC hydration [99]. This really iterates the importance of moving towards more crystalline cellulose based additives in FC [100]. Since not much studies have been conducted on the effect of pulp fibers, AC & MCC on the hydration kinetics, this literature review focuses on summarizing the research done in terms of understanding the hydration kinetics of utilising CNCs in FC. The hydration behaviour of CNCs-reinforced cement paste was studied by Cao *et al*. and the ITC test indicated that the peak heat flow was delayed with the addition of CNCs. In contrast, the degree of hydration (DOH) at a given age (e.g., 7 day) is increased [57]. Similar conclusions were obtained by Flores *et al*. who indicated that even if the size of CNCs used is larger than that used by Cao *et al*. [57] the overall trend in the hydration heat is similar to each other, and CNCs were observed to delay cement hydration at an early age but improve the hydration at a later age. Besides, Ghahari *et al*. indicated that the use of 0.2% and 1% CNCs by volume of cement paste could extend the dormant period of cement hydration that is indicative of the delayed hydration but increase the hydration heat that is indicative of the increased degree of hydration [101].

The delaying effect on the cement hydration (specifically the initiation of hydration) is mainly because CNCs adhere to cement particles and block the cement particles from reacting with water. The increased degree of hydration (DOH) at a given age can be attributed to two possible reasons [57]. One reason is the steric stabilization effect, which is commonly observed in some WRAs, by which CNCs can disperse cement particles more uniformly and thus enhance the reaction efficiency with water. However, the degree of hydration analysis on cement pastes with WRAs indicates that the steric stabilization does not improve the DOH significantly, which indicates that the steric stabilization may not be the dominant reason. The other reason was attributed to a mechanism referred to as short circuit diffusion (SCD). For plain cement pastes, during cement hydration, the hydration products can form a shell around the unhydrated cement particles, which can prevent water from diffusing into the interior unhydrated cement particles and thus slow down the hydration rate. However, for cement pastes with CNCs, the CNCs initially adhere to cement particles and remain inside the hydrated product shell as the hydration progresses. The CNCs can provide some channels for water transportation through hydration products to inner unhydrated cement particles, which can further improve cement hydration. Moreover, the short circuit diffusion mechanism is confirmed to be more dominant than the steric stabilization mechanism in these systems. Furthermore, CNCs from various raw material sources and processing techniques can affect cement hydration differently when cement type varies. Fu *et al*. applied nine different CNCs to cement pastes made using type I/II cement and type V cement, respectively [95]. One important finding was that, although all CNCs increased the degree of hydration at a given age, CNCs produced via transition metal-catalyzed oxidation were particularly effective in enhancing hydration heat release, regardless of the cement type. Another key observation from ITC test was that, at early ages, the retardation effect (i.e., a delay in the time to reach peak heat flow) was more

pronounced in type V cement paste than in type I/II cement paste. However, the total heat release in type V cement paste was greater. This may be attributed to the relatively higher aluminate phase content in the type I/II cement. Hydrated tricalcium aluminate (C_3A) phases (ettringite and monosulfate) tend to adsorb more CNCs than other hydrated phases, leaving fewer CNCs available to interact with silicate phases in the Type I/II cement paste. This leads to a reduced retardation effect on cement hydration. Meanwhile, fewer CNCs on cement particle surfaces reduce the potential for the short-circuit diffusion (SCD) effect, resulting in a lower degree of hydration at a given age. These results suggest that the effectiveness of CNCs is closely tied to the C_3A content in the cement.

1.8.3 Mechanical properties

The strength of a FC composite is critical, as it dictates the type of application to which the cement composite can be employed (structural / non-structural). Over the past couple of decades, extensive research has focused on using pulp fibers as reinforcement in cementitious composites. Key parameters such as pulping techniques [102,103], fiber surface treatment [104], bleaching effects [105], fiber morphology [106], fiber moisture content [107], fiber orientation [108] and fiber durability (wet/dry & freeze thaw cycles) [25,109] have been investigated for their influence on mechanical performance, particularly flexural strength. These studies collectively indicate that pulp fibers represent a promising, sustainable alternative to petrochemical-derived fibers for reinforcing FC.

Recent years have seen the use of CNCs as an additive in cement systems. First, a modest dosage of CNCs (e.g., 0.2% by weight of cement) can improve the mechanical properties, whereas a high dosage of CNCs can result in negative effects [57,101,110–114]. The improvement in the

mechanical properties of cementitious materials at low dosages of CNCs can be attributed to the increased degree of hydration at a given age. Cao *et al*. examined the relationship between the flexural strengths and DOH. Results revealed that, at low CNCs dosages, the flexural strength increased linearly as a function of DOH [57], suggesting that the observed improvement in mechanical properties can be closely related to the increase in DOH. Moreover, by comparing these results with conventional WRAs, Cao *et al*. demonstrated that, CNCs were more effective in improving the flexural strength than WRAs [57]. Since hydration analysis showed that steric stabilization is not the primary mechanism driving the increased degree of hydration, WRAs alone cannot enhance flexural strength solely through steric effects. Furthermore, Cao *et al*. highlighted the potential of CNCs to combat microcracking could contribute to improved mechanical performance in cementitious composites [115]. At high dosages of CNCs, the reduction in the mechanical performance can be attributed to the aggregation of CNCs, that can act as stress concentrators, eventually compromising the structural integrity of the FC [57].

1.9 Cement replacement strategies and matrix modification

The second strategy widely employed to decarbonize the CO_2 emission related to cement production involves modifying the binder matrix to partially or completely replace OPC. This is often facilitated by incorporating supplementary cementitious material as a partial substitute / matrix modifier, that enhances the pozzolanic activity, while reducing its GWP impact.

1.9.1 Low carbon cement blends: SCMs

Conventional SCMs belong to the class of silicate or aluminosilicate, namely metakaolin (MK), silica fume (SF), fly ash (FA - class c/f), granulated blast furnace slag (GBFS) to name a

few, and these materials rely on the presence of silica and alumina in them, which react with portlandite (produced as a result of OPC hydration – note that these SCMs are substituted in proportions to replace cement) to form additional C-S-H and Calcium aluminate hydrate (C-A-H) phases, improving strength and durability [116]. Despite these improvements w.r.t to improved strength and durability, a major issue related to these SCMs is the supply chain constraints [117–119]. For instance, the availability of FA (produced as a byproduct of coal-fired power plants) is declining due to the global shift in moving towards more sustainable and renewable energy-based power generation (especially in economically developed countries) [117,118]. Another example would be that of GBFS (produced as a byproduct from the steel industry) – whose sourcing and production is highly regionally depended /constraint (due to raw material availability, energy demand, industrial infrastructure, environmental and economic regulations and government policies) [117,119]. Additionally, these SCMs exhibit batch to batch variations in both composition / purity – thereby making their standardization difficult – affecting the reliability and performance of the resulting cementitious material. Moreover, certain pozzolans can increase curing time, reduce workability (increasing the water demand) and require optimum formulations to achieve the desired performance, making it difficult to set universal standard or establish consistent regulations [120].

Among these SCMs, MK offers a unique advantage, due to its high pozzolanic activity and ensuring consistent/ reliable quality from batch to batch [121]. This is because, unlike other SCMs, produced as a byproduct of fossil fuel and steel industry, MK is produced by controlled calcination of kaolinite clay (at temperatures significantly lower than clinker production) – thereby produced

with predictable and uniform properties/composition. When supplemented with cement, the resulting cementitious material exhibit improved strength and durability, primarily due to its ability to refine the microstructure, provide chemical resistance (sulfate attacks and low chloride ion permeability) and mitigate efflorescence (white powdery crystalline deposit found on the surface of the cementitious material– typically formed due to the leaching of calcium hydroxide from the cementitious material and its subsequent reaction with CO_2 to form calcium carbonate) by binding free calcium hydroxide in the presence of moisture [121]. However, one of the limitations of MK, compared with other SCMs is its relatively increased GWP (due to the energy demand / environmental implications related to open pit mining (for kaolinite extraction) and calcination) [122]. Despite these limitations, MK is still widely used and is the most preferred choice of binder material/ precursor for alkali activated materials (AAM) and geopolymer systems as its benefit outweighs its drawback [123].

On the other hand, biogenic SCMs have gained a lot of interests, such as the use of effective microorganisms as fillers and cement supplement [124] and biogenic SF [125]. However, microbial based SCMs, struggle with survival challenges of microbes in harsh alkaline environment present in cement matrix [124], while variability of silica content arising from different biogenic sources leads to workability issues and poor mechanical strength in biogenic silica supplemented cement composites [125]. Likewise, waste biomasses, like spent coffee grounds (SCGs) were also reported as the key component of the cement admixture [126]. Although, this proved to be an efficient way to valorise these waste biomass sources which other wise needs to be landfilled, the mechanical properties were severely compromised due to the compatibility issues between inorganic cement matrix and organic-heavy coffee grounds [127].

Over the last decade, BC – as a biogenic material has gained interest for various applications, such as the development of "eco-friendly" structural building materials [128]. In fact, in 2018, the Intergovernmental panel of climate change (IPCC) recognized the use of BC as a promising carbon negative emission technology [129]. BC is a carbon rich solid-waste, co-produced during the biomass-bioenergy generation process via controlled pyrolysis (300−700 °C, little or no oxygen). More details on this are mentioned in the European BC Certificate guidelines [130].

Its amorphous carbon structure results in low H/C (Hydrogen to Carbon) and O/C (Oxygen to Carbon) ratios, which is also observed for soot, carbon black (graphite-like material), to name a few [131]. These ratios indicate chemical stability (i.e., high pH) and relatively higher degree of carbonization [131]. The chemical structure of BC consists of 6-membered aromatic ring with various polar functional groups, like carboxyl, carbonyl, quinone, and lactone, etc. [132]. It is classified as an alkaline material owing to the presence of carbonates (salts of bicarbonate and carbonate), inorganic alkalis (oxides, hydroxides, sulfates, etc.) in addition with soluble and structural organic groups [133]. But understanding and quantification of its alkalinity remain an active area of research [133]. Overall, the chemical composition and physical properties of biomass depend on the biomass type and pyrolysis process parameters [134]. Nonetheless, as a carbon dioxide sequestering material, it offers a pathway to permanently remove CO_2 from the atmosphere by retaining its chemical form. In addition to this, conversion of biomass to BC also serves as effective valorization techniques for these waste biomasses, which otherwise needs to be landfilled (methane emissions during organic decomposition of waste biomasses contributes to GWP [135]). Moreover, it is estimated that the use of BC technology can eliminate up to approximately 1.7 –

3.7 PgCO2-eq of CO_2 [136] from the atmosphere –highlighting the immense potential of utilizing BC in various applications to mitigate climate change.

Beyond carbon sequestration potential, BC has been reported as a SCMs for cement mortar/concrete application and its influence over rheology, cement hydration and mechanical properties to its — attributed to its distinctive pore structure (also topology), surface chemistry and morphology (literature review, *vide infra*).

1.9.2 Effect of BC on the rheo-mechanical performance of FC

In the case of FC, the materials chemistry of BC (particles size, chemical composition and pH) can play a crucial beyond green chemistry, such as improving hydration kinetics and modifying the rheo-mechanical properties. To date, the majority of BC applications as SCMs have focused on cement mortar and ultra-high-performance concrete. One of the noticeable effects of using BC as SCMs is that organic residues in biomass are converted into amorphous carbon (low H/C and O/C), which can delay cement hydration. This retardation extends handling time of the FC slurry and helps maintain workability, both of which are critical for achieving optimal mechanical performance in the final composite.

In a recent report from Roychand *et al*., it was found that BC from spent coffee grounds improved the compatibility between the cement matrix and the biogenic SCMs [127]. Dixit *et al*. explored the particle size effect of BC and examined its dual roles, acting as an internal curing agent and SCMs [137]. Note that manually ground BC was first presoaked in water prior to composite fabrication. Notably, at 5wt.% of finer (< 250 μm) BC particles, cement hydration was ac-

celerated, and higher heat release was observed compared to coarser (>250 μm) ones. It was speculated that finer BC particles could adhere to the positively charged clinker phases owing to higher surface area, creating more nucleation points and thereby accelerating hydration. Furthermore, Gupta *et al*. [138] reported the particle size of BC plays a pivotal role in tuning the rheology (i.e., static yield stress) of cement paste using a ball milling (BM) method [138]. Interestingly, coarser BC particles (avg. particles size ≈ 45 – 50 μm & 2 vol.% addition) increased the static yield stress by 1.8 – 2.7 times compared with BM (avg. particles size: 10 – 18 μm).

In two separate studies by Choi *et al*. [139] and Gupta *et al*. [140], incorporation of BC at 5 wt.% (biomass sources: switchgrass, curing 28 days), and 2 vol.% (biomass sources: locally collected sawdust, curing: 7 days), resulted in compressive strength improvements of 10% and 40%, respectively. However, for non-structural application, Restuccia and Ferro [141] reported that at 0.8 wt.%, flexural strength of the cement mortar (curing: 28 days) increased by 30% [141]. Similar results were obtained by Kushmood *et al.,* at 0.2 & 0.080 wt.%, flexural strength (curing: 28 days) improved by 83% and 80%, respectively [142]. Regarding durability, Sirico *et al*. [128] evaluated the effect of wood waste derived BC on wet/dry strength of concrete – 5 wt.% addition contributed to 30% increase in compressive strength.

To surmise the literature review section, the effect of BC on cement hydration is evident, but the exact mechanism remains unknown. Particle size reduction of BC renders benefits, such as improving compatibility with cement. Regardless of the biomass source, mechanical strength is generally retained or improved. However, none of the reports convey its role in the presence of fiber reinforcement.

1.9.3 AAM

AAMs are a class of binders produced by activating aluminosilicate rich precursor (such as FA, GBFS or MK) with alkaline solutions to replace OPC as the primary binder. The idea of exploring AAM was first investigated by Victor Glukhovsky in 1957 – inspired from the ancient Roman and Egyptian construction [143]. He found that, strength imparting compounds in these construction materials were based on amorphous aluminosilicate calcium hydrate (similar to C-S-H phases formed during OPC hydration) for strength development along with crystalline analcite phases (a specific type of zeolite) which explained durability [143]. Considering these findings as a baseline, he further went on to develop a new class of binder termed as "soil-cement", in which aluminosilicate precursor was combined with alkali rich industrial waste to make AAM (so called soil cement) [143,144]. While the initial motivation for the development of AAM was to valorise industrial waste by-products (such as FA, GBFS, rice husk ash, which were produced in large quantities), recent years have seen a rapid interest in utilizing these materials as OPC replacement to curb the CO_2 emissions related to OPC production.

AAM are broadly classified into two types : (a) High calcium based systems [145,146]: which comprises of aluminosilicate precursors with high calcium oxide content (>10%) such as GBFS, class C FA, to name a few. They are employed in moderately alkaline conditions to from calcium aluminosilicate hydrate (C-A-S-H) gel – and the resulting AAM are known for its faster setting time and early strength development (which is proportional to calcium content in the precursor). (b) Low calcium bases system [145,146] – which utilises aluminosilicate precursor containing relatively lower levels of CaO content (<10 %), (for e.g., MK or class F FA). The final

reaction product of this system is a stable three dimensional inorganic sodium aluminosilicate hydrate (N-A-S-H) gel. These AAM are classified by their longer setting time / prolonged strength development are often referred to as geopolymer systems.

At this juncture it is important to note that, not all AAM are geopolymer but all geopolymers can be classified as AAM. The primary difference lies in the CaO content in the aluminosilicate precursor followed by the difference in their reaction products. AAM hydration product is a monomer precipitate (similar to OPC hydration product) whereas geopolymer reaction product is characterized a true polymer. Additionally, another class of AAM exist known as the hybrid or blended systems where in AAM precursors are blended with OPC clinker to form N-A-S-H and C-A-S-H reaction products [147]. However, this thesis is primarily focused on low calcium AAM or geopolymer system due to the following reasons.

On of the major goal of this thesis to utilize low carbon binder material in FC. As the name suggests, high calcium systems often require precursors that are produced as a result of CO_2 intensive proses (for e.g., BFS is produced as by product of steel industry). Whereas geopolymer systems often employ precursors whose production processes are less carbon intensive (for e.g., MK, FA etc.). Additionally, hybrid system is still dependent on OPC systems, thereby suppressing their sustainability characteristics. Moreover, Low calcium systems, allows the valorization of large quantity of waste materials such as class F FA / calcined clays – aligning with circular economy principles. In addition to the sustainability aspect, geopolymer systems are known to exhibit better chemical/thermal stability and reduced efflorescence compared to high calcium systems (this is because C-A-S-H is more prone to carbonation, acid attack and leaching compared to N-A-S-H reaction product) [147].

In literature disparity still exists in terming systems as AAM / geopolymer systems. For instance, many studies in literature have termed alkali activated BFS system as geopolymer (despite BFS is rich is calcium content and the reaction product is C-A-S-H instead of N-A-S-H).

Therefore, these systems are often misrepresented in literature, deviating from its true definition. Considering these factors, this follows the strict convention of using well defined textbook definition to distinguish between AAM/geopolymer system [148].

1.9.4 Geopolymer binders

Geopolymer, termed coined by French material scientist Joseph Davidovits, refers to inorganic polymer binder developed through the reaction between aluminosilicate materials (source material / binder) and alkali hydroxides and / or soluble silicates [149,150]. This material is known to exhibit superior mechanical strength, durability and high strength to weight (S/W) ratio, compered to OPC counterparts [151,152]. The geopolymerization reaction involves the dissolution of aluminosilicate precursor upon contact with the alkaline activators, which result in the formation of oligomers that undergo polycondensation reaction to form a stable three dimensional framework, namely, polysialate (– Si – O – Al – O), polysialte-siloxo (– Si – O – Al – O – Si – O), polysialate-disiloxo (– Si – O – Al – O – Si – O – Si – O) [149,153,154]. Beyond exceptional mechanical performance, the formation of geopolymer precursors involve much lesser CO_2 emissions compart to manufacturing of cement clinker phases. Commonly used source/ binder materials include industrial and waste/by products such as FA, SF, coconut/rice husk (depending on the calcium content) ash. In addition to this Kaolinite clays are calcined to form MK (high is highly reactive) and is often employed as a geopolymer precursor.

In terms of alkaline activators used to initiate geopolymerization reaction, typically consist of sodium hydroxide (NaOH), Sodium silicate (Na_2SiO_3), sodium carbonate (Na_2CO_3), potassium hydroxide (KOH) and potassium silicate (K_2SiO_3) [155]. Among these, NaOH is often preferred over KOH, due its superior ability to dissolve aluminosilicate precursors, promoting effective geopolymerization. Additionally, the lower cost of NaOH compared to KOH contributes to its widespread use in geopolymer and AAM synthesis. Na_2SiO_3 is also widely used preferred to be employed in conjunction with NaOH as it provides additional soluble silica to facilitate polycondensation reaction – essential for strengthening in the geopolymer gel. The factors that affect geopolymerization reactions are the activator ratio, activator to binder ratio and the Si/Al ratio of geopolymer precursor. Their careful selection of these parameters is required to impart desired rheo-mechanical performance to the resulting geopolymer system. It may be noted that water is not directly added to the geopolymer mix, unless required to main workability (the water typically comes (in diluted form) from the Na_2SiO_3 / NaOH solution and is not chemically bound like OPC system but rather facilitates the dissolution of aluminosilicate precursors.

1.9.5 MK as a precursor in geopolymer synthesis (factors influencing the rheo-mechanical performance)

As mentioned in the earlier sections of the literature review, MK offers a more standardized reliable and highly reactive precursor/binder material as a precursor for geopolymer systems. When Kaolinite clay undergoes the calcination process (typically around 500°C - 850°C), its structure loses the hydroxyl groups and undergoes significant changes (the octahedrally bound aluminum gets converted into penta/tetra coordinated forms, which are known to be highly reactive in alkaline conditions [156,157]. This is crucial to effectively facilitate the first step in geopolymer

synthesis, which involves the dissolution of Si and Al species. In terms of performance, the Si/Al ratio dictates the structural configuration, workability, mechanical strength and durability of resulting synthesized geopolymer [158]. Note that the Si/Al ratio mentioned here refers to the overall molar ratio of silica to alumina in the total mix- including the alkaline activators. In terms of workability, higher Si/Al ratio, promotes more dissolution of Si in the mix – which facilitates the formation of silica chains and gelation in aqueous phase – leading to increased network formation, marked by rise in viscosity and reduced workability [159–161] In terms of setting time, previous research works have indicated that, higher Si/Al ratios (> 1.5) are generally associated with increased setting time – this is because, higher dissolution silicate species would mean more time for the polycondensation reaction to take effect [162]. In addition to this, the type and concentration of alkaline activators also influence the rheological behaviour of MK based geopolymer system. The silicate modulus (defined as the ratio of SiO_2 / Na_2O) significantly affects the workability of geopolymer [163]. A modulus close to 1.5 is essential to maintain balance between reactivity and workability - with higher modulus, reduces the alkalinity which impacts dissolution, whereas lower modulus result sin rapid setting – proving detrimental for the geopolymer [164,165]. Now, following the workable regime, as the geopolymerization proceeds, the alkali cations (from the added activator) play an integral role in stabilizing / balancing out the negative charges generated as a result of the polycondensation reaction (i.e., the silicon present in the aluminosilicate network is substituted by aluminum and each of AlO_4^- repeating unit introduces negative charge that are balanced by alkali cations – leading to the formation of stable aluminosilicate network).

Moreover, the concentration of these alkali activators significantly impacts the performance of the synthesized geopolymer [166,167]. This parameter is often expressed in molar ratios

of Na/Al [168]. An optimal ratio of 1, suggests efficient charge balancing, whereas higher ratios may lead to release of free alkali, that may result in efflorescence. With regards to mechanical properties, the Si/Al ratio plays a vital role [169].

Ratios between 1.7 – 2.0 are considered optimal and geopolymers synthesized with these ratios exhibited the best performance [169]. Additionally compared to geopolymer system composed of other precursors, prior literature studies have indicated that MK based geopolymer system have exhibited the highest compressive strength [169]. Higher ratios are known to enhance Si – O -– Si linkages, contributing to improved strength – however the caveat here is that too high ratios can lead to excess formation of unreacted silica – which acts as stress concentrators eventually leading to the weakening of the geopolymer matrix [168]. Another factor that influences the porosity and workability of geopolymer is the water to solid ratio [170–172]. Extremely higher ratios tend to improve dissolution and improve workability but lead to the formation of interconnected pores increasing tortuosity resulting in crack propagation, while extremely low dosages can reduce workability and yield geopolymer mix that cannot be worked with [170]. Therefore, geopolymer synthesis often deals with formulation challenges (optimizing various mix ratios) and having the right formulation ensures optimum workability with a refined, less porous microstructure that enhances mechanical strength, and long-term durability while ensuring enhanced chemical resistance.

1.10 Research distinction

Despite extensive research into either improving FC with cellulosic additives or decarbonizing cement with alternative binders, the literature lacks a unified investigation that connects rheological, mechanical, and environmental performance across both additive and binder levels. This

thesis distinguishes itself by bridging this gap: it develops a two fold strategy that couples renewable, plant derived reinforcements with tailored binder composites. By integrating mechanistic insights with sustainability metrics such as life cycle analysis, this work goes beyond conventional strength based evaluations to offers a comprehensive pathway for engineering next generation, low carbon construction materials.

Chapter 2: Thesis scope and objective

2.1 Research gap

Despite the recent progress, presented in **Chapter 1**, several important questions remain open:

- While traditional (high CO_2 footprint) FC (non-structural composite) delves with carcinogenic fibers, (i.e., Asbestos) and additives (e.g., densified SF), can we engineer an eco-friendly FC with high performance metrics (i.e., flexural strength) and favorable processibility (i.e., rheology)?
- Can nano/micro cellulosic biomaterials act as suitable, green alternatives to conventionally employed petrochemical derived / silica based additives in FC ?
- Since biomaterials infused cement composite (FC) pose formulation challenges (both economic and engineering), is it possible to develop a cellulosic blend (fiber and additive), which will have low C/P ratio?
- Cement is the predominant choice of matrix material for FC applications (whose production is highly CO_2 intensive). To enhance sustainability, can FC be fabricated using low-carbon cement blends or bio-derived SCMs (e.g., processed waste biomass) as a partial or complete replacement for cement ?

2.2 Research objectives

My thesis is motivated by the open questions listed above and these questions led me to define my primary objective: To develop sustainable, low – carbon, high performance FC compo-

site by replacing conventionally employed petrochemical derived/ silica-based additives with biobased alternatives and to curb cement related CO_2 emissions by transitioning to low-carbon cement blends or waste biomass-derived materials as partial or complete cement replacements. This primary objective is pursued through two key approaches. Their sub-objectives are outlined below:

2.2.1 Reinforcement and additive modification

To incorporate CNCs as a biobased alternative to conventionally employed petrochemical derived additive in pulp FC composites.

- To understand the impacts of CNCs on the key performance metrics of FC system such as rheology, hydration kinetics and mechanical properties (i.e. Flexural strength).
- To benchmark the effect of CNCs on the key performance metrics against the commercial standard (i.e., PCEs).

To incorporate economically viable microcellulosic biomaterials such as MCC & AC, as a biobased alternative to conventionally employed synthetic additives in FC.

- To investigate the effect of these additive/fiber combinations on the rheo-mechanical properties of FC.
- To conduct a C/P of FC system incorporating different cellulose fiber/additive combinations.

2.2.2 Matrix modification

To incorporate BC as a low-carbon SCMs for FC applications.

- To study the effect of BC physicochemical characteristics on the rheo-mechanical properties of FC.
- To understand the mechanism of strength development in BC supplemented FC composites.
- To conduct a cradle to gate life cycle impact assessment and cost / performance analysis to understand the sustainability and economic viability of BC supplemented FC compared to conventional systems.

To develop a low-carbon FC using a Mk-BC geopolymer as a complete replacement for OPC in FC applications.

- To understand the key formulation challenges for developing (Mk-BC) geopolymer (optimising processing parameters such as activator ratio, activator / binder ratio) for ensuring workability and mechanical integrity of the FC system.
- To benchmark the mechanical performance of (MK-BC) geopolymer incorporated FC system with conventional OPC based FC system.
- To assess the environmental impact (using cradle to gate LCA analysis) of Mk-BC geopolymer incorporated FC against OPC based FC.

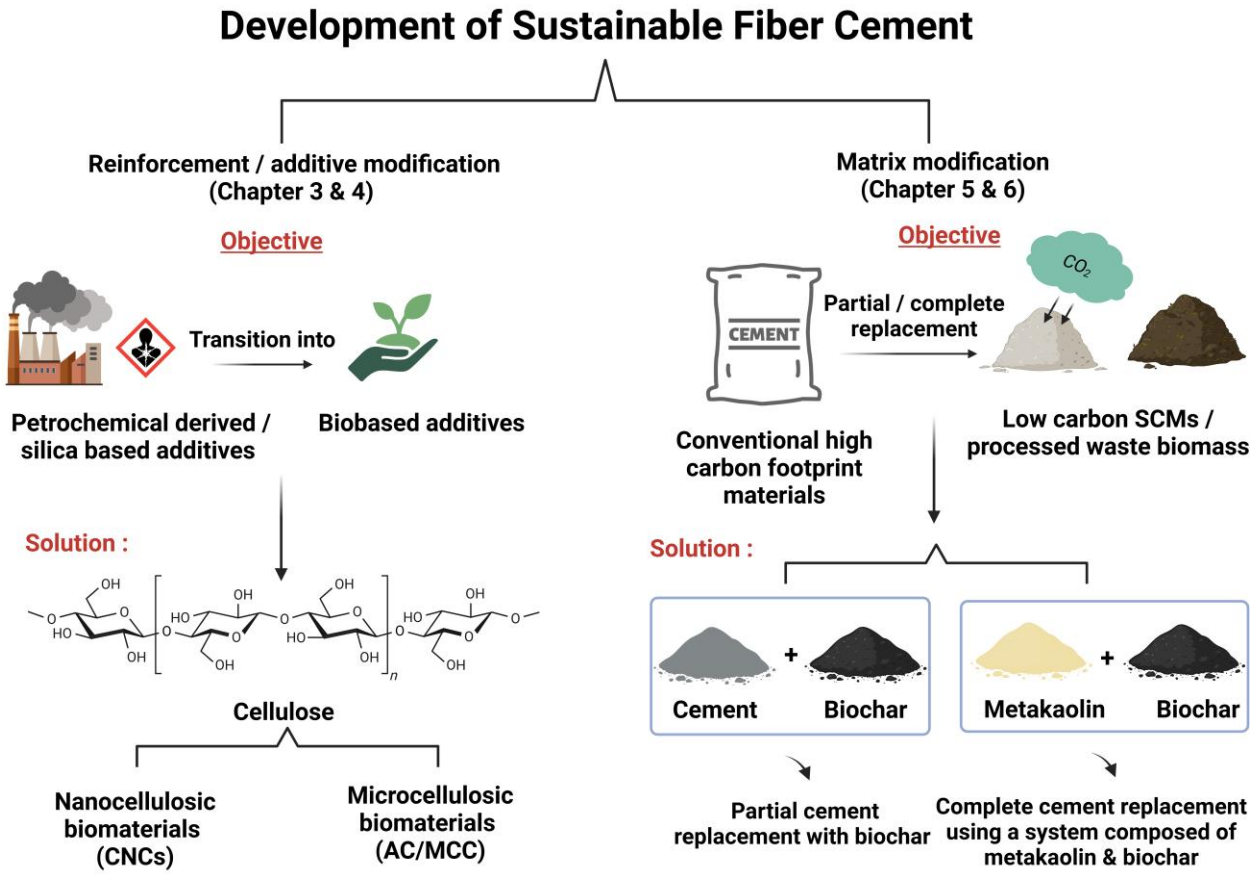

Figure 2.1 Schematic overview of the thesis scope and objectives, investigated through two key approaches: reinforcement/additive modification (chapter 3&4) ad matrix modification (chapter 5&6).

2.3 Thesis organization

This thesis is structured to systematically explore the development of sustainable, low-carbon FC through two primary approaches: reinforcement and additive modification and (b) matrix modification (see **Figure 2.1**). **Chapter 1** presents a comprehensive literature review introducing FC, outlying its composition, applications and challenges, particularly focusing on its environmental impact due to the use of petrochemical/silica-based additives and OPC. This chapter

explores potential solutions, focusing on cellulose-based additives and low carbon cement alternatives, discussing their latest advancement in their area and their potential to reduce carbon footprint of FC system and sets the context for research objectives.

Chapter 2 presents the scope of the research, identifies the potential research problems from the open research questions presented in **Chapter 1**. This chapter sets the objectives of the study, establishing the direction and exploration of biobased additives and alternative cementitious materials through two key approaches (a) reinforcement/additive modification and (b) matrix modification.

Chapter 3 & 4 delves into reinforcement / additive modifications, investigating the incorporation of CNCs (in **Chapter 3**) and cost-efficient microcelluloisc biomaterials such as MCC & AC (in **Chapter 4**) as a biobased alternative to conventional petrochemical derived/ silica-based additives employed in FC. The impacts of these additives on the key performance metrics of FC such as rheology, hydration kinetics and mechanical properties as well as cost / performance characteristics are thoroughly assessed.

Chapter 5 & 6 shift the focus to matrix modifications aimed at reducing OPC consumption. **Chapter 5** examines the use of BC as low-carbon SCMs for FC (partial replacement) whereas **Chapter 6** explores the development of MK-BC geopolymer as a complete replacement to OPC. The impacts of these alternate cementitious systems on the rheo-mechanical properties of FC are assessed thoroughly. The environmental implications of these approaches are evaluated through a cradle to gate LCA analysis in these chapters.

Finally, **Chapter 7**, summarizes the findings from the two key approaches devised to develop sustainable low-carbon FC, discusses the broader implications/limitations for sustainable construction materials and offers recommendations for future research.

Chapter 3: On the roles of CNCs in FC: Implications for rheology, hydration kinetics and mechanical properties.

3.1 Introduction

The adoption of natural fiber-reinforced cement composites in commercial and residential construction has grown steadily in recent decades, due to their potential to lower the embodied carbon of building materials. [173,174]. Fiber reinforcement is typically kept < 8 wt.%, as higher content of fibers has negative ramifications on the physicochemical properties: poor workability, and mechanical strength — a "conundrum" in materials engineering, where the strength requirements of the composite with a reduced CO_2 footprint is essential to achieve SDGs [103,175,176]. Forests, which act as natural carbon sink by sequestering CO_2, play a key role in climate mitigation. A single mature tree can absorb more than 48 pounds of CO_2 annually [177], unless disrupted by wildfires or decomposition. Therefore, utilizing wood-derived pulp fibers offers a promising strategy to reduce the carbon footprint of cement based materials intended for construction applications. Note that pristine (unmodified) wood species will always have the biggest impact on reducing the CO_2 footprint of building materials. For instance, wood-based structural materials (i.e., CTL) can reduce GWP by up to 14% [178], which is significant given that buildings and construction contribute to nearly 40% of energy-related CO_2 emissions. Therefore, incorporation of "low-carbon" yet "high-performing" fibers as well as additives in FC fabrication is of paramount importance; the key performance metrics are workability (rheology) improvement, curing kinetics (hydration), and mechanical strength (reinforcement).

In general, issues in workability can be addressed by using superplasticizers —functional PCEs based polymers — which enhance the flowability of FC at low w/c ratios. In other words,

they can function as high-range water reducers [179], but most of them are still based on petrochemicals. Next, hydration kinetics of cement strongly influence setting time, which in turn governs early strength development — crucial in applications such as in oil-well cementing) [180]. In the context of FC incorporating wood pulp, faster hydration kinetics during curing can help offset the retardation effects caused by sugars present in lignocellulosic pulp [99], while also providing benefits to traditional manufacturing processes, such as facilitating the smooth release of cast cement composites from well-defined molds.

Keep in mind that the use of traditional accelerators, (e.g., inorganic salts/salt-water [181]) is uncommon in FC but widely employed in task-specific concrete, such as seawater concrete. In the case of biomaterials, Plank's research group has pioneered the use of alginate-based biopolymers (water-soluble anionic polysaccharide extracted from the cell walls of brown algae) to accelerate the hydration of calcium aluminate cement in the presence of PCEs. Additionally, Belie et. al. [182] demonstrated that alginate could counterbalance the negative impact of superplasticizers on the mechanical strength of cement mortar. These reports represent notable examples of the emerging use of biobased additives in building materials.

Recent research has shown that cellulosic nanomaterials, such as CNCs, which are rod-shaped crystalline building block of cellulose, can modify the rheology of cement paste [98], influence hydration kinetics, and reinforce concrete [183,184]. A fascinating feature of CNCs is that they can be extracted from a variety of biomass sources (e.g., wood), and they exhibit a high aspect ratio (≈ 6 – 70) [185,186], high stiffness (≈ 110 – 130 GPa), and remarkable tensile strength (≈ 10 GPa) [187]. Moreover, current market research predicts that the nanocellulose market will grow from USD 271.26 million (as of 2017) to approximately USD 1,076.43 million by the end of 2025

[187]. CNCs also offer a broad range of surface functionalities, depending on surface modification, and exhibit resilience in harsh chemical environments, i.e., high pH, making them strong candidates for cement reinforcement [183,188].

Despite these promising attributes, environmental considerations must be accounted for. It is important to note that wood-derived nanocellulose (e.g., CNCs) typically has a higher GWP, as its production process is energy-intensive [177]. However, using CNCs to partly replace cement can help lower the overall CO_2 emissions, since cement has the highest carbon footprint in the mix [189]. Now, in combination with wood-derived pulp fiber, the higher GWP impact of CNCs can be justified, as they can also replace other components in FC, such as PCEs. Traditionally, PCEs are by-products of petrochemicals (e.g., methoxy-polyethylene glycol copolymer); therefore, replacing them with CNCs further contributes to reducing the overall GWP.

In this study, we investigated the roles of CNCs as a rheology modifier (affecting workability), curing agent (influencing hydration kinetics), and mechanical strengthener (providing reinforcement) in FC. We hypothesize that CNCs, due to their nanoscale dimensions and interaction with water, can locally tune the w/c ratio, thereby influencing both the workability and hydration pathways of FC composites. To validate the positive effects of CNCs, we varied their content during fabrication and systematically examined rheology, hydration kinetics, and mechanical strength.

The novelty of this work lies in demonstrating CNCs as a multifunctional additive capable of simultaneously tailoring rheo-mechanical behaviour and hydration kinetics, without the need for additional, property-specific admixtures. Moreover, this is the first study to integrate CNCs into a pulp fiber-reinforced cement system, highlighting the synergistic role of micro–nano cellulose interactions in achieving a high biogenic content (>10 wt.%) while maintaining desirable fresh and

hardened-state properties. These findings offer a potential solution to the current "conundrum" in FC materials engineering: increasing biomaterial content beyond 10 wt.% while preserving mechanical performance and avoiding delays in curing. Furthermore, the beneficial roles of CNCs demonstrated here could be extended to infrastructure concrete casting and the 3D printing of building materials.

3.2 Materials and method

3.2.1 Raw materials

OPC, Type I was received as donation from Lafarge, Canada and then used for composite fabrication (*vide infra*) [190]. CNCs were obtained from the process development center of University of Maine, USA [91]. NBSK pulp was kindly donated by Canfor, Canada [191]. poly (acrylamide-co-acrylic acid) partial sodium salt, the PCEs based additive used in this study was obtained from Sigma Aldrich, Canada and used as received [192]. Unless specified, reverse osmosis (RO) water was used during composite fabrication. The physicochemical properties of raw materials used for this study are listed in **Table A.1 – Table A.3).**

3.2.2 Fabrication of cement composite

Two sets of FC samples were prepared for this comparative study. The first set of samples employed CNCs as a superplasticizer and the second set of samples incorporated PCEs. The non-cementitious additives (CNCs/PCEs) varied in content (0.02, 0.06, 0.2, 0.6, 1, 2, 3, 4 wt.% of cement) were hand mixed for 3 minutes after which they were transferred into the tabletop mixer (Techwood 6-QT 800 watts, high power mixer) along with the refined pulp fiber. Please note that all FC samples prepared for this study contain 8 wt.% of refined NBSK pulp fibers (herein denoted

as ‘FC’) in them and only the additive (CNCs/PCEs) content (*(x)*wt.%) is varied, (see **Figure B.1** for experimental setup diagram). A constant w/c ratio (by weight ratio) of 0.5 is employed for the slurry preparation and mixing was continued for ~7 minutes at 600 rpm; with an intermittent break at every 5 min, using a spatula the adhered FC slurry was scraped from the wall, sides and bottom of the mixing bowl. The slurry preparation was done under a fume hood at temperature of 23 ± 2 °C and relative humidity of 50 ± 4 %. The slurry was then cast in a stainless-steel mold (30 × 20 × 0.8 cm) and then it was air cured. Note that the composite was completely (without releasing agent) demolded after 7 days and then sealed in a plastic bag.

3.2.3 Characterization of sustainable cement composite

3.2.3.1 Rheological characterization

The rheological characterizations were conducted using a Rheometer from NETZSCH Malvern, UK (model: Kinexus Ultra Plus). The testing geometry consisted of a four – vane type geometry with (25 mm diameter). To be consistent across the various specimens, a testing protocol was setup in a way that all the tests were started at an early age of 12 ± 1 min. As the cement pastes were in the dormant period, it was anticipated that the material behaviour would be unperturbed during the testing period owing to the hydration. For each experiment, approximately 33 mL of mixed FC slurry/paste containing additives in varied proportions was poured into the sample holder and steady shear viscometry analysis was carried out with a logarithmic increment of four steps at (25±1°C). The apparent viscosity corresponding to the high shear rate region (100 s^{-1} to 562.4 s^{-1}) was power law fitted to calculate the flow index ‘n’ (using the equation $\eta = k\dot{\gamma}^{n-1}$,

where 'η' – apparent viscosity, 'k' – consistency coefficient, '$\dot{\gamma}$' – shear rate and 'n' – flow index) [193].

3.2.3.2 Hydration kinetics

Hydration kinetics of FC slurry (with CNCs or PCEs) were measured using an isothermal calorimeter from TA instruments, USA (model: TAM III). Upon completion of the slurry/paste mixing process (*vide supra*), approximately 25–35 g of the sample were transferred into a glass ampoule (diameter: 22 mm, height: 55 mm), which was then sealed using a crimp sealer and placed into an instrument chamber, which was kept at constant temperature (25°C) using an oil bath., Prior to data collection, the isothermal condition was held for 15 min to attain equilibrium condition, and the steady-heat measurement was performed for approximately 70 h. The results were normalized by the weight of the sample present in the ampoules.

3.2.3.3 XRD characterization

To characterize the cement hydration product, powder X-ray diffraction (PXRD) was performed using an X-ray diffractometer from Bruker, Germany (model: D8-advance). To perform this experiment, cured FC samples (28 days, air cured) containing additives (CNCs/PCEs) in varied proportions were subjected to mild mechanical pulverization for 2 minutes (with intermittent stops every 30 s) using a low rpm tabletop grinder (700 W, fusion blade digital blending system manufactured by Black + Decker, USA) and sieved through Canadian standard testing sieve (manufactured by W.S. Tyler, USA) with a mesh size of MS 100. The X-ray generator was operating at 40 kV and 40 A producing Cu Ka_1 & Ka_2 ($\lambda 0$ = 0.154056 & 0.154439 nm) [194] radiation and the diffracted X-rays (intensity, I) were recorded as a function of diffraction (Bragg) angle (2θ,

range: 5°–90°) with a step size of 0.03° in a Bragg-Brentano configuration (reflective geometry, distance between the sample and the detector was constant).

3.2.3.4 Microstructural characterization

To investigate the interaction of CNCs with pulp fiber and cement, backscattered SEM images were obtained using Helios Nano Lab 650 equipment. For this study, Microstructural analysis was carried out in two systems. System one focused on investigating the interaction of CNCs with the Pulp fiber and system two was focused on understanding the interaction of CNCs in Pulp fiber – cement matrix. Since all our samples were nonconductive, an iridium coating [195] of thickness (approximately 12 nm) was applied on each specimen using a sputter coater. For system one, CNCs were mixed with approximately 8 grams of Pulp fiber in (4:1) ratio with a water to fiber ratio of 0.5. The resulting mix was probe sonicated for 2 mins, and the sonicated samples were dried in a glass slide. The dried samples were then coated and analyzed for its microstructure. For system two, the cement samples were air cured for 28 days, after which the samples were mechanically pulverized (mild mechanical treatment using a 700 w, fusion blade digital blending system manufactured by Black + Decker, USA) and sieved through Canadian standard testing sieve (manufactured by W.S. Tyler, USA) with a mesh size of MS 100. The resulting powdered samples were coated and analyzed for its microstructure.

3.2.3.5 Mechanical characterization

Three-point bending tests of the cement composite (with CNCs or PCEs) were performed using a universal testing machine from Instron, USA (model: Instron 5969). Rectangular block of size (19.5 cm × 4.5 cm × 0.6 cm) was cut from the cast cement samples for testing their flexural

properties. All the samples were tested at equilibrium condition (as per ASTM C1185 standard requirements) on the 28th day of curing. A crosshead speed of 10 mm/min was used to test the specimens, which was chosen as per the ASTM C 1185 standard requirements [196].

3.3 Results and discussion

3.3.1 Rheological characterization

Rheology of FC slurry not only affects the flow dynamics but also affects the hydration as well as mechanical properties. Rheology (workability) of the FC paste plays a major role in the fabrication (essential in pumping, mixing, spreading and compaction) process of the FC composite. The inclusion of high fiber content in the cementitious system often tends to jeopardize the cement workability and to keep the slurry viscosities in the usable regime, often additives with super plasticizing effects are employed. Therefore, WRAs, e.g., PCEs have revolutionized construction industries with their ability to improve the workability of the FC slurry and currently they are employed as various forms of admixtures, e.g., accelerator admixture, retarder admixture, to name a few. Since cement particles form flocs when they contact water, so, by adding a superplasticizer (i.e., PCEs), their dispersion becomes better through the action of hydrophobic (electrostatic repulsion) and hydrophilic groups (steric repulsion) of the polymer [197].

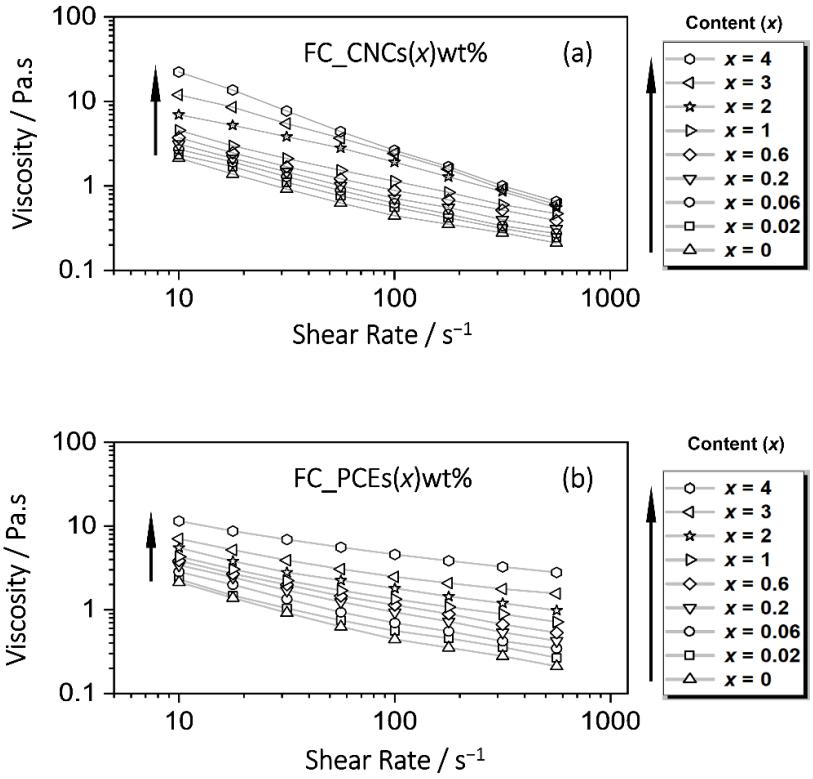

Figure 3.1 Steady-state viscometry (SSV) results of the FC slurry as a function of (a) CNCs wt.% (x) and commercial (b) PCEs wt.% (x) respectively. (Note that the SSV analysis of cement paste (at w/c = 0.5, devoid of any fibers or additives is depicted in Figure B.2).

Figure 3.1 Illustrates the steady state viscometry results of FC in presence of CNCs and PCEs (reference). Since all the samples contain 8 wt.% of cellulose fiber in the mix, all the samples inherently exhibited a shear thinning behaviour (marked by $x = 0$ in **Figure 3.1(a,b)**. The reason could be that the shearing may induce the rupture of fiber flocs and fiber network within the FC slurry, thus making the slurry to flow more freely [198]. Additionally, as proposed by Cui *et al.* that the elastic bending of micro/nanosized cellulose fibers under shear may be another mechanism that contributes to the shear thinning behaviour in bleached pulp fiber suspension [199]. It's important to note that our system contains nanocellulose (CNCs) in varied proportions in addition to

pulp fibers, therefore it is imperative that we understand the influence that the addition of nano-cellulose have on the rheology of cement pastes. The influence of CNFs on the rheological properties of cement pastes were investigated by Mejdoub *et al*., Hisseine *et al*., El Bakkari *et al*., and Nilson and Sargenius [200–202]. However, one of the major limitations that these researchers faced while employing CNFs is that the workability of the cement past considerably decreased with increase in CNFs content, which limits the addition of CNFs at high content (typically CNFs content is kept below 0.5 wt.%) in cementitious system [200–202]. The reason for this was attributed to the swelling effect of CNFs in the presence of water molecules (water molecules tend to adhere onto the outer surface of CNFs), which consumes some of the water that is available for mixing of cement paste and thereby causing the cement paste to thicken, resulting in decreased workability [202]. However, due to the smaller size (100 – 250 nm) of CNCs compared to CNFs (0.2 – 3μm), this swelling effect was minimized, which permits the usage of CNCs at higher content (typically employed up to 1.5 vol%). Although content depended, addition of CNCs in cementitious system demonstrated plasticizing (typically in low content regime (< 0.2 wt.%) as well as viscosity modifying effects (high content regime > 0.5 wt.%) [98].

Now as soon as the non-cementitious additives (i.e., CNCs & PCEs) are introduced (in varied proportions) into our FC system, the viscosity (at any shear rate) is observed to be increased with an increase in additive content. (See, **Figure 3.1(a,b)**).

Now in particular for CNCs, when we consider lower CNCs content (0.02 – 1 wt.%), the increase in viscosities is not significant compared to the viscosity of the control sample containing no additive (marked by $x = 0$ in **Figure 3.1(a)**. This may be because at lower CNCs content, the CNCs may get adhered on the surface of the cement particles and with the addition of water (during

mixing), the CNCs may hold on to these water molecules (rather than getting agglomerated), thereby increasing the bound water associated with the CNCs and when under shear, releases the bound water and disperses the cement particles effectively through electrostatic and steric stabilization [98]. Now as the CNCs content increases, the viscosity is also seen to be increased considerably, which may be attributed to the tendency of CNCs to get agglomerated (especially at higher content) [97,203,204], within the slurry, thereby making the slurry highly viscous. Furthermore, at high CNCs content (1 – 4 wt.%) there could be more alignment of the agglomerated CNCs, in the direction of shear, contributing to higher shear thinning effect. These observations are consistent with the findings reported by Montes *et al*. which indicated that lower content of CNCs in the cement matrix would enable them to act as WRAs whereas higher content enables then behave as VMAs [98]. Our observations (especially when CNCs are employed at low contents) were also similar to biopolymers with superplasticizer properties, which includes starch, cellulose ether, modified chitosan, and acrylamide grafted Kraft lignin polymer[205] have demonstrated plasticizing effect (> 1 wt.%) in concrete (a heterogeneous mixture of cement, sand, and aggregates) and geopolymer mortars [206,207] In contrast to CNCs, the increase in viscosity with increase in PCEs content (depicted in **Figure 3.1(b))** could stem from different mechanism as opposed to CNCs. For instance, steric hindrance from the long side chains that is attached to the polycarboxylate backbone [208] can prevent cement particles from getting agglomerated. We also note that, at higher CNCs content (>2wt%) the viscosity vs shear rate plot of the FC paste appears to be slightly nonlinear and the possible reason for this could be attributed to the improvement in hydration (see **Figure 3.2(a,b)**) resulting in a microstructural evolution causing the curves to be slightly nonlinear. However further rheological studies would be required to validate these effects and is beyond the scope of this study.

Furthermore, behaviour of FC slurry (with CNCs) at high shear rate is important since it could benefit practical large-scale applications (beyond non-structural materials), such as, pumping of concrete and/or as 3D-printing of cementitious materials. Thus, we calculated flow index '*n*' values for the high shear rate regime (see, experimental section for details) and '*n*' was found to decrease with increase in CNCs content (see **Table B.1**). According to the 'power law' model [193], the result indicates that the FC slurry containing CNCs exhibited improved shear behaviour compared to samples incorporating PCEs as an additive.

Overall, it can be inferred from the viscometry results that the rheological characteristics of FC paste can be tuned with CNCs content (lower content facilitates plasticizing effect) whereas higher content enhances the shear thinning effect of the FC slurry.

3.3.2 Hydration kinetics and products characterization

Cement, when it encounters water, an exothermic reaction occurs between clinker phase (e.g., calcium silicate/aluminate) and water, which can be monitored *via* ITC experiments measures the heat released as a function of reaction time (expressed in h).

In recent literature[99,100], it was shown that hydration kinetics is affected by the pulp fibers and/or variety of nanocellulose (additives). However, one of the major limiting factors in FC is that there is a retardation effect on hydration by the non-crystalline saccharides. Kochova *et al*. reported that the incorporation of lignocellulosic fibers in cementitious system can significantly retard (up to 48 hours) OPC hydration [99]. Similar retardation effect was also observed when 0.3 wt.% MCC was incorporated into cement mortar, accompanied by a reduction in the workability of the cement paste [100].

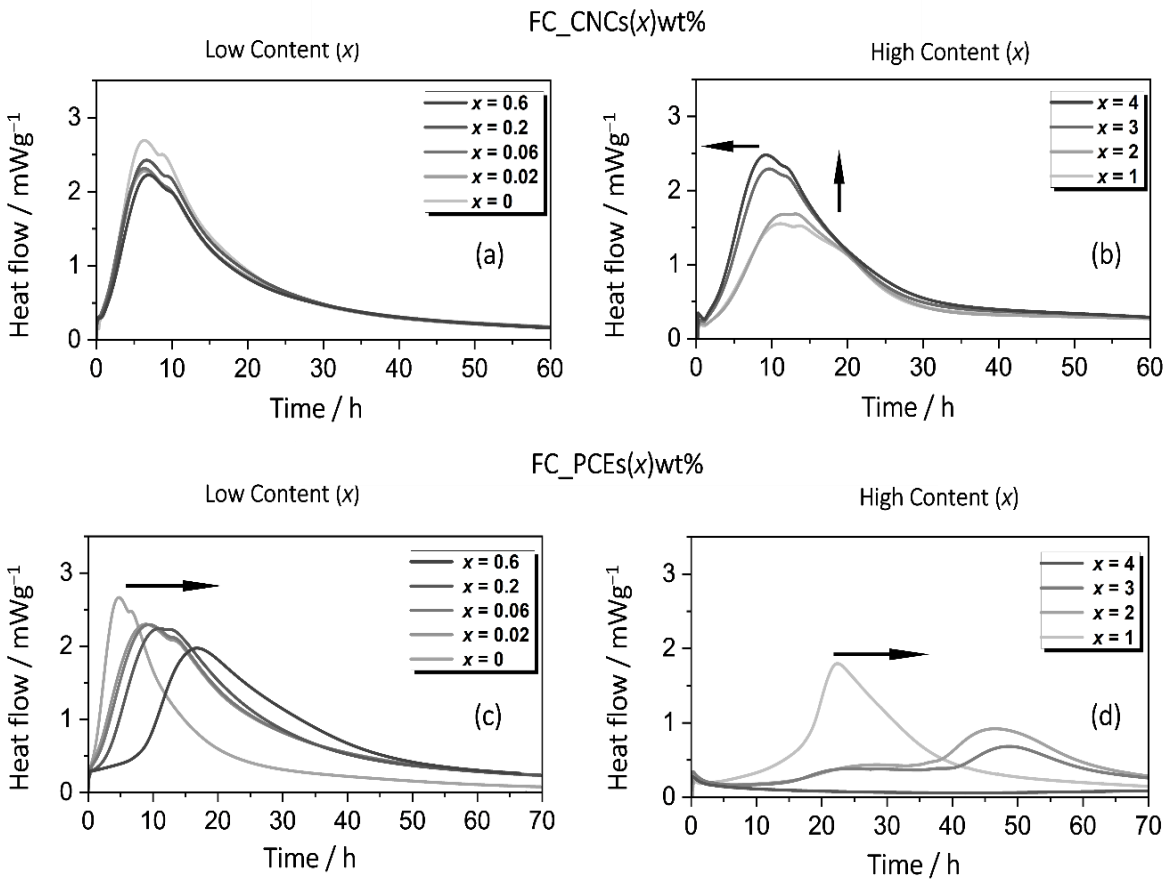

Figure 3.2 Hydration kinetics characterization of FC slurry. ITC curves as a function of (a, b) CNCs wt.% (x) and (c, d) PCEs wt.% (x) respectively. Note, that the horizontal arrow represents the trends pertaining to time it takes for the FC sample containing additives to attain the main peak of hydration (silicate hydration peak) and the vertical arrow indicates the improvement in heat of hydration pertaining to the silicate hydration peak.

Table 3.1 Summary of the ITC results of FC slurry containing CNCs based on the results shown in Figure 3.2.

FC slurry	Content (*x*) of CNCs (wt.%)	Time to attain silicate hydration peak (h)	Calculated heat flow (mWg^{-1})
Control	0	6.4	2.7
	0.02	6.6	2.4

Low CNCs content	0.06	6.6	2.3
	0.2	6.5	2.2
	0.6	6.9	2.2
	1	10.7	1.5
	2	10.8	1.6
High CNCs content	3	9.6	2.3
	4	9.1	2.4

Since in this research, we have combined the pulp (bleached) fiber and CNCs in FC, it is necessary to decouple the individual contributions of the reinforcement and the additive on the rate and extent of cement hydration. It was quite interesting observation that when CNCs are introduced into FC slurry, the trend in ITC curves were content dependent — at lower CNCs content ($x = 0.02$ – 1 wt.%), the heat of hydration (expressed in mWg^{-1}) was decreased (2.4 – 1.5 mWg^{-1}) while the time taken to reach the silicate hydration peak was more or less similar (see **Figure 3.2**, top-left) to the reference/control sample ($x = 0$) with the exception, where $x = 1$ wt. % of CNCs indicated maximum retardation effect. Such behaviour could be borne from the surface chemistries (i.e., negatively charged) and nanoscale characteristics (e. g., surface area) of CNCs. For instance, at lower content, CNCs may act as WRAs, as reported by Montes *et al*.) which may deprive the cement particles from reacting with water, thereby contributing to the delay in hydration (retardation effect).[98]

On the other hand, for samples containing higher CNCs content (2 – 4 wt.%), the hydration delay was minimized, and the specific heat of hydration was increased (see **Figure 3.2(b)** & **Table 3.1**). Reports from Youngbloods' research group [57] highlighted the role of CNCs in improving the hydration kinetics of the cement pastes (degree of hydration (DOH) improved from (~ 55 % to ~ 64 %) producing more hydration products with the increase in CNCs content (0 – 1.6 vol.%). High surface area and water-retention ability of CNCs enabled water-transport from the cement pore solution, across the hydration product shell on cement grains, to the unhydrated cement cores. This mechanism, referred to as "short-circuit diffusion", involves channelling water through CNCs networks, effectively bypassing diffusion barriers [57]. Our hypothesis is that such mechanism could also be in play (especially at high CNCs content domain) in FC, marked by the improvement in hydration kinetics [57,97].

To support our hypothesis, we prepared control samples (only pulp fiber and CNCs) to validate the information regarding the adherence of CNCs on pulp fiber. Interestingly, as shown in the microscopic images (**Figure 3.3(a-e)**), CNCs were observed to form a layer of coating onto the pulp fiber, when compared with a pristine pulp fiber surface (**Figure 3.3(a-e)**). Importantly, the pore-filling effect of CNCs was distinctive as shown in (**Figure 3.3(d,e)**) and **Figure B.4**) where they could form a network, perhaps aiding the transport of water from the cement pore solution [209] and accelerating the cement hydration. Similar accelerating affects in cement hydration were also observed with the addition of ligno and delignified CNFs in cement mortar where the high surface area of CNFs enabled them to act as additional nucleation sites for hydration products to develop [210]. We also note that surface functionality of CNCs improved the hydration of silicate and aluminate in cementitious pastes, and the degree of influence was however dependent on the

cement composition (Type I, II, V) [95] hence we are limiting our current study to only one type of CNCs (sulfated CNCs in this case).

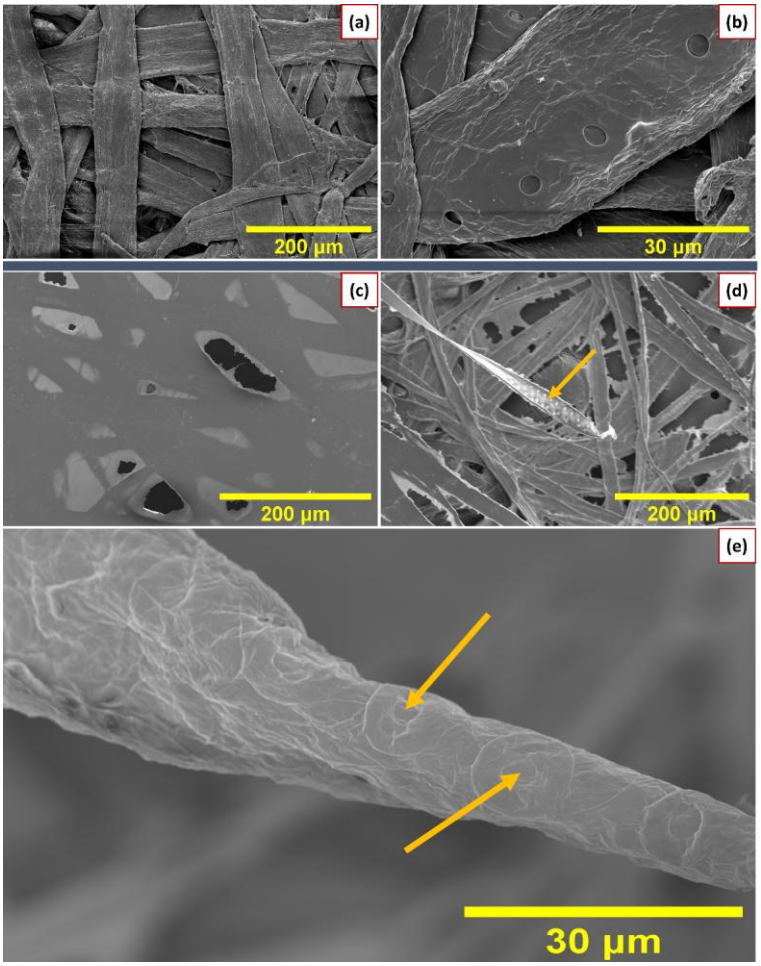

Figure 3.3 Representative SEM images of (a-b) pristine pulp fibers. (c-d) representing CNCs-pulp fiber control samples (x = 4 wt.%) (see experimental section for details). (c) depicts CNCs coating the pulp fiber. (d) CNCs filling in the voids pr present in pulp fiber (marked by the arrow). (e) represents the magnified image of a single strand of pulp fiber representing filled voids by CNCs (marked by the arrow).

In contrast with CNCs, in the case of FC containing PCEs as an additive, specific heat of hydration was decreased considerably with increasing PCEs content, accompanied by significant delay in hydration, highlighted by the onset of silicate hydration peak (for e.g., 4 wt.% PCEs content, the onset of silicate reaction peak was not visible until 70 h) (see **Figure 3.2(c,d)**).

Indeed, retardation effect of PCEs on cement hydration is well documented in literature though they improve cement pastes rheology, — PCEs molecules adsorb on the C_3S cement particles surface and block the reactive surfaces for dissolution.[211] However, the performance of PCEs based polymers strongly dependent on their molecular structures (such as number of side chains, molecular weight) [212,213]. Likewise, beyond conventional PCEs, similar retardation effects were also shown by biobased additives, such as, calcium alginates, natural polysaccharides, which have shown to cause retardation effects in calcium aluminate cements [214] and a CO_2-storing retarder (at 3 wt.%), i.e., *Chlorella* algal biomass, which caused 812% delay in hydration of conventional OPC [215].

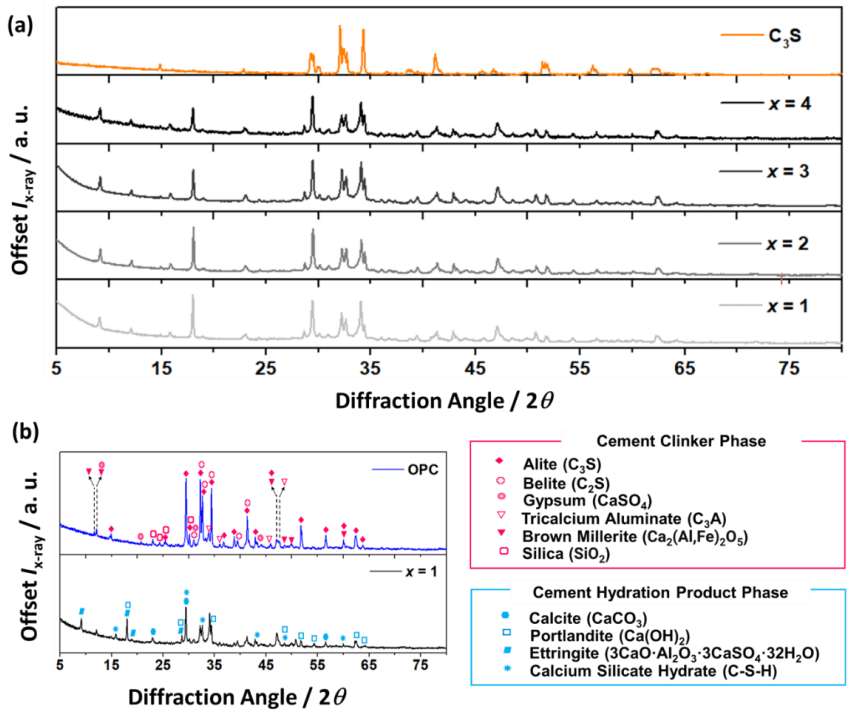

Figure 3.4 (a) Powder X-ray diffraction (PXRD) characterization of the FC as a function of the content of CNCs (x = 1 – 4 wt.%). (b) Representative powder diffractograms of FC with 1 wt.% of CNCs and OPC. The color-coded rectangular boxes on the right indicate the observed cement clinker phase (pink colored) and hydration product phase (sky blue colored) respectively. Since bleached pulp fiber (contains hemicellulose) could increase the amorphous background, samples were sieved to maximize the opportunity for the observation of crystalline hydration products (e.g., portlandite) in FC (CNCs, x = 1 – 4 wt. %). The PDF number related to the cement clinker phases and cement hydration products are as follows: Alite (00-055-0738), Belite (00-033-0302), Gypsum (01-074-1905), Tricalcium aluminate (01-074-7039), Brown millerite (01-074-3674), Silica (01-071-0261), Calcite (01-086-2334), Portlandite (00-001-1079), Ettringite – (01-075-7554).

To this end, to confirm the speciation of the hydration reaction, powder X-ray diffraction (PXRD) is the gold-standard for cement-based materials and composites. Figure 3.4(a) depicts the representative x-ray diffractograms of the FC samples in presence of CNCs and compared with tricalcium silicate (C_3S; alite), which is one key component in cement clinker phase. As shown in

(Figure 3.4(a)), powder diffraction patterns were similar, which was of no surprise since the mechanism of hydration is same while CNCs only affecting the kinetics (rate of hydration reaction). Now, from a qualitative viewpoint, relative intensities between the diffraction peaks (i.e., at 17°) were markedly different but quantitative assessment is challenging owing to the heterogeneous nature of FC. Thus, to highlight the hydration product phase, we present the PXRD (Figure 3.4(b)) of one representative sample, that is, 1 wt.% CNCs and compared that with OPC.

Now, upon phase identification (based on ICSD database), formation of typical cement hydration products was confirmed, such as, portlandite (CH), ettringite, and calcite [216,217]. It is important to note that the amorphous phases are difficult to ascertain (no visible reflexes) via XRD analysis and peak overlaps between different phases (e.g., C-S-H and ettringite) renders uncertainty in phase identification of cement hydration products. Therefore, based on recent study by Maddalena *et. al*., we tentatively assigned the reflection peaks at 16°, 29°, 32° and 49° corresponding to C-S-H [218]. In general, observation of ettringite supported the ITC results (**Figure 3.2**) and although samples were kept inside of a sealed bag, calcite phase was pronounced overlapping with the C-S-H peak at 29°. Also, portlandite and ettringite demonstrated strong reflections at 8° and 17°, which were absent in the raw OPC confirming the presence of these hydration products in the FC. Finally, we note that by employing a model cement clinker component, like C_3S or calcium aluminosilicate (C-A-S), quantification (via Rietveld refinement) of the hydration product in presence of CNCs is thus possible, which is currently underway in our group.

3.3.3 Mechanical characterization (three-point bending test)

It is important to note that in FC, mechanical interlocking (or anchorage) between the surface of cellulose fiber and cement hydration products (see**, Figure B.3**) plays a significant role in

bonding formation amongst these phases which contributes to the strength and toughness of the FC composite [219–223]. Now it is imperative to investigate the effect of CNCs (as additive) on the key mechanical properties (i.e., flexural strength) of FC to corroborate the findings from the ITC investigation (see, **Figure 3.2(a-b)**).

Figure 3.5 illustrates the change in the calculated values of flexural strength/ MOR based on the 3-point bending tests as a function of CNCs content and compared with PCEs. From **(Figure 3.5(a)**), it is observed that, at lower regime of CNCs content (0.02 wt.% – 0.6 wt.%), the MOR was maintained without an appreciable change as compared to the control (without CNCs). Interestingly, at higher regime of CNCs content (1 – 4 wt.%), MOR of the composite exhibited an increasing trend and reached a maximum value of (8.56 MPa) at 4 wt.% of CNCs, (35.4 % increase as compared to the control). Note that at 5 wt.% of CNCs, MOR dropped to 5.38 MPa (see **Table B.2**). On the other hand, as shown in (**Figure 3.5(b)**), MOR also displayed dependency on the content of PCEs, for instance at 2 wt.% of PCEs, there was an increase of 16.7 % (vs control) and then it dropped.

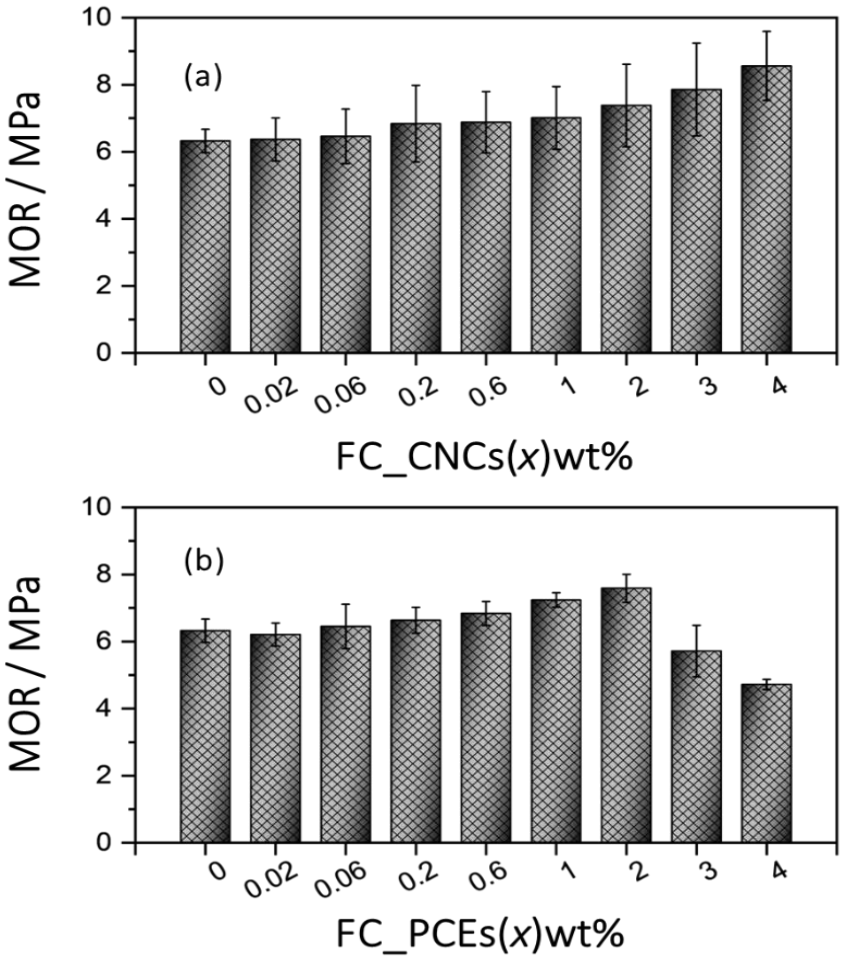

Figure 3.5 MOR values as a function of content (x) of (a) CNCs and (b) PCEs of the hardened pulp FC composite. MOR was calculated from the stress-strain curves of the respective samples. All the experiments were performed under ambient conditions.

In cement composite, improvement in the flexural strength/MOR owing to the cellulosic nanomaterials has been well-documented [57,101,112,113]. One notable mention is the results from youngbloods group work, which revealed that at low CNCs (wood-derived) regime (0.04 – 1.5 wt.%), MOR was increased upto 30% [57]. Also, Mazlan *et al*. employed CNCs (Palm oil derived) resulting 20% increase in MOR at 0.4 wt.% of CNCs (content regime: 0.2 – 0.8 wt.%) [113]. Now, in the context of FC, Lee et. al. demonstrated the beneficial role of CNCs on flexural

strength, i.e., at 0.8 vol% of CNCs, 58% increase in MOR was observed. To this end, it is worth to mention that they employed flax and steel fibers (1 Vol%) whereas in this research only pulp fibers (8 wt.%) were used as reinforcement [112]. Thus, overall, comparing the observed results with the prior studies, we hypothesize that owing to the presence of (bleached) pulp fiber, it was possible to increase the content of CNCs in FC, which lead to the enhancement in the mechanical properties .

Furthermore, the balance between the content of pulp fiber and CNCs is a crucial since > 4 wt.%, mechanical strength of the composite gets reduced, pertinent to agglomeration of CNCs which leads their poor dispersion in the composite. In other words, the aggregated CNCs could act as stress concentrators – composites become more prone to fracture [95,97]. In contrast to CNCs, the surface chemistries of PCEs are quite different, thus at > 2 wt.%, the decrease in MOR could be due to the increased entrained or entrapped air in the cement paste/slurry [224].

Overall, CNCs are unique additive (in combination with pulp fiber) for reinforced cement composite within the class of cellulose nanomaterials. While CNFs can also impart good mechanical properties, the key difference with CNCs lies in the maximum allowable content in the composite [225]. Note that CNFs can only be employed in low content (< 0.5 wt.%), [114,225–227] at higher content regime (> 0.5 wt.%) agglomerated CNFs tend to induce localised stress concentration points in FC, eventually leading to a reduction in flexural strength [225]. Therefore, the combination of pulp fibers and CNCs can produce high strength FC by controlling the content of CNCs, which could unravel new avenues in the quest of sustainable building materials.

3.4 Conclusion

This study explored the use of CNCs as renewable, non-cementitious additives to improve the performance and sustainability of fiber composites. The performance of CNCs was systematically benchmarked against PCEs to assess their viability for use in both structural and non structural building applications. The findings, categorized into fresh-state rheology, hydration kinetics, and hardened mechanical performance are summarized as follows.

(1) Bulk rheological investigation revealed that CNCs significantly enhanced the shear thinning behaviour of the FC slurries, particularly at high shear rates. This behaviour is attributed to the high aspect ratio, colloidal stability and surface charge of CNCs, which facilitate anisotropic alignment under shear and promote lubrication effects between cement particles and fibers. CNCs likely act as a physical dispersant, improving particle distribution `and slurry flowability without the need for synthetic plasticizers.

(2) Isothermal calorimetric studies demonstrated a concentration dependent effect of CNCs on cement hydration. At lower dosages (< 2wt.%), CNCs exhibited a retardation effect, likely due to steric hindrance and physical adsorption on cement particle surfaces, which may obstruct ion diffusion and slow the initiation of hydration reaction. In contrast, at higher CNCs dosages (> 2wt.%), an acceleration in hydration kinetics was observed. This enhancement is attributed to strong water-retention capacity of CNCs and their ability to mediate water transport from cement pore solution to unhydrated cement particles. The physicochemical characteristics of CNCs, including their high surface area, network forming ability, and the presence of surface functional groups promote efficient water delivery into hydration front.

This mechanism supports continuous hydration, particularly in dense cement matrices, leading to faster setting and early age strength development. Such dual behaviour allows CNCs to be strategically utilized to optimize either the workability or the early strength of FC systems, depending on the dosage, particularly where rapid setting and early strength development are desirable.

(3) Results from three point bending tests conducted on 28 day cured FC samples showed that CNCs significantly improved the mechanical performance. At 4 wt.% CNCs addition, the MOR increased by up to 35.4% compared to the control. This enhancement is attributed to the nanoscale reinforcement effect of CNCs, which can bridge microcracks, improve stress transfer between fibers and matrix, and densify the microstructure.

Overall, CNCs demonstrated multifunctional capabilities a biobased additive for FC composites, offering improvements in workability, hydration kinetics and mechanical strength. These improvements stem from the intrinsic physicochemical characteristics of CNCs, particularly their nanoscale dimensions and their interactions with water , which promote enhanced dispersion, fiber-matrix interaction, and crack bridging mechanisms. Given increasing environmental and regulatory guidelines to reduce ethe CO_2 footprint and synthetic polymer usage in construction materials., CNCs offer a promising path forward for developing sustainable, high – performance cementitious composites.

Chapter 4: Sustainable microcellulosic additives for high-density FC: emphasis on rheo-mechanical properties and C/P analysis

4.1 Introduction

The reduction of carbon dioxide (CO_2) emissions from materials like cement is crucial to mitigate global warming, as cement accounts for approximately 8% of global CO_2 emissions. One way to curb cement's impact on climate change is to reduce its content in a range of building materials, e.g., reinforced cement (FC). Importantly, this reduction could play a key role in achieving the UN SDGs, particularly, SDG 12, which focuses on ensuring responsible consumption and production [228]. In this context, wood-derived pulp fibers (with or without lignin) have been widely used in composite (non-structural) engineering [229]. However, their fabrication process often suffers from poor slurry rheology and limited mechanical (flexural) strength of the resulting composite. To overcome these challenges, petrochemical-based superplasticizers (used as rheology modifiers), and siliceous materials as additives (fillers) have been employed to achieve favorable rheo-mechanical properties [230,231].

Although natural fibers have a range of physical attributes, i.e., high aspect ratio, these mechanically strong fibers tend to exhibit poor dispersion in the cement slurry, resulting in inconsistencies that hinder efforts to increase fiber content in the composite. To a degree, it is resolved through VMAs, also known as superplasticizers. These water-soluble admixtures, whether semi-synthetic or fully synthetic, improve rheological behaviour while also affecting other processing parameters such as hydration, setting time and final rheo-mechanical properties [72,232]. Over the years, a wide variety of polymeric superplasticizers, such as PCEs have been developed. These materials balance rheology, micro-mechanical performance, and enhanced hydraulic cement

chemistry [233–235]. On the other hand, biobased superplasticizers — functionalized lignin [236], starch sulphonate [237], methylcellulose [238] and algal biomass derivatives [214,215] have also shown promise in improving the workability of (fiber) cement slurries. However, biopolymers/biomass materials tend to retard cement hydration. For instance, polysaccharides such as starch are well known for their set-retarding effects and are commonly used in ready-mix concrete applications [239].

Another key component in cement-composite design is silica-based additives (e.g., silica sand, SF, and silica flour). These are ubiquitous in the building materials industry and can be tailored to meet specific rheo-mechanical requirements [230,231]. However, due to growing health and environmental concerns surrounding the use and production of crystalline silica-based additives [240], research into sustainable and user-friendly alternatives has gained momentum [241,242]. Cellulosic microparticles have been explored for low-carbon structural building materials, such as microbially induced concrete, due to their abundance in natural plants and waste biomass [242].

In our earlier work, we utilized nanocrystalline cellulose (CNCs) to fabricate FC without any PCEs (superplasticizer) or silica-based additives. Interestingly, CNCs as the sole biobased additive, were able to modify slurry rheology, accelerated hydration kinetics, and improve the mechanical properties of the resulting composite [57,243]. However, at high concentrations (i.e., 4 wt.%), CNCs led to poor workability. Additionally, the high raw material cost (~ USD 5900/t [244]) imposes a significant barrier to commercial scale adoption. Therefore, identifying cost-effective natural additives that retain the material benefits of CNCs is essential [243]. To this end,

polysaccharides present a promising class of biobased materials. Cellulose, the most abundant polysaccharide (accounting for 61.8% of all structural biobased polymers produced as of 2013 [245]) is particularly viable for meeting the volume and supply-chain demands of the construction industry [246].

AC & MCC are among the promising candidates in the polysaccharide class of material, as they offer techno-economic advantages compared to CNCs while rendering similar materials chemistry. Prevalent sources of AC include wood (40–50 %) and cotton (90%), with extraction typically involving alkaline and bleaching treatment. AC can also be extracted from agricultural residues such as rice straw [247] and cocoa pod husk during the chemical pulping process [248]. On the other hand, to produce MCC, often AC extracted from wood/plant sources is often used as a starting material. The purified cellulose is then subjected to a mild acid hydrolysis (e.g., 2 M hydrochloric acid at 105 $^{\circ}$C for 15 min), where the amorphous components in AC are selectively hydrolyzed, resulting in the release of crystallites, which are then mechanically dispersed in solution before drying [249]. Regarding physicochemical features, both materials are chemically similar, exhibiting comparable functional groups, but they are morphologically distinct. However, subjecting the natural materials to chemical and physical treatments significantly affects the size distribution and crystallinity of the processed cellulosic material. Thus, the key differences between the AC and MCC are size and the presence/absence of amorphous hemicellulose (non-crystalline, branched polymer with low molecular weight).

In the context of cement chemistries, the inherently high alkalinity of the cement-matrix (with pore solution pH ranging from $\approx 12 - 13$ [250]) presents additional challenges for the chemical stability of biopolymers. Consequently, crystalline cellulosic materials are considered more

suitable than their amorphous cellulosic or lignocellulosic counterparts [33,251]. Upon surveying the literature, a surprising lack of research on AC and MCC for low-carbon building materials was observed. Notably, AC has yet to be reported as a rheology modifier or as a multifunctional additive in reinforced cement composites. On the other hand, Hoyos et. al. evaluated the effect of MCC on the hydration kinetics of cement paste [100], while Ferreira *et al*. reported a 15% reduction in setting time following MCC addition in cement and geopolymer systems (the latter being inorganic polymeric material composed of three-dimensional aluminosilicate networks). Compressive strength was also enhanced — by approximately 55% in the cement system and ~7% in the geopolymer system. It was hypothesized that geopolymer matrix was more detrimental to MCC than the cement matrix. [252]

Therefore, based on the identified research gap, we selected AC and MCC as additives to develop high-density FC composites without relying on traditional superplasticizers or silica-based (inert) fillers. By minimizing the physicochemical influence of conventional carbon-intensive additives, we evaluated how these biomaterials influence the rheo-mechanical properties of FC. The hypothesis is that morphologically distinct, crystalline microcellulosic additives can modulate the rheo-mechanical properties of FC through their inherent physicochemical characteristics.

In this research, two formulations were developed: one with AC (Combination 1) and the other with MCC (Combination 2), both combined with NBSK. In each case, the relative proportions (wt.%) of the microcellulosic additive (AC or MCC) to NBSK were systematically varied, while keeping the total biobased content fixed at 12 wt.%. Unlike prior studies that primarily explored nano–macro scale cellulose combinations, this study investigates the underexplored micro–macro scale synergy. It offers novel insights into how industrially accessible, morphologically

distinct cellulose forms can be strategically integrated to tailor the rheo-mechanical performance of FC.

Finally, we present performance metrics, including S/W and C/P analyses, to bridge the gap between laboratory findings and commercially relevant benchmarks. We believe the research presented in this work shall inspire stakeholders to accelerate the adoption of biomaterials in next-generation cement admixture industries, which is crucial to improving the sustainability of the construction industry.

4.2 Materials and methodology

4.2.1 Raw materials

Matrix material, the OPC, Type I was procured from Lafarge Canada. The reinforcing fibers (i.e., NBSK) was obtained from Canfor, Canada. We gracefully acknowledge each provider for their kind contribution. MCC (Avicel® PH–101) and AC were procured from Sigma Aldrich, Canada. All these raw materials were used as received during composite fabrication. Reverse Osmosis (RO) water was used to mix the components to form FC slurry. The bulk physico-chemical properties have been detailed in the supporting electronic document **Table A.1–Table A.8**) to conserve space in the main manuscript.

4.2.2 Fabrication process of FC: matrix development and optimization of the content limit for microcellulosic additives

Microcellulosic additives (AC and MCC) were premixed (duration: 2 minutes) with cement prior to the mixing with the refined NBSK fibers (see, **Table A.5** for refined fiber properties). The rest of the steps are mentioned in our previous work [243].

The matrix (FC without additive) was developed first by varying only the reinforcing fiber (NBSK) content (2 – 32 wt.%). We postulated that to develop FC high biomaterials content, the first step is to establish the baseline with a wide range of fiber content (**Table 4.1**). In such a way, we can optimize the formulation recipe with biobased binders, which is not limited to microcellulosic additives. However, high aspect ratio NBSK fibers in a cement matrix is challenging to disperse if superplasticizers are not used. Therefore, the upper limit was experimentally set at 32 wt.% by testing different wood-based pulp fibers. Based on the exploratory work, we observed that the content of bleached and unbleached fiber (high aspect ratio) is possible to extend up to 32 wt.% [33], exhibiting comparable mechanical properties, e.g., flexural strength. We want to note that such a range might vary for natural fiber with different (i.e., low) aspect ratio.

Likewise, the high content of additives in a cement matrix also has detrimental effects, i.e., cracking. (**Figure C.1**) Thus, the maximum allowable content for MCC (additive 2) was 10 wt.%. On the contrary, AC did not render cracking of the FC (withing the composition range). Thus, owing to these limitations, FC with 12 wt.% of NBSK was chosen as the control, and the NBSK to additive (AC/MCC) weight was varied systematically so that the total biomaterial content remained at 12 wt.%. For example, if NBSK is 6 wt.% then additive is 6 wt.%. Such variation af-

forded to observe the physical effect of microcellulosic additives on the rheo-mechanical properties of the FC. In terms terminology, combination 1 and 2 corresponded to AC, and MCC, respectively with NBSK fibers. Compositional details with sample nomenclature are illustrated in **Table 4.1**.

Table 4.1 List of specimens and the corresponding composition. The sample nomenclature and composition of all the FC slurry and cured samples were prepared for this study.

Sample ID	Cellulosic (NBSK) fibers (wt.% of cement)	w/c ratio	Additive (wt.% of cement)	
			AC	MCC
Without additive				
NBSK_2%	2 (8.4 g)	0.5	-	-
NBSK_4%	4 (16.8 g)	0.5	-	-
NBSK_6%	6 (25.2 g)	0.5	-	-
NBSK_8%	8 (33.6 g)	0.5	-	-
NBSK_10%	10 (42 g)	0.5	-	-
NBSK_12% **(Control sample)**	12 (50.4 g)	0.5	-	-
NBSK_16%	16 (67.2 g)	0.5	-	-
NBSK_24%	24 (100.8 g)	0.5	-	-
NBSK_32%	32 (134.4 g)	0.5	-	-

Combination 1: AC and NBSK				
AC_2%	10 (50.4 g)	0.5	2 (8.4 g)	-
AC_4%	8 (33.6 g)	0.5	4 (16.8 g)	-
AC_6%	6 (25.2 g)	0.5	6 (25.2 g)	-
AC_8%	4 (16.8 g)	0.5	8 (33.6 g)	-
AC_10%	2 (8.4 g)	0.5	10 (42 g)	-
Combination 2: MCC and NBSK				
MCC_2%	10 (50.4 g)	0.5	-	2 (8.4 g)
MCC_4%	8 (33.6 g)	0.5	-	4 (16.8 g)
MCC_6%	6 (25.2 g)	0.5	-	6 (25.2 g)
MCC_8%	4 (16.8 g)	0.5	-	8 (33.6 g)

4.2.3 Physicochemical characterization

4.2.3.1 Attenuated total reflectance-Fourier transform infrared spectroscopy (ATR-FTIR)

ATR-FTIR spectra of AC/MCC additives were obtained using Bruker HCT Inventio ATR – FTIR. The additives (used as received) were spread onto the ATR internal reflection element (diamond crystal). The recorded spectral range was from 600 cm^{-1} – 4000 cm^{-1} (4 cm^{-1} resolution), with an average of 32 scans per sample. For brevity, only the mid IR range (600 cm^{-1} – 2000 cm^{-}

[1]) was shown to highlight the functional groups present in the microcellulosic additives (AC and MCC).

4.2.3.2 Raman spectroscopy

Raman spectra of the microcellulosic additives (AC and MCC) were recorded using a dispersive Raman spectrometer from Wasatch Photonics, USA (Model: WP 785). The specimen was loaded on a hollow stainless-steel holder and surface was flattened with a spatula prior to the data acquisition. The recorded spectral range was from 250 cm^{-1} – 2000 cm^{-1} (8 cm^{-1} resolution).

The solid particle/fiber was illuminated with a 785 nm laser since cellulosic material can exhibit autofluorescence under 532 nm excitation. Now, as the Raman scattering intensity will be reduced under higher laser excitation, thus, high (100%) laser power was chosen to achieve best S/N. To reduce the any-laser induced degradation, spectrum was collected at 0.5 ms exposure time. Adaptive iterative penalty least square method (air-PLS) background method was applied on the collected Raman spectra of the microcellulosic additives (AC and MCC).

4.2.4 Microstructural characterization

Microstructural characterization was performed using a SEM from Hitachi, Japan (model: SU3500). Cellulosic (micro and nano) materials are intrinsically non-conductive. As such, they were coated with a thin layer of Iridium (Ir) nanoparticles (ca. 12 nm) using a sputter coater[195] from Leica Microsystems, Germany (model: EM MED020 coating system). The conductive coating suppresses the charging effect as well as beam-induced degradation, which is detrimental to the fragile fibers and soft micro-particles.

4.2.5 Particle/fiber size and shape characterization

Size and shape characterization of anisotropic particle and high aspect ratio fiber is inherently challenging using traditional dynamic light scattering (DLS) technique. Though, a static light scattering (SLS) would be more suitable, however, considering the application prospect of the employed microcellulosic additives, a laser-diffraction based particle (and/or fiber) analyzer technique (solid-state) was adopted in this research.

The average particle diameter of the microcellulosic materials (AC/MCC) was measured in using a dynamic image analyzer (DIA) from Sympatec GMBH, Germany (model: RODOS). Approximately 1g of specimen was fed into a vibrating sample dispenser, which feeds the samples into the DIA for imaging and size analysis. One of the key advantages of using DIA is it accounts for the variation in the shape of the fiber and particle and is free of solvent-induced effects.

During experiment, the sample feed rate was kept constant at 20% (with a gap width of 2 mm) and the particles were dispersed using 1 bar pressure and a vacuum pressure of 14 mbar. System configuration of 175 Hz and trigger condition was maintained at an optical concentration range of $C_{\text{opt, start}} = \geq 0.02\%$ to $C_{\text{opt,end}} \leq 0.02\%$. The accelerated individual particles (open jet aerosol) then pass through an image analyzer and then measured for their properties. The volume means diameter (VMD), computed by the software using the equal area projection method (EQPC) [253,254].

Shape descriptor of irregularly shaped particle computed by calculating its fractal dimensions (Feret) and have a scale from (0–1). Note that '1' means the geometry resembles closely to a fixed shape descriptor (e.g., circle, sphere, and line) while closer to "0" indicates increase in the

complexity of particle/fiber geometry. By default, the software in RODOS computes the fractal dimensions and provides a (0–1) comparison, indicating how complex a geometry, the measured particle/fiber possesses. For instance, aspect ratio*, which is calculated by computing the maximum and minim Feret dimension and dividing them.

4.2.6 Rheological characterization

Rheological characterization was performed using a rotational rheometer from Netzsch, Germany (model: Malvern Kinexus ultra plus) with a vane-in-cup geometry (4 blades, 25 mm diameter, depicted in **Figure 4.2(a**)). The rheological test plan was designed to understand the flow properties, e.g., shear thinning and workability (estimation of the yield stress) of FC slurry. The tests were performed at room temperature (25 ± 1 °C) and the results were repeatable within ± 5%.

Note that all the FC slurries (with and without additive) were assessed to evaluate the specimen at its dormant period, at an early age of 10 ± 1 minute to ensure consistencies in data collection. This is a crucial factor since cement hydration reaction proceeds at the dormant period, and cement starts to set (will harden eventually). Also, this would allow the normal force to reach zero under a stress-free resting period [255].

The rheological experiments were performed under both oscillatory and rotational tests (see, **Figure 4.2(b,c)**). The amplitude sweep experiments were conducted at a constant frequency of 1 Hz, within the shear strain range of 0.01% to 1000% while the steady-state viscometry was performed within the shear rates of (0.01 S^{-1} – 1000 S^{-1}).

4.2.7 Mechanical characterization

Mechanical characterization was performed using a Universal Testing Machine (UTM) from Instron, USA (model: 5969 dual column testing system). Since FC is utilized as a non-structural building material, it is more prone to bending failure. Low thickness (i.e., 8 mm) and high span length induce bending moments more than compression, which is mostly associated with load-bearing applications The flexural strength of the air-cured FC composites was calculated based on the 3-point bending test. Note that the testing parameters were chosen based on ASTM C1185 method. Thus, flexural property-related metric, like MOR is considered for C/P evaluation (detailed in results and discussion section).

In all cases (unless stated otherwise), fabricated composite (with and without additive) was removed from the mold after 28 days of curing and then cut into rectangular blocks of size 19.5 x 4.5 x 0.8 cm before being fed into the UTM to collect load vs deflection curves and to calculate MOR [256].

4.3 Results and discussion

4.3.1 Physicochemical characterization

Chemical functionality of the cellulosic additives employed for this research was probed using complementary vibrational spectroscopic techniques, like ATR-FTIR and Raman. **Figure 4.1(a,b)** illustrates the chemical "*fingerprint*" of AC and MCC, which are identical. It was not surprising as they bear similar functional groups, like hydroxy, and glycosidic ether bond (C—O—C). IR spectra confirmed presence of characteristic cellulosic bands, observed at 1025, and 1155 cm^{-1} corresponding to C—C breathing mode, and C—O—C, respectively. In Raman spectra,

symmetric and asymmetric stretching band of C—O—C were observed at 1096, and 1120 cm^{-1}, respectively. Furthermore, Raman spectrum shed more light on the crystalline structure (and orientation) of the polymorphic cellulose, which could be ascribed to Cellulose I for both AC and MCC, based on the stretching frequencies at 377, 1096, 1378, and 1475 cm^{-1}, which was also observed previously for Avicel I [257]. Thus, based on the chemical analysis using surface-sensitive techniques, AC and MCC exhibit comparable features.

In terms of physical properties, i.e., morphology is a crucial aspect for composite's mechanical performance, could vary for cellulosic materials. **Figure 4.1(c,d)** displays the variability in morphology of microcellulosic additives employed in this study. Structurally, AC is long and fibrous, retaining the morphology of natural pulp fibers, whereas MCC consists of short rod like particles with a granular appearance due to the breakdown of amorphous regions during acid hydrolysis. To further investigate their size disparity, solid-state particle/fiber size and shape analysis was performed as shown in **Figure 4.1(c,d)**. Notably, AC displayed volume mean diameter (VMD) of 134 μm with bimodal distribution curve whereas for MCC, VMD was 64 μm and size distribution was monomodal.

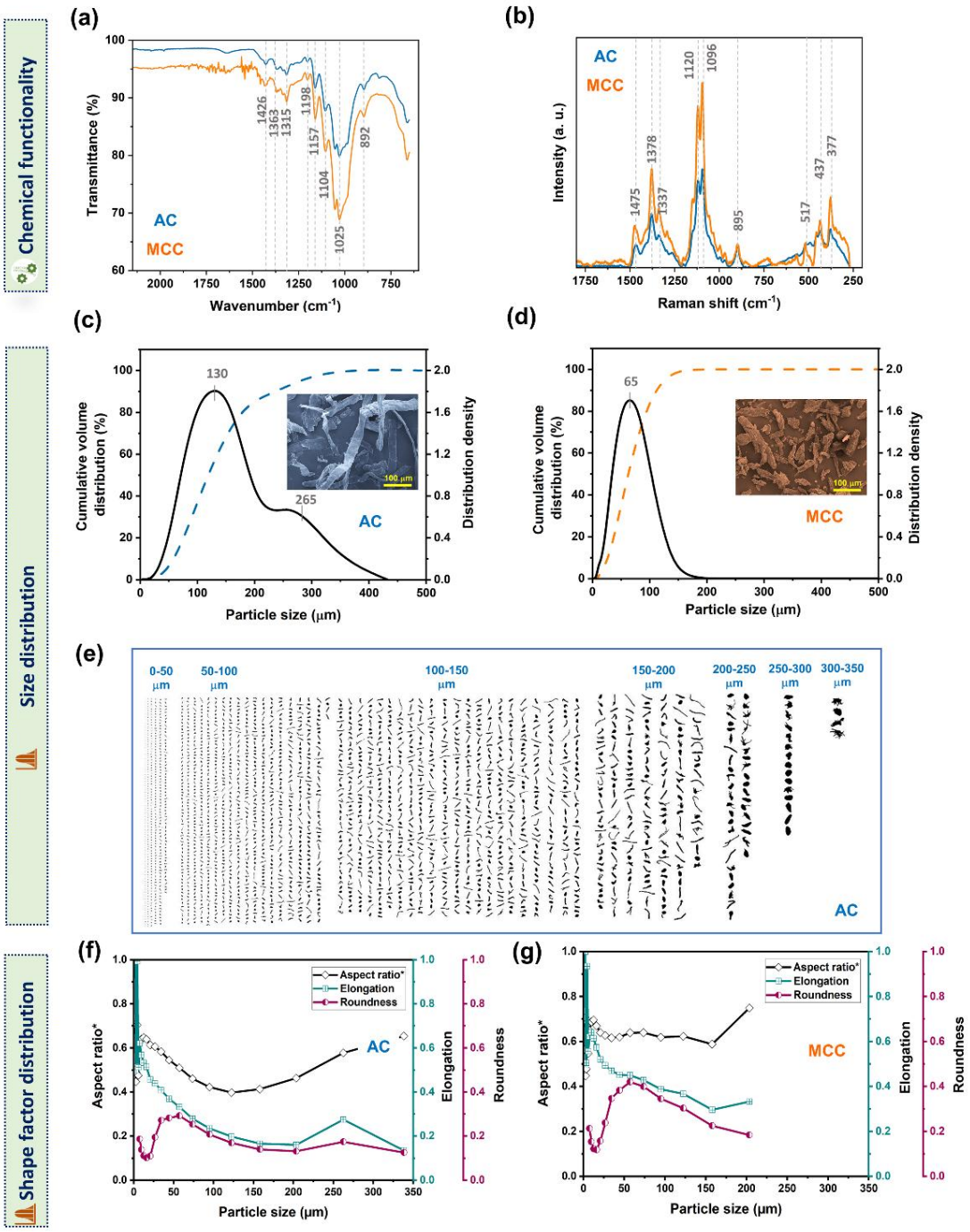

Figure 4.1 Solid-state physico-chemical characterization of microcellulosic additives (AC and MCC) using vibrational spectroscopy and laser-diffraction based particle/fiber shape analysis. (a) ATR-FTIR spectra (b) Raman spectra highlighting the major vibrational bands. Particle/fiber size distribution (LEFI) curves (c) AC

and (d) MCC with inserted SEM micrographs (color coded to match color of the distribution profiles) (e) Illustration of the DIA-enabled size distribution curve of AC with individual particle/fiber captured during the measurement. Variation of shape descriptors (aspect ratio*, elongation, roundness) with particle size of (f) AC (g) MCC. Note that the mentioned VMD corresponds to volume mean diameter. LEFI stands for length of fiber, and elongation is the ratio of DIFI (diameter of the fiber) and LEFI. See, experimental section for details on the aspect ratio* (range: 0–1) calculation method.

In terms of additive shape characteristics, **Figure 4.1(f, g)** indicates the variation in shape descriptors (such as aspect ratio*, roundness, and elongation) with particle size. Key observations from **Figure 4.1(f, g)** were, MCC is more granular in shape as opposed to AC (less spherical and more elongated). Additionally, MCC exhibited uniformity (less variability in shape) whereas the AC shape descriptors, i.e., aspect ratio vary drastically with particle size.

In-depth size and shape factor analysis is particularly critical when we analyse the flow behaviour (rheology) and mechanical characterization of cement composites containing AC and MCC as additives. Recent studies employed using fractal dimensions to compute various shape descriptor of MCC samples to understand its flowability - with particle circularity or roundness contributing to the maximum effect [258].

Therefore, these results suggest to us that the shape and size characteristics of AC and MCC could play a crucial role in imparting specific properties [259] to the FC, discussed in the coming sections. Additionally, the variation of particle shape with respect to particle size can provide valuable insights on the strengthening mechanism of biobased additives in cementitious composite.

4.3.2 Rheological characterization

Understanding the rheology of FC slurry is important — processing cost, interlink to the ease in transportation and storage of the FC slurry. Among different rheological features of cement pastes, the shear-thinning property (see **Figure C.4** for more details) and yield stress are of great importance not only for transportation purposes but also for formulation, and processing.[260] The former quantitatively explains the decrease in viscosity of the slurry upon agitation and the latter elucidates the integrity of the slurry at rest.

During the FC manufacturing (i.e., Hatschek process) [229], after mixing, the FC slurry is transported to the processing line where it will undergo various steps. Yield stress (stress that must be applied to initiate flow) is particularly important when it comes to processing flexibility such as the workability of cement/FC slurry – optimum yield stress ensures workability [261], segregation resistance (a non-homogeneous mix affecting the mechanical strength), bleeding resistance [262] (free water that comes out from the slurry during consolidation), setting time [260] and consolidation (formwork stability) of the cement pastes [263].

Figure 4.2 illustrates the evolution of yield stress as a function of the content of the microcellulosic additive (AC and MCC). There exists a wide range of methods for calculating yield stress in literature such as creep, cross-over of amplitude sweep, stress ramp, and frequency sweep [203]. Here, we calculated the "yield point" *via* two different methodologies (*vide infra*) known as cross-over of amplitude sweep moduli [264] and curve-fitting on the steady-state viscometry results [265]. As presented in **Figure 4.2(b)**, using amplitude sweep results, the transition point from a viscoelastic solid (G' > G") to a liquid-like state (G" > G') may be used as a direct method to measure the "yield point". On the other hand, by fitting the Herschel–Bulkley model on the steady

viscometry results, one may indirectly estimate the yield point as shown in **Figure 4.2(c)**. This rheological model can be described as follows:

$$\tau = \tau_{y_{HB}} + m\,\dot{\gamma}^{n"} \quad (1)$$

where, τ is the shear stress, $\tau_{y_{HB}}$ is yield stress, *m* is consistency coefficient, $\dot{\gamma}$ is the shear rate and *n* represent the flow index [266].

As observed in **Figure 4.2(d,f)**, irrespective of the methods, the "yield point" follows the same trend as a function of the content of the cellulose-based additives (AC and MCC). Note that, the yield stress measured by the cross-over method is higher than the one measured by curve-fitting. The difference between the two yield points has been previously reported in the case of other slurries and suspensions. For some fluids, the cross-over of the amplitude sweep is beyond the *true* "yield point" of the system, introducing a larger magnitude of yield stress [264]. On the other hand, there exist some discrepancies in measuring the "yield point" using curve-fitting — its magnitude is highly dependent on the range of data points and the quality of data acquisition under low shear rates [267].

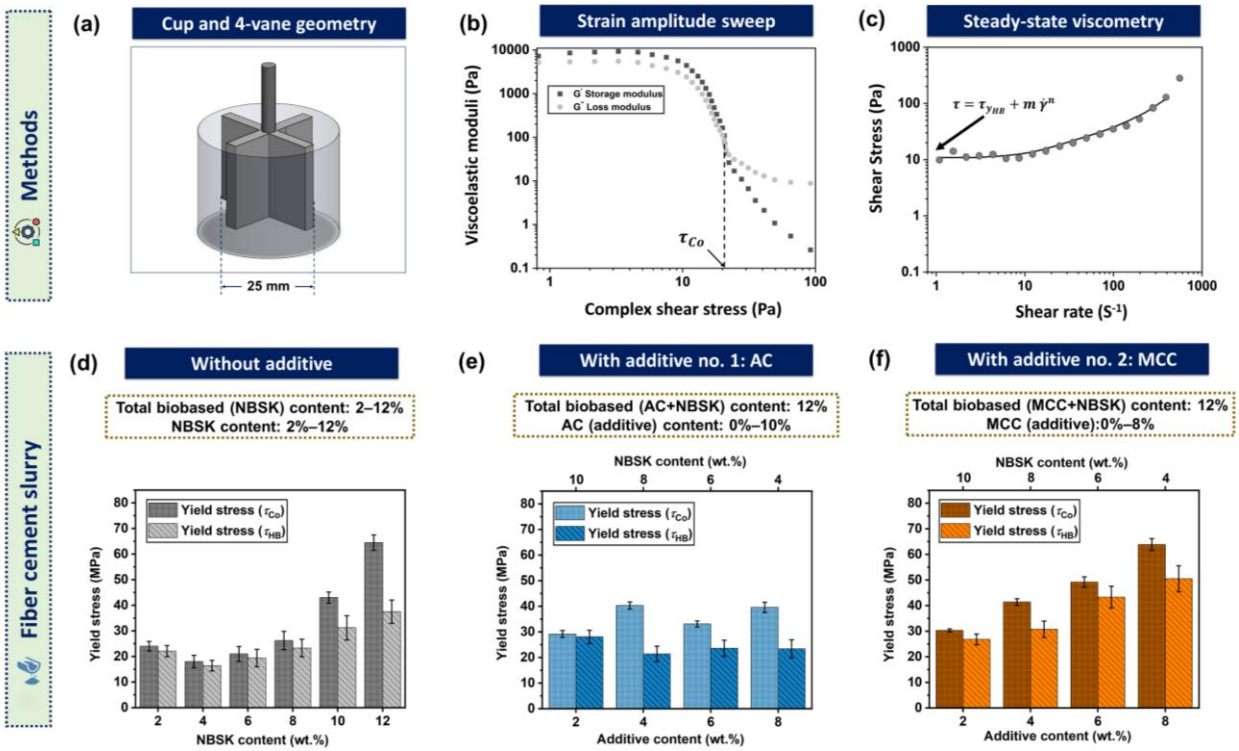

Figure 4.2 Rheological characterization of FC slurry. (a) The cup and 4 vanes rheometer geometry. Methods of computing yield stress using (b) direct method — strain amplitude sweep, and (c) indirect method — steady state viscometry (Herschel–Bulkley model). Reinforcing (NBSK) fiber/additive content dependent yield stress of FC slurry without additive, (d) NBSK; with microcellulosic additive, (e) AC (combination 1: AC and NBSK), and (f) MCC (combination 2: MCC and NBSK).

Figure 4.2(d) represents the yield stress trend of cement paste (without additive) containing varying amounts of NBSK. Notably, with increment of the NBSK content, yield stress exhibited increasing trend and was maintained up to 8 wt.% after which yield stress increases drastically — it reached a maximum 65 Pa at 12 wt.% of NBSK. Such observations are common in the rheology of pulp fiber suspensions. Note that the high aspect ratio pulp fibers tend to undergo bridging and interlocking effects and have high Van der Waals forces of attraction between fibers [268].

Thus, it creates resistance to the flow of any suspension including cement paste and thereby increase the yield stress [269]. Also, long fibers increase the fiber cohesion,[268] which can be a contributing factor to the aggregated state of the cement particles — yield stress increases [269–271]. Moreover, high content of pulp fibers will inadvertently result in less spacing between the fibers within the cement matrix, thereby resulting in a possible hinging/ bending effect between fibers — yield stress increases [198,270,271]. To summarize, yield stress strongly depends in the content of the reinforcing (NBSK in this case) fibers, and since no conventional superplasticizer was employed, to understand the effect of microcellulosic additives, maximum NBSK content was set at 12 wt.% for the rheological (also for mechanical, explained in the respective section) characterization. Also, it affords to benchmark performance metrics of the FC with nanocellulsoic additives [243].

Figure 4.2(e) illustrates the trends in yield stress variation of FC slurry as a function AC content (2–10 wt.%) while keeping the total biomaterials content fixed at 12 wt.%. From absolute point of view, yield stress was low for all the combinations of AC and NBSK (binary materials) as opposed to NBSK (unary biomaterial). But it is interesting to note that it was varied within a narrow range (30–45 Pa) with a maximum of 45 Pa at 6 wt.% AC content. Such a trend could be attributed to the stabilizing agent role of AC, which can improve dispersion, resulting a uniform mix of the components in the FC slurry. Also, due to the lower crystallinity than MCC (see, **Figure C.3** & **Table C.2**), AC affords better water retention. Note that AC is typically used as a stabilizing agent in pharmaceutical applications wherein they facilitate control release of water/moisture with time [272]. This could perhaps mean that the increase in yield stress due to the presence of pulp fibers can be negated by the control addition of AC into the mixture, thereby keeping the yield

stress values at usable regimes preventing a rapid increase of yield stress and viscosity. Also as observed from **Figure 4.1(c,e,f)**, AC consists of a short fiber-like morphology (elongated and less spherical in shape) and so the fiber cohesion between them tends to be minimal compared with macro pulp fibers (high Van der Waals attraction). As a result, the mix consisting of fibers and AC is less prone to getting entangled, resulting in an improved dispersion, and contributing to the reduction in yield stress.

Finally, as displayed in **Figure 4.2(f)**, yield stress was steadily increased for FC slurry with MCC (content: 2–10 wt.%), maximum yield stress of 64 Pa was observed at 8 wt.% of MCC. These results were consistent with the results obtained from the studies conducted by Cao *et al*., wherein they found that for a fixed w/c of 0.35, the incorporation of CNCs in cement paste increased the yield stress from 15 Pa (at 0.04 vol%) to 600 Pa at 0.15 vol.% of CNCs concentration [57]. They have hypothesized it was due to the agglomeration effect of CNCs in fresh cement paste pore solution [57]. We believe that such a mechanism may play a pivotal role in increasing the yield stress in the case of MCC (combination 2 in this study) despite not being nanoscale cellulosic materials. However, MCC has similar physicochemical properties, like, hydrophilicity, crystallinity and narrow particle size distribution as opposed to AC.

Overall, it can be inferred from the rheological studies that, AC and NBSK (combination 1) is more effective than MCC and NBSK (combination 2) in reducing the yield stress (improving the workability) of the FC slurry as compared to MCC.

4.3.3 Mechanical characterization

The strength of a FC composite is crucial as it dictates the feasibility in terms of design, performance, durability, and quality for a particular building materials application, i.e., external cladding/façade materials.

As such, they are more prone to bending (flexural) failure as compared to compression failure (associated with load-bearing components). Factors such as wind loadings, thermal expansion (freeze-thaw), and moisture absorption (wet/dry cycles), to name a few, significantly contribute to flexural loadings when FC is draped around a building structure [273]. Hence, cement, which is inherently brittle, is reinforced via high-aspect ratio fibers to improve its ductile by promoting strain hardening [33]. The incorporation of microcellulosic biomaterials (as additives) can further alter this behaviour depending upon the type, nature, and concentration.

From **Figure 4.3(a),** as the reinforcement content increases (8 – 32%), a decrease in peak strength with an increase in strain hardening behaviour was observed. Pulp fibers enhance the strain-hardening and load transfer ability of cement composites by forming networks that bridge the crack during deformation/failure. However, exceeding a feasible limit can cause weak points within the composite itself, resulting in agglomeration (dispersion challenges) and eventually leading to the failure of the composite. Therefore, based on this observation and being cognizant about the processing challenges without the conventional superplasticizer, the upper limit of the NBSK was 32 wt.%. However, to be consistent with the rheological characterization, we chose 12 wt.% as the limit for total biomaterials (binary components) content for mechanical tests (*vide infra*).

Now, **Figure 4.3(b,c)** depicts the flexural stress-strain behaviour of FC with microcellulosic additives, which are AC (combination 1) and MCC (combination 2), respectively. Interestingly, strain-hardening region and ductility is indeed highest for the control FC (without additive), not surprising as it has the maximum reinforcement. This could be primarily due to the different reinforcing mechanism in presence of additives (AC/MCC), will be discussed in the subsequent section. In **Figure 4.3(b,e)**, with the addition of AC (2–4 wt.%), the ductility and strain hardening region decreased, although the peak strength was improved.

At low content, AC functioned as an inert filler **(see, Figure 4.3(b,e) & Figure 4.1(c,e,f))**, which densifies the composite, while it reduces strain-hardening but improves the peak strength. On the other hand, at higher AC content (i.e., 6–8wt.%), an improvement was observed with both peak strengths as well as the strain-hardening behaviour.

This could be due to the fibrous nature and larger size of AC (see, **Figure 4.1(c,e,f)** and **Figure 4.3(b,e)**), which in combination with NBSK fibers can form network structures (this could be fiber-matrix interlocking network (mechanical interlock) or microfibrillar networks formed between cellulose fibers (chemical interlock), thereby improving the reinforcing ability (by bridging cracks and resisting deformation under load) which makes the composite more ductile. Note that a maximum MOR of 7.9 MPa is observed at 6 wt.% of AC in high-density FC. This originates from the combination of macro-micro reinforcement (combination 1: AC and NBSK) mechanism as evidenced previously for (CNCs and NBSK) combination [243].

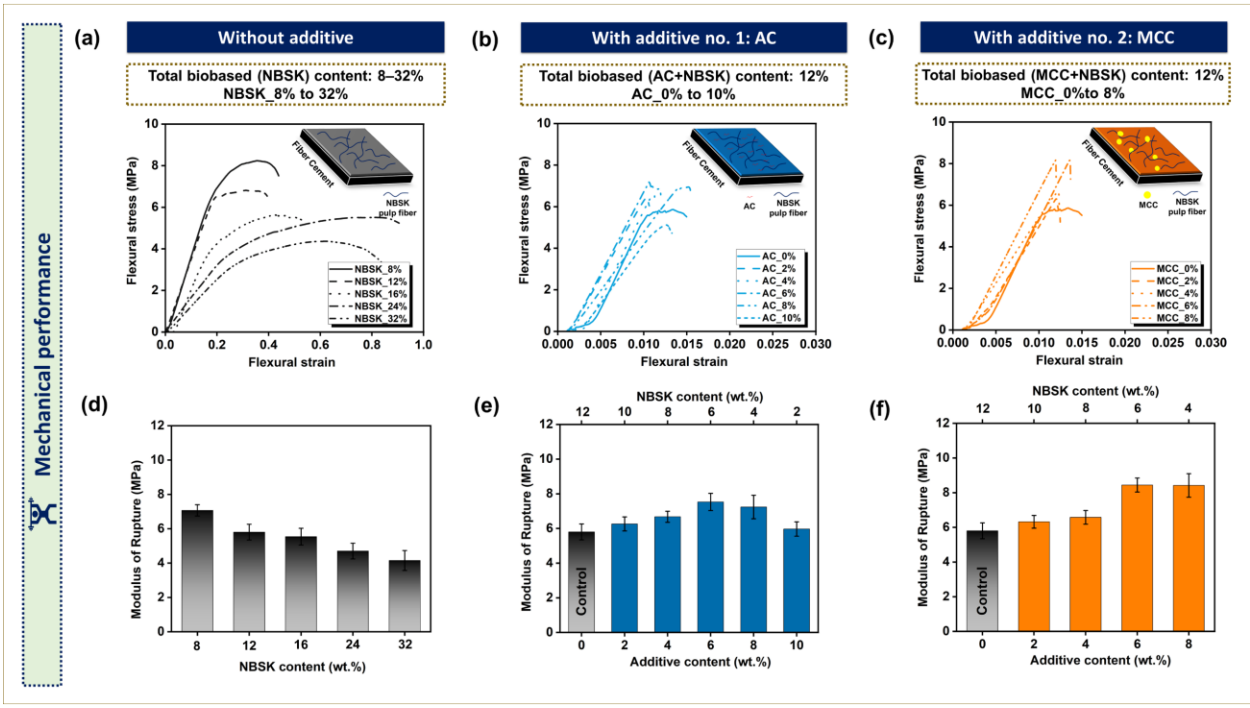

Figure 4.3 Mechanical characterization of the FC. Representative flexural stress-strain curves (a-c) and MOR bar charts (d-f) of cured (28 days) composites. Reinforcing (NBSK) fiber/additive content dependent stress-strain curves and MOR charts of FC slurry without additive, (a, d) NBSK with microcellulosic additive, (b,e) AC (combination 1: AC and NBSK), and (c, f) MCC (combination 2:MCC and NBSK). The "control sample" refers to a FC specimen without any additive ca. 12 wt.% NBSK fibers. FC with microcellulosic additives (AC and MCC), the fiber-to-additive content is varied in such way that the total biobased content kept at 12 wt.%.

Based on the MOR data (**Figure 4.3(d-f)**), it is our speculation that presence of sufficient amount of cellulosic additive (i.e., > 4 wt.% for AC) has an important role to play in maximizing the flexural strength, which would be governed by its morphology and size. In particularly for FC with AC, potential longer cracks are mitigated by the bridging effect of the high aspect-ratio NBSK fibers. Besides, AC can suppress the micro-scale cracks by bridging the micro-cracks. However, upon exceeding the limit, which is 10 wt.% in this case, MOR was decreased due to stress concentration within the span of the composite, compromising its flexibility [57]. However, we note that

the sufficient content of a particular additive will vary if any of the parameter in the formulation changes, hence, at this juncture, we believe there is still scope for new ideas (and evidence) to further understand the failure mechanism of microcellulosic additives, which is beyond the scope of this study.

FC with MCC exhibited brittle fracture (irrespective of content) as opposed to AC, with an increase in the peak strength and MOR. Smaller size and uniform shape characteristics of MCC (**see, Figure 4.1(d, g)** & **Figure C.2**) densifies the cement matrix by filling micro/nano scale voids present in the matrix. Hence, the composite becomes brittle. **Figure 4.3(f)** also illustrates MCC content dependent variation in the MOR. At first, it increased from 6.3MPa to 6.5 MPa (2–4wt.% of MCC) while exhibiting a sudden increase from 6.5 MPa to 8.3 MPa, then stabilized at 8.4 MPa (6–8 wt.% of MCC).

These results were similar to the results observed in recent studies with the addition of MCC on the strength of the geopolymer-OPC hybrid system [252]. The study revealed that the addition of MCC improved the 7-day strength, after which it was dropped due to the chemical degradation of MCC [252]. Likewise, in a study conducted by Souza *et al*., a combination of CNFs /MCC resulted in increasing the MOR (70 % increase at 0.075 wt.%) of the composite [274].

The mechanism of strength development in MCC (hydrophilic) could be also due to improved hydration (see **Figure C.5** for hydration product characterization). Prior studies with CNCs have shown such improvement in hydration, contributing to improved flexural strength of cement composites [57,243]. Their affinity towards water enables them to channel water from hydrated (pore solution) to unhydrated regions during cement hydration [57,243]. As such, the mechanism was termed as short circuit diffusion (SCD) [57].

Moreover, the observed consolidation of MOR values at 6 – 8 wt.% of MCC content as shown in **Figure 4.3(f)** is quite interesting. The reason could be that the effective MCC content that encounters cement particles, which modifies cement properties may have saturated at 6 wt.% of MCC content. Further addition of MCC to 8 wt.% might just function as excess MCC in the cement matrix, which increases the yield stress as observed in **Figure 4.2(f)** but with no further improvement in MOR. It is crucial to mention that increasing MCC content above 8 wt.%, the sample cracked during curing, which could be due to the increased water demand, poor workability, and drying shrinkage effect, to name a few (see**, Figure C.1**). This tells us that we do not need to employ an exceedingly high content of MCC to obtain improved mechanical properties.

We also compared our current results with our past work [243], were in we benchmarked our results with FC with CNCs [243] and a commercially available PCEs superplasticiser (see, **Table C.1** for details) [243]. Comparison of our current results with FC with PCEs, illuminated the beneficial role of microcellulosic additives on the mechanical performance (MOR) of FC. Thereby, once again iterating the potential of this low-cost cellulose based additives in replacing conventionally employed petrochemical based additives in cement/construction industry.

4.3.3.1 S/W analysis

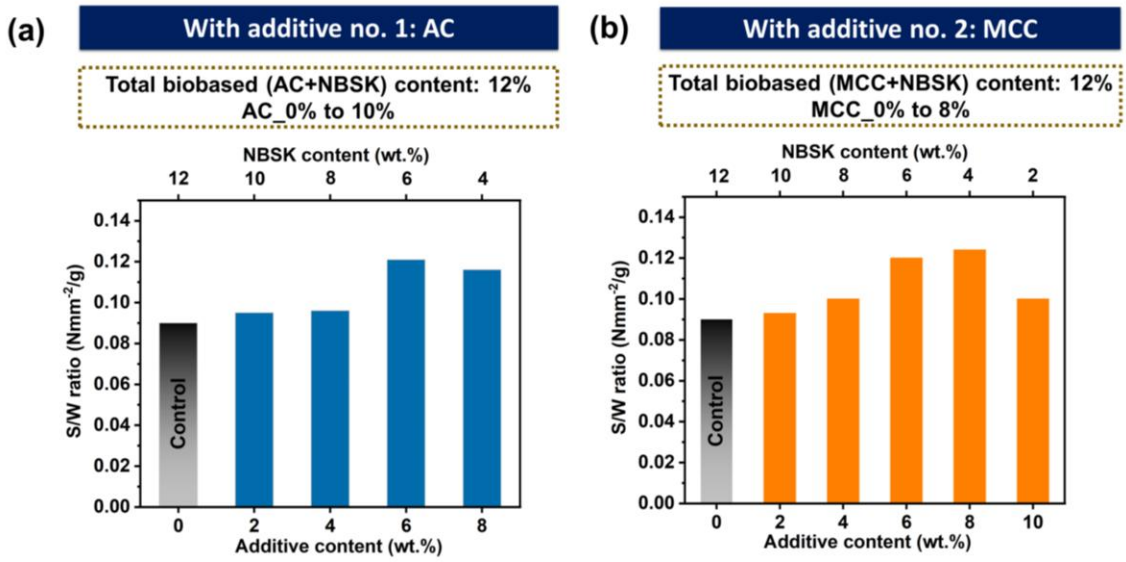

Figure 4.4 S/W ratio analysis of FC with microcellulosic additive (AC and MCC). (a) Combination 1 (AC and NBSK), (b) combination 2 (MCC and NBSK). Note that the ratio here refers to the mean MOR values (in MPa) obtained from the three-point bending test (vide supra) to the weight (g) of the specimen used for the mechanical characterization (Figure 4.3). At MCC content of 10 wt.%, the specimen cracked before curing (see, Figure C.1).

In **Figure 4.4(a,b)**, the addition of both AC/MCC in varied proportions with NBSK improved the strength-to-weight ratio of the FC. However, despite an increase in MOR observed with FC samples containing MCC (versus combination 2), the strength-to-weight ratio was within the same range (0.09–0.12) for FC samples containing both additives. This tells us that the addition of AC reduced the weight of the FC composites whereas the weight of the composite increased with the addition of MCC. This can be attributed to the morphological difference between MCC and AC **(Figure 4.1(c-f)** & **Figure C.2)** resulting in high packing density [275]. These results are encouraging from an application standpoint, where in high strength-to-weight ratio, plays a pivotal

role in various industries, e.g., construction [276] (promotes ease of handling of high-rise buildings, aerospace/automobile [277] (increased payload capacity) and also in specialized applications in challenging environments like offshore marine/construction works, where buoyancy is an important factor [278].

4.3.4 C/P analysis

Cost is one of the most important parameters that dictates the viability of commercialization at the industrial scale. Especially when it comes to the construction industry, the price of raw materials should be as low as possible, and scalability is a crucial aspect in raw material production process. Considering these prospects, we leveraged the findings of this study to conduct a simple cost/performance (C/P) analysis to deem which cellulose-based fiber/additive combination would be the most efficient, in terms of cost/performance (*vide infra*).

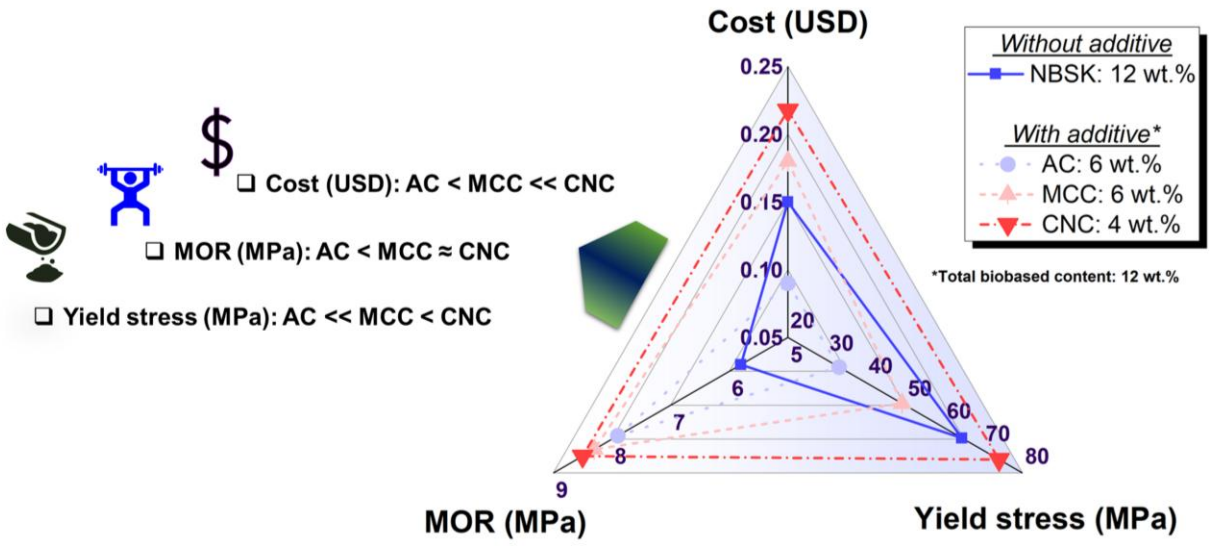

Figure 4.5 C/P analysis of FC with microcellulosic additives (AC and MCC). Spider chart depicting the C/P (performance corresponds to yield stress and MOR). Note that the cost here refers to the total reinforcement/additive cost — does not include the cost of other raw material and processing. In the Appendix, Table C. 3–Table C.4) has detailed background information.

Note that the raw material cost (**Table C.4**) is adapted from previous in-depth techno-economic analysis conducted to ascertain their cost of production. To simplify the analysis, we have chosen samples from both combinations (1 and 2) that exhibited the best mechanical properties **(Figure 4.3(e)** & **Figure 4.3(f))** and drawn a comparison with the control sample. To obtain a broader perspective, we considered the findings from our previous work on FC with the combination of CNCs and NBSK [243]. Now, to compare, we calculated the yield stress of the sample containing CNCs based on the strain amplitude method mentioned in the experimental section as well (see, **Table C.1**).

As shown in **Figure 4.5**, by supplementing the NBSK fibers in proportions with other crystalline cellulose-based additives the total cost of the reinforcement/additive in the system can be

reduced (40% cost reduction) with an increase in MOR by 34% when combination 1 is incorporated (vs control sample). On the other hand, in the case of combination 2 (MCC and NBSK), both cost (20%) and MOR (45%) increases (vs control). This means that the rise in the cost for adding MCC is possible to compensate by the improved mechanical performance in addition to its role in modifying the rheology of the FC slurry. The incorporation of both AC and MCC reduced the yield stress of the FC slurry (with a maximum reduction of 30% and 1.5%, respectively vs control).

With regards to CNCs-NBSK combination (previous research) [243], demonstrated a maximum increase in MOR by 46% (vs control), whereas the yield stress increased by 17% (vs control). However, the downside to CNCs is its cost of production; [244] though AC is majorly found in wood pulp [279], it can be extracted from inexpensive biomass sources, e.g., cotton [280] rendering its economic value proposition for mass production. Note that MCC could be derived from AC using mild acid hydrolysis [281] as mentioned in earlier sections. We also note that the maximum MOR values from **Figure 4.3(d-f)** suggest that there isn't a significant difference between the flexural strength of the FC when either CNCs or microcellulosic biomaterials (AC/MCC) is employed, suggesting that, even by incorporating cost-efficient additives, desirable mechanical properties is possible to achieve.

Finally, **Figure 4.5** summarises the comparison of the C/P of FC samples (based on our current study) using a spider chart. Ideally, the best C/P samples would exhibit low cost and high strength with optimum yield stress. High yield stress would mean that more energy (adds to the processing cost) would require to mix/pump the FC slurry. Therefore, based on these considerations, we infer from **Figure 4.5** that, combination 1 (AC and NBSK) exhibited the best C/P proposition, followed by combination 2 (MCC and NBSK) and CNCs-NBSK combination. Thus, this

analysis iterates the tremendous possibilities of employing additives from biomass sources (i.e., polysaccharides-based) to develop cost-efficient, lightweight, and high-density FC for a sustainable future.

4.4 Conclusion

Owing to the current environmental concerns, the exploration of renewable biomaterials is indeed crucial while maintaining low without sacrificing performance. In this research, we have explored the paradigms of microcellulosic biomaterials as additives and their influence on the rheo-mechanical properties of FC in which traditional materials of choice are either carbon-intensive or carcinogenic.

The key findings of this research listed as below:

- Rheological characterization revealed that the incorporation of both additive combination (1 and 2) led to a reduction in yield stress of the FC slurry. The maximum reduction (30%) was observed for combination 1(AC and NBSK), while combination 2 (MCC and NBSK), showed a marginal decrease (1.5%). These differences were attributed to additives physico-chemical and morphological features (e.g., particle shape and size), which modulate slurry flow behaviour by tuning water mobility and interparticle interactions.
- Mechanical characterization indicated a substantial improvement upon incorporating microcellulosic additives. Combination 1 yielded a 34% increase in flexural strength relative to the control, while combination 2 led to a 42% increase . In addition, AC enhanced ductility and post-cracking toughness, in contrast to MCC, which induced brittleness in the composite. This divergence is hypothesized to result from the larger, more microfibrillar structure

of AC, which may promote stronger fiber matrix bonding and facilitate more efficient load transfer, compared to smaller, more crystalline MCC.

- A correlation analysis revealed that both yield stress and MOR were independent of AC content, while both increased proportionally with higher MCC content. This finding underscores the need to consider not only additive type but also their content specific influence on the composite performance.
- Cost-to-performance evaluation showed that combination 1 achieved a 40% cost reduction while delivering a 34% improvement in flexural strength. Moreover, S/W analysis indicated that AC based systems could be employed to develop lightweight, high performance composites – potentially superior to those containing MCC,CNCs, or no additive.

Overall, this work demonstrates the feasibility of employing microcellulosic additives as sustainable cost-efficient modifiers for FC systems. Their ability to enhance both fresh-state rheology and hardened -state mechanical properties, while reducing material costs, offers a promising pathway for developing low carbon, bio-enhanced cementitious composites. These findings contribute to the broader goal of creating environmentally benign yet functional construction materials in alignment with UN SDGs.

Chapter 5: Engineering low-carbon FC with BC: understanding its physico-chemical properties and their impact on the composite performance and carbon footprint.

5.1 Introduction

Low-carbon building materials are essential in lowering the carbon footprint of construction industries, which predominantly use OPC. FC manufacturing utilizes natural fiber, e.g., wood-derived pulp fiber, and is mixed with OPC, various silica-based fillers, and a plasticizer prior to air or autoclave curing. Thus, recent research on high-density FC, silica-based fillers and petrochemical-derived plasticizers has been replaced with CNCs [243], and micro cellulosic additives [282]. However, these cellulosic additives have limited carbon sequestration potential owing to their lower filler content (in wt.%). While new cement manufacturing or matrix modification methods are being developed [283–285], OPC still dominates global cement production. Substituting OPC with a low-carbon biobased/biogenic material is an excellent material design strategy to reduce current generation of OPC, which contributes to ~8% of global CO_2 emissions under the UN SDGs (especially SDG 11) [286].

As a biogenic material, BC has garnered interest for various applications, one such example being the development of "eco-friendly" structural building materials [128]. BC is a carbon rich solid-waste, produced during biomass-bioenergy generation process via controlled pyrolysis (300−700 °C, with little or no oxygen) [130]. Its amorphous carbon structure renders low ratio of H/C (hydrogen to carbon) and O/C (oxygen to carbon), which is also observed for soot and carbon black [131]. Overall, the chemical composition and morphology of biomass depend on the biomass type and pyrolysis process parameters [134]. Nonetheless, as a carbon sequestering material, it

offers a pathway to remove CO_2 permanently from the atmosphere as it stores carbon in a stable chemical form. In other words, buildings made with BC become a permanent sink for carbon. For instance, it is estimated that the use of BC technology can eliminate up to about 1.7 – 3.7 PgCO2-eq of CO_2 [136] from the atmosphere – which iterates the immense possibility of utilizing BC in various applications to mitigate climate change.

In the case of FC, the materials chemistry of BC (particles size, chemical composition and pH) can play a crucial beyond green chemistry, such as improving hydration kinetics and modifying the rheo-mechanical properties. To date, the majority of BC applications as SCMs have focused on cement mortar and ultra-high-performance concrete. One of the noticeable effects of using BC as SCMs is that organic residues in biomass are converted into amorphous carbon (low H/C and O/C), which can delay cement hydration. This retardation extends handling time of the FC slurry and helps maintain workability, both of which are critical for achieving optimal mechanical performance in the final composite.

In a recent report from Roychand *et al*., it was found that BC from spent coffee grounds improved the compatibility between the cement matrix and the biogenic SCMs [127]. Dixit *et al*. explored the particle size effect of BC and examined its dual roles, acting as an internal curing agent and SCMs [137]. Note that manually ground BC was first presoaked in water prior to composite fabrication. Notably, at 5wt.% of finer (< 250 μm) BC particles, cement hydration was accelerated, and higher heat release was observed compared to coarser (>250 μm) ones. It was speculated that finer BC particles could adhere to the positively charged clinker phases owing to higher surface area, creating more nucleation points and thereby accelerating hydration. Furthermore, Gupta *et al*. [138] reported the particle size of BC plays a pivotal role in tuning the rheology (i.e.,

static yield stress) of cement paste using a ball milling (BM) method [138]. Interestingly, coarser BC particles (avg. particles size ≈ 45 – 50 μm & 2 vol.% addition) increased the static yield stress by 1.8 – 2.7 times compared with BM (avg. particles size: 10 – 18 μm).

In two separate studies by Choi *et al*. [139] and Gupta *et al*. [140], incorporation of BC at 5 wt.% (biomass sources: switchgrass, curing 28 days), and 2 vol.% (biomass sources: locally collected sawdust, curing: 7 days), resulted in compressive strength improvements of 10% and 40%, respectively. However, for non-structural application, Restuccia and Ferro [141] reported that at 0.8 wt.%, flexural strength of the cement mortar (curing: 28 days) increased by 30% [141]. Similar results were obtained by Kushmood *et al.,* at 0.2 & 0.080 wt.%, flexural strength (curing: 28 days) improved by 83% and 80%, respectively [142]. Regarding durability, Sirico *et al*. [128] evaluated the effect of wood waste derived BC on wet/dry strength of concrete – 5 wt.% addition contributed to 30% increase in compressive strength.

Although previous studies demonstrate the influence of BC on cement hydration, the underlying mechanisms remain poorly understood and require further investigation. Given BC's inherently heterogeneous morphology, understanding its particle size and shape is critical to interpreting its behaviour in cementitious matrices. Particle size affects surface area, dispersion, and the potential for filler or pozzolanic effects — factors that are especially important when BC is combined with other components such as reinforcing fibers in the cement matrix. Without adequate characterization of particle size and morphology, it becomes difficult to establish reliable structure–property relationships or optimize performance. While BC addition generally does not compromise mechanical performance, regardless of the biomass source, existing reports have not examined its role in fiber-reinforced systems.

In this research, we have utilized BC as a cement supplement to engineer low-carbon FC. It is hypothesized that BC, due to its porous structure and surface chemistry, can act as both a filler and a chemically active component in FC — enhancing workability, refining pore structure, and reducing the cement content, thereby lowering the GWP while maintaining or improving mechanical performance. Furthermore, to the best of our knowledge, this work is the first to integrate BC into cellulose pulp reinforced FC, establishing a fully biobased system wherein both the reinforcement and the binder modifier are derived from renewable biomass sources. A planetary ball milling method is employed to homogenize BC particle size. BC composition and FC performance are systematically evaluated through complementary techniques, including DIA to capture BC's heterogeneous morphology and rheo-mechanical characterization to assess composite behaviour. We believe this study will advance new avenues in "eco-friendly" building materials development for the low-carbon society, a key driver to reach our SDGs by 2050.

5.2 Material, fabrication and characterization methods

5.2.1 Raw materials

The cement (OPC, Type I) used for this research was procured from Lafarge, Canada, and was used as received. NBSK fibers employed for this research was procured from Canfor (Prince George Paper Mills), Canada. BC was procured from BC, Biocarbon, Canada (brand name: "Black Bear BC", (< 2mm) derived from wood forest residues). Unless otherwise specified, reverse osmosis (RO) water was used for this research. The pulp fibers and BC were subjected to preprocessing steps, which are mentioned in the fabrication section below. The composition and physical properties of the raw materials employed for this research are described in **Table A.1Table A.2**, **Table A. 9**, **Table A.11**).

5.2.2 Fabrication of FC

The first step in FC manufacturing involved refining the pulp fibers to induce fibrillation, which is critical for enhanced fiber-fiber bonding and to promote efficient load transfer. For this, 24 grams of oven dried NBSK were first soaked in 2 liters of deionised (DI) water (overnight, approximately 12 hours). The soaked pulp was then subjected to disintegration, followed by vacuum filtration to remove excess water. The filtered fibers at 10% consistency were then fed into NORAM PFI mill (Model : PPCT1008) and refined for 4500 revolutions of the PFI mill. The refining protocol mentioned was adopted from prior literature studies [287]. Note that for all samples prepared for this study, the refined NBSK fiber content was fixed at 8wt.%, serving as a baseline to systematically evaluate the influence of varying BC content on the FC performance.

BC, which is inherently heterogeneous (particle size, chemical composition, etc.), was subjected to a mechano-chemical process. A planetary ball milling device (PM 400, Retsch, Germany) was used utilizing the stainless-steel ball (bearing size: 6.35 mm in diameter, balls/powder ratio – 20:1) for 45 minutes. The ball milled (BM) BC (labeled as BC_BM, see **Table 5.1** for sample composition) was premixed with cement; NBSK fiber was then added to the mixing bowl under a constant water/binder ratio of 0.5. As a benchtop small-scale mixer, a kitchen-grade Techwood 6QT (power output: 800W) was used, operating at 600 rpm for 6 minutes. The mixing process was carried out at intermittent intervals (i.e., 2 minutes), It is an important step since scraping the cement pastes that adhere to the side and bottom of the mixing bowl, and these breaks ensure the mix is as homogeneous as possible (see **Figure D.1**, for detailed FC fabrication steps).

After the mixing process, the resulting FC slurry was transferred into a metallic mold of dimension (30 x 20 x 0.8 cm) and placed on a vibrating microplate shaker (from Thermo Fisher,

Canada) for 15 mins at 300 rpm for compaction. After compaction, the FC samples were air-cured for 28 days (demolded after 7 days and the samples were placed in a plastic bag). All the sample preparations were carried out at a temperature of 23±2 °C and at a relative humidity of 50±4 °C. For rheological characterization, slurry state samples were utilized and for mechanical, and micro-structural characterization, hardened state samples were utilized. The sample composition is illustrated in **Table 5.1**.

Table 5.1 List of fabricated FC tested to evaluate the rheo-mechanical properties. The sample nomenclature follows the format BC_BM-x, which corresponds to FC containing ball milled BC in varied proportions (i.e., 'x' wt.%). Note all samples contain 8 wt.% of refined NBSK fiber in them and only the binder content (i.e., cement/BC) is varied proportionally). Additionally, the FC constituents is also tabulated in (vol.%) and is used throughout the manuscript were applicable.

sample ID	**Binder**				**NBSK fiber**		**Water**	
	Cement		**BC**					
	wt.%	**vol.%**	**wt.%**	**vol.%**	**wt.%**	**vol.%**	**w/b**	**vol.%**
BC_BM-0 (Control)	100 (420 g)	53.38	0 (0 g)	0	8 (33.6 g)	8.18	0.5	38.44
BC_BM-2	98 (411.6 g)	49.44	2 (8.4 g)	6.51	8 (33.6 g)	7.73	0.5	36.32
BC_BM-4	96 (403.2 g)	45.90	4 (16.8 g)	12.35	8 (33.6 g)	7.32	0.5	34.43
BC_BM-6	94 (394.8 g)	42.71	6 (25.2 g)	17.61	8 (33.6 g)	6.96	0.5	32.72

BC_BM-8	92 (386.4 g)	39.83	8 (33.6 g)	22.37	8 (33.6 g)	6.63	0.5	31.17
BC_BM-10	90 (378 g)	37.21	10 (42 g)	26.70	8 (33.6 g)	6.33	0.5	29.77

From **Table 5.1**, it may be noted that the total binder mass (i.e. cement + BC) was held constants for all samples prepared for this study. The individual proportions of cement and BC was systematically varied for each sample, but the total binder mass remained constant (i.e.., when cement content was decreased ,BC content was increased to match the fixed binder mass). The weight percent of all other FC constituents such as NBSK fibers, water etc., were taken relative to the fixed binder mass. While we acknowledge that replacing cement in proportions with a lower density material such as BC, can affect the solid volume fraction – the use of fixed binder mass was done to maintain a fixed water / binder ratio. This isolates the specific effect of BC on the rheo-mechanical performance of FC. Such experimental design is commonly adopted in cement/composite research and ensures consistency and direct comparison of results [243,282,288].

5.2.3 Solid-state BC and FC characterization

5.2.3.1 Particle size analysis

To understand the effect of ball milling on the particle size of BC, DIA from Sympatec, GMBH, Germany (Model: QICPIC + RODOS) was used. The BC samples (both unmilled and

milled, approximately 3g), were fed (at a constant fed rate of 20%), into the vibrating dispenser of the DIA device. The open jet aerosol disperses particles that pass through an analysis chamber housed with a high-definition camera, that records and computes the shape and size characteristics of individual particles. The EQPC (equal area projection of circle) method was used by the device to calculate the particle size of the BC particles [289].

Compared to conventional laser diffraction system employed for analysing particle size, the QICPIC + RODOS configuration, provides a unique advantage of capturing real time 2D images of individual particles, allowing for simultaneous measurement of both particle shape and size. While laser diffraction based particle analysers, rely on light scattering patterns assuming a spherical shape geometry to generate particle size distribution, image based analysis, does not rely on any assumptions, rather uses fractal dimensions (based on the captured 2D image of the particle) to compute particle shape and size effectively [290]. This makes QICPIC +RODOS particularly useful for analysing irregularly shapes particles such as BC, where particle morphology significantly dictates the resulting composite material performance[290]. In addition to this, the high speed imaging in QICPIC system , enables detection of agglomerates and shape outliers possible, which help us to understand the particle size distribution more effectively, that laser diffraction may not be able to distinguish [290].

5.2.3.2 Raman spectroscopy

Raman spectrograph of the BC samples (before and after ball milling) were recorded through Invia Reflex confocal Raman microscope (Renishaw, UK). Two different laser excitation wavelengths were employed (532 nm & 785 nm) to facilitate the surface and bulk level characterization of both the BC samples. The Raman spectrum was recorded in the range of 1000 to 3000

cm^{-1}. Measurements were made at 5 different spots on the sample, and the respective spectra were averaged.

5.2.3.3 X-ray photoelectron spectroscopy (XPS)

To characterize the surface functional groups and state of the elemental composition of BC, an X-ray photoelectron spectrometer (Kratos AXIS Supra,UK) with a monochromatic Al Kα source (15 mA, 15 kV) was used. The work function of the instrument was calibrated to provide a binding energy (BE) of 83.96 eV for the line of metallic gold ($4f_{7/2}$), whereas the spectrometer dispersion was adjusted to deliver a BE of 932.62 eV for the line of metallic copper (Cu $2P_{3/2}$). Note that all the specimens were subjected to the Kratos charge neutralizer system to compensate for charge buildup, which is synonymous in the case of non-conducting materials. An analysis area of 300 x 700 μm and a pass energy of 160 eV were used for the surface scan. For the high-resolution scan, 300 x 700 μm and a pass energy of 2 eV were utilized. The aliphatic carbon 1_S signal, set to 284.8 eV, was used for the charge correction of all the spectra. Spectrum analyses were carried out using CasaXPS software (Version 2.3.26), and the graphs were plotted using OriginPro 2023 software.

5.2.3.4 Rheological characterization

The rheological characterization of FC slurry was analyzed using a rheometer from NE-TZSCH Malvern, UK (model: Kinexus ultra+). The measuring system was a 4-blade vane-in-cup. To impart consistency and to negate the effect/ interference of cement hydration reaction with the rheological results, all the tests were carried out at an early age of 8±1 min after the mixing process. Approximately 33 mL of the mixed FC slurry was utilized for this analysis.

The FC slurry (supplemented with various proportions of BC) was fed into the sample holder and was subjected to two different analyses (a) steady state viscometry (to understand the trends in viscosity with shear rate) and (b) strain amplitude sweep (to compute static and dynamic yield stress). The steady-state viscometry was carried out within a high-to-low shear rate regime (1000–0.01 S^{-1}) and a temperature of 25±1 °C.

To calculate the static yield stress, a strain amplitude sweep was performed, ranging from 0.01% to 1000%. For the dynamic yield stress, strain amplitude measurements were conducted in reverse order, from 1000% to 0.01%. Both tests were carried out on freshly prepared samples. The yield stress for both static and dynamic measurements was defined as the shear stress at the cross-over point between the elastic (G') and viscous (G") moduli.

5.2.3.5 Mechanical characterization

Mechanical characterization (three-point bending test) was done using a universal testing machine (UTM) from INSTRON, USA (model: 5969) to ascertain the flexural strength of BC-supplemented FC composite. From the casted samples, a rectangular block of size 19.5 x 4.5 x 0.8 cm was cut to perform the test. A crosshead speed of 10 mm/min was chosen for the test. All the tests were carried out on the 28th day of curing and the test itself was carried out as per ASTM C1185 standard requirements [291].

The flexural stress 'σ_f' and strain 'ϵ_f' during a three-point bending test can be calculated using the following formula:

$$\sigma_f = \frac{3PL}{2bd^2} \qquad \textbf{eq 5.1}$$

$$\epsilon_f = \frac{6Dd}{L^2} \qquad \textbf{eq 5.2}$$

Were, σ_f – flexural stress in a material under three point bending test, P – applied load (N), L- span length between supports (mm), b – specimen width (mm), d – specimen thickness (mm), ϵ_f - flexural strain in a material under three point bending test. D - mid-span deflection (mm) obtained from displacement data. For determining the MOR, the value of '*P'* used in the equation (1) corresponds to the maximum load recorded during the test [291].

5.2.3.6 Porous structure analysis

The surface area, pore volume, and pore size distribution of the BC sample (BC_RAW & BC_BM) were measured using a (BELSORP-mini II, high precision surface area and porosity analyzer) from Microtrac, USA using N_2 absorbate at –196 °C. All BC samples were degassed at 110°C under vacuum for 16 hours before conducting the test.

5.2.3.7 PXRD

To analyze the phases, present in the BC as well as to identify the phases of cement hydration products with the addition of BC, PXRD was performed using Bruker D-8 Advance X-ray diffractometer with a Bragg-Brentano configuration. The X-ray radiation (Cu $k\alpha_1$ & $k\alpha_2$, λ_0 =

1.54056 & 1.54439 nm) with a generator specification of 40 kv, 40 mA was used, and a nickel filter was utilized to cut down the $K\alpha_2$ radiation. The specification of the detector slit comprises of 0.6 mm divergent slit, 8 mm anti-scatter slit, 2.5°soller slit, and a LYNXEYE silicon strip detector was employed. The diffraction pattern was recorded from 5 – 90°, and a Bragg angle (2θ) with a step size of 0.03° was used to record the diffractograms.

For probing the phase ID of the BC samples, the sample as received from the vendor (in powdered form) was packed into the sample holder of the PXRD machine and analyzed. For probing the phase ID of cement hydration products with the addition of BC, the 28-day cured FC sample containing BC was subjected to mild mechanical pulverization using a 700 W, mixer from Black + Decker USA. The powdered sample was then sieved through a USA standard testing sieve (mesh size of MS 100, ASTM E-11), this was done to maximize the probability of probing the hydration products. The sieved samples were packed in the PXRD sample holder and analyzed for their hydration products.

5.2.3.8 Electron microscopy

To understand the structural changes in BC before and after ball milling (BM) and to probe the FC interface containing BC, an SEM from Field Emission Instrument (FEI) company, USA (model: Helios Nano Lab 650) was utilized. The BC samples (before and after ball milling) were coated with iridium (since the samples were non-conductive) using a sputter coater (Model: LEICA EM MED020, Germany) and analyzed for their microstructure [195]. To probe the FC interface containing BC, sample preparation involves carrying out the same steps as mentioned in the above section for phase ID of cement hydration products. The pulverized and sieved FC samples were coated using Iridium, as mentioned above, and analyzed for their microstructure.

5.2.3.9 Nuclear magnetic resonance (NMR) spectroscopy

To understand the effect of BC supplementation on the hydration (formation of C-S-H phases, quantification and probing the structure and environment of silicate species) of cement composites, a high resolution ^{29}Si SS (MAS) NMR was carried out using Avance III 400 NMR spectrometer (Bruker) at room temperature. The operation frequency was 400 MHz, and the spectra were recorded at single pulse excitation (with a pulse length of 3.8μs and a delay of 180s). The accumulation number for ^{29}Si was 384 scans. The 7 day cured cement samples (with and without BC, subjected to mild mechanical pulverization, powdered and sieved) were packed in Zirconium rotor (4mm diameter) and spun at a frequency of 10 KHz. Note that for the NMR analysis, samples were prepared without NBSK fibers to effectively study the influence of BC_BM on OPC hydration. The chemical shifts (ppm) were referenced against tetrakis(trimethyl sily) silane (-10.02 ppm and -135.7 ppm). The processing of the NMR data was carried out using Originpro 2023 software.

5.2.3.10 LCA and C/P analysis

A LCA study was carried out, following ISO 14040 & 14044 standards[292], to determine the environmental impact of utilizing BC as a biobased (in six different proportions) supplement to cement for FC manufacturing. Further details pertaining to this LCA study are provided as supplementary information.

The C/P analysis was carried out to evaluate the economic viability and scaling up potential of FC substituted with BC. The performance metric of interest chosen was specific strength of 28 day cured FC composites – obtained by diving the mean MOR to the density of the FC sample. Cost here refers to the total fabrication cost of the FC sample – which was estimated by summing

the cost of all processing steps (including raw material extraction and conversion), based on the system boundary use in LCA . Raw material costs were obtained from prior technoeconomic analysis and published market research (see **Figure D.6** & **Table D.5** –**Table D.6)** for detailed cost breakdown). Cost to performance ratio (CPR) was calculated by dividing the total FC fabrication cost to the specific strength of each sample with varied BC loading.

5.3 Results and discussion

5.3.1 Understanding the physicochemical properties of BC

5.3.1.1 Size and morphology

Figure 5.1 depicts the effect of ball milling on BC particle size distribution. It is observed from **Figure 5.1(a,b)** that BC_RAW and BC_BM exhibited a multimodal particle size distribution peak, with a VMD of 324 µm & 125 µm, respectively; a 61% reduction of VMD for BC_BM (*c.f.* **Table 5.2**). Interestingly, from the DIA images, ball milling contributed to break down of the bigger/coarser BC particles (~500 – 800 µm) into more finer particles. Such a reduction in particle size is vital when BC is used in conjunction with cement as a matrix material to ensure good compatibility. Additionally, the process of ball milling can also influence the shape of the BC particle – from **Figure D.2(a,b)**, it was observed that, larger BC particles (in the range of 600 - 800µm) tend to smoothen out and become more spherical upon balllming, thereby further enhancing the compatibility between two matrix materials.

Now to gain a deeper understanding on the morphology of BC particles, we transitioned from laser diffraction technique to electron microscopy. **Figure 5.1(c,d)** and **Figure 5.1(g,h)** depicts the SEM images of BC particles before and after ball milling. As seen from **Figure 5.1(c,d)**,

BC inherently consists of porous honeycomb like structure – when biomass undergoes pyrolysis, the organic components (such as cellulose, lignin etc.) present in them decomposes, whereas the cell structure (cell walls) often remain intact, giving rise to such structures [293] Due to this, the resulting BC particles tend to possess high surface area and pore volume, which makes them an ideal candidate as an additive/admixture for various applications.

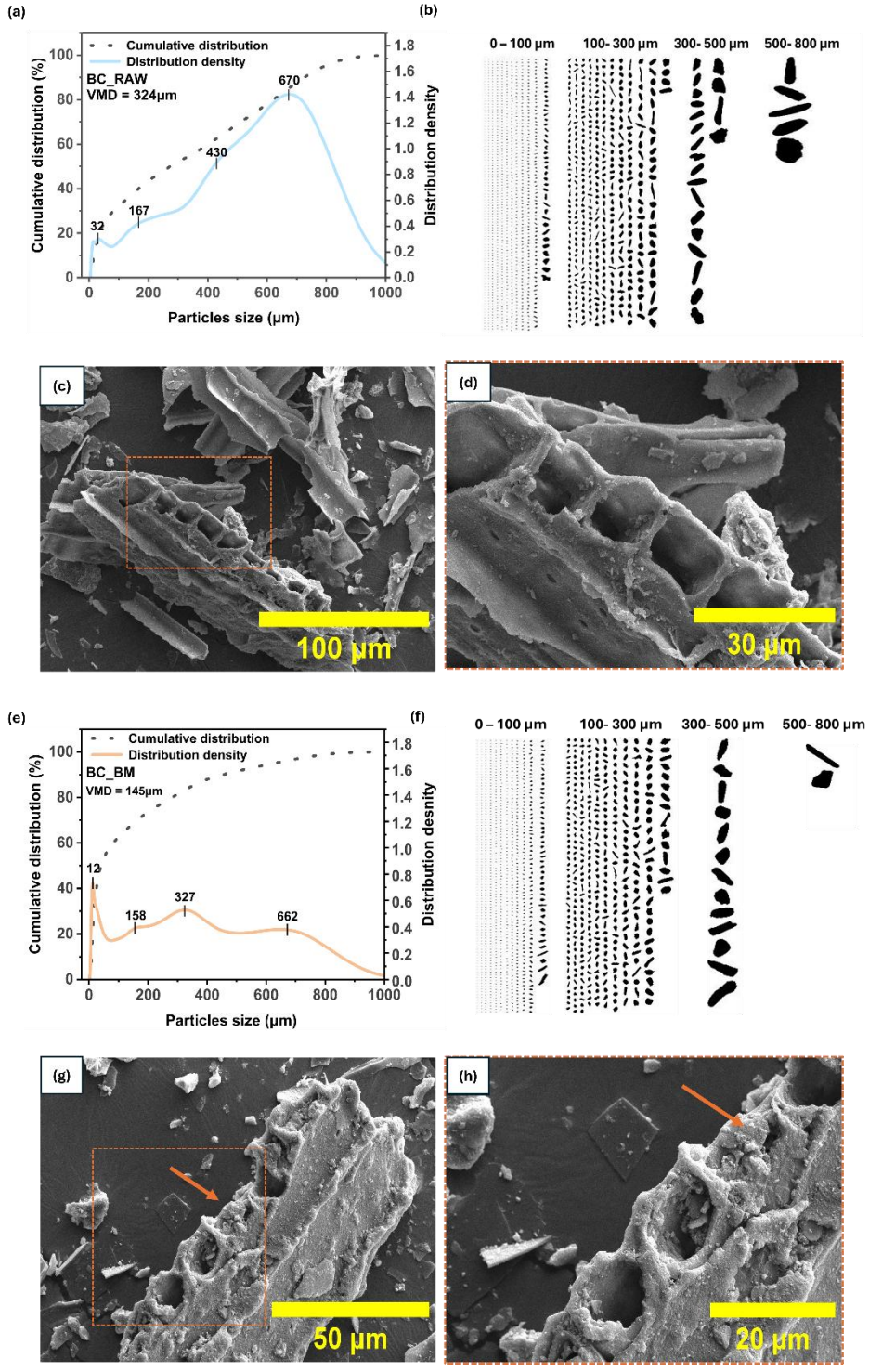

Figure 5.1 Particle size and morphological characterization of BC. Particle size distribution, DIA particle images and SEM micrographs of BC (a–d) before (BC_RAW) and (e–h) after ball milling (BC_BM). In (g and h), the orange arrow indicates the collapsed pore structure.

Now, in addition to reduction in particle size, the process of ball milling can have implications on the morphology of BC structure. As evidenced from **Figure 5.1(e,f)**, some of the larger pores present in the BC structure seemed to have collapsed upon ball milling (marked by the orange arrows, depicted in **Figure 5.1(g,h)**). At this juncture, it is critical to note that high energy milling can indeed jeopardise the structural integrity of BC samples, if the milling parameters were not optimised – therefore upon optimization we chose 45 minutes (milling time), 20:1(ball to powder ratio) and 400 RPM as optimum milling parameters for this study (it may be noted that similar milling parameters were widely employed to reduce the particle size of BC, whilst, keeping the structural integrity of BC intact [294].

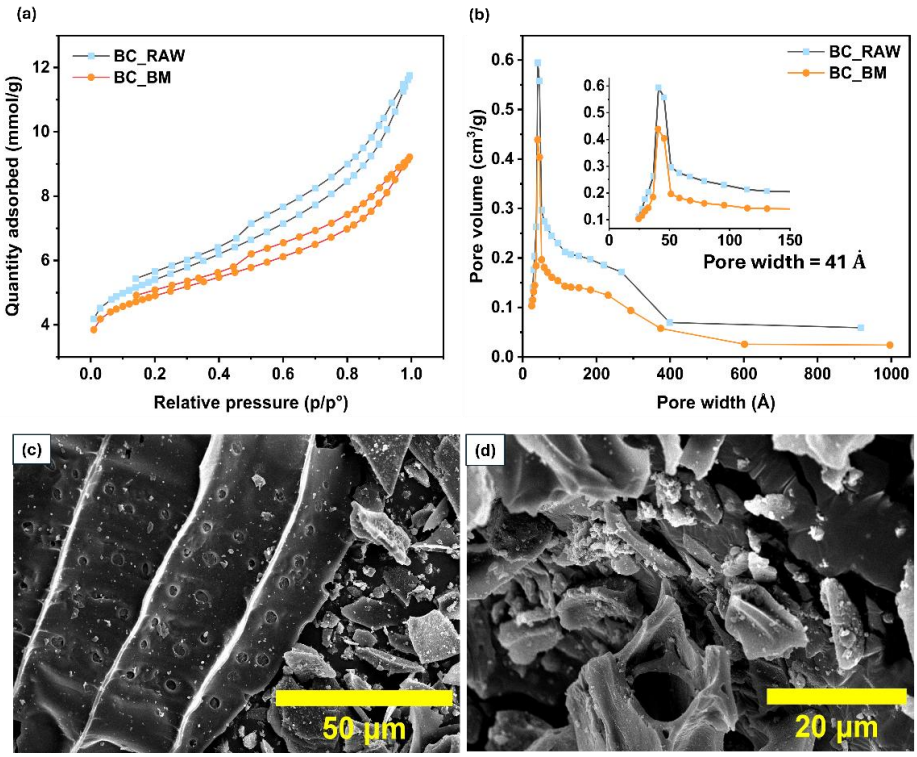

Figure 5.2 Pore characterization and visualization of BC. (a) N_2 adsorption–desorption isotherms and (b) BJH pore size distribution of BC before (BC_RAW) and after ball milling (BC_BM). (c–d) Representative SEM micrographs of BC after ball milling (BC_BM).

Table 5.2 Effect of ball milling on the physical properties of BC.

Sample	Volume mean diameter, VMD (μm)	BET surface area, S_{BET} (m^2/g)	Pore volume, v_p (cm^3/g)
BC_RAW	324	429.4541	0.408102
BC_BM	125	391.1352	0.320178

Additionally, process of ball milling can have ramifications with regards to the physical characteristics of BC such as surface area and porosity. **Figure 5.2(a,b)** depicts the N_2 adsorption desorption isotherm and BJH pore distribution plot of both the BC samples. It could be observed from the N_2 adsorption desorption isotherm, that, both BC samples contain a combination of micro, meso and macro pore and the BJH pore size distribution curve indicated a narrow monomodal distribution centered at the mesoporous region (pore width in the range of ~ 4.1 nm for both the samples). Since the adsorption - desorption occur predominantly in the high relative pressure domain, we can say that both our samples are considered to be mesoporous (2 – 50 nm) in nature (in majority) [295].

Table 5.2 also describes the BET surface area and pore volume of both BC samples - with the measured values in accordance with previously reported surface areas of high temperature pyrolyzed BC.[296] Now, For BC_BM (ball-milled) sample, a slight reduction in both BET surface area as well as the total pore volume by 9% and 21% respectively was observed, compared to BC_RAW sample, which could be attributed to the collapse of some of the BC pore structure (as evidenced in (**Figure 5.1(g,h)**). It may be noted that the BET surface area seemed to reduce slightly

with ball milling process, contrary to our expectation that surface area would increase upon ball milling. However, the contrary trend observed could be due to the reason that, as the milling proceeds, the BC particles may tend to smooth out or form aggregates/agglomerates, which may potentially block the pores from being filled by the gas molecules during the analysis, resulting in a slightly reduced surface area measurement. This result, in a way, highlight the limitation of BET techniques itself in characterizing the physical properties of materials with heterogeneous surface characteristics, especially when biobased materials are analysed – biobased materials often contain volatile organic compounds/ moisture trapped in the pores, which may result in incomplete degassing leading to under estimation of surface area. Despite this, majority of the pores (in the mesoporous region, i.e. between 2 – 50 nm) still remain intact (**Figure 5.2(c,d)**), which suggests that the ball milling (for 45 minutes, in this case) process does not significantly destroy the structural integrity of the BC samples.

Additionally, it is essential to understand the surface characteristics of the BC to effectively probe whether there is any reactivity of the functional groups when integrated with cement clinker phases, or the presence of elements such as silica, which may perhaps allow the BC to participate in pozzolanic activity with cement clinker phases [297].

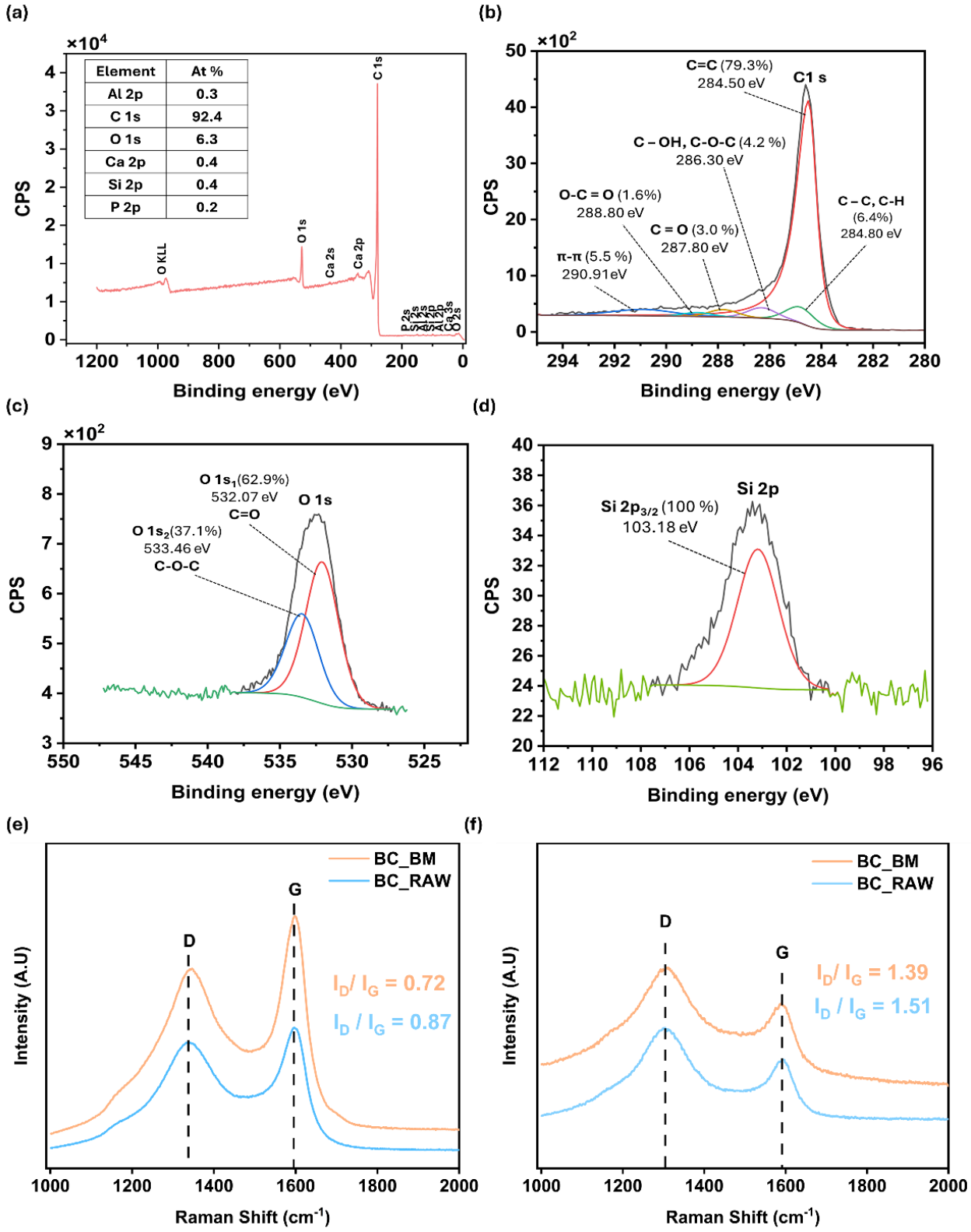
(a)
×10^4
CPS
Binding energy (eV)
Element | At %
Al 2p | 0.3
C 1s | 92.4
O 1s | 6.3
Ca 2p | 0.4
Si 2p | 0.4
P 2p | 0.2
O KLL
O 1s
Ca 2s
Ca 2p
C 1s
(b)
×10^2
C=C (79.3%)
284.50 eV
C1 s
C – OH, C-O-C (4.2 %)
286.30 eV
O-C = O (1.6%)
288.80 eV
C = O (3.0 %)
287.80 eV
π-π (5.5 %)
290.91eV
C – C, C-H
(6.4%)
284.80 eV
(c)
×10^2
O 1s1(62.9%)
532.07 eV
C=O
O 1s
O 1s2(37.1%)
533.46 eV
C-O-C
(d)
Si 2p
Si 2p3/2 (100 %)
103.18 eV
(e)
BC_BM
BC_RAW
D
G
ID/ IG = 0.72
ID / IG = 0.87
Intensity (A.U)
Raman Shift (cm-1)
(f)
BC_BM
BC_RAW
D
G
ID/ IG = 1.39
ID / IG = 1.51
Intensity (A.U)
Raman Shift (cm-1)

Figure 5.3 Surface characterization of BC. (a) Survey and (b–d) HR-XPS spectrum of raw BC and (e–f) Raman spectra of raw and ball milled BC under (e) 532 nm and (f) 785 nm laser excitation.

Figure 5.3(a) depicts the surface XPS scan, revealing that BC surface is primarily composed of C (with a relative proportion of 92.4%) and O (with a relative proportion of 6.3%) followed by trace amounts of Al , Ca , Si & P (at relative proportions of 0.3%, 0.4%, 0.4%, 0.2% respectively) [298].

Figure 5.3(b) depicts the high resolution deconvoluted XPS spectrograph of C1s. From **Figure 5.3(b)**, it can be inferred that surface chemistry of BC is composed of unsaturated C=C bond, polar C-OH and C-O-C, O-C=O, C=O bonds, saturated C-C & C-H bonds [298,299] and π-π satellite [298–300] in relative proportions of 79.3%,4.2%, 1.6%,3.0%,6.4% and 5.5% respectively. The carbon – carbon bonds make up the amorphous and graphitic structure of the BC, which is chemically stable under strong alkaline condition. However, the hydroxyl and carboxyl linkages could be reactive under alkaline cement matrix. Next from the deconvoluted spectrum of O1s as shown in **Figure 5.3(c)** depicts the high resolution deconvoluted spectrum, it can be inferred that $O1_{s1}$ (532.07 eV) and $O1_{s2}$ (533.46 eV) [301] with a relative proportion of 62.9% and 37.1%, respectively were predominantly part of carbonyl and ester groups, respectively. [298,302,303]. **Figure 5.3(d)** presents the high resolution spectrum of Si, and further in-detail deconvolution was not pursed as the proportions of silica present on the BC surface is low.

Since BC is a carbonaceous material, and ball milling can induce changes in its carbon structure, Raman spectroscopy was utilized to understand the effect of mechanochemistry [304]. From **Figure 5.3(e,f)**, two characteristics band appears at around 1354 cm^{-1} (referred to as the 'D' disorder/defect band) and around 1596 cm^{-1} respectively (referred to as the 'G' band which arises

due to the vibrations associated with the sp^2 hybridised carbon atom associated to the crystalline graphitic layer) [305,306]. The ratio of the intensities of 'D' and 'G' band can provide a measure of graphitization degree of the BC samples. If the 'I_D / I_G' ratio is smaller, indicates a better graphitization or ordering of the stacked graphitic chains in BC and a higher ratio is indicative of a less ordered graphitic carbon structure [304]. Two different laser excitation wavelengths of 532 nm and 785 nm were used to probe the graphitization degree. While 532 nm is efficient in probing the surface level characteristics of the BC sample, whereas employing 785 nm, will offer better penetration debt, thereby providing a better insight into the bulk level characteristics of the BC samples. From **Figure 5.3(e,f)**, for two different excitation wavelengths , the 'I_D / I_G' ratio is observed to be slightly smaller in magnitude for ball milled samples compared with raw BC samples, indicating that ball milling is effective in slightly improving the graphitization degree both at the surface level as well as at the bulk level of the BC sample.

Though degree of graphitization of BC may not directly have an influence in terms of the rheo-mechanical performance of FC based composites, however, higher graphitized BC may potentially have longer shelf life in the high alkaline environment of the cement matrix, which could prolong the composites overall performance.

5.3.2 Role of BC on the rheological properties of FC slurry

5.3.2.1 Static and dynamic yield stress analysis: implications on workability

Understanding the flow behaviour/characteristics of FC slurry is of great importance as it dictates the feasibility of FC fabrication process and its application. Cement pastes in general exhibits shear-thinning behaviour (see **Figure D.3**) and possess yield stress. Due to their thixotropic

nature, pastes typically exhibit two distinct yield points: static yield stress (τ_{static}) and dynamic yield stress ($\tau_{dynamic}$) [307]. 'τ_{static}' defines the transition from a solid to a liquid-like state. Whereas '$\tau_{dynamic}$' represents the transition from a liquid to a solid-like state [265]. In the context of the FC fabrication process, 'τ_{static}' provides a measure of flow initiation (crucial to mixing and consolidation of FC slurry) whereas '$\tau_{dynamic}$' becomes a critical parameter in maintaining the flow (useful in the case of pumping the mixed slurry). A variety of factors (such as type and nature of additive/ reinforcement/SCMs employed, their concentration & surface chemical characteristics can influence the magnitude of yield stress of the FC slurry. Therefore, it is essential that we understand the effect of BC and its influence on these critical rheological properties.

Moreover, cement, when encounters water, undergoes an exothermic reaction, leading to the formation of strength imparting hydration products such as C-S-H. This is a continuous, time-sensitive process, leading to ongoing structural evolution /networking in the FC slurry, which often complicates rheological measurements, particularly for long duration tests such as stress ramp or creep tests (which are commonly employed for computing thixotropy and yield stress of viscoelastic material in a rheometer), during the measurement period [38,264]. As a result, these methods often suffer from poor reproducibility and may mask subtle effects introduced by these additives, especially in systems undergoing active reactions [38].

To tackle these limitations, we adopted oscillatory strain amplitude sweep tests, a relatively short-duration method that allows us to study the viscoelastic behaviour of FC slurry, while ensuring minimal disruptions from ongoing hydration effects [260]. This method provides an insight into early-age microstructural transitions and yields both static and dynamic yield stress as well as provide direct measure of thixotropy of the FC slurry. The yield point is typically identified by the

crossover of G' and G"—the point at which the material transitions from an elastic (solid-like) to a viscous (liquid-like) behaviour [264]. The corresponding shear stress at is then taken as the yield stress value [264]. This method provides a direct method of computing yield stress, unlike conventionally used viscometry models (such as e.g., Bingham, Herschel–Bulkley), which are fitted to the steady state viscometry data (indirect method) to compute yield stress viscoelastic materials [308].

Another important factor that can influence the rheological measurement, especially while dealing with suspensions with high yield stress or fibrous content is the effect of wall slip and edge fracture [309,310]. To minimise these effects, we utilised vane-in-cup geometry – which is particularly useful for measuring the rheological properties of highly viscous samples compared to commonly employed parallel plate or concentric cylinder geometry. However, it may be noted that, the complex stress distribution in vane geometry is different from other geometries, therefore absolute comparison of yield stress values is only possible if the test parameters and test geometry employed are similar. Given these critical constraints in terms of model assumptions, test methods, geometric effects, thixotropy and continuous cement hydration – our focus is to understand how BC substitution affects the rheological properties of the FC slurry, within our well defined experimental framework [310]. Importantly the results obtained by employing these well defined protocols turned out to be consistent and reproducible, with varying BC content, offering valuable insights into the rheological characteristics of BC substituted FC slurry.

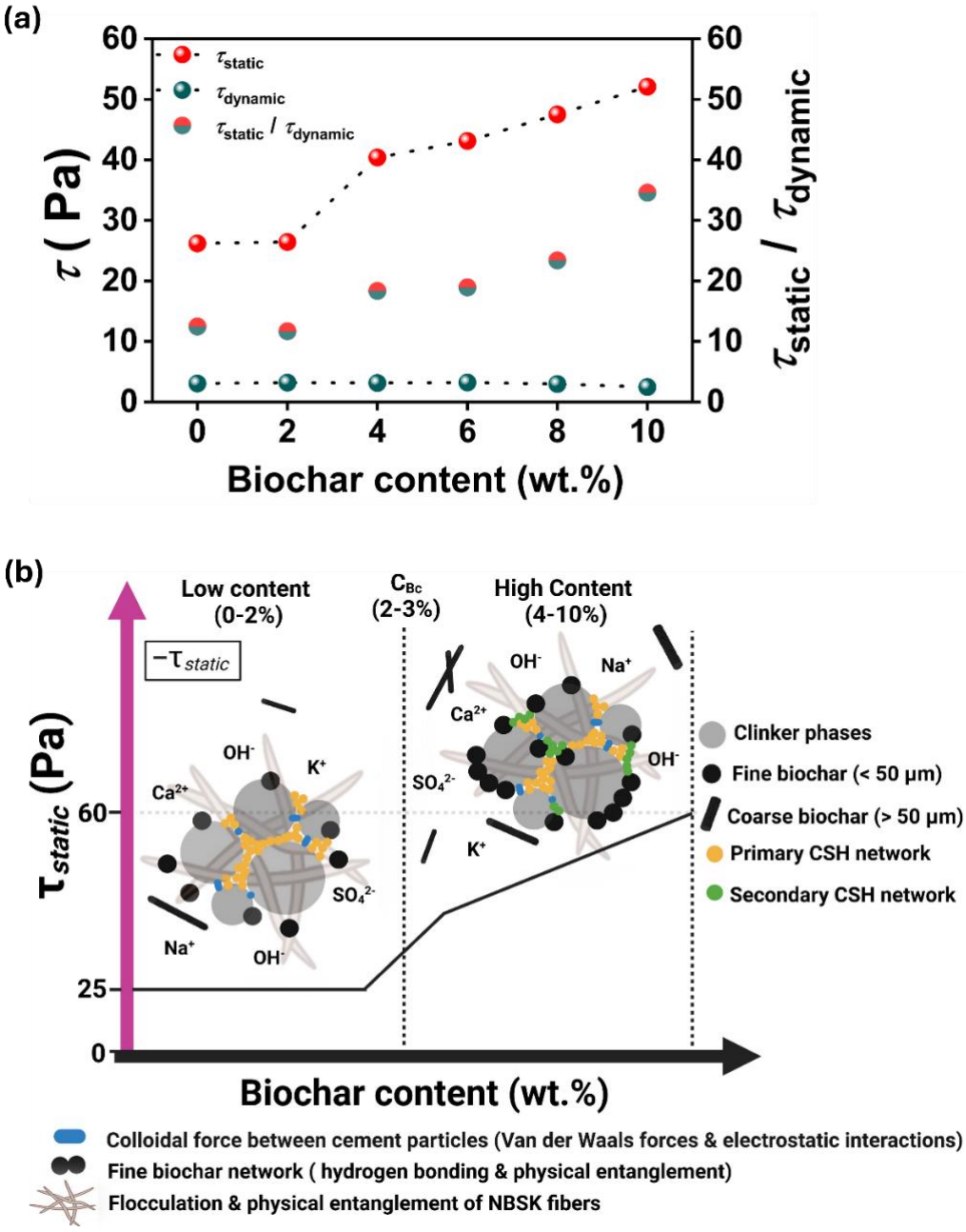

Figure 5.4 Yield stress analysis of FC slurry as a function of BC content. (a) variation of 'τ_static' & 'τ_dynamic' and 'τ_static/τ_dynamic' (b) proposed mechanism of 'τ_static' evolution with BC. Note that Ca^{2+} , Na^{+} , K^{+}, OH^{-} depicted in the Figure 5.4(b) represents the ions present in the cement paste pore solution.

As observed from **Figure 5.4(a)**, 'τ_{static}' of FC slurry is highly dependent on the concentration of BC. At low content (0-2) wt.%, 'τ_{static}' did not change significantly, indicating that the occurrence of yield stress is mostly associated with the colloidal force and electrostatic interaction between the cement clinker phases as well as due to the structural build of cement hydration products (C-S-H network formation, see **Figure 5.4(a,b)**)[311]. Note that, for computing 'τ_{static}' of cement paste, the sample was kept at rest after the mixing process). However additional factors also contribute to 'τ_{static}' development in this domain (see **Figure 5.4(a,b)**) such as - the presence of coarser BC (> 50μm), which may behave as rigid inclusions within the FC slurry or may act as interlocking structures causing resistance to flow [312]. Additionally, the presence of NBSK fibers in FC slurry (8wt.% in this case) can result in complex flocculation and physical entanglement (high aspect ratio fibers tend to entangle under shear) leading to agglomeration and increased resistance to flow (see **Figure 5.4(b)**) [313,314]. Therefore, a combination of these factors contributes to yield stress development; however, we believe that the role of BC is considered minimal in this domain. Now, as the BC concentration rises from (2 – 4) wt.%, the 'τ_{static}' increases rapidly (see **Figure 5.4(b)**). We refer to this concentration range as the critical BC concentration 'C_{BC}' , where an abrupt increase in 'τ_{static}' observed (the concentration range at which BC begins to significantly influence the rheology of FC paste). This rapid increase in 'τ_{static}' could be attributed to the network formation of BC within the FC slurry, causing resistance to flow [315]. During mixing, fine BC particles can buckle against one another (possibly through hydrogen bonding) and form bridges between cement particles via electrostatic interactions. The surface functional groups of fine BC (such as hydroxyl, carboxyl, and carbonyl—identified by XPS, see **Figure 5.3(a,d)**), may facilitate hydrogen bonding both between BC particles and with NBSK fibers, thereby promoting agglomeration and increasing resistance to flow.

At high BC concentration (4 –10 wt.%) the 'τ_{static}' showed a steady increase (reaching a maximum yield stress of 52.07 Pa at 10wt.% (98% increase vs control), see **Figure 5.4(a)**). This increase in 'τ_{static}' could be attributed to the combined effects of (a) BC particles forming networks that bridge cement particles, increasing flow (vide supra), and (b) BC particles adhering to cement particles during mixing, potentially acting as nucleation sites for OPC hydration products to develop [138] (referred to as secondary C-S-H in this study, see **Figure 5.4(b)**). This effect may be due to the high surface area, surface chemical functionality, and porous morphology of ball-milled BC (*Vide supra*), which not only provides additional nucleation sites but also helps retain moisture within the FC slurry. At this juncture it is important to note that, we do not completely exclude the possibility that secondary C-S-H may begin to form even at low BC dosages in FC slurry (as hydration is a time dependent phenomenon), however, based on our results, we propose that their contribution appears to be minimal at low BC dosages.

We propose that fine BC (< 50 μm) contributes primarily to nucleation effects, whereas coarse BC (> 50 μm) acts mainly as rigid, low-reactivity inclusions. Thus, in the low-loading regime, the proportion of fine BC largely determines the extent of secondary C-S-H formation. Additionally, water absorption by NBSK fibers and BC alters the w/b ratio, reducing free water in the slurry and raising yield stress [138]. However, BC can subsequently release stored water, maintaining moisture and promoting continued hydration [138]. This interplay likely explains the steady yield stress increase at high BC loadings. In contrast, it was observed from **Figure 5.4(a)** that '$\tau_{dynamic}$' remained largely independent of the BC content. This may be because network structure formation (as discussed earlier) is delayed under the continuous straining of oscillatory testing. Consequently, '$\tau_{dynamic}$' is primarily influenced by the network formation of the main

matrix material (cement, in this case). Even at higher concentrations, the addition of BC did not significantly affect the $\tau_{dynamic}$ of the cement slurry.

The '$\tau_{static}/\tau_{dynamic}$' ratio can be used as a direct measure of time dependent rheological properties such as thixotropy / rheopexy [203,307]. A ratio greater than unity suggests that the material is thixotropic in nature, meaning the slurry becomes less viscous under stress or strain and gradually recovers its viscosity once the stress is released. It is important to note that various factors can influence this behaviour, and cement pastes often transition from thixotropic to rheopectic behaviour over time. However, in our application — FC mixing and pumping, which typically occurs during the dormant phase of cement hydration — the cement paste predominantly exhibits thixotropic behaviour [39]. As shown in the **Figure 5.4(a)**, '$\tau_{static}/\tau_{dynamic}$' ratio for all BC concentrations is well above 1, indicating that all FC samples (including both BC-containing samples and the control) exhibit thixotropic behaviour. Since '$\tau_{dynamic}$' remained unaffected by BC content, the '$\tau_{static}/\tau_{dynamic}$' ratio mirrored the trend observed in the 'τ_{static}' evolution with varying BC concentrations. Specifically, the ratio remained relatively constant at 0 – 2 wt.% BC and increased significantly from 2 to 10 wt.%.

This behaviour could be attributed to the unique physical properties of BC—such as its surface area, porosity, and water absorption capacity—as discussed earlier. These characteristics promote the development of a stronger network structure within the slurry, enhancing its structural build-up over time. As the BC content increases, the FC samples exhibit a greater degree of thixotropy, meaning they can rebuild their internal structure more effectively after being disrupted. This could also indicate improved restructuring and faster breakdown/deflocculation of the FC

slurry constituents during shear and rapid recovery at rest [316]. Such enhanced thixotropic behaviour is particularly beneficial for processes like pumping and consolidation, where it is desirable for a material to maintain structural stability when at rest yet flow readily when subjected to stress.

5.3.3 Role of BC on the mechanical properties of FC

5.3.3.1 Flexural strength analysis and comparison with conventional carbon based materials

Since FC is designed for non-structural /load-bearing applications, flexural strength, vis a vis, MOR, is characterized to evaluate mechanical performance. In this section, we demonstrate the effect of BC content on the flexural strength of FC, with the derived MOR values compared against those of traditional carbon materials.

Figure 5.5(a) depicts the mechanical characteristics of the FC with BC pertaining to its bending behaviour, a crucial criterion for non-structural building materials, like 8 mm thick building facades. The stress-strain curves in **Figure 5.5(a)**, reveal a relative increase in peak strength with increasing BC content, accompanied by a reduction in post-peak deflection and post crack toughness. This suggests a decline in ductile behaviour and energy absorption after failure of the FC sample (vs control). Such behaviour is common in FC composites and similar trend was observed in our previous studies involving the inclusion of cellulosic nano/micro-particles in FC [243,282]. This transition could be attributed to the high packing density of ball milled BC particles, which provide a void filling effect. Densification of the cement matrix makes the FC stiffer

(more brittle) compared to the control, while enhancing the composites' ability to withstand higher mechanical loads and delay the initiation of microcracks [288,317].

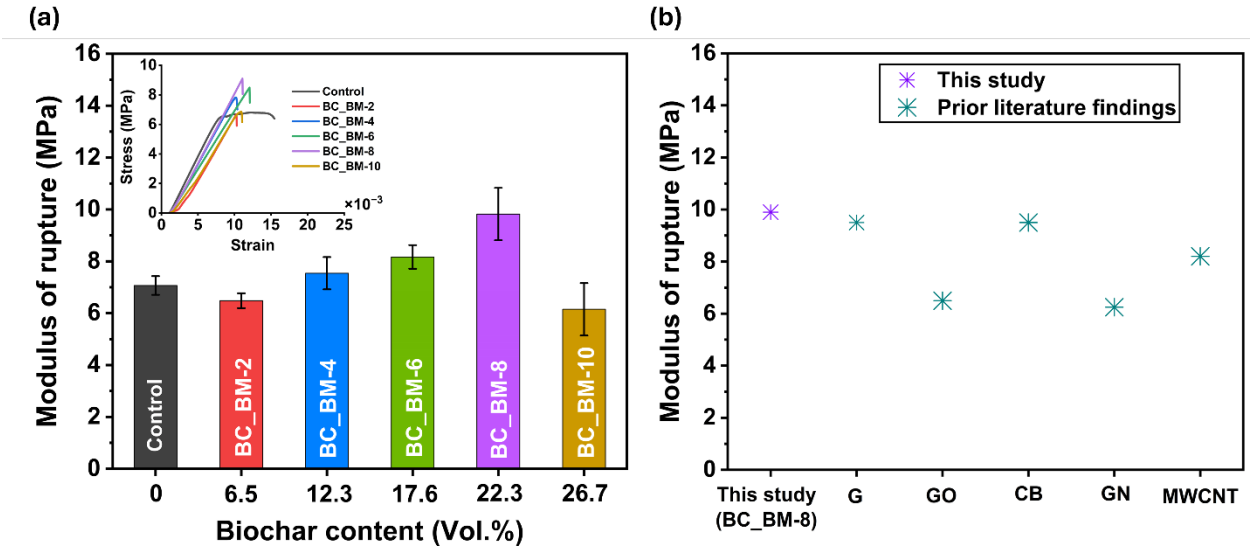

Figure 5.5 Mechanical characterization and performance evaluation of FC with BC as a function of BC content. (a) Stress – strain curves and calculated MOR, (b) MOR comparison between BC and traditional carbon materials as SCMs. In Figure 5.5(d), G, GO, CB, GN, and MWCNT stands for graphene, graphene oxide Carbon black, Graphene nanoparticles and multiwalled carbon nanotubes, respectively.[305–309] More details pertaining to composition, type of dispersant / superplasticizer employed for these materials are mentioned in Appendix D Table D.1. All tested composite was cured for 28d under ambient condition unless stated otherwise.

From **Figure 5.5(a)**, it may also be noted that the control FC exhibited improved strain hardening behaviour under flexural loading, characteristics of effective fiber bridging and crack resistance. However, despite the improvements observed w.r.t peak strength, the inclusion of even low dosage of BC (BC_BM-2) resulted in a significant reduction in post-peak deflection and post-crack toughness of the FC composite. Such a drastic change in the failure response of these FC composite due to flexural loading could be attributed to several reasons, such as matrix densifica-

tion [318], interfacial stress concentration from rigid/ agglomerates of BC [288], potential disruption of fiber-matrix bonding [317] or due to reduced fiber dispersion. Such effects are typical of FC composites and has been reported with the inclusion of fine fillers in FC such as nano silica [318], nano/micro cellulosic additives [243,282], matrix modifiers such as FA (which alter fracture behaviour by modifying the microstructure and interfacial properties) [317] and due to poor/heterogeneous dispersion of fine fillers / additives at extremely low or high loadings [319]. Thus, the observed shift reflects a loss of ductility and toughness due to microstructural and interfacial interactions, rather than a direct transition of failure mode (brittle fracture).

Further analysis of the stress-strain curves indicates that there is less room for the fibers to flex under load, limiting the load transfer, and thereby compromising the ductility of the composite. Note that fibers are tightly embedded (mechanical interlocking) in between the cement-BC matrix. So, as the BC and cement content are varied proportionally while keeping the NBSK fibers content constant, we believe that further optimization—particularly through adjusting fiber dosage (increasing the content of NBSK fibers) and by optimising BC loadings—could improve the composite's strain hardening behaviour. In this study fiber dosages were intentionally kept constant at 8 wt.% , following conventional loading practices adopted in FC research [243]. To this end, our prior work has shown that it is possible to counteract matrix densification and induce flexibility by carefully optimising fiber/additive loading in FC [282]. Although we have demonstrated this potential, further investigation with BC is beyond the scope of this study.

Figure 5.5(a) depicts the variation of MOR with BC content (0–10 wt.%), replacing OPC content in the matrix. Interestingly, at low BC content (i.e., 4 wt.%), MOR increased by 17% and

trend continued until 8 wt.%, reaching a maximum of 9.8 MPa (40% increase vs control). Interestingly, irrespective of BC replacement of cement, the calculated MOR has been higher than the pristine cement matrix (control) for all BC concentration (with an exception at 2wt.% where the MOR was maintained with that of control. This is because the incorporation of BC can have an impact on the packing density [137] while its polar surface chemistry and porous morphology can host nucleation sites favouring the ongoing hydration reactions [320]. In addition to this, the presence of NBSK fibers and BC can retain water, that is available during the mixing of FC slurry (affecting the overall w/b ratio of FC slurry) and release it over time as the FC cures. Such a phenomena affords unhydrated cement to hydrate over time, facilitating a mechanism termed as internal curing, resulting in strength development [137,139]. All these are crucial parts of strengthening mechanism, i.e., increase in peak strength as evidenced by the high MOR values. On the other hand, increasing the content of BC to 10 wt.%, the mean MOR reduced to 6.1 MPa from 9.8 MPa (54% reduction vs BC_BM-8). Such a trend has been reported in prior research where excessive BC in the matrix act as potential stress concentrators owing to the particle agglomeration,[140] especially when no surfactant or dispersing agent are added in the formulation. Another possible reason for such failures, especially at high BC dosages could be attributed to the inherent porous nature of BC that can lead to formation of potential air voids in the tensile plane of the cement composites compromising structural integrity as reported Khushnood *et al*. [142]. Moreover, the evolution of 'τ_{static}' trends observed in this study were in accordance with the MOR trends with increasing BC content (*vide supra*) – indicating a direct correlation with these important rheo-mechanical properties (see **Figure D.4(a,b)**).

Finally, from **Figure 5.5(b)**, MOR of FC with 8wt.% of BC (BC_BM-8) is compared against traditional carbon materials, such as Carbon Black (CB) [321], Graphene (G) [322], Graphene oxide (GO) [323], Graphene Nanoparticles (GN) [324] and MWCNT [325]. As exhibited in **Figure 5.5**(b), MOR of BC_BM-8 is significantly higher (34%, 36% and 17%, respectively) than GO [323], GN [324] and MWNT [325], respectively. However, MOR values of cement composites with G [322] and CB [321] were comparable with BC_BM-8. A crucial point to note that, the reported carbon materials require dispersing agents/surfactants/superplasticiser and fine/coarse aggregates to improve particle distribution, which in turn contribute to flexural strength development (see, **Table D.1** for more details) – not required for wood-derived BC. Mechanical treatment, i.e., ball milling was sufficient to homogenize the BC particle size resulting in improved mechanical performance.

5.3.4 Role of BC on the cement chemistry at FC interface

5.3.4.1 Microstructural and hydration products characterization: implications on hydration

The reaction of cement clinker phases with water results in the formation of hydrates (know as OPC hydration products) imparting strength to cement composite.[326] Now with the addition of BC as a SCMs, it's essential to understand how BC may influence the hydration product formation. Thus, PXRD (for phase ID) and solid-state NMR were employed to understand the structure and speciation of cement hydration products.

Figure 5.6(b) depicts the PXRD patterns of reference OPC (unhydrated) and 28 days cured (hydrated) FC sample containing BC (BC_BM-8). The composition (phase ID) of the cement

clinker phases present in OPC is depicted in the PXRD curves represented in **Figure 5.6(a)** and is adopted from our past study [243]. PXRD of (BC_BM-8) revealed distinct peak at $2\theta = 9^{\circ}$ & 35° for ettringite and $2\theta = 17^{\circ}$ for portlandite respectively, which were absent in the PXRD of OPC, confirming cement hydration [243]. Peaks at $2\theta = 16^{\circ}, 29^{\circ}, 32^{\circ}, 49^{\circ}$ confirmed the presence of C-S-H, hydration product in BC_BM-8 sample [218]. Peak overlap between ettringite and portlandite at $2\theta = 17^{\circ}$ & between C-S-H and calcite peaks at $2\theta = 29^{\circ}$ were observed [243]. No new crystalline phases beyond conventional OPC hydration products were detected.

Visual evidence from SEM suggests the possibility of OPC hydration products formation localised near BC particles - both within the cement-BC matrix **Figure 5.6(a,b)** and within the vicinity of BC particles, that is tightly embedded onto the NBSK fibers (**Figure 5.6(c)**), which maybe indicative of improved hydration. However, SEM analysis alone is inadequate to validate these claims and thus there is a need for advanced characterization. Importantly, the primary OPC hydration product (i.e., C-S-H) is semicrystalline in nature. PXRD technique, though efficient in detecting crystalline phases, is often limited to probe the structural characteristics of semicrystalline or amorphous phases effectively [327]. Additionally, occurrence of overlapped peak between OPC hydration products creates uncertainty in deciphering the appropriate peaks with confidence, making phase quantification difficult [328]. Therefore, the effect (if any) of BC on the structural conformation of silicates in C-S-H may not be effectively studied/quantified with the PXRD techniques.

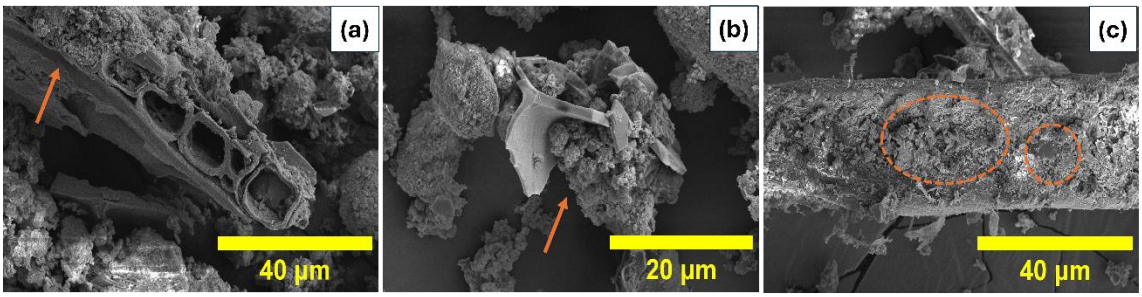

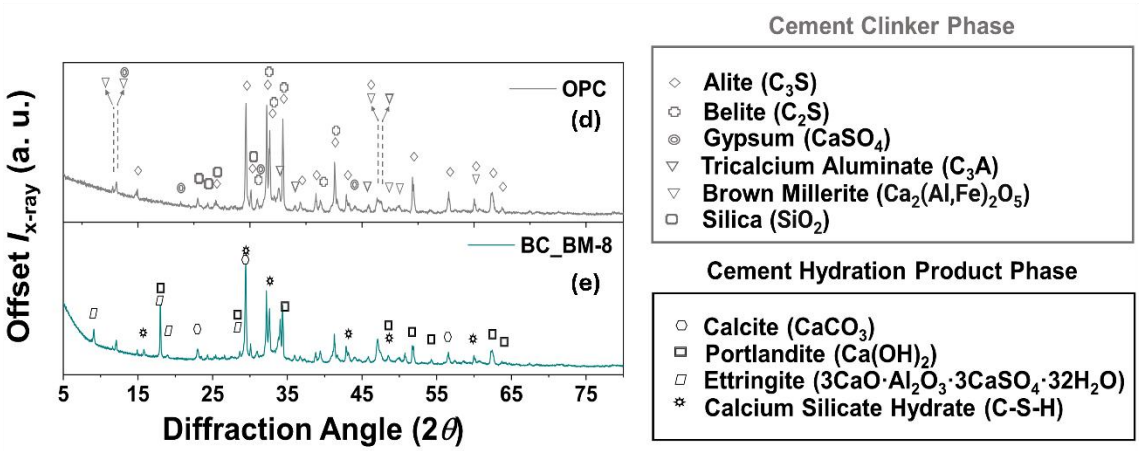

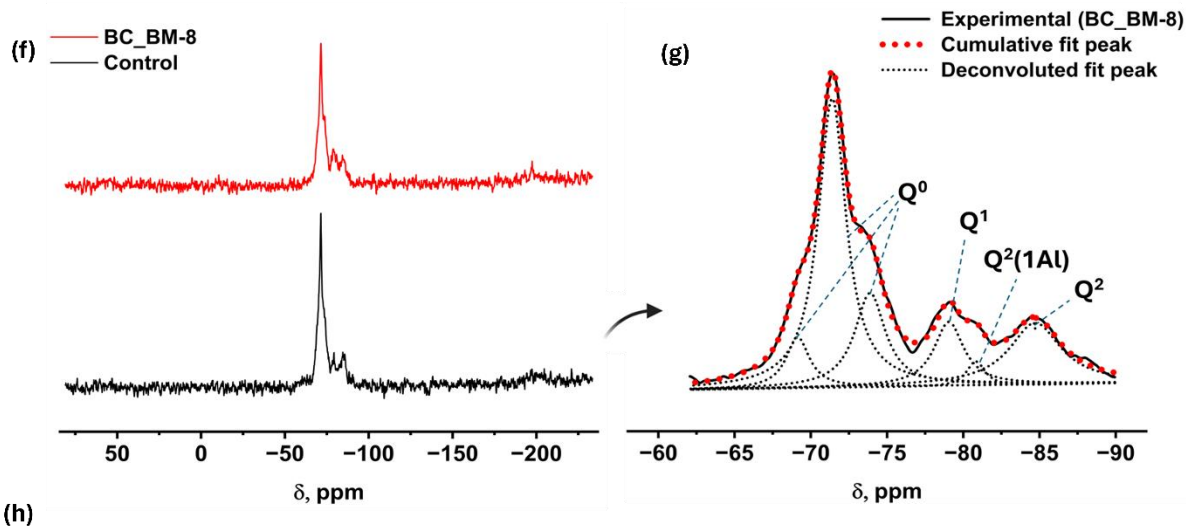

(h)

Sample	Content of Si atom (%)				Degree of hydration of silicate phases of Portland cement (%)
	Q^0	Q^1	$Q^2(1Al)$	Q^2	
Control	75.17127	6.98417	0.90929	16.9385	24.82873
BC_BM_8	70.35583	11.31873	1.77601	16.54943	29.64417

Figure 5.6 Microstructural and hydration product characterization of FC. (a-c) SEM micrographs of FC (BC_BM-8). In (a-b), the orange arrows indicate the growth of OPC hydration products on the BC surface, and in (c), the orange circle indicates the formation of possible hydration product at FC interface.(d-e) PXRD patterns of FC (BC_BM-8) and OPC as a reference. (f) Raw ^{29}Si MAS NMR spectrum of control and BC_BM-8 sample. (g) Deconvoluted ^{29}Si MAS NMR spectrum of BC_BM-8.(h) summary of spectral deconvolution results. Note that for NMR analysis, NBSK fibers were not employed to negate its effect on hydration products and 7 days curing was sufficient. The PXRD diffractogram of Raw BC is shown in Figure D.5.

^{29}Si MAS NMR has been widely used to study the silicate species (degree of hydration and polymerization) around C-S-H, which is the primary OPC hydration product, as discussed in the above sections.[329] The environment around silicate species (conformation of silicates) in ^{29}Si NMR is given by Q^n, where 'n' denotes the number of Si – O – Si linkages. Q^0 represents the isolated silicate species (Silicon oxygen tetrahedra) belonging to the unhydrated cement clinker phases such as di/tricalcium silicates (C_2S/C_3S) and has a chemical shift observed in the range (-68 to -76 ppm) [330,331]. Its important to not that Q^0 comprises of multiple resonances caused due to the presence of alite and belite phases in OPC, with resonance due to C_3S occurring at a higher chemical shift compared to C_2S [331]. This combined resonance results in broadening of the Q^0 peaks, therefore multiple peaks (at δ = -69.1, -71.3, -73.8 ppm) are assigned to deconvolute and quantify the Q^0 species (see **Figure 5.6(g)**).

Now, as OPC undergoes hydration, Q^1 (-76 to -82 ppm) and Q^2 (-82 to -88 ppm) species are formed at the expense of Q^0 species [332]. Therefore, tentative peaks at δ = -79 assigned to Q^1, δ = -80.8 ppm assigned to Q^2 (1 Al) & peak at δ = -84.7 ppm, assigned to Q^2 sites respectively [333]. Additionally prior research from Anderson *et al*. has conformed the resonance of Q^2 (1 Al) sites in corresponding to the aluminate phase in C_3A and C_4AF. In such as case, one of the two

bridging oxygen atoms is bonded to Al, and thereby replacing Si in the silicate tetrahedra [334]. Q^3 and Q^4 (higher polymerised silicate networks) are typically absent in OPC hydration product phases and their presence are often observed with the addition of silicate based admixtures in cement [335].

Figure 5.6(f) depicts the raw ^{29}Si MAS NMR spectrum of 7 day cured control and BC_BM-8 sample respectively. **Figure 5.6(g)** describes the deconvoluted spectrum of BC_BM-8 sample. From **Figure 5.6(b)**, characteristic peaks occurring at chemical shifts (*Vide supra*) are assigned to deconvolute and quantify the different silicate species. **Figure 5.6(h)** summarises the analysis results of deconvolution process for both samples. Now, by quantifying the amount of various silicate species formed, it is possible to quantify the degree of silicate hydration (α) using the formula $\alpha\ (\%) = 100 - Q^0\ (\%)$ [336]. It may be noted that cement curing and subsequent strength development, occur progressively in an interval of 7 days (for e.g., 7, 14, 21, 28 days). 7-day cured samples were used for NMR analysis, as hydration at this stage is advanced enough to identify distinct silicate species, without the complexity introduced by later stage silicate polymerisation.

From **Figure 5.6(h)**, it is inferred that for BC_BM-8 samples, a reduction in Q^0 species (vs control), followed by an increase in degree of hydration is observed (vs control). This suggests to us that the presence of BC may influence the silicate dissolution and favor/promote hydration reactions, indicating that isolated silicate species (Q^0 species), present in clinker phases converted into polymerised silicate species (Q^1, Q^2). Another observation made from **Figure 5.6** is that the amount of Q^1 species formed for BC_BM-8 is higher than (64% increase) that observed with control samples, where as the amount of Q^2 species formed is almost similar for both samples. This

suggests to us that, incorporation of BC may perhaps have altered the environment around silicate species, favouring the formation of fragmented polymerised silicate species (Q^1) compared to the formation of polymerised silicate networks (such as Q^2 species), especially during the early age curing (ie.,7 days in this case). This in a way validates the visual evidence (**Figure 5.6(a-c)**) that BC may have acted as nucleation points for additional precipitation of hydration products (referred to as secondary C-S-H in this case) to develop.

We allude this ability of BC to its physiochemical characteristics, especially surface chemical functionality. The inference derived from the high resolution deconvoluted XPS spectrum of C 1s and O1s, - indicate the presence of surface functional groups (in relatively high proportions) that is capable of being reactive with the cement clinker phases, in the high alkaline environment present in the cement matrix. Additionally, evidence from past studies have show that the presence of hydroxyl and carboxyl linkages in cement admixtures/ additive can form active nucleation sites which could promote the precipitation of early C-S-H [337,338]. This happens because the hydroxyl, carboxyl functional groups present in BC can potentially interact with calcium ions in cement pore solution (wet state while mixing) – which prompts the calcium ions to localise near hydroxyl groups. Simultaneously, silicate ions (from dissolved clinker phases) are also draw to the hydroxyl groups, thus facilitating a close interaction between calcium and silicate species, thereby promoting the formation of poorly crystalline C-S-H [337]. This early precipitation of C-S-H then act as anchoring points for this process to proceed further, and the corresponding binding of these C-S-H phases accumulates to form connected C-S-H networks (at the end of curing, typically after 28 days in an air cured system). Similar nucleating effects have been reported with other carbon based admixture such as graphene/ graphene oxide in cement systems [338].

5.3.5 Role of BC on CO_2 footprint and C/P of FC: balance between performance, cost and sustainability

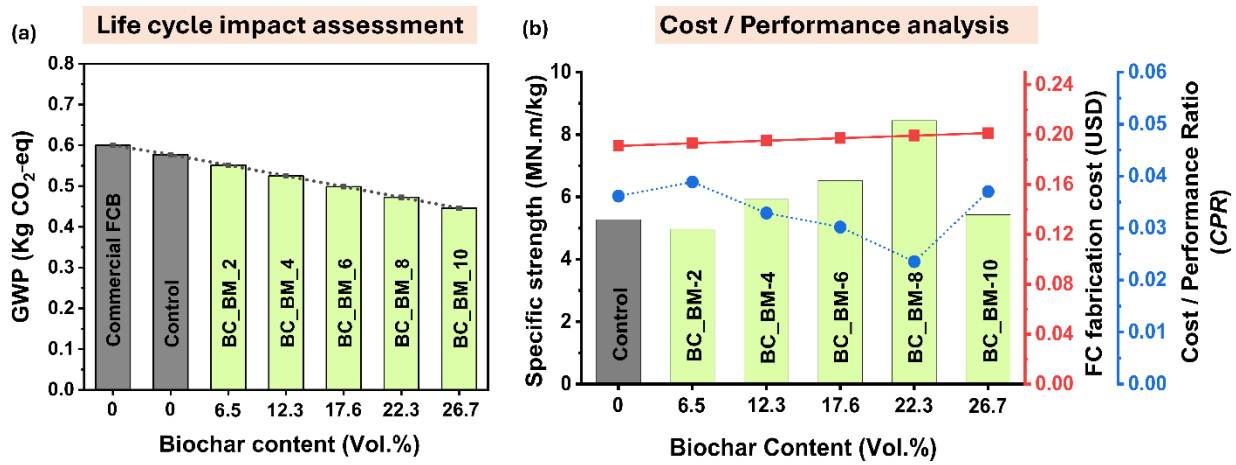

Figure 5.7 Role of BC on CO_2 Footprint and C/P of FC. (a) The accumulative GWP of different BC supplemented FC, calculated using EN 15804 A1:2020 assessment methodology, depicting the GWP impacts related to FC production (accounts for, raw material extraction, conversion and processing, core process involved in the FC fabrication process and the benefit of supplementing different proportion of BC as cement replacement). Note that the GWP results computed from this study were compared with those reported in a published LCA of a leading commercially available cellulose FC board manufacturer (refer Table D.4) and with control sample (BC_BM_0). Refer to ESI (Figure D.6, Table D.2 – Table D.3)) for further information regarding system boundary, functional unit and energy calculations. (b) C/P analysis of FC (performance refers to the specific strength of the FC (which is computed by taking the ratio of mean MOR (in MPa) to the density of FC (in kg/m3) and is compared against the total fabrication cost of FC (see Table D.5 – Table D.6) for background information regarding cost calculations). The CPR index is calculated by the ratio of FC fabrication cost (in USD) to the performance (i.e., specific strength (in MN.m/kg). To provide a quantitative understanding as to the volume occupied by BC (when supplemented in different proportions) in FC, the corresponding BC content is given in Vol%.

The environmental impact of replacing OPC with BC was evaluated using a cradle-to-gate life cycle impact assessment, and the resulting GWP (in kg CO_2eq) as an indication of GHG emissions. Results were compared against the control sample (100% cement) and with the reported GWP of commercial FC. From **Figure 5.7(a)**, it's observed that, with the substitution of BC (2 to 10 wt.%), the net GWP values decreased (from 0.577 to 0.4458 Kg CO_2-eq), leading to a reduction up to 22.8 % (vs control) and 24% (vs commercial FC) for 10wt.% supplementation of BC. This reduction could be attributed to the reduced cement content in the sample due to BC substitution (minor contributor), coupled with the enhanced carbon sequestration potential of the supplemented BC (major contributor). Additionally, from the performance point of view, it was observed from the rheo-mechanical study that, the sample with 8 wt.% addition of BC exhibited the best rheo-mechanical properties (vs control), which corresponds to 18.1% reduction in net GWP result (vs control). Moreover, the presence of cellulosic fibers (as reinforcement) adds to the carbon sequestration potential of our FC system (note that for simplicity of analysis, the carbon sequestration potential of cellulosic fibers is not considered for this study as all the samples contain an equal proportion of fibers). Thus, it can be inferred from this LCA study that the incorporation of BC can pave the way for nurturing strong yet low climate-impact sustainable FC.

Sustainability often comes with a trade-off – in terms of increasing the cost of the material, which could have a negative impact on the product's commercial market viability. Therefore, understanding the cost/performance (C/P) characteristics of FC is of utmost importance as we evaluate the practical implication of transitioning our lab scale product to industrial scale. Considering this, a basic C/P analysis was conducted with the results obtained from this study. Specific flexural strength of the fabricated FC was chosen as the performance metric of interest, compared against

its associated cost of fabrication (in USD). This parameter was chosen considering the importance of light-weight composites for non-structural applications (use as facades). Additionally, a CPR index has been introduced as a measure of the effectiveness of C/P of FC samples. This way, it is possible to gain a quantitate perspective as to how the performance metrics and cost varies with the introduction of BC in the FC system.

From the C/P analysis (**Figure 5.7(b)**), it can be observed that, the specific strength of FC increased with BC content (exception at 10wt.% - specific strength decreased, though slightly higher than control), indicating the potential of BC in reducing the overall density of the FC (ρ_{cement} = 1.44 g/cm^3 , whereas $\rho_{biochar}$ = 0.223 g/cm^3 coupled with its physical characteristics such as high surface area & porosity – enables less amount of BC particles to fill the FC matrix, which otherwise needs to be filled by dense cement particles). With regards to FC fabrication cost - increased linearly with BC substitution (with 8wt.% BC substitution - occupying 22.3 % by volume of FC, resulted in an increase in cost by 4.1% vs control). Despite this increase in FC fabrication cost, the CPR showed a decreasing trend (exception at 10wt.% due to poor mechanical performance) with the substitution of BC, iterating the enormous potential of developing economically viable - low-carbon- high performance (lightweight & high strength) building materials which could find possible application in high rise buildings, offshore systems where – light weight becomes a critical parameter.

5.4 Conclusion

This study delves into developing low-carbon – light weight high – strength FC comprising of cellulosic fibers (as a reinforcement) and wood derived BC in proportions as SCMs. The key findings from this study are as follows:

- Ball milling was found to significantly modify the surface characteristics of BC, thereby improving its compatibility with the cement matrix. Enhanced interfacial compatibility is critical for enabling uniform dispersion and better integration of BC within the composite, contributing to improved mechanical properties and material homogeneity
- Rheological characterization revealed that the static yield stress of FC slurry increased markedly with BC content (reaching a maximum of 52.07 Pa at 10wt.% BC content, exhibiting 98% increase vs control). This enhancement was attributed to :
  (a) Complex physicochemical interactions among BC, NBSK fibers, and cement particles, mediated by mechanisms such as flocculation, electrostatic forces, Van der Waals interactions, hydrogen bonding and fiber entanglement.
  (b) Structural buildup within the slurry driven by cement hydration and the formation of primary and secondary C-S-H networks, facilitated by the nucleating action of BC. Additionally, thixotropic properties improved with increasing BC content, suggesting better resilience to flow disturbances during FC processing. These rheological attributes are especially beneficial for operation such as mixing, pumping, and mold consolidation.
- Results from three point bending tests demonstrated a noticeable improvement in flexural strength, with an optimal substitution of 8wt.% BC (equivalent to 22.3% of the FC matrix)

yielding a 40% increase in MOR compared to control. However, the stress-strain curves indicated a reduction in post-peak deflection, suggesting a reduction in ductility and toughness with increasing BC content.

- Results from a combination of studies (XRD, SEM, ^{29}Si MAS NMR & XPS) indicated that BC plays an active role in influencing degree of hydration and microstructural evolution. The enhanced degree of hydration and matrix densification observed in BC containing systems were likely a consequence of both chemical contributions (e.g., surface functionality promoting hydration reactions) and physical effects (e.g., pore filling and nucleation). These mechanisms collectively contribute to improved mechanical integrity of the final composite.
- A cradle to gate LCA revealed that 8wt.% BC mixture (BC_BM-8) led to an 18% reduction in GWP compared to control mix. Although the integration of BC led to a modest 4.2% increase in fabrication cost, the enhanced cost to performance ratio offsets the added expense.

Overall, the findings from this study demonstrates that mechanochemically processed BC serves as a multifunctional additive that enhances the rheo-mechanical and microstructural properties of FC while significantly lowering their environmental impact, offering a viable pathway towards developing, high performance building materials.

Chapter 6: BC-enhanced low-carbon geopolymer binder: a new paradigm for fiber reinforced building materials with improved performance and sustainability.

6.1 Introduction

Cellulose FC has long been considered as a green and sustainable alternative to asbestos FC due to improved safety, biodegradability and environmental benefits without jeopardizing critical mechanical properties. However, the conventional use of OPC as the primary binder in cellulose FC remains highly carbon intensive, contributing to about 8% of the total anthropogenic CO_2 emissions [7]. To address this challenge, alternative low-carbon binders are being explored, including geopolymer systems. Geopolymers are inorganic, alumino-silicate materials formed through the reaction of alumino-silicate precursors with alkaline activators (e.g., blend of sodium hydroxide and sodium silicate / potassium hydroxide and potassium silicate) [149,150]. Unlike OPC, which produces CO_2 as a result of the calcination reaction in rotating kiln, binders for geopolymer systems are often procured /extracted from naturally occurring earth materials / obtained as industrial byproducts, thus requires less energy for its production - significantly reducing GHG emissions [6]. Additionally, geopolymer systems are known to exhibit superior strength (early age) and chemical stability compared to OPC counterpart.

Commonly used precursors in geopolymer binders include FA (byproduct of coal combustion in powerplant) [339,340], GBFS (waste byproduct from iron and steel production) [119] and SF (silicon metal/alloy byproduct) [341]. Over the years a variety of researchers studied the effect of

geopolymer system with these precursors for the development of low-carbon construction materials. It was observed that FA based geopolymer system exhibited superior strength / durability and chemical stability [342,343] (vs conventional OPC based concrete), whereas GBFS and SF based geopolymer systems are often reactive (facilitating pozzolanic activity, thereby densifying matrix, while reducing permeability) and are known for their early strength characteristics [344–347]. While these precursors offer sustainability benefits (valorization of industrial waste / by product), their availability is subject to fluctuations in industrial production, making their long-term supply chain uncertain (especially when competing against cement industry and its scale of production to meet the construction demand) [117–119,348].

On the other hand, MK, derived from the calcination of kaolinite clay, offers a more reliable and consistent alternative to other SCMs. Kaolinite clay is the most abundant clay mineral found on Earth's crust – making it easily accessible and scalable as a low-carbon binder [156]. While sourcing (open pit mining) and processing (calcination) of kaolinite do involve direct environmental impacts and energy usage, its production is not dependent on fossil fuel based industries (conventional SCMs are often produced as a byproduct of polluting/ declining industries [349]). Additionally, the production of MK is more standardized, leaving less compositional differences / batch to batch variations, ensuring consistent reactivity. This may not hold true for conventional SCMs, which often exhibit variability in chemical composition and reactivity. Over the years, a variety of researchers investigated the performance of MK based geopolymer systems and the results revealed superior compressive strength, chemical resistance, thermal stability and durability (resistance to free-thaw cycles) [123]. Despite these merits, key challenge exists, that prevents the widespread adoption of MK in geopolymer system – such as increased cost along with its

increased water demand (arising due to the physicochemical characteristics of MK). Increased water demand can adversely affect workability, curing kinetics and the hardened geopolymer properties. To address this issue, the incorporation of cellulosic pulp fibers offers a promising solution. Our prior research (detailed in **Chapter 3 & 5**) has extensively demonstrated these capabilities. Based on these insights, we believe that the integration of pulp fibers into the MK based geopolymer system could mitigate such challenges and enhance their practical applicability.

In parallel, BC, a carbon rich material produced as a result of biomass pyrolysis, has emerged as a promising partial substitute for OPC, which negates environmental and socio-economic impacts associated with clicker production [128]. Our prior study (**Chapter 5**) systematically investigated the impact of these substitutions and their positive ramifications on the FC rheo-mechanical performance and environmental impact. These benefits further inspire us to translate the use of BC as a partial substitute to MK (the precursor / binder) geopolymer system.

This approach not only aims to curb the CO_2 emissions but also enhances the overall sustainability of FC building materials by incorporating a blend of low-carbon binders in geopolymer systems. Emerging literature studies have begun to explore the co-utilization of BC with geopolymer precursors, although research remains limited. For instance, studies from Egodagamage *et al*. investigated the effects of three different BC (derived from sewage sludge from two different wastewater sources and from locally sources rice husk derived BC) - in a AAM/ geopolymer blend composed of GBFS, using sodium carbonate and sodium hydroxide as activator [350]. Results revealed that 2 wt.% rice husk BC (containing 10% Na_2O) imparted a 12.2 % increase 56-day compressive strength vs control (i.e. without BC) and reduced the workability and setting time by 10% and 28% respectively [350].

This performance enhancement was attributed to high reactive silica content in rice husk derived BC – contributing to improved geopolymerization [350]. Other studies have investigated BC in MK based systems. For e.g., Khamlue *et al*. examined the incorporation of coconut shell derived BC in MK – aluminum oxide geopolymer system (activated by a blend of: Na_2SiO_3 – 15M NaOH) and analyzed its microstructural effects [351]. Similarly, Piccolo *et al*. evaluated the effects of municipal incinerator bottom ash (IBA) as a partial replacement in MK based geopolymer system (activated by blend of Na_2SiO_3 – 8M NaOH), focusing on porosity, reaction mechanism and water absorption of these geopolymer systems. However, both studies primarily focused on microstructural characteristics and chemical interactions, with limited or no assessment of rheo-mechanical properties [352].

These findings highlight the growing interest in hybrid geopolymer binders that combine BC and aluminosilicate materials. However, there is limited research on their mechanical performance, particularly in systems reinforced with NBSK fibers. Mechanochemical processing using planetary ball milling was employed as a pre-mixing step to integrate the two different binder materials. In addition to mechanical characterization, in dept particle shape/size and morphological analysis of the premixed binder via DIA & SEM analysis and we employed PXRD analysis to phase ID and confirm the extent of geopolymerization reaction. Furthermore, a cradle to gate LCA to assess the environmental impact of utilizing these hybrid geopolymer binders. We believe that this study will pave the way for the next generation, low-carbon FC geopolymer that are both technically robust and environmentally sustainable, offering a scalable solution for green construction.

6.2 Material and methods

6.2.1 Raw materials

MK used in this study was procured from Advanced Cement Technologies (ATC), USA (brand name: Powerpozz™). BC and pulp fibers employed for this study remained same as those employed in the previous section (see **Table A. 9**). Sodium silicate solution and sodium hydroxide pellets used for this were procured from Sigma Aldrich, Canada. Unless otherwise specified, DI water was used for this study. The physicochemical properties of all the raw materials employed for this research are mentioned in **Table A.12Table A.13)** & **Figure E.1**.

6.2.2 Fabrication of FR-BEMG

As indicated in **Figure 6.1**, the first step involved in fabricating FR_BEMG is to combine both binder components that are morphologically and compositionally distinct.

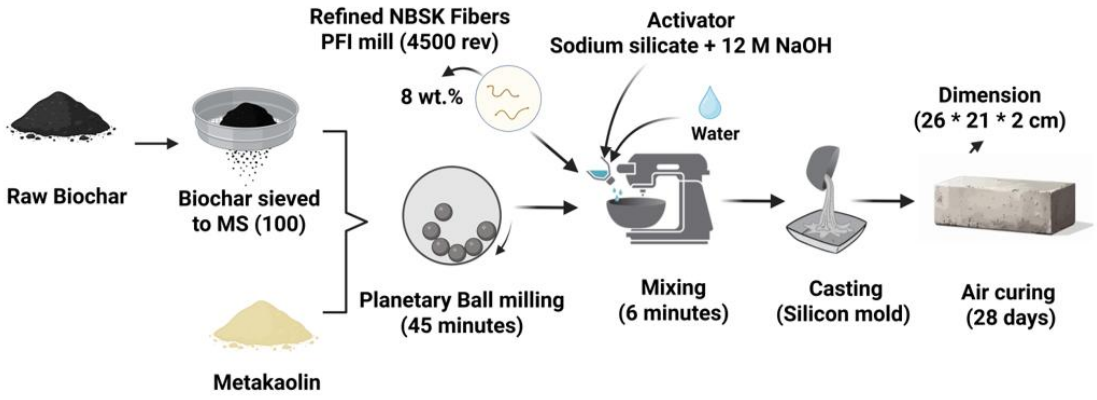

Figure 6.1 Schematic representation depicting the key steps involved in the fabrication of FR_BEMG

The BC (mixture of coarse and fine, irregularly shaped particles) was first sieved using a Canadian Standard Sieve (MS 100) to ensure size compatibility with MK (which has a uniform

particle shape/size). The sieved BC, along with MK (used as received) were then loaded into metallic jar at appropriate proportions and mixed using planetary ball milling technique (following the same milling parameters outlined in **Chapter 4**).

Next step involves preparing the activator, that is added at the processing stage of FC to initiate the geopolymer reactions. The activator used for this study involves a blend of sodium silicate and 12 Molar NaOH solution mixed at a constant activator ratio of 1.14 and then added to the binder at an activator/ binder ratio of 0.5 for all samples (the activator type and their appropriate ratio used were selected based on relevant literature in geopolymer research and further optimized through trial and error to achieve a stable and workable composition for this study) [353]. After this, the binder – activator mix along with refined pulp fibers (see section **5.2.2** for refining protocols) were transferred into a mixing bowl using a kitchen-grade Techwood 6QT (power output: 800W), operating at 600 rpm for 6 minutes (as shown in **Figure 6.1**).

Note that additional water was added during the mixing process for some samples so as to maintain the slurry consistency. After mixing, the slurry was transferred onto a silicon mold (of dimension 26*21*2 cm), compacted using a vibrating shaker and air cured for 54 days. Note that while the samples were curing, a wet burlap/hessian cloth was placed over the sample. This was done to maintain moisture over time and to support optimal reaction condition and prevent premature / early age cracking. The sample composition used for this research is mentioned in **Table 6.1**.

Table 6.1 Mix design of all the geopolymer samples prepared in this study.

Binder	Activator	Refined	Extra

MK		BC		Sodium silicate solution		Sodium hydroxide (12 Molar)		NBSK fiber		Extra water	
Wt. %	**Vol. %**	**Wt. %**	**Vol. %**	**ml**	**Vol. %**	**ml**	**Vol. %**	**Wt. %**	**Vol. %**	**ml**	**Vol. %**
100 (150 g)	86.18	0	0	28.7	5.8	23.6	4.77	8 (12 g)	3.22	-	-
98 (147 g)	83.62	2 (3 g)	2.6	28.7	5.75	23.6	4.73	8 (12 g)	3.19	-	-
96 (144 g)	80.63	4 (6 g)	5.3	28.7	5.66	23.6	4.65	8 (12 g)	3.14	3	0.59
94 (141 g)	78.19	6 (9 g)	7.8	28.7	5.60	23.6	4.61	8 (12 g)	3.11	3	0.58
92 (138 g)	75.65	8 (12 g)	10.3	28.7	5.44	23.6	4.55	8 (12 g)	3.07	4	0.77
90 (135 g)	73.16	10 (15 g)	12.8	28.7	5.48	23.6	4.50	8 (12 g)	3.04	5	0.95

6.2.3 Particle shape / size analysis

To understand the effectiveness of different mixing techniques on particle shape/ size characteristics of MK-BC blends, a comparative study was conducted using conventional hand mixing and mechanochemical ball milling. A higher concentration of BC was used in this blend (10 wt.%) to evaluate potential challenges in combing these two fundamentally different particles together (such as possible agglomeration, etc.). This approach provides a measure of mixing efficiency and its implication on the microstructure of the binder material. For the hand mixed samples, both MK and BC were combined in predetermined ratios (MK – 90 wt.% an BC – 10 wt.%) and manually mixed using a spatula in a petri dish for 3 minutes until visual consistency was achieved. Whereas for the ball milled samples, samples with the same ratios were placed into the planetary ball milling jar and premixed under ideal milling conditions (refer to section **5.2.2**). Once the mixing process is complete, both the samples were analysed using a DIA from Sympatec, GMBH, Germany (Model: QICPIC + RODOS). Measurement settings and processing algorithms were kept consistent with those previously described in (**Chapter 4 & 5**).

6.2.4 Morphological analysis

To complement the particle shape/size analysis obtained through DIA, SEM from Field Emission Instrument (FEI) company, USA (model: Helios Nano Lab 650) was employed to further examine the morphological characteristics of different mixing techniques of hybrid binder blend (MK + BC). The samples probed for SEM was same as those probed by DIA. Due to the nonconductive nature of the samples, the powdered samples were coated using iridium using a sputter coater (Model: LEICA EM MED020, Germany) and analyzed for their microstructure [195].

6.2.5 Mechanical characterization

The mechanical performance (flexural strength) of FR_BEMG was evaluated by three point bending test using a universal testing machine from Instron, USA (model: Instron 5969). The samples were air cured for 54 days prior to testing and the tests were carried out in accordance with ASTM C348[354], at a loading rate of 10 mm/min. This loading rate was chosen to draw a comparison with previous studies (**Chapter 3 & 4**) that utilised similar conditions for FC. Note that the specimens were tested in their original cast dimensions, with no additional cutting / trimming required.

6.2.6 Microstructural characterization

Microstructural characterization via Powder X-Ray Diffraction (PXRD) using Bruker D-8 Advance X-ray diffractometer (with a Bragg-Brentano configuration) was carried out to confirm the occurrence of geopolymerization reaction and to probe the effect of BC on the geopolymerization of FR-BEMG. The measurement parameters employed were the same as those described in **Chapter 5**. The 54 day air cured FR-BEMG samples were subjected mild mechanical pulverisation, followed by sieving (following the same procedure mentioned in **Chapter 5**). The powdered and sieved FR-BEMG samples were analysed for their microstructure.

6.3 LCA

A cradle to gate LCA study was carried out in accordance with ISO 14040 and ISO 14044 standards [292], to evaluate the environmental impact of fabricating FR-BEMG. The assessment involves quantifying the potential benefits of incorporating wood -derived BC as a partial replacement of MK across six different substitution levels. The functional unit of this study was defined

as 0.05 $m^2$of cured FR-BEMG panel with a target thickness of 2 cm, representing a standardised volume of material that reflects the dimensions of the laboratory fabricated samples. All relevant foreground data, including raw material extraction and conversion, core processes involved – were derived based on the experimental procedures detailed in system boundary (see **Figure 6.6(a)**) . Background data for raw materials (binder + activator) and electricity were sourced from the ecoinvent v3.8 database and the LCA modeling was performed using OpenLCA software. The primary impact category assessed was GWP. The energy consumption associated with core processes, raw material processing was assumed to be consistent with the values described in **Chapter 5**, (please refer to **Appendix D Figure D.6** & **Table D.2**, **Table D.4**) for more details). The sequestration potential of the BC employed in this study was assumed to be the same as that used in **Chapter 5**, based on the same production process and material source. The underlying assumptions and justifications for this values are detailed in **Appendix D**, **Figure D.6** & **Table D.2**, **Table D.4).**

6.4 Results and Discussion

6.4.1 Particle shape/ size and morphological characterization

The shape and size of the geopolymer precursors / binder plays a critical role in determining the reactivity, workability and packing density of the resulting geopolymer system. Prior studies have indicated that finer and more uniform binder materials led to more efficient geopolymerization, leading to improved matrix densification and better mechanical integrity. This is extremely crucial to evaluate hybrid systems such as this, were, fundamentally distinct precursors are combined to form geopolymer binder. To facilitate this hybrid blend, we relied on mechanochemical processes such as planetary ball milling as a premixing step in our geopolymer fabrication step.

Furthermore, to effectively decipher the influence of mixing technique on the dispersion/morphology and its impact on the resulting mechanical performance, particle shape/size analysis was performed on samples prepared via (a) hand mixing and (b) mechanochemical mixing using planetary ball milling. While planetary ball milling was employed as the premixing technique in this study, a comparative analysis with hand mixed samples was included to highlight the drawbacks of manual blending in achieving desired particle homogeneity.

Figure 6.2 depicts the particle size distribution of hybrid MK-BC binders subjected to (a) hand mixing and (b) planetary ball milling. From **Figure 6.2(a)**, it can be observed that, the hand mixed samples revealed a broad and multimodal particle size distribution, with a volume mean diameter (VMD) of 38.1μm. This was backed by the actual 2D DIA images **Figure 6.2(c)**), which indicate presence of coarse agglomerates and irregularly shaped particles, especially at high particle size regime.

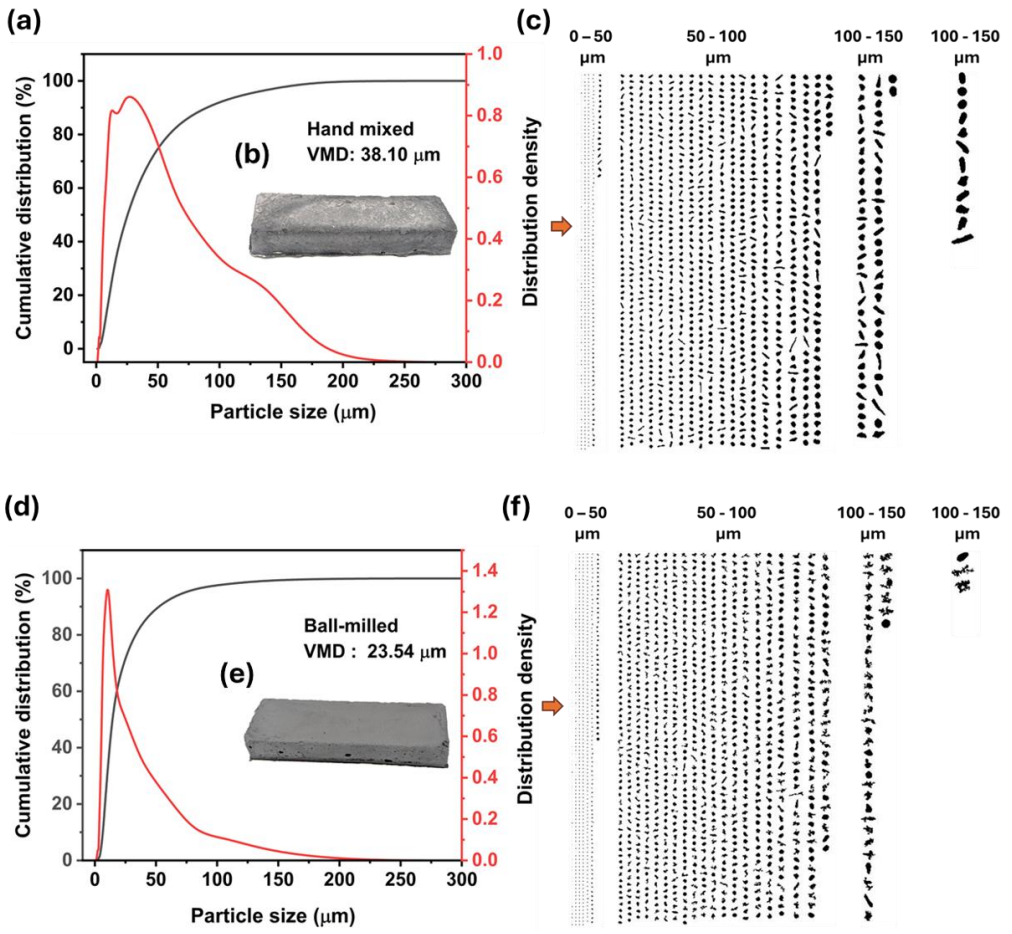

Figure 6.2 Particle size distribution and 2D particle images of hybrid MK-BC blends, along with actual digital images of cured geopolymer samples fabricated using two premixing technique (a -c) Hand mixing and (d-f) mechanochemical ball-milling technique.

This non-uniformity among two fundamentally different binders could be attributed to the differences in their particle density, surface energy and cohesion arising during hand mixing technique. Due to this, the resulting geopolymer system exhibited poor dispersion, proving to be detrimental for the mechanical integrity of the geopolymer samples (see **Figure 6.2(b)**). In contrast, the samples processed via mechanochemical processes (i.e. ball milling), exhibited a significantly narrow, monomodal particle size distribution with a VMD of 23.54 μm (38 % reduction in VMD

vs hand mixed samples) (see **Figure 6.2(d-f)**). Evidence from 2D-DIA images suggest significantly lower agglomeration and improved particle size reduction compared to hand mixed samples. The reason for this could be attributed to the following : In planetary ball milling process, the two distinct binder materials are subjected to high energy collision and shear forces, which increases particle to particle contact, which can result in surface activation via defect generation (as evidenced from **Figure 6.2(d-f)** that the particles seem to be fused upon ball milling, which introduces defects / dislocations in their surfaces, which increases their surface reactivity). The effect of this enhanced dispersion between binders as a result of ball milling, resulted in the formation of a stable geopolymer sample (see **Figure 6.2(d)**).

Now, in order to gain further insight into the microstructural attributes of these hybrid binders, particle morphology was analyzed using DIA (for particle shape analysis) and SEM. **Figure 6.3(a)**, iterates the variation of hybrid binder shape w.r.t increasing particle size subjected to different mixing techniques discussed in this chapter. Note that the shape descriptor evaluated for this study is the binder aspect ratio (in this context, aspect ratio is derived from the fractal dimensions, defined as the ratio of maximum to minimum fret diameter of a particle, which serves as a indicator of particle elongation and shape irregularity. More details regarding the computation of these shape descriptors are elaborated in **Chapter 4**. As observed from **Figure 6.3**, the hand mixed samples displayed a broader and a more scattered distribution of aspect ratios, particularly for larger particle sizes (> 150 μm), indicating the presence of irregularly / elongated shaped particles, giving rise to a non-uniform mixture. Whereas in the case of ball milled samples, morphological analysis demonstrated a relatively uniform aspect ratio variation with increasing particle size, mostly centered around (0.7-0.8), which is characteristic of a rounder and more uniform particle

blend leading to a more homogeneous and interfacial blending of binder mixture. These results are indicative of the critical role of employing a mechanochemical process such as ball milling to integrate physiochemically distant species together for various applications.

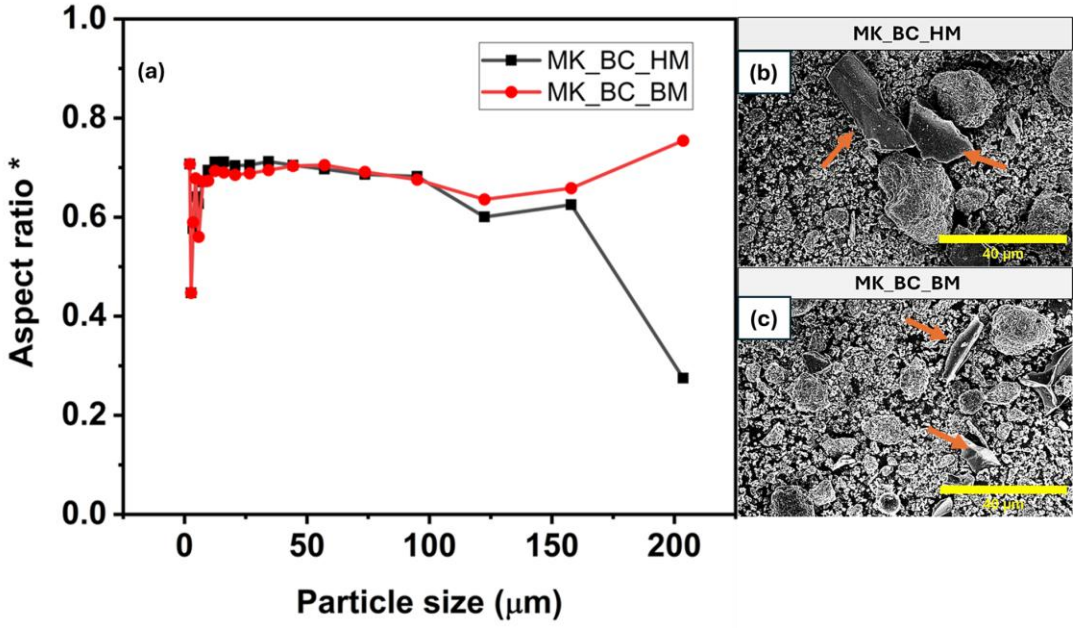

Figure 6.3 DIA based particle shape analysis and morphological analysis of hybrid geopolymer precursor blended using two premixing techniques: hand mixed (MK_BC_HM) and ballmilled (MK_BC_BM) (a) variation of shape descriptor (aspect ratio in this case) with increasing particle size (b) SEM micrographs depicting the microstructure of both premixed samples. Note that the orange arrow indicates the coarser BC particles in the microstructure.

Furthermore, the SEM micrographs presented in **Figure 6.3(b,c)** further substantiate the observations made from DIA. From **Figure 6.3(b)**, the hand mixed binder samples, exhibit coarse, irregularly shaped and agglomerated chunks of both MK and BC particles (marked by orange arrow). Additionally, a significant disparity exists between particle sizes, severely affecting dispersion and reactivity of these binder materials. On the other hand, the SEM images pertaining to ball milled

binders (**Figure 6.3(c)**) exhibited better compatibility between two distinct binder materials, with fewer large/elongated fragments and higher percentage of uniformly distributed particles, leading to more homogeneous mixture, once again iterating the enormous potential of mechanochemical processing in cement/ geopolymer applications.

6.4.2 Mechanical characterization

Role of BC supplementation on the flexural strength and specific strength of FR-BEMG.

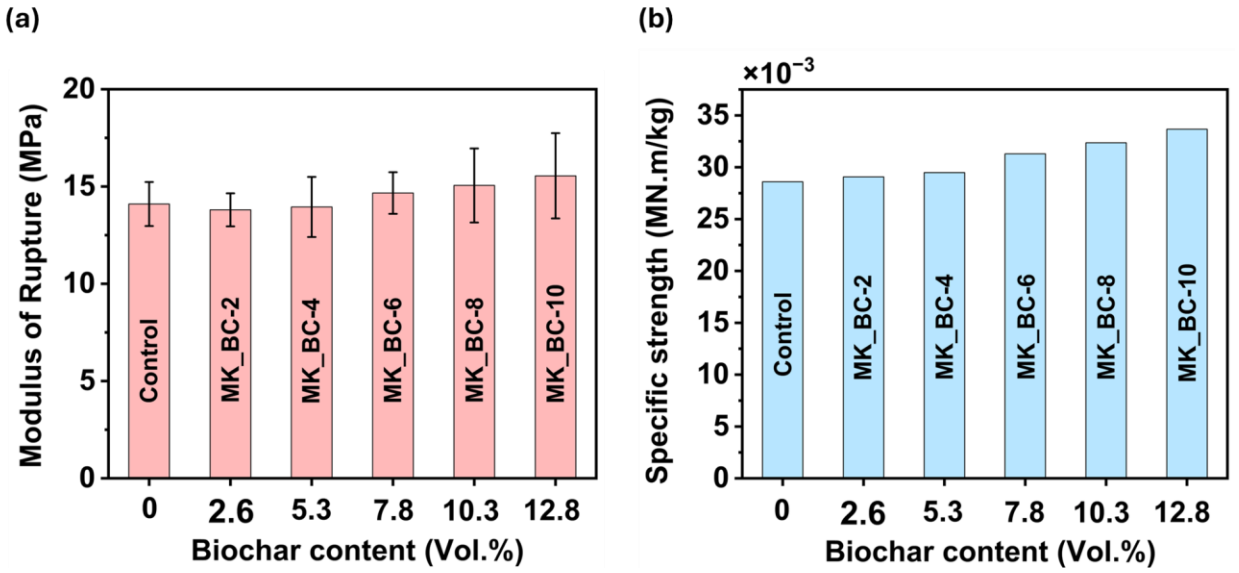

Figure 6.4 Mechanical characterization of (54 day cured) FR-BEMG as a function of BC content depicting (a) MOR and (b) specific strength (mean MOR normalized by overall density of the geopolymer).

Evaluating the mechanical performance of geopolymer system is critical as it dictates the viability of these materials to be employed for both structural and non-structural composites – particularly when incorporating additive/ admixtures such a BC, which inherently exhibit a high degree of variability due to their heterogeneous nature. Among various mechanical properties, flexural strength is of critical importance in our context, as the targeted application include non-structural

application such as for use as external claddings/ partition walls / facades etc., which are more prone to bending failure than compression, making it's a key design criterion for ensuring enhanced shelf life.

Figure 6.4(a) depicts the variation of flexural strength and specific strength as a function of increasing BC content. The control specimen (without BC) serves as a base line for this comparison and exhibited a mean MOR of about 13.6 MPa. Now as the BC content increased, the MOR values remained more or less independent, with a slight increase to 15.4 MPa at 10 wt.% BC addition (demonstrating a 12 % increase vs control). Furthermore, it may be noted that the error margins increased at high BC content (possibly due to heterogeneity of BC particles) indicating the statistical similarity in flexural strength among all samples. However, the retention of flexural strength, despite supplementing the primary binder (i.e., MK) upto 10wt.%, showcases the enormous potential of BC as a viable, low-carbon geopolymer precursor. This maintained MOR could be attributed to microstructural improvement such as matrix densification and improved fiber -matrix bonding, likely due to the micro filler effect of BC. Similar effects were observed with the addition of BC in FC in our previous chapter (**Chapter 5**). Now, increasing the BC content beyond 10 wt.%, it was difficult to evaluate the mechanical performance due to geopolymer formulation challenges, such as high-water demand and poor dispersion (which is typical of MK based geopolymer system [350]). As such 10 wt.% was identified as the critical BC concentration, which yielded the best flexural strength without jeopardizing workability.

Additionally, **Figure 6.4(b)** indicates the variation of specific strength (i.e., MOR normalized by density of the geopolymer sample) as a function of increasing BC content. From **Figure 6.4(b)**, it can be observed that, unlike the trends observed with MOR, specific strength exhibited a moderate

increase with increasing BC content. This outcome was expected due to the relatively lower density of BC (compared to MK), which reduces the overall density of the geopolymer system. Additionally, since the magnitude of MOR remained relatively independent with BC supplementation (with slight increase observed at high dosages) across all samples. The rise of specific strength was dictated by density reduction effect of BC, upon its incorporation into the geopolymer matrix. This property is particularly useful, especially for use in high rise applications, where minimizing the dead load, without compromising the composites mechanical integrity becomes critical.

6.4.3 Microstructural characterization

Probing geopolymerization of FR-BEMG via PXRD

PXRD was conducted to confirm the geopolymerization of FR_BEMG composites and to probe structural evolution (if any) due to the incorporation of BC. As observed from **Figure 6.5**, PXRD analysis was conducted for 4 samples – raw MK and three geopolymer binders supplemented with 0, 6 and 12wt.% of BC. From **Figure 6.6**, the raw MK exhibited sharp reflection peaks, primarily arising from quartz (at $2\theta = 20.8°, 26.6°$) and a broad amorphous hump located between $2\theta \approx 15°$-$25°$ [355–358].

This amorphous hump arises due to the dehydroxylation of anhydrous kaolinite upon calcination at high temperatures to produce MK [358]. In addition to this, PXRD of MK also shows weak reflection peaks corresponding to phases such as anatase, muscovite, Illite and albite, which are often present in kaolinite as impurities. Now, upon alkali activation, the MK-BC system undergoes geopolymerization. The alkali activators (blend of sodium silicate + 12 M NaOH) serve two pur-

poses. Sodium hydroxide creates an alkaline environment that facilitates the dissolution of aluminosilicate structure of MK, releasing reactive silicate and aluminate species into the pore solution [359–362].

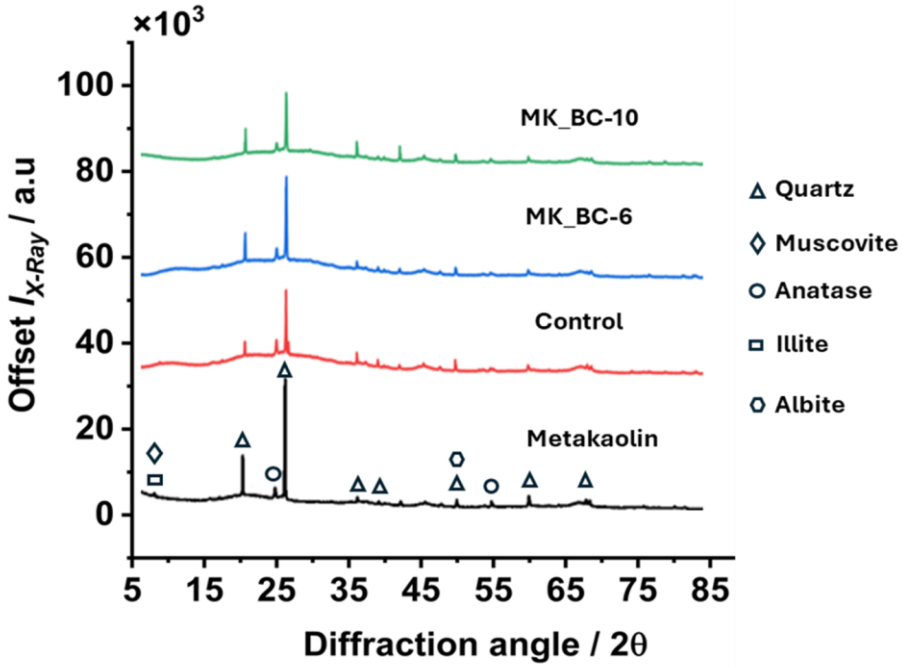

Figure 6.5 Microstructural characterization of FR-BEMG depicting the representative PXRD diffractograms and phase ID of (a) raw MK and FR-BEMG at (b) intermediate (MK_BC-6) and high (BC_BM-10) dosages. The PDF number associated with the identified phases are as follows: Quartz (00-046-1045), muscovite (00-05-2035), Anatase (01-084-1285), Ilite (00-026-0911) and Albite (00-009-0466).

It may be noted that the dissolution of aluminosilicate is highly influenced by the concentration of NaOH – with higher molarities enhancing the dissolution capacity [363]. Previous studies have reported alkali activation, utilizing upto 18 Molar NaOH [364], however considering the presence of NBSK fibers as a reinforcement in our system and its susceptibility to alkaline medium, we refrained from going beyond 12 Molar concentration. At this juncture the sodium silicate present in the activator supplies additional soluble silica, that is necessary for the subsequent steps, such

as polycondensation reaction [365]. The next step in geopolymerization involves rearrangement and transportation of dissolved species. After the dissolution phase, these species undergo a reorientation or rearrangement process, which sets the stage for the formation of geopolymer network [366]. Now, a variety of factors can influence this rearrangement process (concentration and ratio of activator, Si/Al ratio of the geopolymer precursor etc.,) however the exact mechanism or the critical parameter that governs this effect is not well documented in literature and always talked about with a certain degree of uncertainty or skepticism. After rearrangement state, these species undergo polycondensation reaction (eliminating water as a by product) via shared oxygen atom to form Si-O-Al & Si-O-Si bonds [149,153,154] This process results in the formation of a continuous, amorphous aluminosilicate network (i.e., the geopolymer matrix).

Now, as the polycondensation reaction proceeds, the oligomer species formed, further link to create a three-dimensional network comprising repeated units of SiO_4 and AlO_4 tetrahedra, connected via shared oxygen atom. The sodium ions from the activator help balance the negative charge associated with the repeated units, stabilizes the structure and forms the primary binding phase termed as sodium alumino silicate hydrate (N-A-S-H) gel [362,367,368]. These transformations as a result of the geopolymerization are evident in the PXRD pattern (**Figure 6.5**) through a reduction in crystalline quartz peak intensity, followed by a shift and broadening of the amorphous hump towards $2\theta \approx 25° - 35°$ (vs PXRD spectrum of raw MK), which is typical of geopolymer gel formation, confirming geopolymerization reaction [355–357].

Notably, the supplementation of BC at intermediate (6wt.%) and high concentration (12 wt.%) did not contribute to any detectable changes in the PXRD patterns and remained similar to

what was observed with the PXRD of control. However, we do not completely exclude ethe possibility of subtle chemical/microstructural changes due to the supplementation of BC and may require further investigation to effectively probe these effects, which is beyond the scope of this work. Additionally, geopolymer reaction product (i.e., N-A-S-H) formed is highly amorphous in nature, therefore its quantification, w.r.t increasing BC content remains hard to probe, due to the limitation of XRD technique in quantifying amorphous phases.

Moreover, it is important to emphasize that PXRD patterns of geopolymer systems were devoid of calcite, portlandite or C-A-S-H formation, despite the supplemented BC contains relatively high proportions of CaO, which characterizes these materials as geopolymer system instead of AAM [148].

6.4.4 Life cycle impact analysis

Role of FR-BEMG on the CO_2 footprint

The environmental impact of utilizing hybrid geopolymer binder precursors was evaluated by a cradle to gate life cycle impact assessment. **Figure 6.6(a)** depicts the system boundary adopted for this analysis and encompasses all processes involved in the geopolymer fabrication, starting from raw material extraction, conversion and processing (includes both binder and activator) to core process involved (such as mixing , compaction , casting and curing). The background information regarding the raw materials, were taken from ecoinvent database. The functional unit was fixed at 0.05 m^2 of the fabricated geopolymer.

Figure 6.6(b) depicts the life cycle impact assessment, indicating the net emission related to geopolymer fabrication, the impact of BC substitution and the reduction in net emission due to

decrease in MK content. Although the emissions related to alkaline activators and MK remains the largest contributor to total GWP, partial replacement of MK with BC significantly offsets these emissions through carbon sequestration. Considering these results, the 10 wt.% BC-substituted geopolymer offered the greatest environmental benefit (19% reduction) and highest mechanical performance (12% increase in MOR) compared to the control.

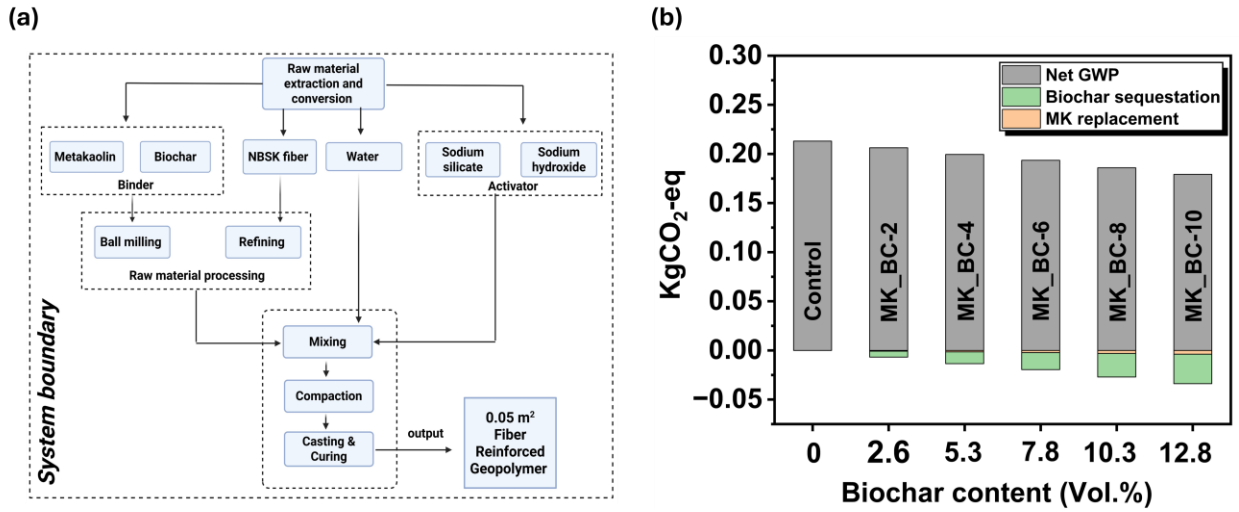

Figure 6.6 Figure Cradle to gate LCA of FR_BEMG depicting (a) system boundary adapted to incorporate all the processing steps involved in laboratory scale processing (starting from raw material extra and conversion to core process involved for the production of 0.05 m2 (functional unit) of geopolymer sample) and (b) GWP per sample as a function of BC content, indicating contributions BC carbon sequestration and MK replacement.

Additionally, the GWP of commercial FC board (Hardie VL Plank) , presented in **Chapter 5** was normalised to match the functional unit and dimensions of the FR-BEMG sample, resulting in a corrected GWP of 1.37 kg CO_2-eq for the commercial sample – representing a reduction of approximately 95% in GWP compared to the FR-BEMG sample (0.06315 kg CO_2-eq). These findings emphasize the dual characteristics of BC in reducing GWP, whilst maintaining the structural

integrity of the geopolymer system, thus paving the way for the development of green construction materials.

6.5 Conclusion

This study investigated the development and characterization of FR-BEMG. The key findings are as follows:

- The process of ball milling was a critical step in combining two fundamentally distinct binder materials together thereby ensuring optimum particle shape and size. This is critical to impart good mechanical integrity to the resulting geopolymer (as evidenced with the hand mixed samples, which resulted in poor dispersion, resulting in poor mechanical integrity/incomplete geopolymerization due to increased porosity and other issues).
- Results from mechanical characterization revealed that the MOR remained relatively independent of the BC content (exhibited a range around (13 -16 MPa) for all samples, whereas the specific strength of the FC moderately increased with BC addition. This could be attributed to the low density of calcined clay – capable of significantly reducing the density of the FR-BEMG (compared to OPC, which posses' high density).
- PXRD analysis confirmed the geopolymerization process. This was characterized by a broad hump around $2\theta \approx 25° - 35°$ in the PXRD spectrum of all MK geopolymer samples (with/without BC), which was absent in the PXRD of geopolymer precursor (i.e., MK). No changes in the PXRD spectrum were observed with the incorporation of BC, indicating its limited/no influence on the geopolymerization process.

- Cradle to gate LCA analysis revealed that incorporating BC into FR-BEMG system, significantly reduced the GWP impact (with 10wt.% substitution resulting in a reduction of GWP by 19%). Additionally, when compared to GWP of commercial FC (OPC based) the FR-BEMG demonstrated a substantially lower carbon footprint (≈ 95% reduction in GWP for FR-BEMG), underlying its immense potential as an alternative construction material.

Chapter 7: Conclusions and Recommendations

7.1 Conclusion

This thesis presents a comprehensive approach to decarbonizing FC composites by innovating both the reinforcing / additive constituent and the binder system. In the first approach (**Chapter 3 & 4**), cellulose based additives – including CNCs, MCC, and AC were introduced as sustainable alternatives to synthetic cement admixtures. These additives enhanced rheological properties such as shear thinning behaviour, static yield stress and influenced hydration kinetics through their interaction with water and intrinsic physicochemical characteristics.

CNCs exhibited a content depended effect on hydration kinetics: at low contents (< 2wt.%), they delayed hydration, while at higher contents (> 2wt.%), they accelerated cement hydration – likely due to improved water accessibility and surface–mediated transport mechanisms. MCC and AC emerged as cost effective alternatives to CNCs. While both contributed to enhanced flexural strength, AC uniquely improved post-crack toughness and ductility, which is attributed to its microfibrillar morphology that facilitated improved fiber matrix interaction and efficient load transfer. In contrast, MCC increased composite brittleness. Although CNCs and MCC achieved higher peak strengths, they did not enhance post–peak toughness, as confirmed by stress–strain analysis.

In the second approach (**Chapter 5 & 6**), the thesis focused on matrix decarbonization by incorporating BC both as a partial cement replacement in OPC based systems and as a functional component in alkali activated (geopolymer) binders. Rheological investigations revealed that the inclusion of BC significantly improved the static yield stress and enhanced time dependent thixotropic behaviour, thereby improving workability and handling time during mixing and casting.

These improvements were attributed to a synergistic combination of chemical interactions between BC and the cementitious matrix, as well as the formation of a weak network structure arising from early age cement hydration and along with physical effects such as fiber entanglement.

Microstructural and spectroscopic analysis confirmed that BC contributed to improved hydration and matrix densification through both filler effects and chemical interactions. Notably, BC's porous structure and surface functional groups provided additional water – accessible surfaces and acted as potential nucleation sites for hydration products to develop – improving hydration kinetics and contributing to matrix refinement. LCA further supported the environmental viability of this approach, with 8wt.% BC replacement reduced the GWP by 18 % (compared to a pure cementitious system), with only a 4.2% increase in fabrication cost – offset by gains in sustainability and specific strength. The reduction in composite density with increasing BC content led to the development of lightweight FC systems with enhanced specific strength, although a moderate increase in brittleness was observed at higher dosages due to reduced post cracking deformation.

In the final chapter **(Chapter 6,** a cement free geopolymer binder system was developed using wood derived BC and MK that were premixed via planetary ball milling and subsequently reinforced with softwood kraft fibers. The composite system achieved flexural strength in the range of 13–15 MPa, representing a significant enhancement over conventional cement based counterparts in this study, which exhibited flexural strength 6–10 MPa. The mechanochemical premixing process effectively modified the surface characteristics of BC, improving its physicochemical characteristics thereby improving its compatibility and reactivity within the alkali-activated matrix.

In summary, this thesis provides a dual strategy to engineer low-carbon, high performance FC composites by integrating renewable reinforcements with tailored binder chemistry. The outcomes demonstrate that by utilising cellulosic additives and BC based systems can improve workability, enhance strength, modify stress-strain response, and reduce environmental impact, offering a viable pathway toward sustainable construction materials.

7.2 Final remarks

As a concluding remark, correlation plot (**Figure 7.1**) provides a comparative understanding of the relationship between flexural strength and density for both conventional OPC based FC systems and the alternative geopolymer based system.

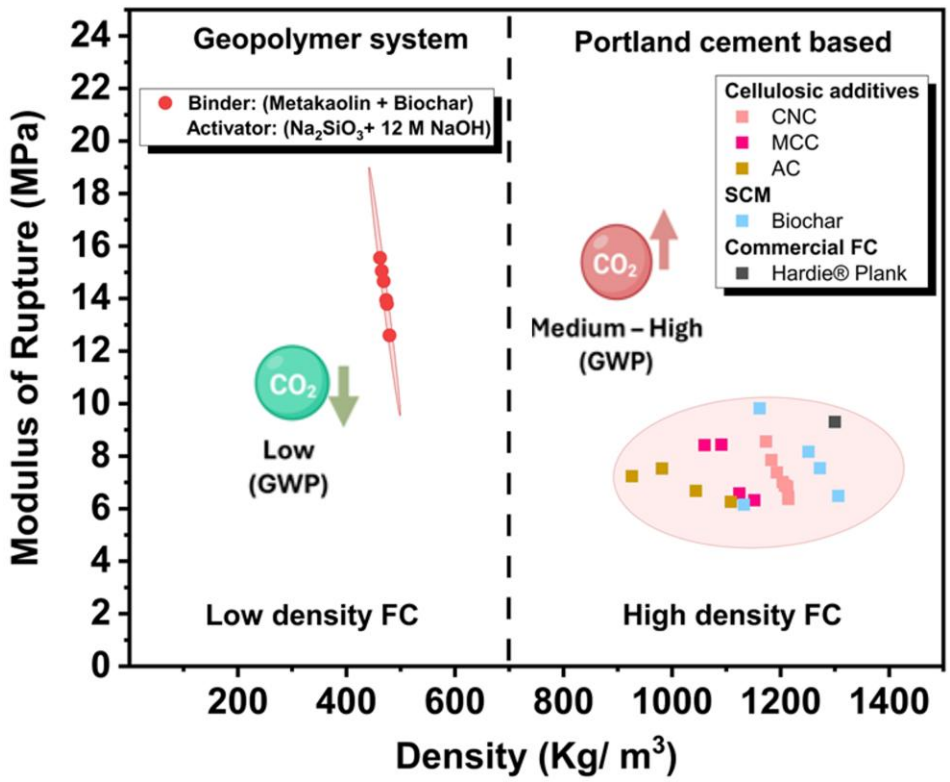

Figure 7.1 Correlation plot depicting the variation in MOR as a function of FC density, for samples developed in this study, including OPC based systems modified using cellulosic additives and BC and MK based geopolymer system enhanced with BC. This plot also includes a commercial standard (Hardie® Plank) for benchmarking. This density-based clustering system allows for material classification across various application domains.

On the right (see **Figure 7.1**), OPC based FC enhanced with various strategies (such as reinforcement/ additive modifications with CNCs, MCC and AC) and (matrix modification with the use of BC as SCMs) are represented – which cluster in the high density domain (≈ 1000 to 1300 kg/m^3), with MOR (ranging from ≈ 6 – 11 MPa). Notably, these results (both MOR and density) obtained were in close proximity (or even higher in some cases) with the commercial standard (Hardie® Plank, included in the cluster) – acting as a valuable benchmark for gauging

the industrial relevance of the samples explored in this thesis. These results are extremely significant as they demonstrate that, critical FC performance can be retained or improved while enhancing sustainability (replating conventional petrochemical/silica based additives with cellulosic additives) and reducing the CO_2 footprint (through the incorporation of waste derived BC as a SCMs) in FC – further reinforces the immense potential for innovation in OPC based systems.

To complement these advancements within OPC based systems, transitioning into geopolymer based system offers a promising solution that pushes the existing boundaries for the innovation of lightweight high performance low-carbon designs (see **Figure 7.1**). The system comprising of hybrid (MK + BC) geopolymer precursor activated by Na_2SiO_3 and 12 M NaOH – exhibited superior MOR (in the range of ≈ 13 -16 MPa) at substantially lower densities (≈ 450 kg/m^3) – highlighting its immense potential as a low embodied carbon, high performance (high specific strength) alternative to traditional OPC based FC. Despite, these substantial improvements, widespread adoption of geopolymer system , is constraint by both regulatory and standardization requirements. However, this thesis identifies viable pathways in both domains – enhancing sustainability and reducing GWP impact of existing OPC based system for imminent scalable interventions as well as advancing geopolymer technologies for the development of future ready sustainable / low-carbon construction material.

7.3 Limitations

While this thesis demonstrates promising approaches for decarbonizing and improving, the sustainability of FC, several limitations must be acknowledged:

- One of the key challenges, in transition to biobased / sustainable additives such as CNCs, MCC or AC, possess challenges in terms of cost and availability. Petrochemical / silica-based additives on the other hand are more easily available and lower in cost, which may cause issues related to scalability and limited regional accessibility.
- The long terms durability and performance of FC containing nano/micro cellulosic additive in the highly alkaline environment of cementitious matrices also remain an area of concern. Cellulosic additives employed in this research, though crystalline, may still be susceptible to degradation over time, affecting the integrity and longevity of composite.
- BC, while effective as a partial cement substitute, also suffers variability in terms of its physicochemical properties, driven primarily by its biomass source and processing parameters (pyrolysis conditions). This variability could pose problems related to establishing standard usage guidelines and ensuring consistent and reproducible performance.
- With regards to complete OPC replacement with geopolymer systems, issues arise regarding the consistent supply and quality of precursors such as MK. Its availability is often geographically limited to regions with suitable clay deposits (in terms of quantity and permission /government policies w.r.t to open pit mining, that can have environmental implications). In addition to this, variations in the purity of kaolinite and calcination conditions, can significantly affect the reactivity and consistency of MK, posing challenges in standardization and achieving uniform/ consistent performance across geopolymer mixes.
- While rheological and mechanical characteristics of FC with the incorporation of additives and SCMs were extensively studied in his thesis, their practical/ real world use case scenario requires us to evaluate critical properties such as fire resistance, acoustic properties

– especially when these are employed for non-structural applications such as external claddings, partition walls etc.

- To translate these findings into more structural applications, such as concrete, further in-depth research and validation is essential. This is because unlike non-structural materials, load bearing application are governed by strict design codes and performance standards, which requires formulation that fits well within the well-defined boundaries/ guidelines of workability, hydration and strength development – therefore extensive benchmarking, testing and certification is essential.

7.4 Future direction

Building upon the findings from this Theis, several important research directions can be pursued for development, such as:

- Though cost/ performance metric was evaluated for the incorporation of cellulosic additives in FC, its sustainability aspect is yet to be investigated. Therefore, conducting an in depth LCA would be critical to draw a comparison between performance and sustainability between various cellulosic additives employed in this study.
- Despite in depth rheo-mechanical studies were investigated in this thesis, the durability of FC containing cellulosic additives and waste biomasses, subjected to wet/dry and freeze thaw cycle, still remains an area of concern and requires in depth investigations.
- The rheological characterization of FR-BEMG system (such as yield stress, thixotropy) are critical in the context of geopolymer Synthesis and need extensive investigation.

- Development of standardized testing protocols and regulatory frameworks of these systems will be essential for widespread adoption of these technologies as a mainstream low-carbon construction material.
- Finally, transitioning these findings to more structural / load bearing applications requires further investigation to evaluate its load bearing capacity (such as extensive compressive testing) and resistance to environmental degradation (such as sulphate attacks, chloride ion permeability etc.) are critical.

Put together, the insights gained from this thesis provide a strong platform for continued exploration and development of low-carbon sustainable construction materials – critical step towards decarbonizing cement industry and achieving global net-zero emissions target by 2050.

Bibliography

[1] Global Cement Industry Outlook: Trends and Forecasts - World Cement Association n.d. https://www.worldcementassociation.org/blog/news/global-cement-industry-outlook-trends-and-forecasts?itid=lk_inline_enhanced-template (accessed May 17, 2025).

[2] Global cement production has plateaued over the last decade - Our World in Data n.d. https://ourworldindata.org/data-insights/global-cement-production-has-plateaued-over-the-last-decade (accessed October 28, 2025).

[3] U.S. Geological Survey Mineral Commodity Summaries 2024 Data Release (ver. 2.0, March 2024) - ScienceBase-Catalog n.d. https://www.sciencebase.gov/catalog/item/65a6e45fd34e5af967a46749 (accessed October 28, 2025).

[4] CO_2 emissions by fuel - Our World in Data n.d. https://ourworldindata.org/emissions-by-fuel (accessed October 28, 2025).

[5] Cement production global 2024| Statista n.d. https://www.statista.com/statistics/1087115/global-cement-production-volume/ (accessed May 17, 2025).

[6] Cement and Concrete Manufacturing | Department of Energy n.d. https://www.energy.gov/eere/iedo/cement-and-concrete-manufacturing (accessed May 17, 2025).

[7] Andrew RM. Global CO2 emissions from cement production. Earth Syst Sci Data 2018;10:195–217. https://doi.org/10.5194/ESSD-10-195-2018,.

[8] Kajaste R, Hurme M. Cement industry greenhouse gas emissions – management options and abatement cost. J Clean Prod 2016;112:4041–52. https://doi.org/10.1016/J.JCLEPRO.2015.07.055.

[9] Environmental & Ecological Impacts of Cement | UKGBC n.d. https://ukgbc.org/our-work/topics/embodied-ecological-impacts/cement/ (accessed May 17, 2025).

[10] Roadmap to Net-Zero Carbon Concrete by 2050 n.d. https://ised-isde.canada.ca/site/clean-growth-hub/en/cement-and-concrete-canada/roadmap-net-zero-carbon-concrete-2050 (accessed May 17, 2025).

[11] Klos H. Asbestos cement : Technology and project planning. Springer Vienna; 1967. https://doi.org/10.1007/978-3-7091-8169-0.

[12] Ludwig Hatschek. Process for the production of artificial stone slabs from fiber materials and hydraulic binders. AT5970B, 1901.

[13] Murray R. Asbestos: a chronology of its origins and health effects. Occup Environ Med 1990;47:361–5. https://doi.org/10.1136/OEM.47.6.361.

[14] Coutts RSP. A review of Australian research into natural fibre cement composites. Cem Concr Compos 2005;27:518–26. https://doi.org/10.1016/J.CEMCONCOMP.2004.09.003.

[15] Corn JK, Starr J. Historical perspective on asbestos: Policies and protective measures in world war ii shipbuilding. Am J Ind Med 1987;11:359–73. https://doi.org/10.1002/AJIM.4700110311.

[16] Atalla RH, VanderHart DL. Native Cellulose: A Composite of Two Distinct Crystalline Forms. Science (1979) 1984;223:283–5. https://doi.org/10.1126/SCIENCE.223.4633.283.

[17] Wiedenhoeft AC, Miller RB. Structure and function of wood. Handbook of Wood Chemistry and Wood Composites Boca Raton, Fla : CRC Press, 2005: Pages 9-33 2005.
[18] Barnett JR. TREE PHYSIOLOGY | Xylem Physiology. Encyclopedia of Forest Sciences 2004:1583–90. https://doi.org/10.1016/B0-12-145160-7/00099-5.
[19] Rowell RM, Pettersen R, Tshabalala MA. Chapter 3 Cell Wall Chemistry. In:Handbook of Wood Chemistry and Wood Composites, 2nd Edition; Chapter 3 Pp 33-72 2013 2012;3:33–72.
[20] Arzola-Villegas X, Lakes R, Plaza NZ, Jakes JE. Wood Moisture-Induced Swelling at the Cellular Scale—Ab Intra. Forests 2019, Vol 10, Page 996 2019;10:996. https://doi.org/10.3390/F10110996.
[21] Kirker GT, Blodgett AB, Arango RA, Lebow PK, Clausen CA. The role of extractives in naturally durable wood species. Int Biodeterior Biodegradation 2013;82:53–8. https://doi.org/10.1016/J.IBIOD.2013.03.007.
[22] R. S. P. Coutts. Wood fibre reinforced cement composites. Research Review, Division of Chemical Technology, CSIRO 1979:1–16.
[23] Coutts RSP, Campbell MD. Coupling agents in wood fibre-reinforced cement composites. Composites 1979;10:228–32. https://doi.org/10.1016/0010-4361(79)90024-7.
[24] Qian G, Xu G, Li H, Li A. The Effect of Autoclave Temperature on the Expansion and Hydrothermal Products of High-MgO Blended Cements. Cem Concr Res 1998;28:1–6. https://doi.org/10.1016/S0008-8846(97)00202-0.
[25] Mohr BJ, Nanko H, Kurtis KE. Durability of kraft pulp fiber–cement composites to wet/dry cycling. Cem Concr Compos 2005;27:435–48. https://doi.org/10.1016/J.CEMCONCOMP.2004.07.006.
[26] Britt KW. Handbook of Pulp and Paper Technology. New York: Van Nostrand Reinhold; 1970.
[27] Coutts RSP, Ridikas V. Refined wood fibre-cement products. Appita 1982;35:395–400.
[28] Coutts RSP, Kightly P. Microstructure of autoclaved refined wood-fibre cement mortars. J Mater Sci 1982;17:1801–6. https://doi.org/10.1007/BF00540809/METRICS.
[29] Morgan PW. Brief History of Fibers from Synthetic Polymers. Journal of Macromolecular Science—Chemistry 1981;15:1113–31. https://doi.org/10.1080/00222338108066456.
[30] Rabenold RR. Handbook of fiberglass and advanced plastics composites, edited by George Lubin, Van Nostrand Reinhold, New York, New York, 1969. 912 pages. $27.50. J Polym Sci B 1970;8:447–8. https://doi.org/10.1002/POL.1970.110080611.
[31] Wenzel RW. Resistance of Solid Surfaces to Wetting by Water. Ind Eng Chem 1936;28:988–94.
[32] Mohr BJ, Biernacki JJ, Kurtis KE. Microstructural and chemical effects of wet/dry cycling on pulp fiber–cement composites. Cem Concr Res 2006;36:1240–51. https://doi.org/10.1016/J.CEMCONRES.2006.03.020.

[33] Hoque M, Kamal S, Raghunath S, Foster EJ. Unraveling lignin degradation in fibre cement via multidimensional fluorometry. Sci Rep 2023;13:1–13. https://doi.org/10.1038/S41598-023-35560-3;SUBJMETA=166,301,638,639;KWRD=CHEMISTRY,ENGINEERING,MATERIALS+SCIENCE.
[34] Booya E, Gorospe K, Das S. Performance of engineered pulp fibre reinforced composites subjected to weathering conditions. Journal of Building Engineering 2019;25:100816. https://doi.org/10.1016/J.JOBE.2019.100816.
[35] A. Abed M, L. Balázs G. Concrete Performance in Cold Regions: Understanding Concrete's Resistance to Freezing/Thawing Cycles. Sustainability of Concrete With Synthetic and Recycled Aggregates, IntechOpen; 2022. https://doi.org/10.5772/intechopen.99968.
[36] Kibblewhite RP. Effects of pulp freezing and frozen pulp storage on fibre characteristics. Wood Sci Technol 1980;14:143–58. https://doi.org/10.1007/BF00584043/METRICS.
[37] Paul R. Blankenhorn, Michael R. Silsbee. Process for enhancing the characteristics and durability of wood fiber cement and wood fiber concrete composites. WO2000071336A1, 2000.
[38] Møller PCF, Mewis J, Bonn D. Yield stress and thixotropy: on the difficulty of measuring yield stresses in practice. Soft Matter 2006;2:274–83. https://doi.org/10.1039/B517840A.
[39] Roussel N, Ovarlez G, Garrault S, Brumaud C. The origins of thixotropy of fresh cement pastes. Cem Concr Res 2012;42:148–57. https://doi.org/10.1016/J.CEMCONRES.2011.09.004.
[40] Wallevik JE. Rheological properties of cement paste: Thixotropic behaviour and structural breakdown. Cem Concr Res 2009;39:14–29. https://doi.org/10.1016/J.CEMCONRES.2008.10.001.
[41] Perrot A, Lecompte T, Khelifi H, Brumaud C, Hot J, Roussel N. Yield stress and bleeding of fresh cement pastes. Cem Concr Res 2012;42:937–44. https://doi.org/10.1016/J.CEMCONRES.2012.03.015.
[42] Gwon S, Choi YC, Shin M. Effect of plant cellulose microfibers on hydration of cement composites. Constr Build Mater 2021;267:121734. https://doi.org/10.1016/J.CONBUILDMAT.2020.121734.
[43] Bilba K, Arsene MA, Ouensanga A. Sugar cane bagasse fibre reinforced cement composites. Part I. Influence of the botanical components of bagasse on the setting of bagasse/cement composite. Cem Concr Compos 2003;25:91–6. https://doi.org/10.1016/S0958-9465(02)00003-3.
[44] Stancato AC, Burke AK, Beraldo AL. Mechanism of a vegetable waste composite with polymer-modified cement (VWCPMC). Cem Concr Compos 2005;27:599–603. https://doi.org/10.1016/J.CEMCONCOMP.2004.09.011.

[45] Jongvisuttisun P, Negrello C, Kurtis KE. Effect of processing variables on efficiency of eucalyptus pulps for internal curing. Cem Concr Compos 2013;37:126–35. https://doi.org/10.1016/J.CEMCONCOMP.2012.11.006.
[46] Kawashima S, Shah SP. Early-age autogenous and drying shrinkage behavior of cellulose fiber-reinforced cementitious materials. Cem Concr Compos 2011;33:201–8. https://doi.org/10.1016/J.CEMCONCOMP.2010.10.018.
[47] Jongvisuttisun P, Leisen J, Kurtis KE. Key mechanisms controlling internal curing performance of natural fibers. Cem Concr Res 2018;107:206–20. https://doi.org/10.1016/J.CEMCONRES.2018.02.007.
[48] Justs J, Wyrzykowski M, Bajare D, Lura P. Internal curing by superabsorbent polymers in ultra-high performance concrete. Cem Concr Res 2015;76:82–90. https://doi.org/10.1016/J.CEMCONRES.2015.05.005.
[49] Toledo Filho RD, Ghavami K, Sanjuán MA, England GL. Free, restrained and drying shrinkage of cement mortar composites reinforced with vegetable fibres. Cem Concr Compos 2005;27:537–46. https://doi.org/10.1016/J.CEMCONCOMP.2004.09.005.
[50] Silva F de A, Filho RDT, Filho J de AM, Fairbairn E de MR. Physical and mechanical properties of durable sisal fiber–cement composites. Constr Build Mater 2010;24:777–85. https://doi.org/10.1016/J.CONBUILDMAT.2009.10.030.
[51] Boghossian E, Wegner LD. Use of flax fibres to reduce plastic shrinkage cracking in concrete. Cem Concr Compos 2008;30:929–37. https://doi.org/10.1016/J.CEMCONCOMP.2008.09.003.
[52] Khorami M, Ganjian E, Srivastav A. Feasibility Study on Production of Fiber Cement Board Using Waste Kraft Pulp in Corporation with Polypropylene and Acrylic Fibers. Mater Today Proc 2016;3:376–80. https://doi.org/10.1016/J.MATPR.2016.01.023.
[53] Tonoli GHD, Mendes RF, Siqueira G, Bras J, Belgacem MN, Savastano H. Isocyanate-treated cellulose pulp and its effect on the alkali resistance and performance of fiber cement composites. Holzforschung 2013;67:853–61. https://doi.org/10.1515/HF-2012-0195/MACHINEREADABLECITATION/RIS.
[54] Khorami M, Ganjian E. The effect of limestone powder, silica fume and fibre content on flexural behaviour of cement composite reinforced by waste Kraft pulp. Constr Build Mater 2013;46:142–9. https://doi.org/10.1016/J.CONBUILDMAT.2013.03.099.
[55] Mohr BJ, Biernacki JJ, Kurtis KE. Supplementary cementitious materials for mitigating degradation of kraft pulp fiber-cement composites. Cem Concr Res 2007;37:1531–43. https://doi.org/10.1016/J.CEMCONRES.2007.08.001.
[56] El-Ashkar NH, Nanko H, Kurtis KE. Effect of Moisture State on Mechanical Behavior and Microstructure of Pulp Fiber-Cement Mortars. Journal of Materials in Civil Engineering 2007;19:691–9. https://doi.org/10.1061/(ASCE)0899-1561(2007)19:8(691).

[57] Cao Y, Zavaterri P, Youngblood J, Moon R, Weiss J. The influence of cellulose nanocrystal additions on the performance of cement paste. Cem Concr Compos 2015;56:73–83. https://doi.org/10.1016/J.CEMCONCOMP.2014.11.008.
[58] Claramunt J, Ardanuy M, Fernandez-Carrasco LJ. Wet/Dry Cycling Durability of Cement Mortar Composites Reinforced with Micro- and Nanoscale Cellulose Pulps. Bioresources 2015;10. https://doi.org/10.15376/biores.10.2.3045-3055.
[59] Sant G, Ferraris CF, Weiss J. Rheological properties of cement pastes: A discussion of structure formation and mechanical property development. Cem Concr Res 2008;38:1286–96. https://doi.org/10.1016/J.CEMCONRES.2008.06.008.
[60] Förster S, Konrad M, Lindner P. Shear thinning and orientational ordering of Wormlike Micelles. Phys Rev Lett 2005;94:017803. https://doi.org/10.1103/PHYSREVLETT.94.017803/FIGURES/3/THUMBNAIL.
[61] Phung TN, Brady JF, Bossis G. Stokesian Dynamics simulation of Brownian suspensions. J Fluid Mech 1996;313:181–207. https://doi.org/10.1017/S0022112096002170.
[62] Brader JM. Nonlinear rheology of colloidal dispersions. Journal of Physics: Condensed Matter 2010;22:363101. https://doi.org/10.1088/0953-8984/22/36/363101.
[63] Nilsson J, Sargenius Principal P, Billberg P, Ali Farhang C, Abe K. Effect of microfibrillar cellulose on concrete equivalent mortar fresh and hardened properties 2011.
[64] Karimi H, Gauvin F, Brouwers HJH, Cardinaels R, Yu Q. On the versatility of paper pulp as a viscosity modifying admixture for cement composites. Constr Build Mater 2020;265:120660. https://doi.org/10.1016/J.CONBUILDMAT.2020.120660.
[65] Baykoff M. On the Theory of the Hardening of Hydraulic Cements. Proceedings of the Weekly Meetings of the Academy of Sciences 1926:128–9.
[66] John E, Lothenbach B. Cement hydration mechanisms through time – a review. J Mater Sci 2023;58:9805–33. https://doi.org/10.1007/S10853-023-08651-9/FIGURES/4.
[67] Bullard JW, Jennings HM, Livingston RA, Nonat A, Scherer GW, Schweitzer JS, et al. Mechanisms of cement hydration. Cem Concr Res 2011;41:1208–23. https://doi.org/10.1016/J.CEMCONRES.2010.09.011.
[68] Jones FE. The Formation of the Sulfoaluminates and Sulfoferrites of Calcium in the Portland Cement-Water System. Journal of Physical Chemistry 1945;49:344–58.
[69] Climate Change | United Nations n.d. https://www.un.org/en/global-issues/climate-change (accessed May 21, 2025).
[70] THE 17 GOALS | Sustainable Development n.d. https://sdgs.un.org/goals (accessed May 21, 2025).
[71] Khayat KH, Mikanovic N. Viscosity-enhancing admixtures and the rheology of concrete. Understanding the Rheology of Concrete 2012:209–28. https://doi.org/10.1533/9780857095282.2.209.

[72] Palacios M, Flatt RJ. Working mechanism of viscosity-modifying admixtures. Science and Technology of Concrete Admixtures 2016:415–32. https://doi.org/10.1016/B978-0-08-100693-1.00020-5.
[73] Wang S, Zhou H, Bi Y, Li X, Wang J, Xiong L, et al. Influence of a new Viscosity Modifying Admixture (VMA) on the rheological properties of cement paste 2016:619–23. https://doi.org/10.2991/ICMMBE-16.2016.115.
[74] Payen A. Memoir on the Composition of the Tissue of Plants and of Woody Material. Proceedings of the Academy of Sciences, 1838, p. 1052–6.
[75] Atalla RH. The Structures of Cellulose. MRS Proceedings 1990;197:89–98. https://doi.org/10.1557/PROC-197-89/METRICS.
[76] Blackwell J. The Macromolecular Organization of Cellulose and Chitin 1982:403–28. https://doi.org/10.1007/978-1-4684-1116-4_20.
[77] Kolpak FJ, Blackwell J. Determination of the Structure of Cellulose II. Macromolecules 1976;9:273–8. https://doi.org/10.1021/MA60050A019/SUPPL_FILE/MA60050A019_SI_001.PDF.
[78] Wada M, Chanzy H, Nishiyama Y, Langan P. Cellulose III I crystal structure and hydrogen bonding by synchrotron X-ray and neutron fiber diffraction. Macromolecules 2004;37:8548–55. https://doi.org/10.1021/MA0485585;SUBPAGE:STRING:ABSTRACT;WGROUP:STRING:ACHS.
[79] Wada M, Heux L, Sugiyama J. Polymorphism of cellulose I family: Reinvestigation of cellulose IVl. Biomacromolecules 2004;5:1385–91. https://doi.org/10.1021/BM0345357;PAGEGROUP:STRING:PUBLICATION.
[80] Delucis R de A, Cademartori PHG de, Fajardo AR, Amico SC. Cellulose and its Derivatives: Properties and Applications. Polysaccharides 2021:221–52. https://doi.org/10.1002/9781119711414.CH11.
[81] Wise LE, Murphy M, d'Addieco AA. Chlorite holocellulose, its fractionnation and bearing on summative wood analysis and on studies on the hemicelluloses. 1946;122:35–43.
[82] Adeleye OA, Bamiro OA, Albalawi DA, Alotaibi AS, Iqbal H, Sanyaolu S, et al. Characterizations of Alpha-Cellulose and Microcrystalline Cellulose Isolated from Cocoa Pod Husk as a Potential Pharmaceutical Excipient. Materials 2022, Vol 15, Page 5992 2022;15:5992. https://doi.org/10.3390/MA15175992.
[83] Battista OA, Smith PA. Microcrystalline cellulose. Ind Eng Chem 1962;54:20–9. https://doi.org/10.1021/IE50633A003/ASSET/IE50633A003.FP.PNG_V03.
[84] Adel AM, Abd El-Wahab ZH, Ibrahim AA, Al-Shemy MT. Characterization of microcrystalline cellulose prepared from lignocellulosic materials. Part II: Physicochemical properties. Carbohydr Polym 2011;83:676–87. https://doi.org/10.1016/J.CARBPOL.2010.08.039.

[85] Yulina R, Srie Gustiani R, Kasipah C, Danny Sukardan Balai Besar Tekstil M, Perindustrian K, Jenderal Ahmad Yani No J. Preparation of Microcrystalline Cellulose from Cotton Yarn Spinning Mills Wastes: Effect of Pretreatment and Hydrolysis Reaction Condition on the Product Characteristics. E3S Web of Conferences 2020;148:02004. https://doi.org/10.1051/E3SCONF/202014802004.
[86] Karchangi ZK, Behrooz R. Preparation of Microcrystalline Cellulose Using Cotton Yarn Waste from the Textile Industry and Evaluation of its Characteristics. Bioresources 2023;18:1115–27. https://doi.org/10.15376/BIORES.18.1.1115-1127.
[87] An NN, Le Chi PT. Extraction of microcrystalline cellulose from cotton fiber, and application to block natural rubber as reinforcing agent. Vietnam Journal of Chemistry 2023;61:73–80. https://doi.org/10.1002/VJCH.202300070.
[88] Vanhatalo KM, Parviainen KE,, Dahl OP. Techno-economic analysis of simplified microcrystalline cellulose process :: BioResources 2014. https://bioresources.cnr.ncsu.edu/resources/techno-economic-analysis-of-simplified-microcrystalline-cellulose-process/ (accessed January 1, 2024).
[89] Chaerunisaa AY, Sriwidodo S, Abdassah M, Chaerunisaa AY, Sriwidodo S, Abdassah M. Microcrystalline Cellulose as Pharmaceutical Excipient. Pharmaceutical Formulation Design - Recent Practices 2019. https://doi.org/10.5772/INTECHOPEN.88092.
[90] Moon RJ, Martini A, Nairn J, Simonsen J, Youngblood J. Cellulose nanomaterials review: structure, properties and nanocomposites. Chem Soc Rev 2011;40:3941. https://doi.org/10.1039/c0cs00108b.
[91] Nanocellulose Data Sheets - The Process Development Center - University of Maine n.d. https://umaine.edu/pdc/nanocellulose/nanocellulose-spec-sheets-and-safety-data-sheets/ (accessed August 4, 2022).
[92] Šturcová A, Davies GR, Eichhorn SJ. Elastic modulus and stress-transfer properties of tunicate cellulose whiskers. Biomacromolecules 2005;6:1055–61. https://doi.org/10.1021/BM049291K;PAGE:STRING:ARTICLE/CHAPTER.
[93] Habibi Y, Lucia LA, Rojas OJ. Cellulose nanocrystals: Chemistry, self-assembly, and applications. Chem Rev 2010;110:3479–500. https://doi.org/10.1021/CR900339W/ASSET/IMAGES/MEDIUM/CR-2009-00339W_0022.GIF.
[94] Nawa T. Effect of Chemical Structure on Steric Stabilization of Polycarboxylate-based Superplasticizer. Journal of Advanced Concrete Technology 2006;4:225–32. https://doi.org/10.3151/JACT.4.225.
[95] Fu T, Montes F, Suraneni P, Youngblood J, Weiss J. The Influence of Cellulose Nanocrystals on the Hydration and Flexural Strength of Portland Cement Pastes. Polymers 2017, Vol 9, Page 424 2017;9:424. https://doi.org/10.3390/POLYM9090424.
[96] Cao Y, Zavattieri P, Youngblood J, Moon R, Weiss J. The relationship between cellulose nanocrystal dispersion and strength. Constr Build Mater 2016;119:71–9. https://doi.org/10.1016/J.CONBUILDMAT.2016.03.077.

[97] Cao Y, Tian N, Bahr D, Zavattieri PD, Youngblood J, Moon RJ, et al. The influence of cellulose nanocrystals on the microstructure of cement paste. Cem Concr Compos 2016;74:164–73. https://doi.org/10.1016/J.CEMCONCOMP.2016.09.008.
[98] Montes F, Fu T, Youngblood JP, Weiss J. Rheological impact of using cellulose nanocrystals (CNC) in cement pastes. Constr Build Mater 2020;235:117497. https://doi.org/10.1016/J.CONBUILDMAT.2019.117497.
[99] Kochova K, Schollbach K, Gauvin F, Brouwers HJH. Effect of saccharides on the hydration of ordinary Portland cement. Constr Build Mater 2017;150:268–75. https://doi.org/10.1016/J.CONBUILDMAT.2017.05.149.
[100] Gómez Hoyos C, Cristia E, Vázquez A. Effect of cellulose microcrystalline particles on properties of cement based composites. Mater Des 2013;51:810–8. https://doi.org/10.1016/J.MATDES.2013.04.060.
[101] Ghahari SA, Assi LN, Alsalman A, Alyamaç KE. Fracture Properties Evaluation of Cellulose Nanocrystals Cement Paste. Materials 2020, Vol 13, Page 2507 2020;13:2507. https://doi.org/10.3390/MA13112507.
[102] Campbell MD, Coutts RSP. Wood fibre-reinforced cement composites. J Mater Sci 1980;15:1962–70. https://doi.org/10.1007/BF00550621/METRICS.
[103] Booya E, Ghaednia H, Das S, Pande H. Durability of cementitious materials reinforced with various Kraft pulp fibers. Constr Build Mater 2018;191:1191–200. https://doi.org/10.1016/J.CONBUILDMAT.2018.10.139.
[104] Blankenhorn PR, Blankenhorn BD, Silsbee MR, DiCola M. Effects of fiber surface treatments on mechanical properties of wood fiber–cement composites. Cem Concr Res 2001;31:1049–55. https://doi.org/10.1016/S0008-8846(01)00528-2.
[105] US20110248421A1 - Fiber cement composite materials using bleached cellulose fibers - Google Patents n.d. https://patents.google.com/patent/US20110248421A1/en (accessed November 9, 2023).
[106] Tonoli GHD, Fuente E, Monte C, Savastano H, Lahr FAR, Blanco A. Effect of fibre morphology on flocculation of fibre–cement suspensions. Cem Concr Res 2009;39:1017–22. https://doi.org/10.1016/J.CEMCONRES.2009.07.010.
[107] Soroushian P, Marikunte S. Moisture Effects on Flexural Performance of Wood FiberCement Composites. Journal of Materials in Civil Engineering 1992;4:275–91. https://doi.org/10.1061/(ASCE)0899-1561(1992)4:3(275).
[108] Mohr BJ, Nanko H, Kurtis KE. Aligned kraft pulp fiber sheets for reinforcing mortar. Cem Concr Compos 2006;28:161–72. https://doi.org/10.1016/J.CEMCONCOMP.2005.08.004.
[109] Soroushian P, Marikunte S, Won J. Wood Fiber Reinforced Cement Composites under WettingDrying and FreezingThawing Cycles. Journal of Materials in Civil Engineering 1994;6:595–611. https://doi.org/10.1061/(ASCE)0899-1561(1994)6:4(595).

[110] Filipak Vanin DV, Andrade VD, Fiorentin TA, Recouvreux D de OS, Carminatti CA, Al-Qureshi HA. Cement pastes modified by cellulose nanocrystals: A dynamic moduli evolution assessment by the Impulse Excitation Technique. Mater Chem Phys 2020;239:122038. https://doi.org/10.1016/J.MATCHEMPHYS.2019.122038.
[111] Lee HJ, Kim W. Long-term durability evaluation of fiber-reinforced ECC using wood-based cellulose nanocrystals. Constr Build Mater 2020;238:117754. https://doi.org/10.1016/J.CONBUILDMAT.2019.117754.
[112] Lee HJ, Kim SK, Lee HS, Kim W. A Study on the Drying Shrinkage and Mechanical Properties of Fiber Reinforced Cement Composites Using Cellulose Nanocrystals. Int J Concr Struct Mater 2019;13:1–11. https://doi.org/10.1186/S40069-019-0351-2/FIGURES/12.
[113] Mazlan D, Krishnan S, Din MFM, Tokoro C, Khalid NHA, Ibrahim IS, et al. Effect of Cellulose Nanocrystals Extracted from Oil Palm Empty Fruit Bunch as Green Admixture for Mortar. Scientific Reports 2020 10:1 2020;10:1–11. https://doi.org/10.1038/s41598-020-63575-7.
[114] Claramunt J, Ventura H, Toledo Filho RD, Ardanuy M. Effect of nanocelluloses on the microstructure and mechanical performance of CAC cementitious matrices. Cem Concr Res 2019;119:64–76. https://doi.org/10.1016/J.CEMCONRES.2019.02.006.
[115] M.T. Postek, R.J. Moon, A.W. Rudie and MAB. Production and Applications of Cellulose Nanomaterials. Production and Applications of Cellulose Nanomaterials 2013:1–28.
[116] Juenger MCG, Siddique R. Recent advances in understanding the role of supplementary cementitious materials in concrete. Cem Concr Res 2015;78:71–80. https://doi.org/10.1016/J.CEMCONRES.2015.03.018.
[117] Ahmad MR, Fernàndez-Jimenez A, Chen B, Leng Z, Dai JG. Low-carbon cementitious materials: Scale-up potential, environmental impact and barriers. Constr Build Mater 2024;455:139087. https://doi.org/10.1016/J.CONBUILDMAT.2024.139087.
[118] Bouckaert S, Pales AF, McGlade C, Remme U, Wanner B, Varro L, et al. Net Zero by 2050: A Roadmap for the Global Energy Sector 2021.
[119] Low Carbon Roadmap: Pathways to a CO2-neutral European steel industry n.d. https://www.eurofer.eu/publications/reports-or-studies/low-carbon-roadmap-pathways-to-a-co2-neutral-european-steel-industry (accessed June 11, 2025).
[120] Wijayanti SC, Anggara F, Petrus HTBM. Effect of Fly Ash (FA) Characteristic on Geopolymer Product Quality. Advances in Science, Technology and Innovation 2024:95–8. https://doi.org/10.1007/978-3-031-48758-3_22/FIGURES/3.
[121] Sabir B, Wild S, Bai J. Metakaolin and calcined clays as pozzolans for concrete: a review. Cem Concr Compos 2001;23:441–54. https://doi.org/10.1016/S0958-9465(00)00092-5.
[122] Scrivener KL, John VM, Gartner EM. Eco-efficient cements: Potential economically viable solutions for a low-CO2 cement-based materials industry. Cem Concr Res 2018;114:2–26. https://doi.org/10.1016/J.CEMCONRES.2018.03.015.

[123] Qader DN, Jamil AS, Bahrami A, Ali M, Arunachalam KP. A systematic review of metakaolin-based alkali-activated and geopolymer concrete: A step toward green concrete. Reviews on Advanced Materials Science 2025;64. https://doi.org/10.1515/RAMS-2024-0076/ASSET/GRAPHIC/J_RAMS-2024-0076_FIG_007.JPG.
[124] Nathaniel O, Sam ARM, Lim NHAS, Adebisi O, Abdulkareem M. Biogenic approach for concrete durability and sustainability using effective microorganisms: A review. Constr Build Mater 2020;261:119664. https://doi.org/10.1016/J.CONBUILDMAT.2020.119664.
[125] Stamatakis MG, Fragoulis D, Csirik G, Bedelean I, Pedersen S. The influence of biogenic micro-silica-rich rocks on the properties of blended cements. Cem Concr Compos 2003;25:177–84. https://doi.org/10.1016/S0958-9465(02)00019-7.
[126] Sena Da Fonseca B, Vilão A, Galhano C, Simão JAR. Reusing coffee waste in manufacture of ceramics for construction. Advances in Applied Ceramics 2014;113:159–66. https://doi.org/10.1179/1743676113Y.0000000131.
[127] Roychand R, Kilmartin-Lynch S, Saberian M, Li J, Zhang G, Li CQ. Transforming spent coffee grounds into a valuable resource for the enhancement of concrete strength. J Clean Prod 2023;419:138205. https://doi.org/10.1016/J.JCLEPRO.2023.138205.
[128] Sirico A, Bernardi P, Sciancalepore C, Vecchi F, Malcevschi A, Belletti B, et al. Biochar from wood waste as additive for structural concrete. Constr Build Mater 2021;303:124500. https://doi.org/10.1016/J.CONBUILDMAT.2021.124500.
[129] de Coninck H, Revi A, Babiker M, Bertoldi P, Buckeridge M, Bertoldi P, et al. Strengthening and Implementing the Global Response. In: Masson-Delmotte V, P Z, Pörtner H-O, Roberts D, Skea J, Shukla PR, et al., editors. Global Warming of 1.5°C., Cambridge University Press, Cambridge UK and New York, NY, USA; 2018, p. 313–444. https://doi.org/10.1017/9781009157940.006.
[130] A biochar classification system and associated test methods. Biochar for Environmental Management 2015:165–93. https://doi.org/10.4324/9780203762264-8.
[131] Ippolito JA, Cui L, Kammann C, Wrage-Mönnig N, Estavillo JM, Fuertes-Mendizabal T, et al. Feedstock choice, pyrolysis temperature and type influence biochar characteristics: a comprehensive meta-data analysis review. Biochar 2020;2:421–38. https://doi.org/10.1007/S42773-020-00067-X/TABLES/6.
[132] Bardestani R, Kaliaguine S. Steam activation and mild air oxidation of vacuum pyrolysis biochar. Biomass Bioenergy 2018;108:101–12. https://doi.org/10.1016/J.BIOMBIOE.2017.10.011.
[133] Fidel RB, Laird DA, Thompson ML, Lawrinenko M. Characterization and quantification of biochar alkalinity. Chemosphere 2017;167:367–73. https://doi.org/10.1016/J.CHEMOSPHERE.2016.09.151.
[134] Tomczyk A, Sokołowska Z, Boguta P. Biochar physicochemical properties: pyrolysis temperature and feedstock kind effects. Rev Environ Sci Biotechnol 2020;19:191–215. https://doi.org/10.1007/S11157-020-09523-3/TABLES/3.

[135] Basic Information about Landfill Gas | US EPA n.d. https://www.epa.gov/lmop/basic-information-about-landfill-gas (accessed November 2, 2024).
[136] Lehmann J, Cowie A, Masiello CA, Kammann C, Woolf D, Amonette JE, et al. Biochar in climate change mitigation. Nature Geoscience 2021 14:12 2021;14:883–92. https://doi.org/10.1038/s41561-021-00852-8.
[137] Dixit A, Gupta S, Pang SD, Kua HW. Waste Valorisation using biochar for cement replacement and internal curing in ultra-high performance concrete. J Clean Prod 2019;238:117876. https://doi.org/10.1016/J.JCLEPRO.2019.117876.
[138] Gupta S, Tulliani JM, Kua HW. Carbonaceous admixtures in cementitious building materials: Effect of particle size blending on rheology, packing, early age properties and processing energy demand. Science of The Total Environment 2022;807:150884. https://doi.org/10.1016/J.SCITOTENV.2021.150884.
[139] Choi WC, Yun H Do, Lee JY. Mechanical Properties of Mortar Containing Bio-Char From Pyrolysis. Journal of the Korea Institute for Structural Maintenance and Inspection 2012;16:67–74. https://doi.org/10.11112/JKSMI.2012.16.3.067.
[140] Gupta S, Kua HW, Pang SD. Biochar-mortar composite: Manufacturing, evaluation of physical properties and economic viability. Constr Build Mater 2018;167:874–89. https://doi.org/10.1016/J.CONBUILDMAT.2018.02.104.
[141] Restuccia L, Ferro GA. Nanoparticles from food waste: a “green” future for traditional building materials. Proceedings of the 9th International Conference on Fracture Mechanics of Concrete and Concrete Structures, IA-FraMCoS; 2016. https://doi.org/10.21012/FC9.276.
[142] Khushnood RA, Ahmad S, Restuccia L, Spoto C, Jagdale P, Tulliani JM, et al. Carbonized nano/microparticles for enhanced mechanical properties and electromagnetic interference shielding of cementitious materials. Frontiers of Structural and Civil Engineering 2016;10:209–13. https://doi.org/10.1007/S11709-016-0330-5/METRICS.
[143] V. D. Glukhovsky. Soil Silicate-Based Products and Structures. Moscow: Gosstroiizdat Publ.; 1957.
[144] V. D. Glukhovsky. Soil Silicates. Kiev: Gosstroyizdat; 1959.
[145] Pacheco-Torgal F. Introduction to Handbook of Alkali-activated Cements, Mortars and Concretes. Handbook of Alkali-Activated Cements, Mortars and Concretes 2015:1–16. https://doi.org/10.1533/9781782422884.1.
[146] Nodehi M, Taghvaee VM. Alkali-Activated Materials and Geopolymer: a Review of Common Precursors and Activators Addressing Circular Economy. Circular Economy and Sustainability 2021 2:1 2021;2:165–96. https://doi.org/10.1007/S43615-021-00029-W.
[147] Martínez A, Miller SA. A review of drivers for implementing geopolymers in construction: Codes and constructability. Resour Conserv Recycl 2023;199:107238. https://doi.org/10.1016/J.RESCONREC.2023.107238.

[148] Shoaei P, Ameri F, Karimzadeh M, Atabakhsh E, Zareei SA, Behforouz B. Difference between geopolymers and alkali-activated materials. Handbook of Sustainable Concrete and Industrial Waste Management: Recycled and Artificial Aggregate, Innovative Eco-Friendly Binders, and Life Cycle Assessment 2022:421–35. https://doi.org/10.1016/B978-0-12-821730-6.00018-8.
[149] Davidovits J. Geopolymers - Inorganic polymeric new materials. Journal of Thermal Analysis 1991;37:1633–56. https://doi.org/10.1007/BF01912193/METRICS.
[150] Joseph Davidovits. Mineral polymers and methods of making them. US4349386A, 1982.
[151] Singh NB, Saxena SK, Kumar M. Effect of nanomaterials on the properties of geopolymer mortars and concrete. Mater Today Proc 2018;5:9035–40. https://doi.org/10.1016/J.MATPR.2017.10.018.
[152] Duxson P, Fernández-Jiménez A, Provis JL, Lukey GC, Palomo A, Van Deventer JSJ. Geopolymer technology: The current state of the art. J Mater Sci 2007;42:2917–33. https://doi.org/10.1007/S10853-006-0637-Z/FIGURES/15.
[153] Amritphale SS, Bhardwaj P, Gupta R, Amritphale SS, Bhardwaj P, Gupta R. Advanced Geopolymerization Technology. Geopolymers and Other Geosynthetics 2019. https://doi.org/10.5772/INTECHOPEN.87250.
[154] Vrålstad T, Saasen A, Fjær E, Øia T, Ytrehus JD, Khalifeh M. Plug & abandonment of offshore wells: Ensuring long-term well integrity and cost-efficiency. J Pet Sci Eng 2019;173:478–91. https://doi.org/10.1016/J.PETROL.2018.10.049.
[155] Shi C, Roy D, Krivenko P. Alkali-Activated Cements and Concretes. Alkali-Activated Cements and Concretes 2003. https://doi.org/10.1201/9781482266900.
[156] Murat M. Hydration reaction and hardening of calcined clays and related minerals. I. Preliminary investigation on metakaolinite. Cem Concr Res 1983;13:259–66. https://doi.org/10.1016/0008-8846(83)90109-6.
[157] Khatib JM, Wild S. Pore size distribution of metakaolin paste. Cem Concr Res 1996;26:1545–53. https://doi.org/10.1016/0008-8846(96)00147-0.
[158] Duxson P, Provis JL, Lukey GC, Mallicoat SW, Kriven WM, Van Deventer JSJ. Understanding the relationship between geopolymer composition, microstructure and mechanical properties. Colloids Surf A Physicochem Eng Asp 2005;269:47–58. https://doi.org/10.1016/J.COLSURFA.2005.06.060.
[159] Huang W, Wang H. Formulation development of metakaolin geopolymer with good workability for strength improvement and shrinkage reduction. J Clean Prod 2024;434:140431. https://doi.org/10.1016/J.JCLEPRO.2023.140431.
[160] Sagoe-Crentsil K, Weng L. Dissolution processes, hydrolysis and condensation reactions during geopolymer synthesis: Part II. High Si/Al ratio systems. J Mater Sci 2007;42:3007–14. https://doi.org/10.1007/S10853-006-0818-9/FIGURES/6.

[161] Weng L, Sagoe-Crentsil K. Dissolution processes, hydrolysis and condensation reactions during geopolymer synthesis: Part I-Low Si/Al ratio systems. J Mater Sci 2007;42:2997–3006. https://doi.org/10.1007/S10853-006-0820-2/FIGURES/3.
[162] Yaseri S, Hajiaghaei G, Mohammadi F, Mahdikhani M, Farokhzad R. The role of synthesis parameters on the workability, setting and strength properties of binary binder based geopolymer paste. Constr Build Mater 2017;157:534–45. https://doi.org/10.1016/J.CONBUILDMAT.2017.09.102.
[163] Firdous R, Stephan D. Effect of silica modulus on the geopolymerization activity of natural pozzolans. Constr Build Mater 2019;219:31–43. https://doi.org/10.1016/J.CONBUILDMAT.2019.05.161.
[164] Gharzouni A, Joussein E, Samet B, Baklouti S, Pronier S, Sobrados I, et al. The effect of an activation solution with siliceous species on the chemical reactivity and mechanical properties of geopolymers. J Solgel Sci Technol 2015;73:250–9. https://doi.org/10.1007/S10971-014-3524-0/FIGURES/10.
[165] Bondar D, Lynsdale CJ, Milestone NB, Hassani N, Ramezanianpour AA. Effect of type, form, and dosage of activators on strength of alkali-activated natural pozzolans. Cem Concr Compos 2011;33:251–60. https://doi.org/10.1016/J.CEMCONCOMP.2010.10.021.
[166] Hounsi AD, Lecomte-Nana G, Djétéli G, Blanchart P, Alowanou D, Kpelou P, et al. How does Na, K alkali metal concentration change the early age structural characteristic of kaolin-based geopolymers. Ceram Int 2014;40:8953–62. https://doi.org/10.1016/J.CERAMINT.2014.02.052.
[167] Xu H, Van Deventer JSJ. The geopolymerisation of alumino-silicate minerals. Int J Miner Process 2000;59:247–66. https://doi.org/10.1016/S0301-7516(99)00074-5.
[168] Liu J, Li X, Lu Y, Bai X. Effects of Na/Al ratio on mechanical properties and microstructure of red mud-coal metakaolin geopolymer. Constr Build Mater 2020;263:120653. https://doi.org/10.1016/J.CONBUILDMAT.2020.120653.
[169] He P, Wang M, Fu S, Jia D, Yan S, Yuan J, et al. Effects of Si/Al ratio on the structure and properties of metakaolin based geopolymer. Ceram Int 2016;42:14416–22. https://doi.org/10.1016/J.CERAMINT.2016.06.033.
[170] Lizcano M, Gonzalez A, Basu S, Lozano K, Radovic M. Effects of water content and chemical composition on structural properties of alkaline activated metakaolin-based geopolymers. Journal of the American Ceramic Society 2012;95:2169–77. https://doi.org/10.1111/J.1551-2916.2012.05184.X;WGROUP:STRING:PUBLICATION.
[171] Pouhet R, Cyr M, Bucher R. Influence of the initial water content in flash calcined metakaolin-based geopolymer. Constr Build Mater 2019;201:421–9. https://doi.org/10.1016/J.CONBUILDMAT.2018.12.201.

[172] Bowen F, Jiesheng L, Jing W, Yaohua C, Tongtong Z, Xiaoming T, et al. Investigation on the impact of different activator to solid ratio on properties and micro-structure of metakaolin geopolymer. Case Studies in Construction Materials 2022;16:e01127. https://doi.org/10.1016/J.CSCM.2022.E01127.
[173] Kidalova L, Stevulova N, Geffert A. Possibility of Using Wood Pulp in the Preparation of Cement Composites. Selected Scientific Papers - Journal of Civil Engineering 2014;9:51–8. https://doi.org/10.2478/SSPJCE-2014-0006.
[174] Faruk O, Bledzki AK, Fink HP, Sain M. Progress Report on Natural Fiber Reinforced Composites. Macromol Mater Eng 2014;299:9–26. https://doi.org/10.1002/MAME.201300008.
[175] Booya E, Gorospe K, Ghaednia H, Das S. Durability properties of engineered pulp fibre reinforced concretes made with and without supplementary cementitious materials. Compos B Eng 2019;172:376–86. https://doi.org/10.1016/J.COMPOSITESB.2019.05.070.
[176] Ardanuy M, Claramunt J, Toledo Filho RD. Cellulosic fiber reinforced cement-based composites: A review of recent research. Constr Build Mater 2015;79:115–28. https://doi.org/10.1016/J.CONBUILDMAT.2015.01.035.
[177] Trees Are Climate Change, Carbon Storage Heroes | US Forest Service n.d. https://www.fs.usda.gov/features/trees-are-climate-change-carbon-storage-heroes (accessed May 15, 2023).
[178] Sahoo K, Bergman R, Alanya-Rosenbaum S, Gu H, Liang S. Life Cycle Assessment of Forest-Based Products: A Review. Sustainability 2019, Vol 11, Page 4722 2019;11:4722. https://doi.org/10.3390/SU11174722.
[179] Javadi A, Jamil T, Abouzari-Lotf E, Soucek MD, Heinz H. Working Mechanisms and Design Principles of Comb-like Polycarboxylate Ether Superplasticizers in Cement Hydration: Quantitative Insights for a Series of Well-Defined Copolymers. ACS Sustain Chem Eng 2021;9:8354–71. https://doi.org/10.1021/ACSSUSCHEMENG.0C08566/ASSET/IMAGES/LARGE/SC0C08566_0008.JPEG.
[180] Bishop M, Barron AR. Cement Hydration Inhibition with Sucrose, Tartaric Acid, and Lignosulfonate: Analytical and Spectroscopic Study. Ind Eng Chem Res 2006;45:7042–9. https://doi.org/10.1021/ie060806t.
[181] Sun Y, Zhang Y, Cai Y, Lam WL, Lu J-X, Shen P, et al. Mechanisms on Accelerating Hydration of Alite Mixed with Inorganic Salts in Seawater and Characteristics of Hydration Products. ACS Sustain Chem Eng 2021;9:10479–90. https://doi.org/10.1021/acssuschemeng.1c01730.
[182] Mignon A, Snoeck D, D'Halluin K, Balcaen L, Vanhaecke F, Dubruel P, et al. Alginate biopolymers: Counteracting the impact of superabsorbent polymers on mortar strength. Constr Build Mater 2016;110:169–74. https://doi.org/10.1016/J.CONBUILDMAT.2016.02.033.

[183] Fu T, Moon RJ, Zavattieri P, Youngblood J, Weiss WJ. Cellulose nanomaterials as additives for cementitious materials. Cellulose-Reinforced Nanofibre Composites, Elsevier; 2017, p. 455–82. https://doi.org/10.1016/B978-0-08-100957-4.00020-6.
[184] Guo A, Sun Z, Sathitsuksanoh N, Feng H. A Review on the Application of Nanocellulose in Cementitious Materials. Nanomaterials 2020;10:2476. https://doi.org/10.3390/nano10122476.
[185] Dong S, Roman M. Fluorescently Labeled Cellulose Nanocrystals for Bioimaging Applications. J Am Chem Soc 2007;129:13810–1. https://doi.org/10.1021/ja076196l.
[186] Panchal P, Ogunsona E, Mekonnen T. Trends in Advanced Functional Material Applications of Nanocellulose. Processes 2019, Vol 7, Page 10 2018;7:10. https://doi.org/10.3390/PR7010010.
[187] Shojaeiarani J, Bajwa DS, Chanda S. Cellulose nanocrystal based composites: A review. Composites Part C: Open Access 2021;5:100164. https://doi.org/10.1016/J.JCOMC.2021.100164.
[188] Moon RJ, Martini A, Nairn J, Simonsen J, Youngblood J. Cellulose nanomaterials review: structure, properties and nanocomposites. Chem Soc Rev 2011;40:3941. https://doi.org/10.1039/c0cs00108b.
[189] Becerril AP. THE INFLUENCE OF CELLULOSE NANOCRYSTALS ON PERFORMANCE AND TRANSPORT PROPERTIES OF CEMENTITIOUS MATERIALS AND GYPSUM 2020. https://doi.org/10.25394/PGS.13270457.V1.
[190] Portland cement n.d. https://www.lafarge.ca/en/portland-cement (accessed November 6, 2022).
[191] Bleached Softwood Kraft Pulp | Canfor n.d. https://www.canfor.com/products/pulp-and-paper/pulp/bleached-softwood-pulp (accessed August 4, 2022).
[192] Poly(acrylamide-co-acrylic acid) Mw 520,000, Mn 150,000 Typical, acrylamide 80wt. 62649-23-4 n.d. https://www.sigmaaldrich.com/CA/en/product/aldrich/511471 (accessed November 6, 2022).
[193] Paul CW. Adhesion Science and Engineering. Elsevier; 2002.
[194] Deutsch M, Hölzer G, Härtwig J, Wolf J, Fritsch M, Förster E. K alpha and K beta x-ray emission spectra of copper. Phys Rev A 1995;51:283–96. https://doi.org/10.1103/PHYSREVA.51.283.
[195] Heu R, Shahbazmohamadi S, Yorston J, Capeder P. Target Material Selection for Sputter Coating of SEM Samples. Micros Today 2019;27:32–6. https://doi.org/10.1017/S1551929519000610.
[196] ASTM C1185, 2016, Standard Test Methods for Sampling and Testing Non-Asbestos Fiber-Cement Flat Sheet, Roofing and Siding Shingles, and Clapboards. ASTM International 2016.

[197] Lei L, Plank J. A concept for a polycarboxylate superplasticizer possessing enhanced clay tolerance. Cem Concr Res 2012;42:1299–306. https://doi.org/10.1016/j.cemconres.2012.07.001.
[198] Derakhshandeh B, Kerekes RJ, Hatzikiriakos SG, Bennington CPJ. Rheology of pulp fibre suspensions: A critical review. Chem Eng Sci 2011;66:3460–70. https://doi.org/10.1016/J.CES.2011.04.017.
[199] Cui H, Grace JR. Flow of pulp fibre suspension and slurries: A review. International Journal of Multiphase Flow 2007;33:921–34. https://doi.org/10.1016/J.IJMULTIPHASEFLOW.2007.03.004.
[200] Mejdoub R, Hammi H, Suñol JJ, Khitouni M, M'nif A, Boufi S. Nanofibrillated cellulose as nanoreinforcement in Portland cement: Thermal, mechanical and microstructural properties. Http://DxDoiOrg/101177/0021998316672090 2016;51:2491–503. https://doi.org/10.1177/0021998316672090.
[201] Hisseine OA, Omran AF, Tagnit-Hamou A. Influence of Cellulose Filaments on Cement Paste and Concrete. Journal of Materials in Civil Engineering 2018;30:04018109. https://doi.org/10.1061/(ASCE)MT.1943-5533.0002287.
[202] Bakkari M El, Bindiganavile V, Goncalves J, Boluk Y. Preparation of cellulose nanofibers by TEMPO-oxidation of bleached chemi-thermomechanical pulp for cement applications. Carbohydr Polym 2019;203:238–45. https://doi.org/10.1016/J.CARBPOL.2018.09.036.
[203] Zakani B, Grecov D. Yield stress analysis of cellulose nanocrystalline gels. Cellulose 2020;27:9337–53. https://doi.org/10.1007/S10570-020-03429-7/FIGURES/17.
[204] Xu Y, Atrens AD, Stokes JR. Rheology and microstructure of aqueous suspensions of nanocrystalline cellulose rods. J Colloid Interface Sci 2017;496:130–40. https://doi.org/10.1016/J.JCIS.2017.02.020.
[205] Gupta C, Nadelman E, Washburn NR, Kurtis KE. Lignopolymer Superplasticizers for Low-CO_2 Cements. ACS Sustain Chem Eng 2017;5:4041–9. https://doi.org/10.1021/acssuschemeng.7b00021.
[206] Bezerra UT. Biopolymers with superplasticizer properties for concrete. Biopolymers and Biotech Admixtures for Eco-Efficient Construction Materials, Elsevier; 2016, p. 195–220. https://doi.org/10.1016/B978-0-08-100214-8.00010-5.
[207] Plank J. Applications of biopolymers and other biotechnological products in building materials. Appl Microbiol Biotechnol 2004;66:1–9. https://doi.org/10.1007/S00253-004-1714-3/TABLES/6.
[208] Banfill PFG. Additivity effects in the rheology of fresh concrete containing water-reducing admixtures. Constr Build Mater 2011;25:2955–60. https://doi.org/10.1016/J.CONBUILDMAT.2010.12.001.
[209] Vollpracht A, Lothenbach B, Snellings R, Haufe J. The pore solution of blended cements: a review. Materials and Structures/Materiaux et Constructions 2016;49:3341–67. https://doi.org/10.1617/S11527-015-0724-1/FIGURES/26.

[210] Kamasamudram KS, Ashraf W, Landis EN, Khan RI. Effects of ligno– and delignified–cellulose nanofibrils on the performance of cement-based materials. Journal of Materials Research and Technology 2021;13:321–35. https://doi.org/10.1016/J.JMRT.2021.04.090.
[211] Cadix A, James S. Cementing additives. Fluid Chemistry, Drilling and Completion 2022:187–254. https://doi.org/10.1016/B978-0-12-822721-3.00008-3.
[212] Sha S, Wang M, Shi C, Xiao Y. Influence of the structures of polycarboxylate superplasticizer on its performance in cement-based materials-A review. Constr Build Mater 2020;233:117257. https://doi.org/10.1016/J.CONBUILDMAT.2019.117257.
[213] Chen XQ, Cheng X, Wen XD, Xun J, Shen YF. Research on the effectiveness of polycarboxylate superplasticisers with different side-chain lengths. Https://DoiOrg/101680/Jadcr1800232 2021;33:39–45. https://doi.org/10.1680/JADCR.18.00232.
[214] Engbert A, Gruber S, Plank J. The effect of alginates on the hydration of calcium aluminate cement. Carbohydr Polym 2020;236. https://doi.org/10.1016/J.CARBPOL.2020.116038.
[215] Chen X, Matar MG, Beatty DN, Srubar W V. Retardation of Portland Cement Hydration with Photosynthetic Algal Biomass. ACS Sustain Chem Eng 2021;9:13726–34. https://doi.org/10.1021/acssuschemeng.1c04033.
[216] Double DD, Hellawell A. The hydration of Portland Cement. Nature 1976 261:5560 1976;261:486–8. https://doi.org/10.1038/261486a0.
[217] Richardson IG. The nature of the hydration products in hardened cement pastes. Cem Concr Compos 2000;22:97–113. https://doi.org/10.1016/S0958-9465(99)00036-0.
[218] Maddalena R, Li K, Chater PA, Michalik S, Hamilton A. Direct synthesis of a solid calcium-silicate-hydrate (C-S-H). Constr Build Mater 2019;223:554–65. https://doi.org/10.1016/J.CONBUILDMAT.2019.06.024.
[219] Michell AJ, Freischmidt G. Effect of fibre curl on the properties of wood pulp fibre-cement and silica sheets. Journal of Materials Science 1990 25:12 1990;25:5225–30. https://doi.org/10.1007/BF00580155.
[220] Bentur A. Role of Interfaces in Controlling Durability of Fiber-Reinforced Cements. Journal of Materials in Civil Engineering 2000;12:2–7. https://doi.org/10.1061/(ASCE)0899-1561(2000)12:1(2).
[221] Savastano H, Warden PG, Coutts RSP. Potential of alternative fibre cements as building materials for developing areas. Cem Concr Compos 2003;25:585–92. https://doi.org/10.1016/S0958-9465(02)00071-9.
[222] Savastano H, Warden PG, Coutts RSP. Microstructure and mechanical properties of waste fibre–cement composites. Cem Concr Compos 2005;27:583–92. https://doi.org/10.1016/J.CEMCONCOMP.2004.09.009.
[223] Coutts RSP, Kightly P. Bonding in wood fibre-cement composites. Journal of Materials Science 1984 19:10 1984;19:3355–9. https://doi.org/10.1007/BF00549827.

[224] Jang JG, Lee NK, Lee HK. Fresh and hardened properties of alkali-activated fly ash/slag pastes with superplasticizers. Constr Build Mater 2014;50:169–76. https://doi.org/10.1016/J.CONBUILDMAT.2013.09.048.
[225] Barnat-Hunek D, Szymańska-Chargot M, Jarosz-Hadam M, Łagód G. Effect of cellulose nanofibrils and nanocrystals on physical properties of concrete. Constr Build Mater 2019;223:1–11. https://doi.org/10.1016/J.CONBUILDMAT.2019.06.145.
[226] Kolour HH, Ashraf W, Landis EN. Hydration and Early Age Properties of Cement Pastes Modified with Cellulose Nanofibrils. Https://DoiOrg/101177/0361198120945993 2020;2675:38–46. https://doi.org/10.1177/0361198120945993.
[227] Sun X, Wu Q, Lee S, Qing Y, Wu Y. Cellulose Nanofibers as a Modifier for Rheology, Curing and Mechanical Performance of Oil Well Cement. Scientific Reports 2016 6:1 2016;6:1–9. https://doi.org/10.1038/srep31654.
[228] Sustainable consumption and production n.d. https://www.un.org/sustainabledevelopment/sustainable-consumption-production/ (accessed January 14, 2024).
[229] Ranachowski Z. The fabrication, testing and application of fibre cement boards 2018:125.
[230] Chung DDL. Cement-Matrix Composites. Carbon Composites 2017:333–86. https://doi.org/10.1016/B978-0-12-804459-9.00006-3.
[231] El-Sheikhy R. Resisting spread of environmental-pollution diseases due to Portland-cement industries: green nanoclay applications. Scientific Reports 2023 13:1 2023;13:1–27. https://doi.org/10.1038/s41598-023-27759-1.
[232] Bouras R, Kaci A, Chaouche M. Influence of viscosity modifying admixtures on the rheological behavior of cement and mortar pastes. Korea Australia Rheology Journal 2012;24:35–44. https://doi.org/10.1007/S13367-012-0004-3/METRICS.
[233] Altun MG, Özen S, Mardani-Aghabaglou A. Effect of side chain length change of polycarboxylate-ether based high range water reducing admixture on properties of self-compacting concrete. Constr Build Mater 2020;246:118427. https://doi.org/https://doi.org/10.1016/j.jobe.2021.102259.
[234] Antoni, Halim JG, Kusuma OC, Hardjito D. Optimizing Polycarboxylate Based Superplasticizer Dosage with Different Cement Type. Procedia Eng 2017;171:752–9. https://doi.org/10.1016/J.PROENG.2017.01.442.
[235] Shin JY, Hong JS, Suh JK, Lee YS. Effects of polycarboxylate-type superplasticizer on fluidity and hydration behavior of cement paste. Korean Journal of Chemical Engineering 2008 25:6 2008;25:1553–61. https://doi.org/10.1007/S11814-008-0255-3.
[236] Ng S, Justnes H. Influence of lignosulfonate on the early age rheology and hydration characteristics of cement pastes. J Sustain Cem Based Mater 2015;4:15–24. https://doi.org/10.1080/21650373.2014.894952.
[237] Zhang DF, Ju BZ, Zhang SF, He L, Yang JZ. The study on the dispersing mechanism of starch sulfonate as a water-reducing agent for cement. Carbohydr Polym 2007;70:363–8. https://doi.org/10.1016/J.CARBPOL.2007.04.024.

[238] Vieira JG, Oliveira G de C, Filho GR, Assunção RMN de, Meireles C da S, Cerqueira DA, et al. Production, characterization and evaluation of methylcellulose from sugarcane bagasse for applications as viscosity enhancing admixture for cement based material. Carbohydr Polym 2009;78:779–83. https://doi.org/10.1016/J.CARBPOL.2009.06.016.
[239] Peschard A, Govin A, Pourchez J, Fredon E, Bertrand L, Maximilien S, et al. Effect of polysaccharides on the hydration of cement suspension. J Eur Ceram Soc 2006;26:1439–45. https://doi.org/10.1016/J.JEURCERAMSOC.2005.02.005.
[240] Penkała M, Ogrodnik P, Rogula-Kozłowska W. Silica Dust as an Additive in Concrete with Proven Impact on Human Health. Pol J Environ Stud 2019;28:4057–71. https://doi.org/10.15244/PJOES/99241.
[241] Bourbia S, Kazeoui H, Belarbi R. A review on recent research on bio-based building materials and their applications. Materials for Renewable and Sustainable Energy 2023 12:2 2023;12:117–39. https://doi.org/10.1007/S40243-023-00234-7.
[242] Smirnova M, Nething C, Stolz A, Gröning JAD, Funaro DP, Eppinger E, et al. High strength bio-concrete for the production of building components. Npj Materials Sustainability 2023 1:1 2023;1:1–15. https://doi.org/10.1038/s44296-023-00004-6.
[243] Raghunath S, Hoque M, Foster EJ. On the Roles of Cellulose Nanocrystals in Fiber Cement: Implications for Rheology, Hydration Kinetics, and Mechanical Properties. ACS Sustain Chem Eng 2023;11. https://doi.org/10.1021/acssuschemeng.3c01392.
[244] Abbati De Assis C, Houtman C, Phillips R, Bilek T, Rojas OJ, Peresin MS, et al. Understanding the Conversion Economics of Cellulose Nanocrystals: Understanding the Conversion Economics of Cellulose Nanocrystals 2017. https://doi.org/10.1002/bbb.1782.
[245] Shaghaleh H, Xu X, Wang S. Current progress in production of biopolymeric materials based on cellulose, cellulose nanofibers, and cellulose derivatives. RSC Adv 2018;8:825–42. https://doi.org/10.1039/C7RA11157F.
[246] Lei L, Hirata T, Plank J. 40 years of PCE superplasticizers - History, current state-of-the-art and an outlook. Cem Concr Res 2022;157:106826. https://doi.org/10.1016/J.CEMCONRES.2022.106826.
[247] Rivai H, Hamdani AS, Ramdani R, Lalfari RS, Andayani R, Armin F, et al. Research on Production and Characterization of Alpha Cellulose Derived from Rice Straw (Oryza sativa L.). Technological Innovation in Pharmaceutical Research Vol 3 2021:68–75. https://doi.org/10.9734/BPI/TIPR/V3/1698C.
[248] Adeleye OA, Bamiro OA, Albalawi DA, Alotaibi AS, Iqbal H, Sanyaolu S, et al. Characterizations of Alpha-Cellulose and Microcrystalline Cellulose Isolated from Cocoa Pod Husk as a Potential Pharmaceutical Excipient. Materials 2022, Vol 15, Page 5992 2022;15:5992. https://doi.org/10.3390/MA15175992.
[249] Xuan Truong Nguyen. US7005514B2 - Process for preparing microcrystalline cellulose - Google Patents. 2002 n.d. https://patents.google.com/patent/US7005514B2/en (accessed December 3, 2023).

[250] Sumra Y, Payam S, Zainah I. The pH of Cement-based Materials: A Review. Journal of Wuhan University of Technology-Mater Sci Ed 2020 35:5 2020;35:908–24. https://doi.org/10.1007/S11595-020-2337-Y.
[251] Van Loon LR, Glaus MA, Laube A, Stallone S. Degradation of Cellulosic Materials Under the Alkaline Conditions of a Cementitious Repository for Low- and Intermediate-Level Radioactive Waste. II. Degradation Kinetics. Journal of Environmental Polymer Degradation 1999 7:1 1999;7:41–51. https://doi.org/10.1023/A:1021894102937.
[252] Rocha Ferreira S, Ukrainczyk N, Defáveri do Carmo e Silva K, Eduardo Silva L, Koenders E. Effect of microcrystalline cellulose on geopolymer and Portland cement pastes mechanical performance. Constr Build Mater 2021;288:123053. https://doi.org/10.1016/J.CONBUILDMAT.2021.123053.
[253] Xu R, Di Guida OA. Comparison of sizing small particles using different technologies. Powder Technol 2003;132:145–53. https://doi.org/10.1016/S0032-5910(03)00048-2.
[254] RODOS n.d. https://www.sympatec.com/en/particle-measurement/dispersing-units/rodos (accessed August 27, 2024).
[255] Han D, Ferron RD. Effect of mixing method on microstructure and rheology of cement paste. Constr Build Mater 2015;93:278–88. https://doi.org/10.1016/J.CONBUILDMAT.2015.05.124.
[256] ASTM C1185. ASTM C1185, 2016, Standard Test Methods for Sampling and Testing Non-Asbestos Fiber-Cement Flat Sheet, Roofing and Siding Shingles, and Clapboards. ASTM International 2016.
[257] Wiley JH, Atalla RH. Band assignments in the raman spectra of celluloses. Carbohydr Res 1987;160:113–29. https://doi.org/10.1016/0008-6215(87)80306-3.
[258] Xiu H, Ma F, Li J, Zhao X, Liu L, Feng P, et al. Using fractal dimension and shape factors to characterize the microcrystalline cellulose (MCC) particle morphology and powder flowability. Powder Technol 2020;364:241–50. https://doi.org/10.1016/J.POWTEC.2020.01.045.
[259] Kurpińska M, Pawelska-Mazur M, Gu Y, Kurpiński F. The impact of natural fibers' characteristics on mechanical properties of the cement composites. Scientific Reports 2022 12:1 2022;12:1–14. https://doi.org/10.1038/s41598-022-25085-6.
[260] Mbasha W, Masalova I, Haldenwang R, Malkin A. The yield stress of cement pastes as obtained by different rheological approaches. Applied Rheology 2015;25:9–19. https://doi.org/10.3933/APPLRHEOL-25-53517/MACHINEREADABLECITATION/RIS.
[261] Feneuil B, Roussel N, Pitois O. Optimal cement paste yield stress for the production of stable cement foams. Cem Concr Res 2019;120:142–51. https://doi.org/10.1016/J.CEMCONRES.2019.03.002.

[262] Perrot A, Lecompte T, Khelifi H, Brumaud C, Hot J, Roussel N. Yield stress and bleeding of fresh cement pastes. Cem Concr Res 2012;42:937–44. https://doi.org/10.1016/J.CEMCONRES.2012.03.015.
[263] Mzwandile J, Willy M, Rainer H. Cement paste yield stress and self-compacting mortar stability. Constr Build Mater 2023;393:131917. https://doi.org/10.1016/J.CONBUILDMAT.2023.131917.
[264] Dinkgreve M, Paredes J, Denn MM, Bonn D. On different ways of measuring "the" yield stress. J Nonnewton Fluid Mech 2016;238:233–41. https://doi.org/10.1016/J.JNNFM.2016.11.001.
[265] Moller P, Fall A, Chikkadi V, Derks D, Bonn D. An attempt to categorize yield stress fluid behaviour. Philosophical Transactions of the Royal Society A: Mathematical, Physical and Engineering Sciences 2009;367:5139–55. https://doi.org/10.1098/RSTA.2009.0194.
[266] De Larrard F, Ferraris CF, Sedran T. Fresh concrete: A Herschel-Bulkley material. Materials and Structures/Materiaux et Constructions 1996;31:494–8. https://doi.org/10.1007/BF02480474/METRICS.
[267] De Kee D. Yield stress measurement techniques: A review. Physics of Fluids 2021;33. https://doi.org/10.1063/5.0070209/1058940.
[268] Hirn U, Schennach R. Comprehensive analysis of individual pulp fiber bonds quantifies the mechanisms of fiber bonding in paper. Scientific Reports 2015 5:1 2015;5:1–9. https://doi.org/10.1038/srep10503.
[269] Wikström T, Rasmuson A. Yield stress of pulp suspensions: The influence of fibre properties and processing conditions. Nord Pulp Paper Res J 1998;13:243–50. https://doi.org/10.3183/NPPRJ-1998-13-03-P243-246/HTML.
[270] Bennington CPJ, Kerekes RJ, Grace JR. The yield stress of fibre suspensions. Can J Chem Eng 1990;68:748–57. https://doi.org/10.1002/CJCE.5450680503.
[271] Derakhshandeh B, Hatzikiriakos SG, Bennington CPJ. The apparent yield stress of pulp fiber suspensions. J Rheol (N Y N Y) 2010;54:1137–54. https://doi.org/10.1122/1.3473923.
[272] Shokri J, Adibkia K, Shokri J, Adibkia K. Application of Cellulose and Cellulose Derivatives in Pharmaceutical Industries. IntechOpen; 2013. https://doi.org/10.5772/55178.
[273] Adamczak-Bugno A, Świt G, Krampikowska A, Proverbio E. Analysis of the Significance of Changes in the Number and Energy Parameters of Acoustic Emission Signals on the Assessment of the Strength of Fibre–Cement Boards. Materials 2022, Vol 15, Page 5757 2022;15:5757. https://doi.org/10.3390/MA15165757.
[274] de Souza LO, Liebscher M, de Souza LMS, de Andrade Silva F, Mechtcherine V. Effect of microcrystalline and nano-fibrillated cellulose on the mechanical behavior and microstructure of cement pastes. Constr Build Mater 2023;408:133812. https://doi.org/10.1016/J.CONBUILDMAT.2023.133812.

[275] Silva L, Parveen S, Filho A, Zottis A, Rana S, Vanderlei R, et al. A facile approach of developing micro crystalline cellulose reinforced cementitious composites with improved microstructure and mechanical performance. Powder Technol 2018;338:654–63. https://doi.org/10.1016/J.POWTEC.2018.07.076.
[276] Sifan M, Nagaratnam B, Thamboo J, Poologanathan K, Corradi M. Development and prospectives of lightweight high strength concrete using lightweight aggregates. Constr Build Mater 2023;362:129628. https://doi.org/10.1016/J.CONBUILDMAT.2022.129628.
[277] Zhang W, Xu J. Advanced lightweight materials for Automobiles: A review. Mater Des 2022;221:110994. https://doi.org/10.1016/J.MATDES.2022.110994.
[278] Yan JB, Wang JY, Liew JYR, Qian X. Applications of ultra-lightweight cement composite in flat slabs and double skin composite structures. Constr Build Mater 2016;111:774–93. https://doi.org/10.1016/J.CONBUILDMAT.2016.02.122.
[279] Chinmay Mondal, Ramesh Shetar. A process for obtaining alpha-cellulose - Google Patent (WO2012070072A2). WO 2012/070072A2, 2011.
[280] Ritter GJ. Determination of Alpha-Cellulose: Report of Work of Sub-Committee 2 of the Division of Cellulose Chemistry of the American Chemical Society. Industrial and Engineering Chemistry - Analytical Edition 1929;1:52–4. https://doi.org/10.1021/AC50065A027/ASSET/AC50065A027.FP.PNG_V03.
[281] Yulina R, Srie Gustiani R, Kasipah C, Danny Sukardan Balai Besar Tekstil M, Perindustrian K, Jenderal Ahmad Yani No J. Preparation of Microcrystalline Cellulose from Cotton Yarn Spinning Mills Wastes: Effect of Pretreatment and Hydrolysis Reaction Condition on the Product Characteristics. E3S Web of Conferences 2020;148:02004. https://doi.org/10.1051/E3SCONF/202014802004.
[282] Raghunath S, Hoque M, Zakani B, Gondaliya AM, Foster EJ. Sustainable micro-cellulosic additives for high-density fiber cement: emphasis on rheo-mechanical properties and cost–performance analysis. RSC Sustainability 2024. https://doi.org/10.1039/D4SU00287C.
[283] Herring A, King PL, Saadatfar M, Mahdini F, Kemis Yahyah AM, Andò E. 3D microstructure controls on mineral carbonation. Journal of CO2 Utilization 2021;47:101494. https://doi.org/10.1016/J.JCOU.2021.101494.
[284] Hargis CW, Chen IA, Devenney M, Fernandez MJ, Gilliam RJ, Thatcher RP. Calcium Carbonate Cement: A Carbon Capture, Utilization, and Storage (CCUS) Technique. Materials 2021, Vol 14, Page 2709 2021;14:2709. https://doi.org/10.3390/MA14112709.
[285] Dunant CF, Joseph S, Prajapati R, Allwood JM. Electric recycling of Portland cement at scale. Nature 2024 629:8014 2024;629:1055–61. https://doi.org/10.1038/s41586-024-07338-8.
[286] Climate change: The massive CO2 emitter you may not know about n.d. https://www.bbc.com/news/science-environment-46455844 (accessed November 2, 2024).

[287] Chakraborty A, Sain M, Kortschot M. Cellulose microfibrils: A novel method of preparation using high shear refining and cryocrushing. Holzforschung 2005;59:102–7. https://doi.org/10.1515/HF.2005.016/MACHINEREADABLECITATION/RIS.
[288] Gupta S, Kua HW, Low CY. Use of biochar as carbon sequestering additive in cement mortar. Cem Concr Compos 2018;87:110–29. https://doi.org/10.1016/J.CEMCONCOMP.2017.12.009.
[289] Particle Size n.d. https://www.sympatec.com/en/particle-measurement/glossary/fundamentals-of-particle-characterisation/particle-size (accessed December 12, 2024).
[290] QICPIC-RODOS-L-VIBRI-L n.d. https://www.sympatec.com/en/particle-measurement/sensors/dynamic-image-analysis/qicpic/qicpic-rodos-l-vibri-l (accessed April 16, 2025).
[291] ASTM C1185. Standard Test Methods for Sampling and Testing Non-Asbestos Fiber-Cement Flat Sheet, Roofing and Siding Shingles, and Clapboards. West Conshohocken: 2016.
[292] Finkbeiner M, Inaba A, Tan RBH, Christiansen K, Klüppel HJ. The new international standards for life cycle assessment: ISO 14040 and ISO 14044. International Journal of Life Cycle Assessment 2006;11:80–5. https://doi.org/10.1065/LCA2006.02.002/METRICS.
[293] Conte P, Bertani R, Sgarbossa P, Bambina P, Schmidt HP, Raga R, et al. Recent Developments in Understanding Biochar's Physical–Chemistry. Agronomy 2021, Vol 11, Page 615 2021;11:615. https://doi.org/10.3390/AGRONOMY11040615.
[294] Peterson SC, Jackson MA, Kim S, Palmquist DE. Increasing biochar surface area: Optimization of ball milling parameters. Powder Technol 2012;228:115–20. https://doi.org/10.1016/J.POWTEC.2012.05.005.
[295] Jamal MU, Fletcher AJ. Design of Experiments Study on Scottish Wood Biochars and Process Parameter Influence on Final Biochar Characteristics. Bioenergy Res 2023;16:2342–55. https://doi.org/10.1007/S12155-023-10595-6/FIGURES/6.
[296] James G, Sabatini DA, Chiou CT, Rutherford D, Scott AC, Karapanagioti HK. Evaluating phenanthrene sorption on various wood chars. Water Res 2005;39:549–58. https://doi.org/10.1016/J.WATRES.2004.10.015.
[297] Li Y, Lin H, Li Y, Shen J, Yang C, Wang K. Carbon Sequestration of Silica-Rich Biochar in Cement Accompanied by the Pozzolanic Effect. ACS Sustain Chem Eng 2024. https://doi.org/10.1021/ACSSUSCHEMENG.4C03831/ASSET/IMAGES/LARGE/SC4C03831_0013.JPEG.
[298] Wang Z, Pan X, Kuang S, Chen C, Wang X, Xu J, et al. Amelioration of Coastal Salt-Affected Soils with Biochar, Acid Modified Biochar and Wood Vinegar: Enhanced Nutrient Availability and Bacterial Community Modulation. Int J Environ Res Public Health 2022;19:7282. https://doi.org/10.3390/IJERPH19127282/S1.

[299] Fang Q, Chen B, Lin Y, Guan Y. Aromatic and hydrophobic surfaces of wood-derived biochar enhance perchlorate adsorption via hydrogen bonding to oxygen-containing organic groups. Environ Sci Technol 2014;48:279–88. https://doi.org/10.1021/ES403711Y/SUPPL_FILE/ES403711Y_SI_001.PDF.
[300] Jung J, Macdonald AH. Tight-binding model for graphene π-bands from maximally localized Wannier functions. Phys Rev B Condens Matter Mater Phys 2013;87:195450. https://doi.org/10.1103/PHYSREVB.87.195450/FIGURES/5/MEDIUM.
[301] Arias B, Pevida C, Fermoso J, Plaza MG, Rubiera F, Pis JJ. Influence of torrefaction on the grindability and reactivity of woody biomass. Fuel Processing Technology 2008;89:169–75. https://doi.org/10.1016/J.FUPROC.2007.09.002.
[302] Terzyk AP. The influence of activated carbon surface chemical composition on the adsorption of acetaminophen (paracetamol) in vitro: Part II. TG, FTIR, and XPS analysis of carbons and the temperature dependence of adsorption kinetics at the neutral pH. Colloids Surf A Physicochem Eng Asp 2001;177:23–45. https://doi.org/10.1016/S0927-7757(00)00594-X.
[303] Li Y, Zhang X, Yang R, Li G, Hu C. The role of H3PO4 in the preparation of activated carbon from NaOH-treated rice husk residue. RSC Adv 2015;5:32626–36. https://doi.org/10.1039/C5RA04634C.
[304] Ferrari A, Robertson J. Interpretation of Raman spectra of disordered and amorphous carbon. Phys Rev B 2000;61:14095. https://doi.org/10.1103/PhysRevB.61.14095.
[305] Dos Reis GS, Larsson SH, Thyrel M, Pham TN, Lima EC, de Oliveira HP, et al. Preparation and Application of Efficient Biobased Carbon Adsorbents Prepared from Spruce Bark Residues for Efficient Removal of Reactive Dyes and Colors from Synthetic Effluents. Coatings 2021, Vol 11, Page 772 2021;11:772. https://doi.org/10.3390/COATINGS11070772.
[306] González-Hourcade M, Simões dos Reis G, Grimm A, Dinh VM, Lima EC, Larsson SH, et al. Microalgae biomass as a sustainable precursor to produce nitrogen-doped biochar for efficient removal of emerging pollutants from aqueous media. J Clean Prod 2022;348:131280. https://doi.org/10.1016/J.JCLEPRO.2022.131280.
[307] Balmforth NJ, Frigaard IA, Ovarlez G. Yielding to stress: Recent developments in viscoplastic fluid mechanics. Annu Rev Fluid Mech 2014;46:121–46. https://doi.org/10.1146/ANNUREV-FLUID-010313-141424/CITE/REFWORKS.
[308] Zhang C, Wang M, Liu R, Li X, Liu Y, Jiang P, et al. Rheological properties of cement-based slurry and evaluation of rheological model: Influence of particle size and shape. Constr Build Mater 2023;406:133498. https://doi.org/10.1016/J.CONBUILDMAT.2023.133498.
[309] Marchesini FH, Naccache MF, Abdu A, Alicke AA, de Souza Mendes PR. Rheological characterization of yield-stress materials: Flow pattern and apparent wall slip. Applied

Rheology 2015;25:32–41. https://doi.org/10.3933/APPLRHEOL-25-53883/MACHINEREADABLECITATION/RIS.
[310] Cloitre M, Bonnecaze RT. A review on wall slip in high solid dispersions. Rheologica Acta 2017 56:3 2017;56:283–305. https://doi.org/10.1007/S00397-017-1002-7.
[311] Ma S, Qian Y, Kawashima S. Experimental and modeling study on the non-linear structural build-up of fresh cement pastes incorporating viscosity modifying admixtures. Cem Concr Res 2018;108:1–9. https://doi.org/10.1016/J.CEMCONRES.2018.02.022.
[312] Zhang J, Su Y, Zhang C, Li M, Zhu X, Zhang Y, et al. Alterations in rheo-viscoelastic properties of cement composites with biochar incorporation as bio-based admixture. Constr Build Mater 2024;439:137358. https://doi.org/10.1016/J.CONBUILDMAT.2024.137358.
[313] Wikström T, Rasmuson A. Yield stress of pulp suspensions: The influence of fibre properties and processing conditions. Nord Pulp Paper Res J 1998;13:243–50. https://doi.org/10.3183/NPPRJ-1998-13-03-P243-246/MACHINEREADABLECITATION/RIS.
[314] Kerekes RJ, Soszynski RM, Tam Doo PA. The Flocculation of Pulp Fibres. In: Punton V, editor. Trans. of the VIIIth Fund. Res. Symp. Oxford, 1985, Fundamental Research Committee (FRC), Manchester; 1985, p. 265–310. https://doi.org/10.15376/frc.1985.1.265.
[315] Börzsönyi T, Szabó B, Wegner S, Harth K, Török J, Somfai E, et al. Shear-induced alignment and dynamics of elongated granular particles. Phys Rev E Stat Nonlin Soft Matter Phys 2012;86:051304. https://doi.org/10.1103/PHYSREVE.86.051304/FIGURES/12/MEDIUM.
[316] Ye H, Zhang J, Gao X, Ling J, Zhu X, Jiao D. Showing the role of weakly-bound particles flocculation in the reversibility of thixotropic behavior for fresh cement paste. Constr Build Mater 2024;411:134624. https://doi.org/10.1016/J.CONBUILDMAT.2023.134624.
[317] Tosun-Felekoglu K, Felekoglu B. Effects of fiber–matrix interaction on multiple cracking performance of polymeric fiber reinforced cementitious composites. Compos B Eng 2013;52:62–71. https://doi.org/10.1016/J.COMPOSITESB.2013.03.043.
[318] Du H. Properties of ultra-lightweight cement composites with nano-silica. Constr Build Mater 2019;199:696–704. https://doi.org/10.1016/J.CONBUILDMAT.2018.11.225.
[319] Lin Y, Du H. Graphene reinforced cement composites: A review. Constr Build Mater 2020;265:120312. https://doi.org/10.1016/J.CONBUILDMAT.2020.120312.
[320] Gupta S, Krishnan P, Kashani A, Kua HW. Application of biochar from coconut and wood waste to reduce shrinkage and improve physical properties of silica fume-cement mortar. Constr Build Mater 2020;262:120688. https://doi.org/10.1016/J.CONBUILDMAT.2020.120688.
[321] Zhang Q, Luan C, Yu C, Huang Y, Zhou Z. Mechanisms of carbon black in multifunctional cement matrix: Hydration and microstructure perspectives. Constr Build Mater 2022;346:128455. https://doi.org/10.1016/J.CONBUILDMAT.2022.128455.

[322] Liu J, Fu J, Yang Y, Gu C. Study on dispersion, mechanical and microstructure properties of cement paste incorporating graphene sheets. Constr Build Mater 2019;199:1–11. https://doi.org/10.1016/J.CONBUILDMAT.2018.12.006.
[323] Pan Z, He L, Qiu L, Korayem AH, Li G, Zhu JW, et al. Mechanical properties and microstructure of a graphene oxide–cement composite. Cem Concr Compos 2015;58:140–7. https://doi.org/10.1016/J.CEMCONCOMP.2015.02.001.
[324] Sixuan HUANG. Multifunctional graphite nanoplatelets (GNP) reinforced cementitious composites. Master's Theses. National University of Singapore, 2012.
[325] Cerro-Prada E, Pacheco-Torres R, Varela F. Effect of Multi-Walled Carbon Nanotubes on Strength and Electrical Properties of Cement Mortar. Materials 2021;14:1–13. https://doi.org/10.3390/MA14010079.
[326] Taylor HFW, Barret P, Brown PW, Double DD, Frohnsdorff G, Johansen V, et al. The hydration of tricalcium silicate - RILEM committee 68-MMH, Task Group 3. Matériaux et Constructions 1984;17:457–68. https://doi.org/10.1007/BF02473986/METRICS.
[327] Madsen IC, Scarlett NVY, Kern A. Description and survey of methodologies for the determination of amorphous content via X-ray powder diffraction. Zeitschrift Fur Kristallographie 2011;226:944–55. https://doi.org/10.1524/ZKRI.2011.1437/MACHINEREADABLECITATION/RIS.
[328] Snellings R, Salze A, Scrivener KL. Use of X-ray diffraction to quantify amorphous supplementary cementitious materials in anhydrous and hydrated blended cements. Cem Concr Res 2014;64:89–98. https://doi.org/10.1016/J.CEMCONRES.2014.06.011.
[329] Francis Young J. Investigations of Calcium Silicate Hydrate Structure Using Silicon-29 Nuclear Magnetic Resonance Spectroscopy. Journal of the American Ceramic Society 1988;71:C–118. https://doi.org/10.1111/J.1151-2916.1988.TB05028.X.
[330] Hjorth J, Skibsted J, Jakobsen HJ. 29Si MAS NMR studies of portland cement components and effects of microsilica on the hydration reaction. Cem Concr Res 1988;18:789–98. https://doi.org/10.1016/0008-8846(88)90104-4.
[331] Dong Y, Feng C, Zhao Q, Liang X. Study on the Structure of C-S-H Gels of Slag–Cement Hardened Paste by 29Si, 27Al MAS NMR. Appl Magn Reson 2019;50:1345–57. https://doi.org/10.1007/S00723-019-01152-6/FIGURES/9.
[332] Brykov AS, Vasil'Ev AS, Mokeev M V. Hydration of Portland cement in the presence of high activity aluminum hydroxides. Russian Journal of Applied Chemistry 2012;85:1793–9. https://doi.org/10.1134/S1070427212120014/METRICS.
[333] Parry-Jones G, Al-Tayyib AJ, Al-Dulaijan SU, Al-Mana AI. 29Si MAS-NMR hydration and compressive strength study in cement paste. Cem Concr Res 1989;19:228–34. https://doi.org/10.1016/0008-8846(89)90087-2.
[334] Daugaard Andersen M, Jakobsen HJ, Skibsted Jø. Incorporation of aluminum in the calcium silicate hydrate (C-S-H) of hydrated Portland cements: A high-field 27Al and 29Si

MAS NMR investigation. Inorg Chem 2003;42:2280–7. https://doi.org/10.1021/IC020607B/ASSET/IMAGES/MEDIUM/IC020607BN00001.GIF.
[335] Kjellsen KO. A discussion of the paper “Kinetics of the hydration reactions in the cement paste with mechanochemically modified cement 29Si magic-angle-spinning NMR study” by K. Johansson, C. Larsson, O.N. Antzutkin, W. Forsling, H.R. Kota and V. Ronin. Cem Concr Res 2000;30:1323. https://doi.org/10.1016/S0008-8846(00)00301-X.
[336] Le Saout G, Lécolier E, Rivereau A, Zanni H. Chemical structure of cement aged at normal and elevated temperatures and pressures: Part I. Class G oilwell cement. Cem Concr Res 2006;36:71–8. https://doi.org/10.1016/J.CEMCONRES.2004.09.018.
[337] Huang CY, Lin YC, Chung JHY, Chiu HY, Yeh NL, Chang SJ, et al. Enhancing Cementitious Composites with Functionalized Graphene Oxide-Based Materials: Surface Chemistry and Mechanisms. International Journal of Molecular Sciences 2023, Vol 24, Page 10461 2023;24:10461. https://doi.org/10.3390/IJMS241310461.
[338] Meng S, Ouyang X, Fu J, Niu Y, Ma Y. The role of graphene/graphene oxide in cement hydration. Nanotechnol Rev 2021;10:768–78. https://doi.org/10.1515/NTREV-2021-0055/ASSET/GRAPHIC/J_NTREV-2021-0055_FIG_008.JPG.
[339] Ravina D, Mehta PK. Properties of fresh concrete containing large amounts of fly ash. Cem Concr Res 1986;16:227–38. https://doi.org/10.1016/0008-8846(86)90139-0.
[340] Matković B, Gržeta B, Paljević M, Rogić V, Dasović D, Dimic D. Hydrated fly ash with SiO2 fume and/or portland cement addition. Reactions in pastes and strength development in mortars. Cem Concr Res 1990;20:475–83. https://doi.org/10.1016/0008-8846(90)90039-Z.
[341] Delage P, Altcin PC. Influence of Condensed Silica Fume on the Pore-Size Distribution of Concretes. Industrial and Engineering Chemistry Product Research and Development 1983;22:286–90. https://doi.org/10.1021/I300010A024/ASSET/I300010A024.FP.PNG_V03.
[342] Hardjito D, Wallah SE, Sumajouw DMJ, Rangan BV. On the Development of Fly Ash-Based Geopolymer Concrete. Materials Journal 2004;101:467–72. https://doi.org/10.14359/13485.
[343] Lv Q, Yu J, Ji F, Gu L, Chen Y, Shan X. Mechanical Property and Microstructure of Fly Ash-Based Geopolymer Activated by Sodium Silicate. KSCE Journal of Civil Engineering 2021;25:1765–77. https://doi.org/10.1007/S12205-021-0025-X/METRICS.
[344] Khater HM. Effect of silica fume on the characterization of the geopolymer materials. International Journal of Advanced Structural Engineering 2013;5:1–10. https://doi.org/10.1186/2008-6695-5-12/FIGURES/9.
[345] Hamed YR, Yousry Elshikh MM, Elshami AA, Matthana MHS, Youssf O. Mechanical properties of fly ash and silica fume based geopolymer concrete made with magnetized water activator. Constr Build Mater 2024;411:134376. https://doi.org/10.1016/J.CONBUILDMAT.2023.134376.

[346] Sawarkar PG, Pote A, Lal Murmu A. Properties of blast furnace slag geopolymer concrete. Mater Today Proc 2023. https://doi.org/10.1016/J.MATPR.2023.03.179.
[347] Boumaza A, Khouadjia MLK, Isleem HF, Hamdi OM, Khishe M. Effect of blast furnace slag on the fresh and hardened properties of volcanic tuff-based geopolymer mortars. Sci Rep 2025;15:1–16. https://doi.org/10.1038/S41598-025-98382-5;SUBJMETA=1023,166,301,639,986;KWRD=CIVIL+ENGINEERING,STRUCTURAL+MATERIALS.
[348] The future of supplementary cementitious materials | McKinsey n.d. https://www.mckinsey.com/industries/engineering-construction-and-building-materials/our-insights/the-future-cement-industry-a-cementitious-golden-age?utm_source=chatgpt.com (accessed June 11, 2025).
[349] Rashad AM. Metakaolin as cementitious material: History, scours, production and composition – A comprehensive overview. Constr Build Mater 2013;41:303–18. https://doi.org/10.1016/J.CONBUILDMAT.2012.12.001.
[350] Egodagamage H, Yapa HD, Samith Buddika HAD, Navaratnam S, Nguyen K. Effective use of biochar as an additive for alkali-activated slag mortar production. Constr Build Mater 2023;370:130487. https://doi.org/10.1016/J.CONBUILDMAT.2023.130487.
[351] Khamlue P, Lertcumfu N, Jaita P, Manotham S, Tunkasiri T, Malasri P, et al. The Effects of Biochar Additive on the Properties of Geopolymer Materials. Key Eng Mater 2019;798:273–8. https://doi.org/10.4028/WWW.SCIENTIFIC.NET/KEM.798.273.
[352] Piccolo F, Andreola F, Barbieri L, Lancellotti I. Synthesis and Characterization of Biochar-Based Geopolymer Materials. Applied Sciences 2021, Vol 11, Page 10945 2021;11:10945. https://doi.org/10.3390/APP112210945.
[353] Segura IP, Jensen PA, Damø AJ, Ranjbar N, Jensen LS, Canut M. Influence of sodium-based activators and water content on the fresh and hardened properties of metakaolin geopolymers. SN Appl Sci 2022;4:1–16. https://doi.org/10.1007/S42452-022-05167-W/FIGURES/10.
[354] Test Method for Flexural Strength of Hydraulic-Cement Mortars 2021. https://doi.org/10.1520/C0348-21.
[355] Chen L, Wang Z, Wang Y, Feng J. Preparation and Properties of Alkali Activated Metakaolin-Based Geopolymer. Materials 2016, Vol 9, Page 767 2016;9:767. https://doi.org/10.3390/MA9090767.
[356] DUXSON P. The structure and thermal evolution of metakaolin geopolymers 2006.
[357] Rahier H, Van Mele B, Biesemans M, Wastiels J, Wu X. Low-temperature synthesized aluminosilicate glasses: Part I. Low-temperature reaction stoichiometry and structure of a model compound. J Mater Sci 1996;31:71–9. https://doi.org/10.1007/BF00355128/METRICS.

[358] Zhang M, Guo H, El-Korchi T, Zhang G, Tao M. Experimental feasibility study of geopolymer as the next-generation soil stabilizer. Constr Build Mater 2013;47:1468–78. https://doi.org/10.1016/J.CONBUILDMAT.2013.06.017.
[359] El Alouani M, Alehyen S, El Achouri M, Hajjaji A, Ennawaoui C, Taibi M. Influence of the Nature and Rate of Alkaline Activator on the Physicochemical Properties of Fly Ash-Based Geopolymers. Advances in Civil Engineering 2020;2020:8880906. https://doi.org/10.1155/2020/8880906.
[360] Oelkers EH. General kinetic description of multioxide silicate mineral and glass dissolution. Geochim Cosmochim Acta 2001;65:3703–19. https://doi.org/10.1016/S0016-7037(01)00710-4.
[361] Walther J V. Relation between rates of aluminosilicate mineral dissolution, pH, temperature, and surface charge. Am J Sci 1996;296:693–728. https://doi.org/10.2475/AJS.296.7.693.
[362] Provis JL, Bernal SA. Geopolymers and related alkali-activated materials. Annu Rev Mater Res 2014;44:299–327. https://doi.org/10.1146/ANNUREV-MATSCI-070813-113515/CITE/REFWORKS.
[363] Pundienė I, Pranckevičienė J, Zhu C, Kligys M. The role of temperature and activator solution molarity on the viscosity and hard structure formation of geopolymer pastes. Constr Build Mater 2021;272:121661. https://doi.org/10.1016/J.CONBUILDMAT.2020.121661.
[364] Hanjitsuwan S, Hunpratub S, Thongbai P, Maensiri S, Sata V, Chindaprasirt P. Effects of NaOH concentrations on physical and electrical properties of high calcium fly ash geopolymer paste. Cem Concr Compos 2014;45:9–14. https://doi.org/10.1016/J.CEMCONCOMP.2013.09.012.
[365] Hajimohammadi A, Provis JL, Van Deventer JSJ. The effect of silica availability on the mechanism of geopolymerisation. Cem Concr Res 2011;41:210–6. https://doi.org/10.1016/J.CEMCONRES.2011.02.001.
[366] Poulesquen A, Gomes Rodrigues D, Keshavarz B, Courtois N, Ilavsky J, McKinley GH. Aluminosilicate colloidal gels: from the early age to the precipitation of zeolites. Soft Matter 2024;20:5538–52. https://doi.org/10.1039/D4SM00181H.
[367] Das S, Yang P, Singh SS, Mertens JCE, Xiao X, Chawla N, et al. Effective properties of a fly ash geopolymer: Synergistic application of X-ray synchrotron tomography, nanoindentation, and homogenization models. Cem Concr Res 2015;78:252–62. https://doi.org/10.1016/J.CEMCONRES.2015.08.004.
[368] Ruiz-Santaquiteria C, Skibsted J, Fernández-Jiménez A, Palomo A. Alkaline solution/binder ratio as a determining factor in the alkaline activation of aluminosilicates. Cem Concr Res 2012;42:1242–51. https://doi.org/10.1016/J.CEMCONRES.2012.05.019.
[369] Singh NB. Properties of cement and concrete in presence of nanomaterials. Smart Nanoconcretes and Cement-Based Materials: Properties, Modelling and Applications 2020:9–39. https://doi.org/10.1016/B978-0-12-817854-6.00002-7.

[370] Portland Cement | Lafarge Canada n.d. https://www.lafarge.ca/en/portland-cement (accessed January 1, 2024).
[371] Pulp bleaching sequences | pulp paper mill n.d. https://www.pulppapermill.com/pulp-bleaching-sequences/ (accessed January 1, 2024).
[372] Avicel® PH-101 - Cellulose, Cellulose powder n.d. https://www.sigmaaldrich.com/CA/en/substance/avicelph101123459004346 (accessed August 2, 2023).
[373] BLACK BEAR BIOCHAR | BC Biocarbon n.d. https://www.bcbiocarbon.com/black-bear-biochar-specs (accessed November 20, 2024).
[374] Metakaolin – We Supply Metakaolin and Silica Fume : Advanced Cement Technologies, LLC (ACT) n.d. https://www.metakaolin.com/metakaolin/ (accessed April 12, 2025).
[375] Greenberg SA, Meyer LM. Rheology of Fresh Portland Cement Pastes Influence of Calcium Sulfates n.d.
[376] Segal L, Creely JJ, Martin AE, Conrad CM. An Empirical Method for Estimating the Degree of Crystallinity of Native Cellulose Using the X-Ray Diffractometer. Textile Research Journal 1959;29:786–94. https://doi.org/10.1177/004051755902901003.
[377] Khenblouche A, Bechki D, Gouamid M, Charradi K, Segni L, Hadjadj M, et al. Extraction and characterization of cellulose microfibers from Retama raetam stems. Polímeros 2019;29:e2019011. https://doi.org/10.1590/0104-1428.05218.
[378] Adeleye OA, Bamiro OA, Albalawi DA, Alotaibi AS, Iqbal H, Sanyaolu S, et al. Characterizations of Alpha-Cellulose and Microcrystalline Cellulose Isolated from Cocoa Pod Husk as a Potential Pharmaceutical Excipient. Materials 2022;15. https://doi.org/10.3390/MA15175992.
[379] Park S, Baker JO, Himmel ME, Parilla PA, Johnson DK. Cellulose crystallinity index: Measurement techniques and their impact on interpreting cellulase performance. Biotechnol Biofuels 2010;3:1–10. https://doi.org/10.1186/1754-6834-3-10/TABLES/2.
[380] Cellulose nanowhiskers isolation and properties from acid hydrolysis combined with high pressure homogenization :: BioResources n.d. https://bioresources.cnr.ncsu.edu/resources/cellulose-nanowhiskers-isolation-and-properties-from-acid-hydrolysis-combined-with-high-pressure-homogenization/ (accessed August 25, 2024).
[381] Piasta W, Zarzycki B. The effect of cement paste volume and w/c ratio on shrinkage strain, water absorption and compressive strength of high performance concrete. Constr Build Mater 2017;140:395–402. https://doi.org/10.1016/J.CONBUILDMAT.2017.02.033.
[382] Pignon F, Challamel M, De Geyer A, Elchamaa M, Semeraro EF, Hengl N, et al. Breakdown and buildup mechanisms of cellulose nanocrystal suspensions under shear and upon relaxation probed by SAXS and SALS. Carbohydr Polym 2021;260:117751. https://doi.org/10.1016/J.CARBPOL.2021.117751.
[383] Wissbrun KF. Rheology of Rod-like Polymers in the Liquid Crystalline State. J Rheol (N Y N Y) 1981;25:619–62. https://doi.org/10.1122/1.549634.

[384] Ahuja A, Potanin A, Joshi YM. Two step yielding in soft materials. Adv Colloid Interface Sci 2020;282:102179. https://doi.org/10.1016/J.CIS.2020.102179.
[385] Zakani B, Salem H, Entezami S, Sedaghat A, Grecov D. Effect of particle concentration on lubrication performance of cellulose nanocrystalline (CNC) water-based lubricants: mixed lubrication regime. Cellulose 2022;29:3963–84. https://doi.org/10.1007/S10570-022-04510-Z/FIGURES/3.
[386] Canfor. CANFOR PULP REPORTS RESULTS FOR SECOND QUARTER OF 2023. 2023.
[387] Chakraborty A, Sain MM, Kortschot MT, Ghosh SB. Modeling energy consumption for the generation of microfibres from bleached kraft pulp fibres in a PFI mill :: BioResources 2007. https://bioresources.cnr.ncsu.edu/resources/modeling-energy-consumption-for-the-generation-of-microfibres-from-bleached-kraft-pulp-fibres-in-a-pfi-mill/ (accessed November 27, 2023).
[388] Alpha Cellulose (Cotton) n.d. https://www.indiamart.com/proddetail/alpha-cellulose-fiber-2852563247262.html (accessed January 1, 2024).
[389] Sri Bhanupratap Rathod R, Sahoo P, Gupta S. Application of micro-crystalline cellulose as additive in Portland cement-based and alkali activated slag-fly ash mortar: Comparison of compressive strength, hydration and shrinkage. Constr Build Mater 2023;385:131531. https://doi.org/10.1016/J.CONBUILDMAT.2023.131531.
[390] Vanhatalo KM, Parviainen KE,, Dahl OP. Techno-economic analysis of simplified micro-crystalline cellulose process :: BioResources 2014. https://bioresources.cnr.ncsu.edu/resources/techno-economic-analysis-of-simplified-microcrystalline-cellulose-process/ (accessed January 1, 2024).
[391] Ciriminna R, Ghahremani M, Karimi B, Pagliaro M. Emerging green routes to nanocellulose. Biofuels, Bioproducts and Biorefining 2023;17:10–7. https://doi.org/10.1002/BBB.2423.
[392] Oguntola O, Simske S. Continuous Assessment of the Environmental Impact and Economic Viability of Decarbonization Improvements in Cement Production. Resources 2023, Vol 12, Page 95 2023;12:95. https://doi.org/10.3390/RESOURCES12080095.
[393] PCE, (2024) n.d. https://www.zauba.com/import-polycarboxylate-ether-cement-hs-code.html (accessed January 1, 2024).
[394] Silica fume price per kg - HSA Microsilica n.d. https://microsilica-fume.com/silica-fume-price-per-kg.html (accessed June 2, 2024).
[395] Silica Sand Price in Canada - 2023 - Charts and Tables - IndexBox n.d. https://www.indexbox.io/search/silica-sand-price-canada/ (accessed June 2, 2024).
[396] Nano Silica Price, 2024 Nano Silica Price Manufacturers & Suppliers | Made-in-China.com n.d. https://www.made-in-china.com/products-search/hot-china-products/Nano_Silica_Price.html (accessed June 2, 2024).

[397] Technical Committee ISO/TC 207. Environmental Management. Environmental management-life cycle assessment-principles and framework. International Organization for Standardization; 2006.
[398] O.I.d. Normalización. ISO 14044: Environmental Management, Life Cycle Assessment, Requirements and Guidelines. ISO; 2006.
[399] Cen EN. 15804: A1: 2020. —sustainability of construction works—environmental product declarations—core rules for the product category of construction products. 2020.
[400] ISO E. 14025. Environmental Labels and Declarations—Type III Environmental Declarations—Principles and Procedures. Edited in. 2010.
[401] Elias M, Sanchez DL, Saksa P, Hunt J, Remucal J. Market analysis of coupled biochar and carbon credit production from wildfire fuel reduction projects in the western USA. Biofuels, Bioproducts and Biorefining 2024. https://doi.org/10.1002/BBB.2614.
[402] Carvalho J, Nascimento L, Soares M, Valério N, Ribeiro A, Faria L, et al. Life Cycle Assessment (LCA) of Biochar Production from a Circular Economy Perspective. Processes 2022, Vol 10, Page 2684 2022;10:2684. https://doi.org/10.3390/PR10122684.
[403] Greenhouse gas lifecycle assessment of biochar and biocoal applications in British Columbia | University of Northern British Columbia Institutional Repository n.d. https://unbc.arcabc.ca/islandora/object/unbc%3A58978 (accessed August 1, 2024).
[404] Biochar Summary – Climate Solutions Advancement Network (ClimateSAN) n.d. https://climatesan.org/biochar-summary/ (accessed August 1, 2024).
[405] Chakraborty A, Sain MM, Kortschot MT, Ghosh SB. Modeling energy consumption for the generation of microfibres from bleached kraft pulp fibres in a PFI mill. BioRes 2007;2:210–22.
[406] Database - ecoinvent n.d. https://ecoinvent.org/database/ (accessed August 1, 2024).
[407] openLCA.org | openLCA is a free, professional Life Cycle Assessment (LCA) and footprint software with a broad range of features and many available databases, created by GreenDelta since 2006 n.d. https://www.openlca.org/ (accessed August 1, 2024).
[408] Price of Cement - United States | IBISWorld n.d. https://www.ibisworld.com/us/bed/price-of-cement/190/ (accessed November 20, 2024).
[409] Li W, Dang Q, Smith R, Brown RC, Wright MM. Techno-economic analysis of the stabilization of bio-oil fractions for insertion into petroleum refineries. ACS Sustain Chem Eng 2017;5:1528–37. https://doi.org/10.1021/ACSSUSCHEMENG.6B02222/ASSET/IMAGES/MEDIUM/SC-2016-02222R_0009.GIF.
[410] Sahoo K, Bilek E, Bergman R, Mani S. Techno-economic analysis of producing solid biofuels and biochar from forest residues using portable systems. Appl Energy 2019;235:578–90. https://doi.org/10.1016/J.APENERGY.2018.10.076.
[411] Utility meter rates for water, sewer, and energy | City of Vancouver n.d. https://vancouver.ca/home-property-development/metered-rates.aspx (accessed November 20, 2024).

[412] Current lumber, pulp and panel prices n.d. https://natural-resources.canada.ca/our-natural-resources/domestic-and-international-markets/current-lumber-pulp-panel-prices/13309#pulp (accessed November 20, 2024).
[413] Electricity rates n.d. https://www.fortisbc.com/about-us/corporate-information/regulatory-affairs/our-electricity-utility/electric-bcuc-submissions/electricity-rates (accessed July 7, 2024).

Appendices

Appendix A Physiochemical properties of all the raw materials employed in this thesis

Table A.1 General Composition of OPC [369].

Clinker Phases	Quantity (%)
Tricalcium silicates (C_3S)	30-55
Dicalcium silicates (C_2S)	20-50
Tricalcium aluminate (C_3A)	7-12
Tetracalcium aluminoferrite (C_4AF)	6-11

Table A.2 Physio-chemical properties of OPC (procured from Lafarge, Canada) used for this research [370].

Components	Quantity (%)
Limestone	≤15
Gypsum	2-10
Magnesium Oxide	≤4
Quartz	≤0.2
Physiochemical properties	
Physical state	Solid
Color	Gray, off white or white powder
PH	12 -13 (in water)
Boiling point	> 1000 °C
Specific Gravity	3.15 (water = 1)

Table A.3 Properties of cellulose nanocrystals (CNC), which was procured from the product development center, University of Maine, USA) for this research.[91].

Properties	
Appearance	White / off white
Density	1.5 g/cm^3
Width	5 -20 nm
Length	150 – 200 nm
Aspect ratio	10 - 30
Sulphur content (in dry CNCs)	0.85 wt.% Sulphur
Solid content	98% dry powder

Table A.4 Properties of NBSK pulp [191,371].

Properties	
Species	Lodgepole pine – Pinus contorta, white spruce – Picea glauca, Sub–alpine fir–Abies lasiocarpa
Bleaching Process	ECF

Bleaching sequence	$DE_{OP}DE_{P}D$

The bleaching process, ECF stands for Enhanced – Elemental chlorine free. And the beaching sequence, $DE_{OP}DE_{P}D$ stands for D- Chlorine dioxide reacts with pulp in acidic medium. E – Dissolution of reaction product with oxygen. O- Molecular oxygen reacts with pulp in alkaline medium at high pressure. P – Peroxide reacts with pulp in alkaline medium.

Table A.5 Refined (PFI mill) properties of NBSK fiber used for this research.

Properties	
Revolutions	4500
Coarseness	0.157 mg/m
Freeness	621.3 ml
Curl Index (Length weighted)	0.184
Kink Index	2.11 (1/mm)
Total Kink angle	71.88 Degrees
Kinks /mm	0.94 (1/mm)

Table A.6 Physical properties of the commercial PCEs based superplasticizer, that is, poly (acrylamide-co-acrylic acid) partial sodium salt.

Appearance	**White to off white**
Molecular weight (kDa)	M_w: 520
	M_n: 150
Viscosity (cP) 25 °C	150-700
Particle size (μm)	150.05

Table A.7 Physiochemical properties of Avicel® Ph 101 (procured from sigma Aldrich, Canada) used for this research [372].

Properties	
CAS number	9004-34-6
Appearance	White, powder
Moisture content	3 – 5 %
Loose bulk density	0.26-0.31 gcm^{-1}
BET surface area	1220 m^2/kg
PH	5.5 – 7.0
Degree of polymerization	NMT 350 units

Table A.8 Physiochemical properties of Alpha cellulose (sigma Aldrich, Canada) used for this research.

Properties	
CAS number	9004 -34 -6
Source	Plant
Appearance	White / off white (fiber) powder
Bulk density	5.6 – 6.8 cc/g

Table A. 9 Physical properties of BC sourced from BC Biocarbon, used in this research [373].

Properties	
Brand name	Black bear BC
Source	Wood forest residues
pH	9
Dry density (g/cm^3)	0.223
Size (cub sized)	< 2 mm
Pyrolysis temperature (°C)	600 – 800

Table A.10 Trace elemental analysis of BC used in this research measured using Ash content and X-Ray fluorescence.

Elements	**Ash content (%)**	**X – Ray fluorescence (ASTM D4326) (wt.%)**
SiO_2	24.02	28.57
Al_2O_3	8.30	4.60
TiO_2	0.36	0.28
Fe_2O_3	14.80	13.93
CaO	28.06	22.33
MgO	7.48	4.67
Na_2O	2.10	0.96
K_2O	7.73	8.20
P_2O_5	1.96	1.630
SO_3	2.35	0.86
Undetected	2.85	-
BaO	-	0.157
SrO	-	0.109
V_2O_5	-	0.008
NiO	-	0.013
MnO	-	1.280
Cr_2O_3	-	0.022
CuO	-	0.04
ZnO	-	0.11
Loss of fusion	-	12.23
Sum	-	100

Table A.11 Trace metal analysis of BC sample measured using inductively coupled plasma mass spectroscopy (ICPMS).

Elements	Results	RL	Units
Aluminum	65	40	mg/kg dry
Antimony	< 0.1	0.1	mg/kg dry
Arsenic	<0.30	0.3	mg/kg dry
Barium	7.5	1	mg/kg dry
Beryllium	<0.1	0.1	mg/kg dry
Bismuth	<0.1	0.1	mg/kg dry
Boron	4.4	2.0	mg/kg dry
Cadmium	< 0.04	0.04	mg/kg dry
Calcium	2280	100	mg/kg dry
Chromium	4.3	1	mg/kg dry
Cobalt	0.2	0.1	mg/kg dry
Copper	1.27	0.4	mg/kg dry
Iron	461	20	mg/kg dry
Lead	0.48	0.2	mg/kg dry
Lithium	0.13	0.1	mg/kg dry
Magnesium	122	10	mg/kg dry
Manganese	36.1	0.4	mg/kg dry
Mercury	< 0.04	0.04	mg/kg dry
Molybdenum	2.44	0.10	mg/kg dry
Nickel	7.09	0.60	mg/kg dry
Phosphorus	86	10	mg/kg dry
Potassium	904	40	mg/kg dry
Selenium	< 0.20	0.20	mg/kg dry
Silver	< 0.10	0.10	mg/kg dry
Sodium	< 50	50	mg/kg dry
Strontium	10.1	0.20	mg/kg dry
Sulfur	< 1000	1000	mg/kg dry
Tellurium	< 0.10	0.10	mg/kg dry
Thallium	< 0.10	0.10	mg/kg dry
Thorium	< 0.50	0.50	mg/kg dry
Tin	0.34	0.20	mg/kg dry
Titanium	2.4	1.0	mg/kg dry
Tungsten	< 0.20	0.20	mg/kg dry
Uranium	< 0.050	0.050	mg/kg dry
Vanadium	< 1.0	1	mg/kg dry
Zinc	5.3	2	mg/kg dry
Zirconium	< 2.0	2	mg/kg dry

*Note that the samples were digested using (HNO_3 + HCL , block digestion) prior to ICPMS analysis.

Table A.12 Chemical composition of high reactivity MK (HRM) binder (PowerPozzTM), manufactured by Advanced Cement Technologies, LLC (ACT), USA [372].

Chemical composition	Wt.%
SiO_2	52.4
Al_2O_3	42.1 – 44.3
Fe_2O_3	0.30 – 0.50
TiO_2	1.56 – 2.50

Table A.13 Physiochemical properties of HRM (PowerPozz^{TM}), procured from ACT, USA [374].

Properties	
Physical form	Amorphous
Specific gravity	2.2
Color	Cream white
Bulk density	0.288 - 0.35 g/cm^3
pH	4.0
BET (Surface area)	20 m^2/g

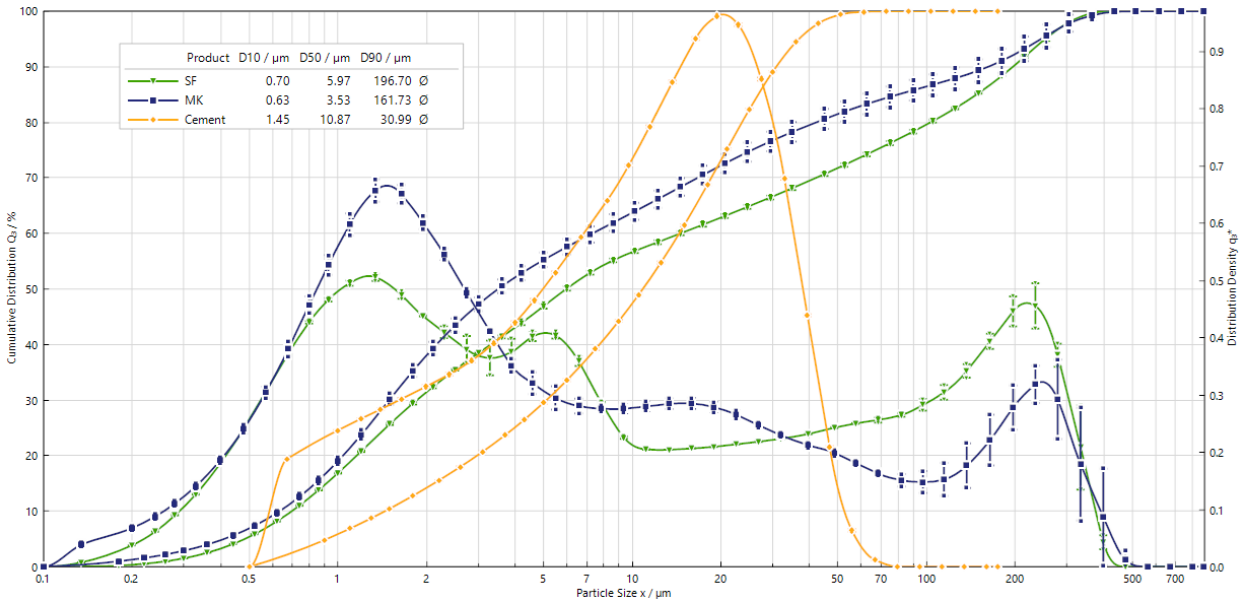

Figure A.1 Particle size distribution (measured via laser diffraction) of all the cementitious binder material used in this thesis (i.e., cement and MK). Note that particle size of SF was also measured, to obtain a comparative measure of how the particle size varies between different cementitious binders (SF was not used as a binder in this thesis).

Appendix B Chapter 3 supplementary materials

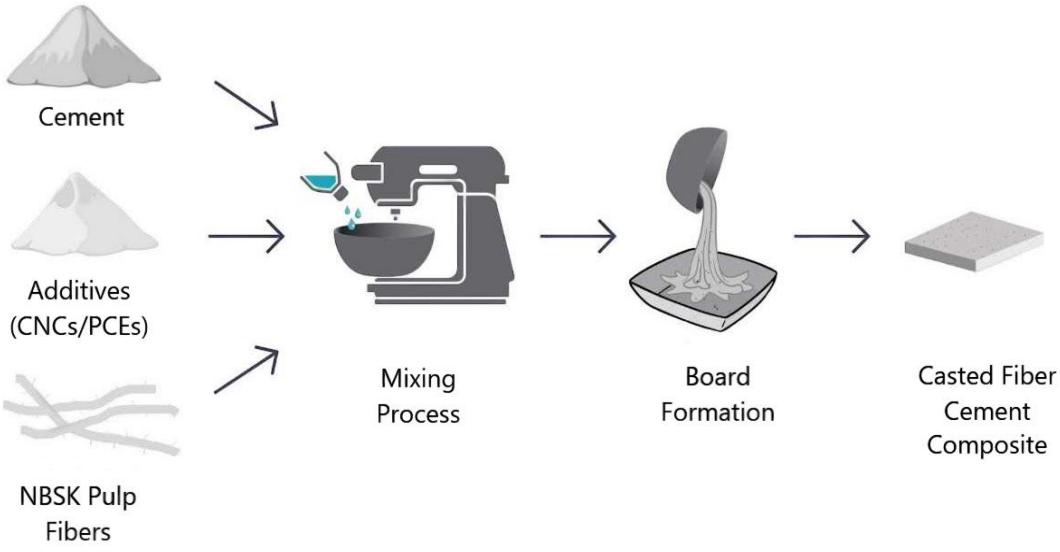

Figure B.1 Schematic illustration of the fiber-reinforced cement composites containing additives (CNCs/PCE).

Table B.1 Power law fit (shear-thinning regime) parameters based on rheological characterization (viscosity versus shear rate) of the FC slurry (non-Newtonian fluids) containing additives (CNCs/PCEs).

Additive content (wt%)	Consistency Coefficient '*m*' (CNCs)	Flow index '*n*' (CNCs)	R^2 Fit (CNCs)	Consistency Coefficient '*m*' (PCEs)	Flow index '*n*' (PCEs)	R^2 Fit (PCEs)
0	3.424	0.5608	0.9985	3.424	0.5608	0.9985
0.02	4.838	0.5388	0.9989	4.568	0.553	0.995
0.06	4.995	0.5272	0.9931	4.356	0.5984	0.9972
0.2	6.747	0.519	0.9975	7.606	0.6189	0.9973
0.6	8.195	0.5127	0.9996	8.61	0.6293	0.9978
1	11.29	0.4958	0.9945	7.072	0.6383	0.9998
2	53.45	0.2789	0.9962	8.613	0.6586	0.9998
3	107.4	0.184	0.9189	7.731	0.6819	0.9991
4	113.2	0.1787	0.9554	16.53	0.7187	0.9998

B.1 Rheological characterization (OPC paste)

In general, cement paste does exhibit both shear thinning and shear thickening behaviour. However, the extent of this behaviour is dependent on the cement composition, which includes C_2S (Belite), C_3S (Alite), Calcium sulfates, Gypsum, C_3A and C_4AF, to name a few, and process parameters, which includes, w/c ratio, mixing time, and curing time [375].

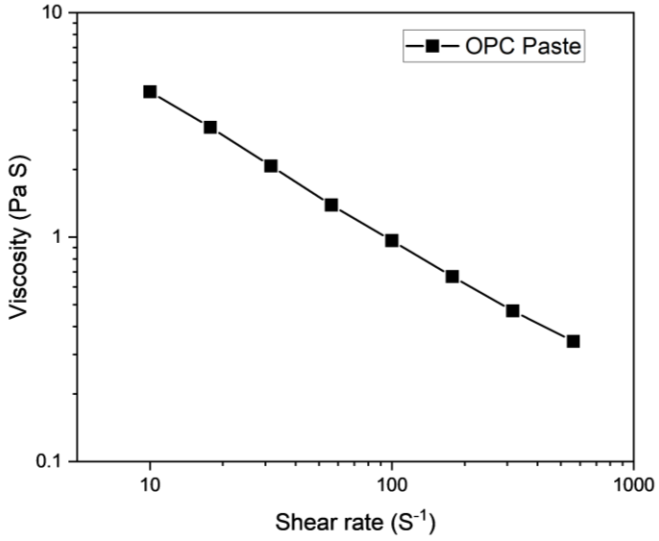

Figure B.2 Rheological characterization of OPC pastes without any reinforcing bleached fiber and additive. Variation of viscosity as a function of shear rate. Note that a water/cement ratio of 0.5 (used in this study) was employed for testing the steady state viscometry of OPC paste.

It is important to note that in the compositional paradigm, Gypsum is an important component in OPC that is added to delay cement setting. However, in the absence of Gypsum cement would rapidly set, causing excessive cracking and loss of strength to the cured cementitious material. Furthermore, excessive gypsum could cause shear thickening behaviour in cement pastes due to the formation of a large amount of plaster set, due to the presence of anhydrite gypsum in the cement and a higher water-cement will free up the spaces between cement particles hence contribute to shear thinning effects [375].

Regarding the process parameter, for water-to-cement ratio of 0.5 (used in this study) the viscosity vs shear rate plot for cement pastes does indicate a shear thinning. However, the addition of pulp fibers increases the "pot life" of the FC system, which means keeping the viscosities of the FC paste in a usable regime (prevent the rapid increase of viscosities with time). In other words, it increases the handling time of the FC pastes.

In addition to this, the shear thinning effect of the cement pastes is improved with the addition of pulp fibers as fiber flocks tend to break down and align in the direction of shear, resulting in decreased viscosity with the increase in shear rate [198].

B.2 Mechanical characterization

Table B.2 Mechanical characterization of cured cementitious sample based on the three-point bending tests.

Cured Sample (cement board)	MOR	Standard Deviation (S.D)
OPC (without reinforcement and additive)	4.8	0.81
FC_CNCs(*5*)wt.% (reinforced and with additive)	5.38	0.998

Calculated MOR values of the OPC and FC board (thickness: ca. 8 mm). OPC board does not contain any reinforcing pulp fibers and additives while the FC board contains 8 wt.% of pulp fiber (reinforcement) and 5 wt.% CNCs (additive).

B.3 Microstructural characterization

Field emission–SEM (FE–SEM)

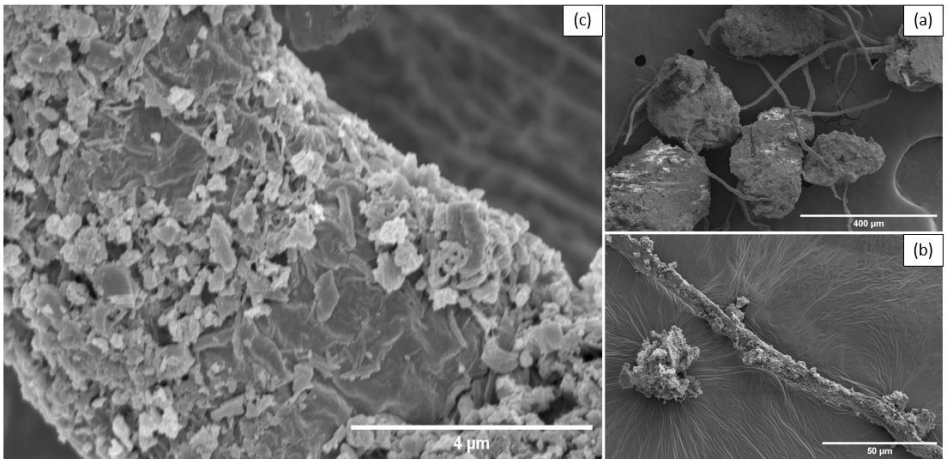

Figure B.3 FE–SEM images of FC interface (from low to high magnification (Figure S3 (a-c)), representing the FC interfaces containing CNCs.

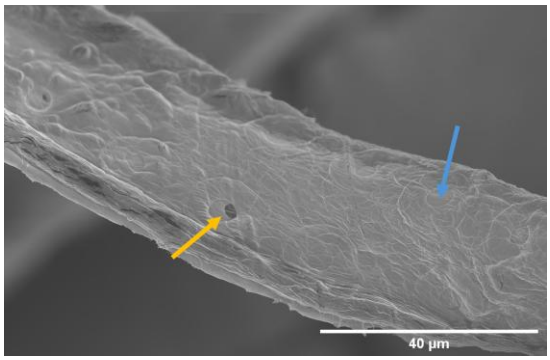

Figure B.4 FE–SEM micrograph of fiber–CNCs interface. The image depicts voids (pores) filling effect (indicated by the blue arrow) of CNCs deposited to the bleached pulp fiber. The unfilled void (pore) of the pulp fibers is indicated by the yellow arrow.

Appendix C Chapter 4 supplementary materials

Table C.1 The yield stress and MOR values of FC paste containing varying proportions of NBSK fibers and cellulose nanocrystals (CNCs). * Indicates that the value was obtained from the current study.

Sample name	MOR (MPa)	Yield stress (Pa)	NBSK content (wt.%)	CNC content (wt.%)
FC_NBSK_10%_CNCs_2%	8.2 [243]	68*	10	2
FC_NBSK_8%_CNCs_4%	8.5 [243]	74*	8	4

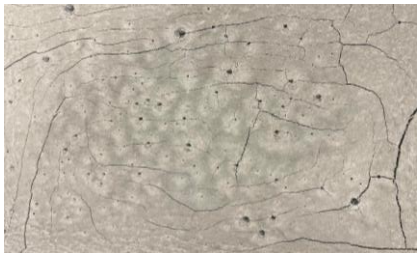

Figure C.1 Image of FC sample containing 10 wt.% MCC content and 2 wt.% NBSK fibers. Note that the samples cracked within one day of curing.

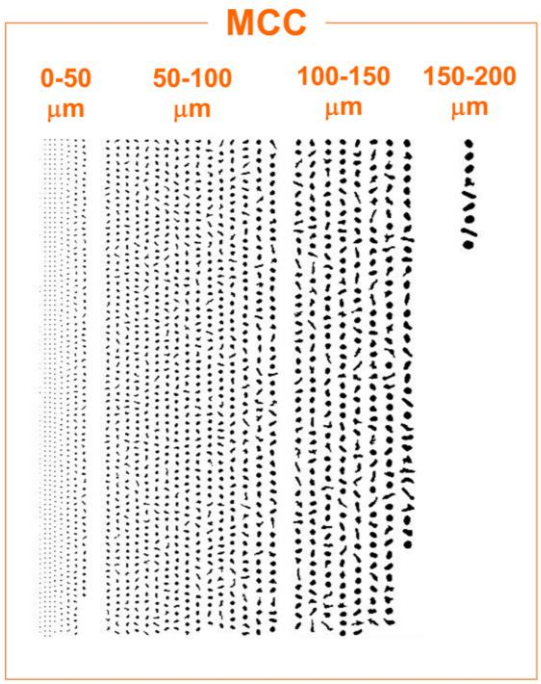

Figure C.2 A digital mosaic of individual MCC particle in motion as a function of particle size. Image captured during the DIA measurement.

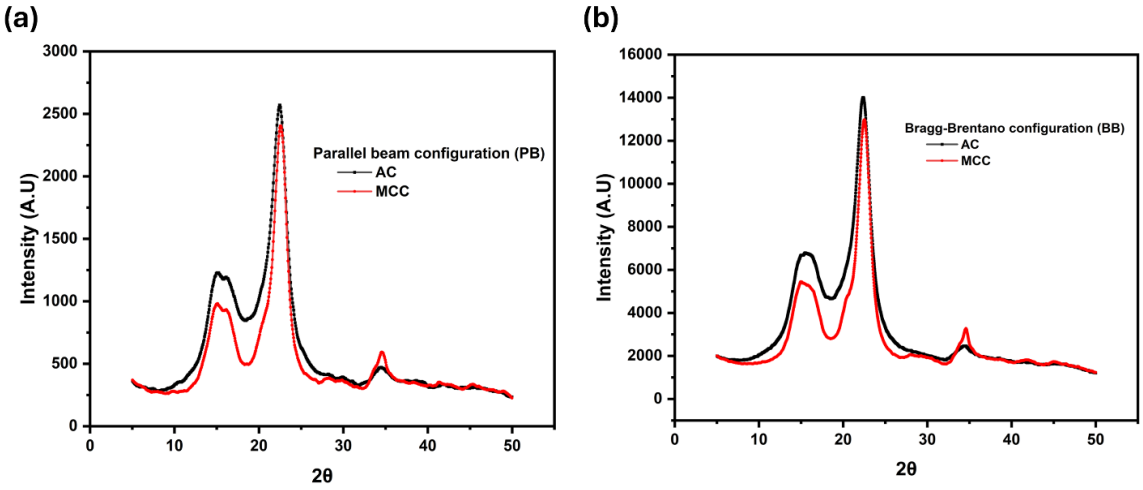

Figure C.3 Representative PXRD diffractograms of micro-additives (AC and MCC) employed for this study computed using two different configuration modes (a) Parallel beam (PB) and (b) Bragg-Brentano configurations respectively.

Table C.2 Crystallinity index (C*ri*) of AC and MCC, calculated using Segal's method [376]**.**

Additives	Crystallinity index (*CI*) % (PB configuration)	Crystallinity index (C*I*) % (BB configuration)
AC	67.4%	67.1 %
MCC	79.62%	78.57%

The calculated *CI* values were in accordance reported in literatures [377–380].

C.1 Rheological characterization

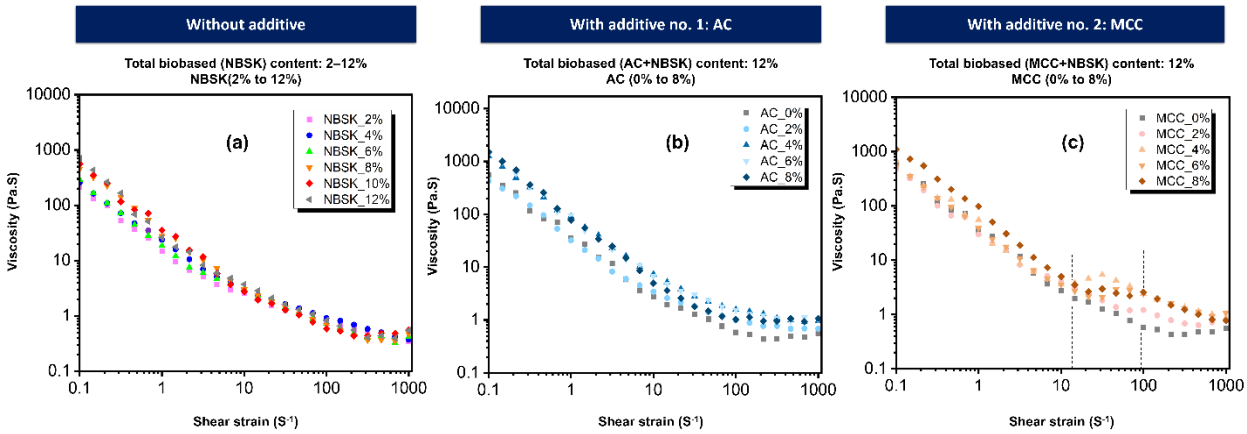

Figure C.4 Steady-state viscometry of FC slurry. The steady-state viscometry analysis of FC samples containing varying proportions of reinforcing fibers and microcellulosic materials (a) NBSK fibers (b) NBSK and AC (c) NBSK and MCC, which are denoted as combination 1 and combination 2, respectively. Note that the dotted arrow tentatively depicts the boundaries of the constant viscosity region (observed with the addition of MCC in FC slurry).

Figure C.4 represents the evolution of shear viscosity by shear rate, under steady-state viscometry. As observed, in the case of all cement pastes, they follow a shear-thinning behaviour [243]. Under high shear rates, the difference between shear viscosities of all formulations is minimal and they all reach a plateau. This is useful for applications where the slurry needs to be agitated at a high speed (e.g., >1000 rpm for pumping application of cement slurry) and an estimate of shear viscosity is required for determining the mixing requirements (factors such as binder ratio, water/cement ratio, content of fibers/additives) [255,381].

Under low shear rates, the shear viscosity of the FC slurry increased as a function of the content of NBSK (from 2–12wt.%), AC, and MCC (from 2–8wt.%) as displayed in **Figure C.4(a-c)** respectively. Such behaviour was also observed with the addition of CNCs in FC slurry [243]. Note that, unlike NBSK fibers and AC, when MCC was added, the shear viscosity plot did not manifest a shear-thinning plot followed by the plateau in viscosity. Interestingly, the slurries follow a three-region shear-thinning flow, followed by a constant shear viscosity, which was previously reported for the case of biobased colloidal suspensions [382], emulsions [383], and slurries [384] (for e.g. CNC suspension/colloids in water) [385]. Now, in some of these systems, aggregation of the agglomerates and their following de-aggregation under shear forces would introduce secondary shear-thinning behaviours in the viscosity plots [384].

C.2 Microstructural characterization

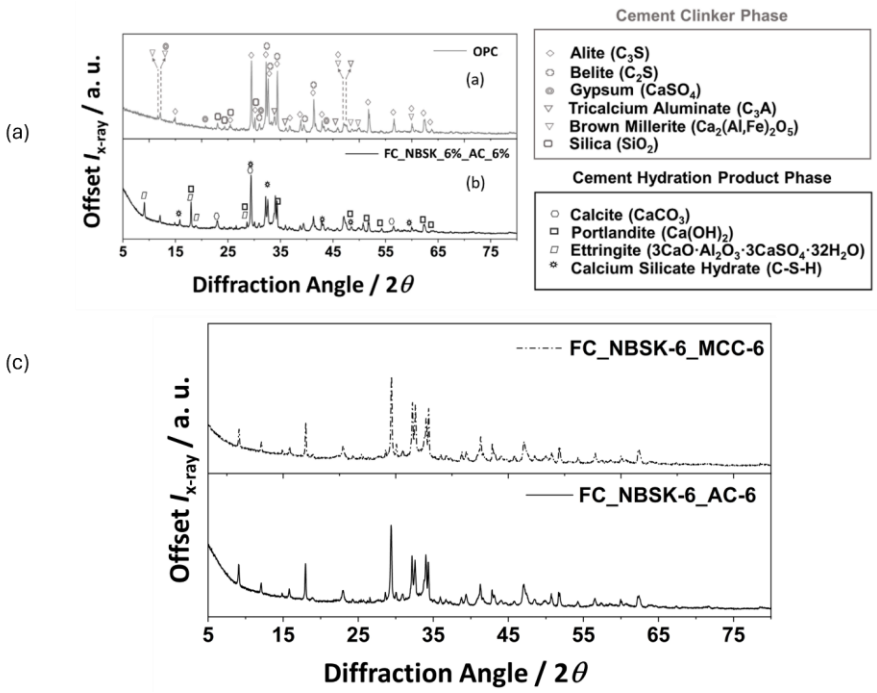

Figure C.5 Hydration products characterization. Powder X- Ray diffractogram (PXRD) of (a) OPC clinker phases (b) and (c) representative FC sample containing both combinations, depicting their OPC hydration products.

The powder diffraction file (PDF) number associated with the OPC clinker phases and FC hydration products (as obtained from ICSD database) is as follows: Alite (00-055-0738), Belite (00-033-0302), Gypsum (01-074-1905), Tricalcium aluminate (01-074-7039), Brownmillerite (01-074-3674), Silica (01-071-0261), calcite (01-086-2334), portlandite (00-001-1079), Ettringite (01-075-7554).

Table C. 3 The table depicting the material cost (reinforcement/additive) for fabricating all the FC samples used in this research.

Sample ID	NBSK fibers (wt.% of cement)	w/c ratio	Additive (wt.% of cement)		Cost of reinforcement (USD/g)	Cost of additive (USD/g)	Total Cost (USD)
	Without additive						
			AC	MCC			
NBSK_2%	2 (8.4 g)	0.5	-	-	0.003	-	0.02

NBSK_4%	4 (16.8 g)	0.5	-	-	0.003	-	0.05
NBSK_6%	6 (25.2 g)	0.5	-	-	0.003	-	0.07
NBSK_8%	8 (33.6 g)	0.5	-	-	0.003	-	0.1
NBSK_10%	10 (42 g)	0.5	-	-	0.003	-	0.12
NBSK_12% (Control sample)	12 (50.4 g)	0.5	-	-	0.003		0.15
NBSK 16%	16 (67.2 g)	0.5	-	-	0.003	-	0.2016
NBSK 24%	24 (100.8 g)	0.5	-	-	0.003	-	0.3024
NBSK 32%	32 (134.4 g)	0.5	-	-	0.003	-	0.4032
Combination 1: AC and NBSK							
			AC	**MCC**			
AC_2%	10 (50.4 g)	0.5	2 (8.4 g)	-	0.003	0.0008	0.126
AC_4%	8 (33.6 g)	0.5	4 (16.8 g)	-	0.003	0.0008	0.113
AC_6%	6 (25.2 g)	0.5	6 (25.2 g)	-	0.003	0.0008	0.09
AC_8%	4 (16.8 g)	0.5	8 (33.6 g)	-	0.003	0.0008	0.07
AC_10%	2 (8.4 g)	0.5	10 (42 g)	-	0.003	0.0008	0.0588
Combination 2: MCC and NBSK							
				AC	**MCC**		
MCC_2%	10 (50.4 g)	0.5	-	2 (8.4 g)	0.003	0.0045	0.16
MCC_4%	8 (33.6 g)	0.5	-	4 (16.8 g)	0.003	0.0045	0.17
MCC_6%	6 (25.2 g)	0.5	-	6 (25.2 g)	0.003	0.0045	0.18
MCC_8%	4 (16.8 g)	0.5	-	8 (33.6 g)	0.003	0.0045	0.20
Combination 3: CNC and NBSK (previous study)[243]							
Sample ID	**NBSK fibers (wt.% of cement)**	**w/c ratio**	**Additive (wt.% of cement)**		**Cost of reinforcement (USD/g)**	**Cost of additive (CNC) (USD/g)**	**Total Cost (USD)**
CNC_2%	8 (33.6 g)	0.5	2 (8.4 g)		0.003	0.007	0.1588
CNC_4%	8 (33.6 g)	0.5	4 (16.8 g)		0.003	0.007	0.2176

The cost of NBSK fibers is inclusive of the refining cost mentioned in **Table C.4** Note that the total cost here refers to the total (reinforcement + additive) cost that is required to produce a FC composite as mentioned in the manuscript. The raw material cost is derived from **Table C.4** (*vide infra*) to tabulate the total reinforcement cost.

Table C.4 Table representing the reinforcement/additive cost (adapted from current market prices and prior in depth technoeconomic studies conducted to ascertain the production cost of these additives) along with their references.

Materials	Cost (USD / Mt)		Reference
	Cellulosic fiber		
NBSK	Raw material	≈ 700	[386,387]

	Refining	≈ 1720	
	Total	≈ 2420	
Cellulosic additive			
AC	≈ 800		[244,388]
MCC	≈ 4500		[389,390]
CNC	≈ 7000		[244,391]

As shown in **Table C.4**, the total production cost of NBSK fibers (raw material cost + cost of refining) makes them an expensive component in the FC, where the cost of production of cement is around only 60 USD/tonne) [392]. Additionally, fiber refining is an energy-intensive process and modeling studies from Chakraborty *et al*. reveals that the cost of refining 1 kg of NBSK fibers (to 1 μm length) in a PFI mill was accounted to about USD 1.72/kg (ca. two times the cost to procure 1 tonne of NBSK fibers) [387].

High content of NBSK fibers demands the use of additional rheology modifiers/superplasticizer, which is another significant contributor to carbon dioxide emissions as well as added cost to a FC fabrication process. For example, the cost of production of PCE superplasticizer is about 850–1440 USD/tonne) [393]. Thus, "*less is more*" is the philosophy followed in this research work so that we do not have to compromise with performance metrics without incorporating property-specific additives like curing accelerators, and retarders, to name a few.

Table C.5 Cost of silica-based additives used in construction industry. Note that these prices can fluctuate depending on market trends and product availability.

	Cost USD/mt	**Reference**
SF (Micro silica)	≈200 – 800	[394]
Silica sand	≈90	[395]
Nano silica	≈1500 – 4000 *Could be even higher depending upon the size and purity	[396]

As seen from **Table C.5,** the cost of silica-based additives varies with the size and type of silica, most common are silica sand (low-cost) and micro silica. Though silica sand is cheap, extracting sand would involve quarrying activities to be conducted, causing significant environmental impact. In terms of micro silica, the prices can be compared with that of AC, indicating the cost feasibility in replacing silica-based additives with biobased (cellulosic) additives for building materials.

Appendix D Chapter 5 supplementary materials

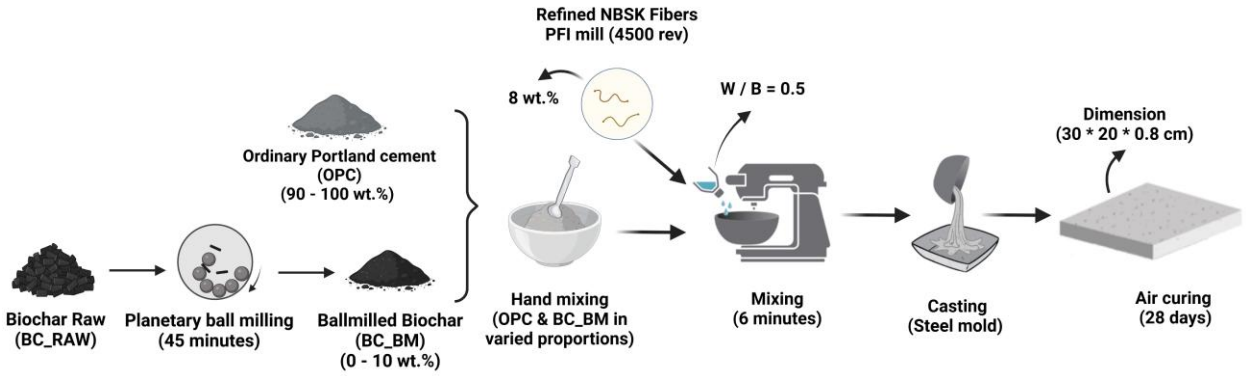

"Created in BioRender. Raghunath, S. (2025) https://BioRender.com/r88j542"

Figure D.1 Steps involved in FC manufacturing. Note that for rheological characterization, the FC slurry after mixing is used , whereas for mechanical as well as microstructural characterization, cured FC samples are utilised.

D.1 Rheological characterization

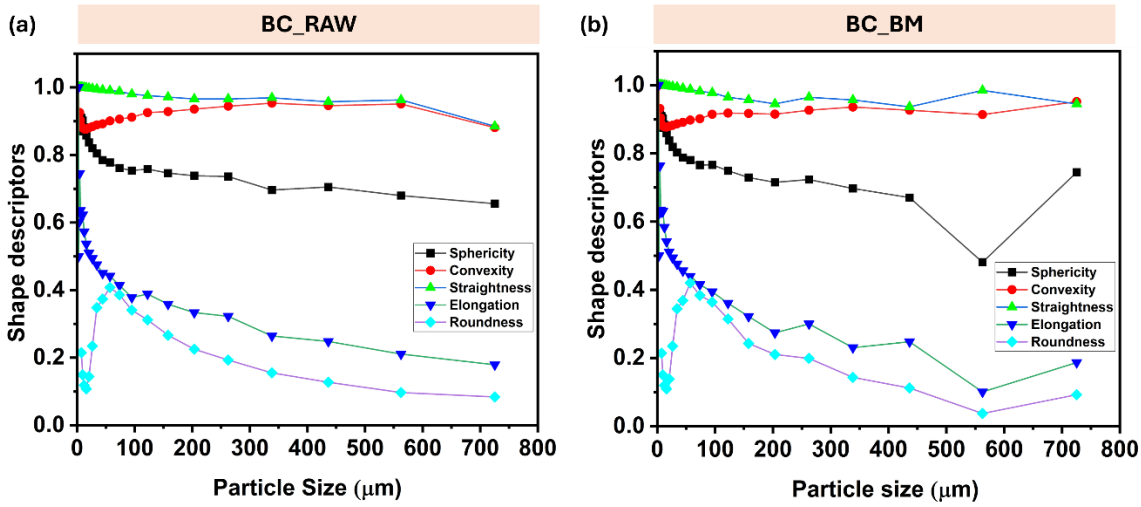

Figure D.2 Variation of Particle shape descriptors (sphericity, convexity, straightness, elongation and roundness) with particle size of (a) raw BC samples (b) ball milled BC samples.

Figure D.2(a,b) depicts the variation in different BC shape descriptors with respect to increasing BC particle size. It can be inferred from **Figure D.2(a,b)** that the shape of the BC significantly varies with particle

shape. For BC_RAW samples, as the particle size increases (>150 μm), the general trend observed is that the particle tends to be less elongated, less spherical and round compared to finer BC particles (<150μm). However, the particle straightness and convexity remain independent (although a slight decrease is observed at particle size > 550μm) with increasing particle size. It is important to note that the convexity of the BC particles (which is a measure of the compactness of a particle) is high and consistent for both BC_RAW as well as for BC_BM samples. High convexity indicates that the particles have less indentation and outwardly smooth (more compact), thus can potentially affect the packing density and particle interlocking which can aid in improved mechanical properties as well as the flow behaviour for the FC slurry. From **Figure D.2(b)**, it can be observed that, the effect of ball milling is more pronounced at higher particle size domain (> 550μm) compared to finer BC particles. In this domain, it is observed that ball milling is effective in improving the sphericity, roundness, elongation and convexity to a small extent, whereas the straightness of the BC particles reduces slightly.

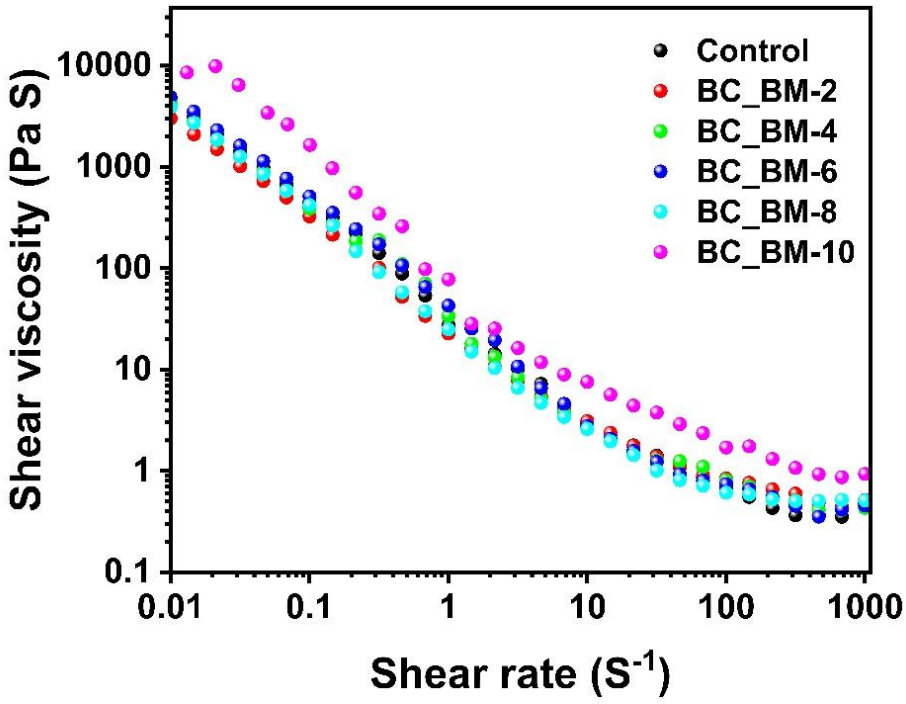

Figure D.3 Steady state viscometry analysis of FC slurry as a function of BC content.

General observation made from **Figure D.3** is that, despite the concentration of BC, all FC samples exhibited shear thinning behaviour. Now at high BC content (6 - 10 wt.%), viscosity of the FC slurry at every shear rate seemed to increase whereas at low BC content (0 - 2wt.%) the steady state viscometry results

showed similar trends to that of control sample (in terms of magnitude and trendlines). This in a way suggests that the BC content needs to exceed the C_{BC} (i.e. 3-4wt.% range) to tune the rheological properties of the FC slurry, which is in accordance with the trends observed with the evolution of static yield stress with increasing BC content (see **Figure 5.4(a)**).

Table D.1 Properties (MOR) of cement composites which employed different carbon different based materials as an additive/reinforcement/SCMs, used to benchmark mechanical characterization results from this study.

Carbon based material	Content at which the composite exhibited maximum MOR	Dispersion method	MOR (MPa)	References
Carbon black (CB)	2 wt.%	Sand and superplasticiser	9.5	[321]
Graphene (G)	0.01wt.%	Polycarboxylate superplasticizer,	9.5	[322]
Graphene oxide (GO)	0.05 wt.%	Ultrasonification	6.5	[323]
Graphene nanoparticles (GN)	0.05wt.%	Darex S 20 - 2 ml, ultrasonification 2 hours	6.25	[324]
Multi-Walled Carbon nanotubes (MWCNT)	0.02 wt.%	Mechanical stirring for 3 min, followed by magnetic stirring for 30 min and ultrasonication for 1 h.	8.2	[325]

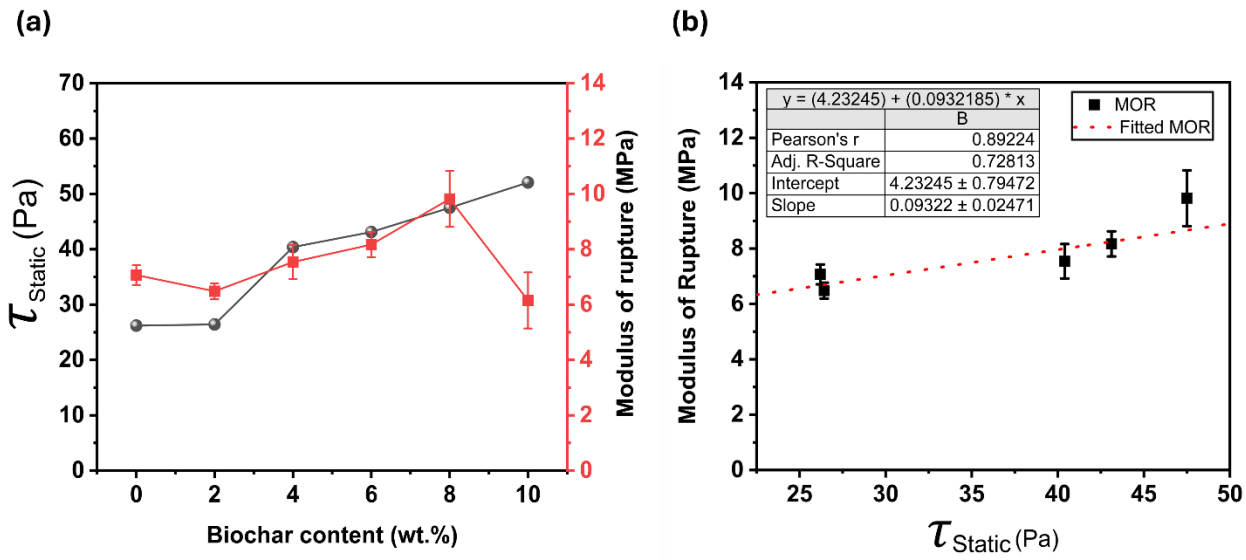

Figure D.4 Rheo-mechanical characterization of FC function of BC content depicting (a) Variation of τ_{Static} & MOR (b) linear correlation existing between τ_{Static} & MOR.

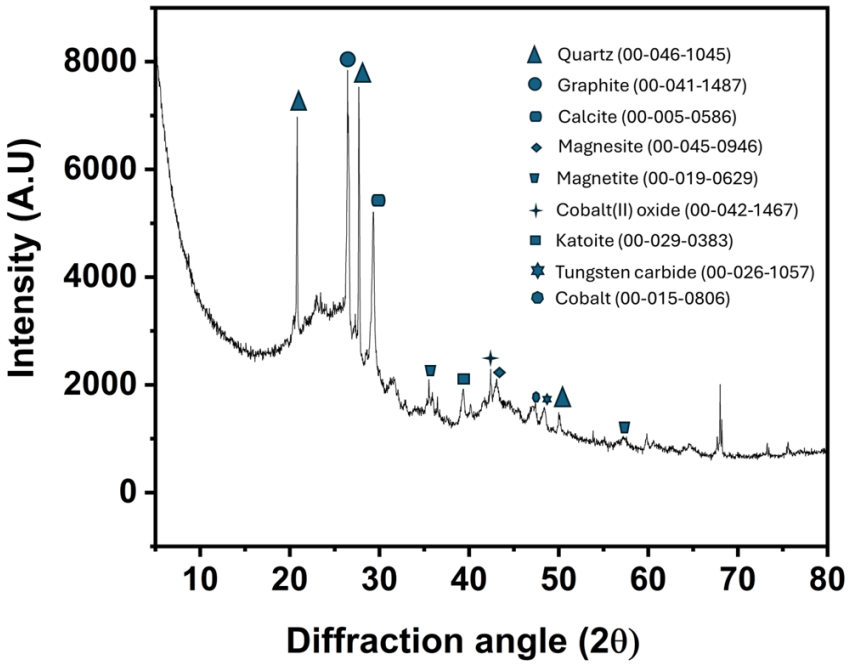

Figure D.5 Powder X-Ray diffractogram (depicting the phase ID) of BC used for this research. Note that the PDF number associated with each identified phase is mentioned alongside with the phases.

D.2 LCA

A LCA study was carried out, in accordance with ISO 14040[397] & 14044 [398] standard, to determine the environmental impact of utilising BC as a biobased (in six different proportions) supplement to cement for FC manufacturing. Further details pertaining to this LCA study is provided as supplementary information [292].

Goal and Scope : A system boundary (cradle to gate) was developed to evaluate the environmental impact of utilising BC as a biobased supplement to cement in FC manufacturing (**Figure D.6**). Cement was supplemented with 6 different BC contents (0 -10 wt.%) and assessed for their respective environmental impacts. The life cycle impact category of interest to this study was GWP. EN 15804 A1:2020 assessment method[399], which is the specialised European standard for assessing the environmental impact and product category rules (PCR) of construction product and services (within the framework of type 111 EPD according to ISO 14025) [400] was utilised for GWP evaluation. The functional unit for this LCA analysis was defined as 0.05 m^2 of FC.

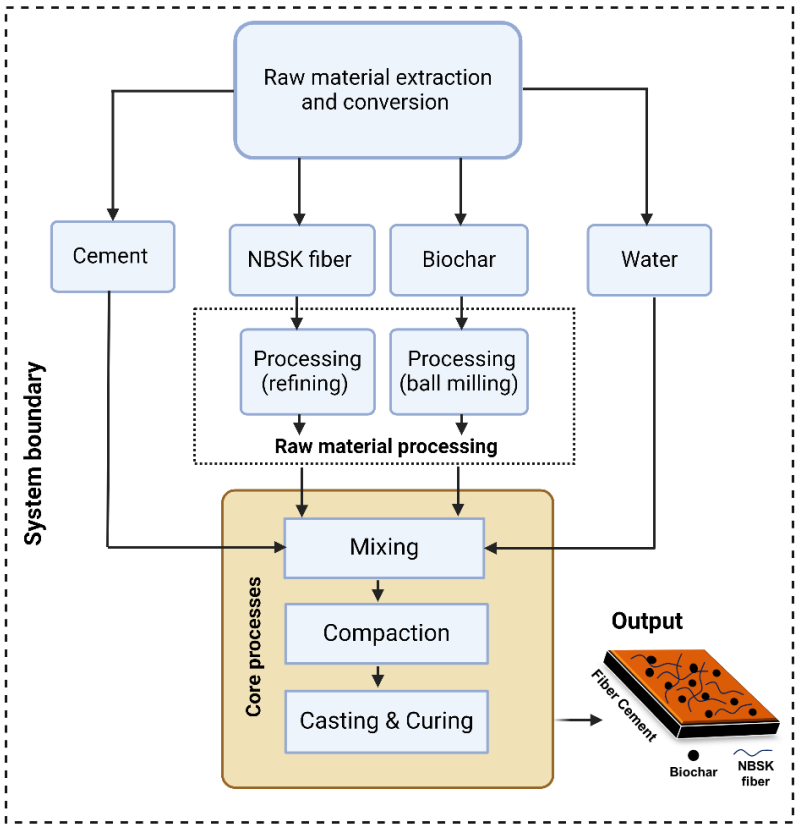

Figure D.6 A cradle to gate system boundary of lab scale FC production

We relied on peer-reviewed literature for the GWP and carbon sequestration values of BC, in order to obtain a wider perspective as to how different biomass sources and pyrolysis conditions can contribute to the GWP of BC production in USA and Canada. Now it may be noted that the conversion of woody biomass into BC (pyrolysis) process requires energy and does contribute to GWP. However, this valorization process (pyrolysis) converts about 60 - 80% of carbon presents in biomass into stable form of carbon (i.e. BC), which outweighs the carbon emission during its production stage, resulting in a net negative process [288]. Additionally, if these waste biomasses were to be landfilled or incinerated, it results in the release of CO_2 and C_2H_4 contributing to increase in GWP [288]. Thus, when carbon counting or LCA analysis are carried out related to BC production, often these factors are considered, which results in a net negative GWP for BC. Now depending upon the pyrolysis process, the valorization or end use pathways of pyrolysis gases and taking into consideration the potential end use application of the produced BC, the sequestration potential of BC (although negative) can vary significantly. Thus, from the literature studies it was estimated that 1 tonne of BC can sequester up to 1.9 to 2.7 [401,402]tonnes of CO_2 -eq and for this analysis, an average of 2.3 tonnes of CO_2 -eq was chosen as an input to this analysis (this average value was taken from the LCA study conducted for BC Biocarbon, from where the BC was procured) [403,404]. The energy consumption related to pulp fiber refining was adapted from the modelling studies conducted by Chakraborty *et al.* [405].

Life cycle inventory

The detailed foreground inventory details pertaining to the production of BC supplemented FC composite are provided in (**Table D.2 - Table D.3**). The background data pertaining to each process was derived from the ecoinvent_38_en15804gd_v3 database [406] and the LCA modeling was carried out using OpenLCA software (version 2.0, 2023) [407].The “market for cement”, “sulphate pulp” and “water” was modeled to |EN15804 -RoW. “RoW” was chosen to promote a comprehensive LCA analysis considering the global data and impacts. Now, according to the EN 15804 and PCR standard requirements, the cutoff criteria indicates that any flows in the LCA core processes can be cut off, if it contributes to less than 1% of the total mass of material input or 1 % of the total energy. With regards to this, we assumed that the environmental impact related to the equipment usage for raw material processing and core process involved in the FC manufacturing process to be negligible and was omitted from the analysis. Note that all the samples were prepared in the University of British Columbia (UBC) laboratory, located in BC, Canada. Hence the electricity consumption of all the processes related to FC production was modelled to “market for electricity, low voltage | EN15804 – CA -BC”.

Table D.2 Energy consumption related to raw material processing and core process for FC production as input to the LCA analysis.

Process	Rated Power (Watts)	Time employed (mins)	Energy (kWh)
Mixing (Techwood tabletop mixer)	400	6	0.04
Compaction (Fisher incubating micro-plate shaker)	450	15	0.1125
BC Processing (Retsch 400 PT , Ball milling device)	1500	45	0.596

Table D.3 Life cycle inventory of all the processes involved in FC production, used for this analysis.

Inventory	Unit	Samples					
Input							
		FC_BC-0	**FC_BC-2**	**FC_BC-4**	**FC_BC-6**	**FC_BC-8**	**FC_BC-10**
Cement	g	420	411.6	403.2	394.8	386.4	378
Water	g	210	210	210	210	210	210
NBSK fiber	g	33.6	33.6	33.6	33.6	33.6	33.6
BC	g	0	8.4	16.8	25.2	33.6	42
Raw material Processing							
Refining	kWh	0.963	0.963	0.963	0.963	0.963	0.963
Ball milling	kWh	0.596	0.596	0.596	0.596	0.596	0.596
Core processes							
Mixing	kWh	0.04	0.04	0.04	0.04	0.04	0.04
Compaction	kWh	0.1125	0.1125	0.1125	0.1125	0.1125	0.1125
Casting & curing	NA	NA (The samples were air-cured for 28 days, hence no energy consumption)					
Output							
FC	m^2	0.05	0.05	0.05	0.05	0.05	0.05
Sample wastage	The mix composition of the FC manufacturing scheme was designed in such a way that there is minimal wastage – therefore zero wastage was considered for this LCA analysis.						

Table D.4 The composition, mechanical properties and LCA parameters of commercial FC used as a benchmark for this study.

Manufacturer : James Hardy **Environmental product declaration no : S-P-01432** **(In accordance with ISO 14025 & EN 15804 : 2012 +A1 :2013)**

Issued :2019 -04 -12 **Valid till : 2023-12-13** **Revised: 2022 -03 -14** **LCA conducted by : EuGeos Limited, UK**	
Composition	**Wt.% (as per declared functional unit)**
Crystalline silica	38 -45
Calcium silicate (hydrate)	40 -45
Cellulose	4-9
Calcium aluminium silicate hydrate	5-12
Acrylic polymers	<1%
Physical and mechanical properties	
Thickness Hardie Panel Hardie Plank Hardie VL Plank	 8 mm 8mm 11 mm
Flexural strength (EN12467: 2012)	>7 Saturated MPa > 10 Equilibrium conditioned
LCA Parameters and Results	
Functional unit	1 m^2
GWP (Modules, A1 – A3) Hardie Panel Hardie Plank Hardie VL Plank	 8.94 $KgCO_2$-eq 7.34 $KgCO_2$-eq 1.20$KgCO_2$-eq

* Note that for comparison and benchmarking, we compared our sample with Hardie VL Plank boards.

Table D.5 Cost of raw material (obtained from current market research & prior technoeconomic analysis) and the energy requirement with cost pertaining to all the core processes (including raw material processing) used for C/P calculation and analysis.

Raw material cost	
Cement	157 USD/Mt [408]
BC	400 USD/ Mt [409,410]
Water	2.027 USD/m^3 [411]
NBSK fiber	1735 USD/Mt [412]
Electricity (commercial rate)	5.98 ¢ per kWh[413] (Fortis BC, price in USD)
Raw material processing cost	
NBSK fiber refining	0.028694 KWh /g Now all the samples contain 8wt.% (33.6 g) of NBSK fiber, Therefore, Total refining energy

	= 0.028694 kWh * 33.6 g = 0.9641184 KWh Total refining cost = Total refining energy (kWh) * Cost of electricity (commercial rate , ¢ per kWh) = 0.9641184 kWh * 5.98 ¢ per kWh = 0.0576 USD (for refining 33.6 g of NBSK pulp)
Ball milling	Total energy = 0.596 kWh Total cost = Total energy * cost of electricity = 0.0356 USD
Other processing cost (Mixing + Compaction)	= 0.0091195 USD

Note that for consistency of cost calculations, Prices in CAD were converted into USD (using a conversion factor, 1 CAD = 0.7163 USD).

Table D.6 Total fabrication cost (calculated from information derived from Table D.3) of all the FC samples fabricated in this research for C/P analysis.

Sample	Total FC production cost for 0.05 m (USD)	% increase in cost w.r.t control
Control	0.19096117	NA
2wt.%	0.19301077	1.073307207
4wt.%	0.19506037	2.146614414
6wt.%	0.19710997	3.219921621
8.wt%	0.19915957	4.293228828
10.wt.%	0.20120917	5.366536035

Appendix E Chapter 6 supplementary materials

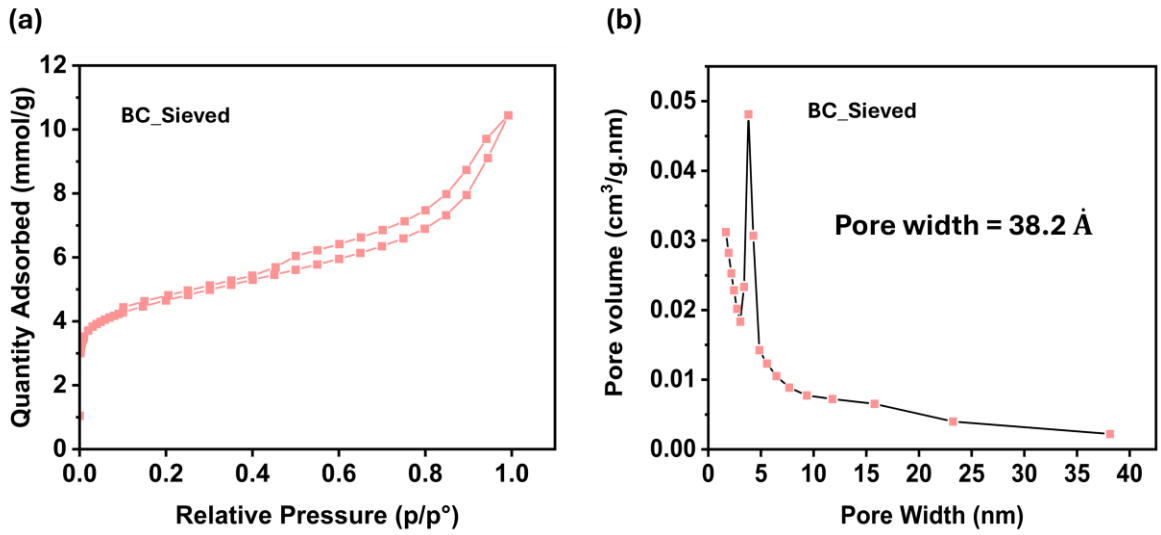

Figure E.1 Porous structure analysis of raw BC (sieved through MS 100) Depicting (a) N_2 adsorption – desorption isotherm and (b) BJH pore size distribution.